UiT The Arctic University of Norway

Faculty of Biosciences, Fisheries and Economics

The Norwegian College of Fishery Science

Antimicrobial activities and mechanisms of action of peptide analogues of marine origin

Hymonti Dey

A dissertation for the degree of Philosophiae Doctor

April 2024

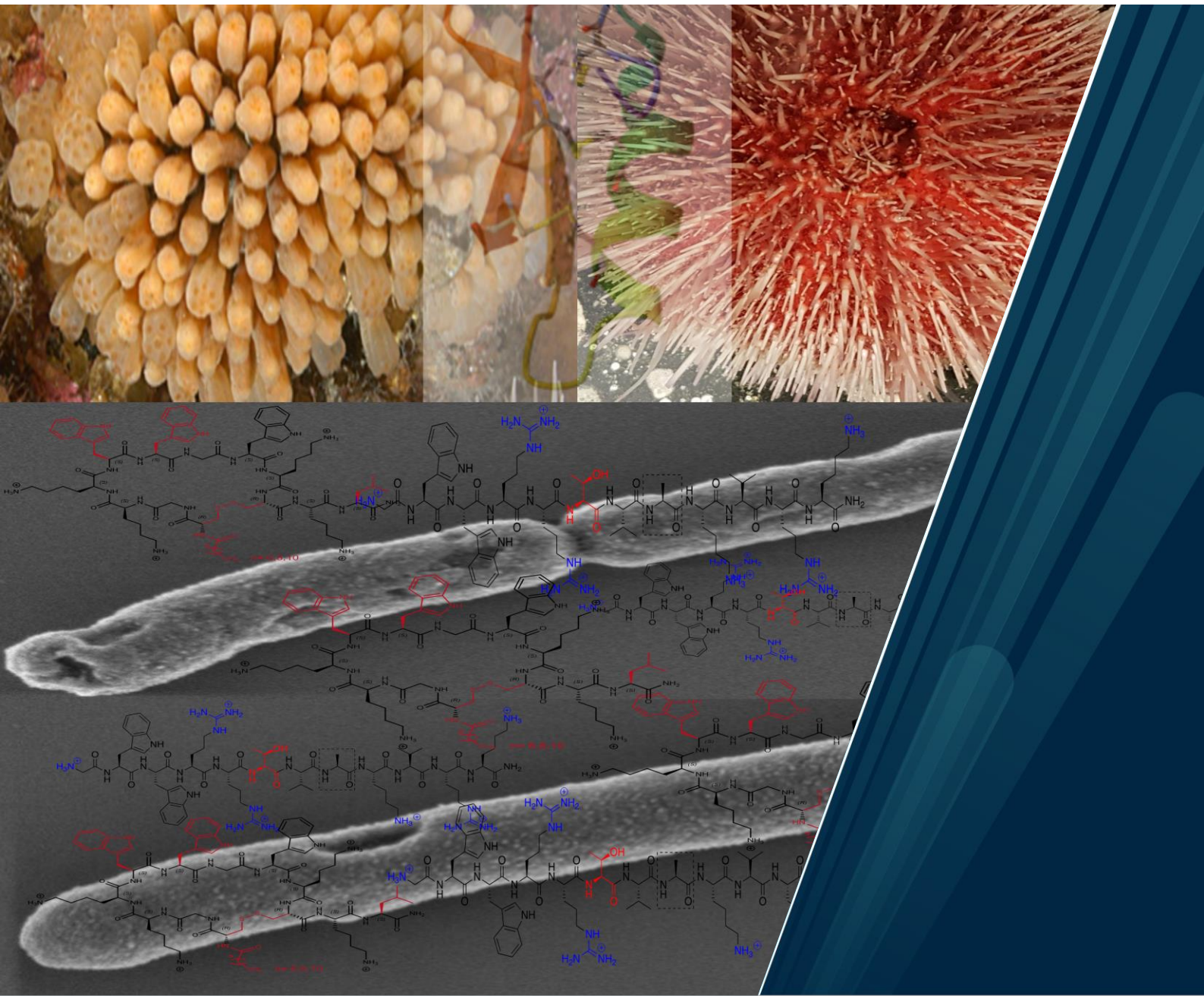

A dissertation for the degree of Philosophiae Doctor

Antimicrobial activities and mechanisms of action of peptide analogues of marine origin

Hymonti Dey

April 2024, Tromsø

The work for this thesis was carried out from August 2019 to April 2024 at the Marine Bioprospecting Group, Norwegian College of Fishery Science (NFH), Faculty of Biosciences, Fisheries and Economics, UiT – The Arctic University of Norway. The work was part of the LeadScAMR project funded by UiT - The Arctic University of Norway.

Acknowledgements

This thesis work was carried out at the Norwegian College of Fishery Science, UiT – The Arctic University of Norway, Tromsø and was a part of Lead-ScAMR project with financial support from UiT.

First of all, I would like to thank my team of supervisors for their enormous support. I feel fortunate to receive all the invaluable insights for the completion of this thesis work. I would start by expressing my deepest gratitude to my main supervisor Prof. Tor Haug. Thank you for the encouragement and support. Your thoughtful and patient attitude gave me the strength of pursuing my goals even if it was challenging sometimes. You always kept your door open and greeted me with a smile and made me feel like “this is good enough”, now stop. I know you were stressed too.

My heartfelt thanks to Assoc. Prof. Hans-Matti Blencke for the unwavering support and mentorship in shaping my academic and professional growth. Your way of thinking provided me with helpful directions for the microbiology work. I would say you are an amazing person with an incredible brain. I feel fortunate to have those hours-long discussions to find solutions to the problems I was facing both in science and life. Your guidance during writing of this thesis means a lot to me. I am also thankful to Prof. Morten B. Strøm and Assoc. Prof. Elizabeth GA Fredheim for being supportive when I really needed it. Your insightful feedback and encouragement have enriched my knowledge.

I am thankful to all my PhD colleagues, specially Danijela, Céline, Ataur, and Manuel for this wonderful collaborative work and intellectual exchange. I want to acknowledge all my co-authors for your contributions. Without your help this work wouldn’t have been done yet. All my NFH colleagues (current and former), especially Ida, Hege, Andrea, Christopher, Pauke, Frode, Jonathan and Katya, your cooperation helped me integrate into the group easily. Tromsø felt more like home because of all of you. Special thanks to Prof. Klara Stensvåg for being the heart of our group. You are a true inspiration for all of us in the marine bioprospecting group. I would also like to express my gratitude to Roger Simm for providing resources and a friendly environment at the Institute of Oral Biology (IOB), UiO, Oslo. Your guidance and support enriched my research experience.

Life in the Arctic would not have been more amazing without the experience I gathered with all the amazing people throughout the whole PhD journey. Thanks to UiT The Arctic University of Norway, for providing me with this opportunity. I am forever grateful.

A big thanks to all my friends in Norway, specially Mariusz, thank you for your love, encouragement, and understanding. Also, I want to extend my deepest appreciation to my family, my mother Geetashree and brother Anindya who live far away, but long distance couldn’t weaken our support for each other. Finally, my son Arijeet, thank you for your belief in my abilities. You were my source of strength and motivation during the challenging times. Ma loves you to the moon and back.

Hymonti Dey

April 2024

Abstract

Modern medicine is threatened by the emergence of antimicrobial resistance (AMR). New agents with unique structures and mechanisms of action are urgently needed to address the problems associated with AMR. To effectively address this challenge, a proper understanding of the structure-activity relationship is required to decipher the mechanism of action of novel compounds. Template-based design inspired by the structural motif of natural antimicrobial peptides (AMPs) could open new ways to develop antimicrobial agents with novel mechanisms of action. In this thesis, the biological effects of altering the amino acid composition, cyclization, and addition of *N*-terminal fatty acid chains on short synthetic marine AMP derivatives were studied. A rational peptide design approach based on well-known physicochemical features, such as hydrophobicity and cationic properties was applied on templates derived from the marine AMPs Turgencin A and EeCentrocin 1. Antimicrobial screening was conducted using different Gram-positive and Gram-negative bacterial strains as well as different fungal strains. Several bacterial biosensors including novel MoA-specific whole-cell biosensors were used to study the mechanism of action (MoA).

The incorporation of tryptophan into the core sequence of Turgencin A analogues as well as the substitution of lysine with arginine and cyclization via disulfide bridges, increased the potency of the derivates. This indicates the importance of arginine and tryptophan residues in the improvement of amphipathic properties. The highest antimicrobial activity was observed for cyclic lipopeptides **C_{12}-cTurg-1** and **C_8-cTurg-2,** indicating the importance of acylation in enhancing both activity and stability via increased hydrophobicity and cyclization. Similarly, modification with arginine and tryptophan or head-to-tail cyclization of a previously reported lead peptide (P6) derived from the heavy chain of the marine heterodimeric peptide EeCentrocin 1 resulted in the potent derivatives **P6-W6R8** and **cP6-W6R8**. Structure-activity studies showed that derivatives with increased antibacterial and membranolytic activities and low toxicity can be generated by fine-tuning several modifications. In addition to their effects on the cytoplasmic membrane, a secondary mechanism, involving outer membrane (OM) disruption in Gram-negative bacteria and the induction of stress responses related to membrane damage, suggests a concentration-dependent mechanism of action. In subsequent MoA studies, the application of a novel bacterial biosensor for measuring OM activity confirmed the primary interaction of the synthetic derivatives with the OM of *Escherichia coli*.

In studies involving combined treatment with either erythromycin or vancomycin, synergy against *E. coli* occurred more frequently with the OM active peptides, whereas no synergy was observed against Gram-positive bacteria. Most analogues were able to inhibit the formation of both Gram-positive and Gram-negative bacterial biofilms, which may be attributed to their membranolytic and killing effect. However, the biofilm inhibitory effects of moderately active analogues were independent of their growth inhibition effects. Synergistic combinations were also able to inhibit biofilm formation by *Salmonella enterica* serovar Typhimurium UMR1 and *Pseudomonas aeruginosa* PA01. The findings of the present study support previous research which shows that OM-acting AMPs potentiates the effects of antibiotics, by facilitating their access to the intracellular target molecules.

In summary, this thesis demonstrates that the targeted modifications of the structural motifs of marine AMPs can improve their antimicrobial and membranolytic activities, as well as their potential as synergists - to potentiate the antimicrobial and antibiofilm effects of commercial antibiotics.

List of papers

This thesis is based on the following papers, two published articles and two completed manuscripts, which are referred to in the text of the thesis by their Roman numerals.

Paper I

Dey, H. *, Simonovic, D. *, Hagen, I.N.-S., Vasskog, T., Fredheim, E.G.A., Blencke, H.M., Anderssen, T., Strøm, M.B., & Haug, T. (2022). Synthesis and Antimicrobial Activity of Short Analogues of the Marine Antimicrobial Peptide Turgencin A: Effects of SAR Optimizations, Cys-Cys Cyclization and Lipopeptide Modifications. International journal of molecular sciences, 23(22), 13844. https://doi.org/10.3390/ijms232213844.

Paper II

Simonovic, D. *, **Dey, H.** *, Johansen, N., Anderssen, T., Hansen, I.K.Ø., Devold, H., Vasskog, T., Blencke, H.M., Øyen, F.J., Fredheim, E. G. A., Haug, T., & Strøm, M. B. Antimicrobial activity of short analogues of the marine peptide EeCentrocin 1: Synthesis of lipopeptides and head-to-tail cyclic peptides and mechanism of action studies. (**Manuscript**)

Paper III

Richard, C.S.M., **Dey, H.**, Øyen, F., Maqsood, M., & Blencke, H.M. (2023). Outer Membrane Integrity-Dependent Fluorescence of the Japanese Eel UnaG Protein in Live *Escherichia coli* Cells. Biosensors, 13(2), 232. https://doi.org/10.3390/bios13020232.

Paper IV

Dey, H., Simonovic, D., Richard, C.S.M., Hagen, I.N.-S., Johansen, N., Fredheim, E. G. A., Strøm, M.B., Simm, R., Haug, T., & Blencke, H.M. Combining outer membrane active synthetic antimicrobial peptides with vancomycin or erythromycin increases antibacterial and antibiofilm activities. (**Manuscript**)

* Shared 1st authorship.

Contributions to/division of work

Contributions/roles	Paper I	Paper II	Paper III	Paper IV
Concept and idea	**MBS, TH**	**MBS, TH**	**CSMR, MM, HMB**	**HD, HMB, EGAF, MBS, TH**
Study design and methods	**DS, HD, TV, TA, HMB, INSH, EGAF, MBS, TH**	**DS, HD, TV, IKØH, TA, FJØ, HeD, NJ, TH, HMB, MBS**	**CSMR, HD, HMB**	**HD, DS, RS, INSH, NJ, CSMR, HMB**
Data gathering and interpretation	**DS, HD, TA, MBS, HMB, EGAF, TH**	**HD, DS, TA, MBS, HMB, EGAF, TH**	**CSMR, HMB, HD**	**HD, HMB, CSMR, INSH, RS, EGAF**
Manuscript preparation	**DS, HD, HMB, EGAF, MBS, TH**	**HD, DS, EGAF, MBS, HMB, TH**	**CSMR, HMB**	**HD, HMB, EGAF, TH**

Abbreviations

AMPs	Antimicrobial peptides
AMR	Antimicrobial resistance
ATP	Adenosine triphosphate
BR	Billirubin
FDA	Food and drug administration
FICI	Fractional inhibitory concentration index
HGT	Horizontal gene transfer
IM	Inner membrane
LPS	Lipopolysaccharides
MALDI-Tof	Matrix assisted laser desorption/ionization-Time-of-flight
MBC	Minimum bactericidal concentration
MoA	Mode of Action
MDR	Multidrug resistant
MIC	Minimum inhibitory concentration
NPN	1-*N*-phenylnapthylamine
NRPS	Nonribosomal peptide synthetase
OM	Outer membrane
PM	Plasma membrane
PMBN	Polymyxin B nonapeptide
SAR	Structure-activity-relationship

Table of Contents

1 Introduction

1.1 Urgent need for new strategies in the age of antimicrobial resistance

Infectious diseases are one of the leading contributors to mortality worldwide [1]. Currently, more than 700,000 fatalities annually are attributed to multidrug-resistant bacterial infections [2-4]. Without the new class of antibiotics available to treat bacterial infections, current predictions estimate an increase of more than 10 million deaths annually by 2050 [5,6].

The number of multidrug-resistant (MDR) bacteria has increased significantly in recent decades [1]. Many antibiotics that can reliably cure bacterial infections, are no longer effective because of the high prevalence of resistant strains. The spread of MDR pathogens within the community and healthcare settings contributes to high mortality rates, prolonged hospital stays, and more than $105 billion in global healthcare cost [7]. Antimicrobial resistance (AMR) is an ancient natural process that stems from an enduring battle among microorganisms, commonly referred to as nature's counter defense for survival advantages [8-10]. Unfortunately, the recurrent and prolonged exposure of microbial communities to antibiotics provides strong selective pressure, accelerating antibiotic-induced resistance and tolerance, ultimately leading to a major threat to human health [11,12]. While bacterial resistance to certain antibiotics can be intrinsic, due to their inherent structural and functional properties, in most cases, it is acquired by horizontal gene transfer (HGT) or *de novo* mutations [10]. General mechanisms of bacterial resistance are based on inhibition of drug entry, increased drug efflux, target mutation and modification, or chemical modification/inactivation/breakdown of the antibiotic itself [13-15] (summarized in **Figure 1**).

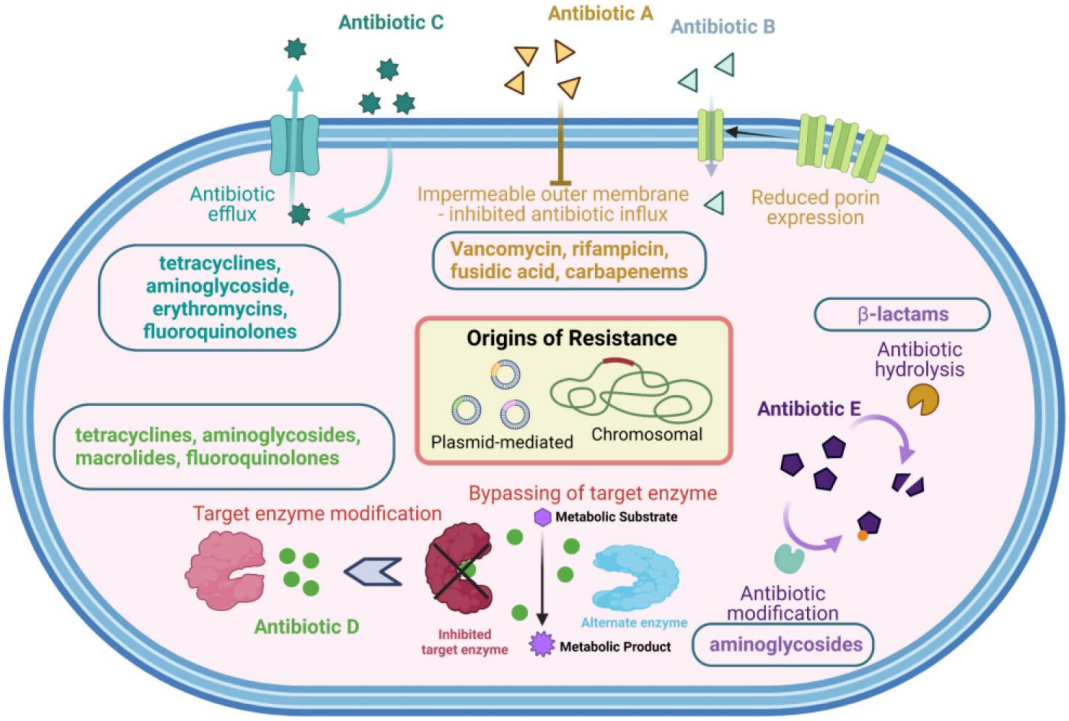

Figure 1. *Mechanism of antibiotic resistance; reproduced with permission by ACS publications: Dhanda et al. (2023) [15].*

However, AMR represents only part of the challenges associated with antibiotic failure, other concerns, such as biofilms and the protective outer membrane (OM) of Gram-negative bacteria continue to complicate treatment efficacy. The lack of new drug discovery and empty development pipelines are only amplifying these threats to modern healthcare. This has led to the distressing reality where microbes develop resistance to antimicrobials more rapidly than novel agents can be discovered to counteract them [16].

Biofilms are one of the main causes of persistent infections [17]. They provide a protected niche for the microbial community embedded in the extracellular matrix, allowing bacteria to tolerate high doses of antibiotics, environmental stressors, and host defense [17-19]. Recurrent hospital-acquired infections can be caused by biofilm-forming bacteria, especially those belonging to the ESKAPE pathogen group [20]. Similarly, Gram-negative bacteria resist many antibiotics because of the barrier function of their OM, which renders them intrinsically resistant to large scaffold molecules or stressors [21,22]. The last novel antibiotic class effective against Gram-negative bacteria, the quinolones, was introduced into the market more than 55 years ago [22,23]. Unfortunately, very few novel antibiotics designed to combat Gram-negative bacteria and biofilms are currently in the clinical and preclinical research pipelines [11,24]. The discovery of penicillin by Alexander Fleming almost a century ago initiated the 'antibiotic golden era, with the subsequent development of several novel classes of antibiotics (summarized in **Figure 2**) [2,3]. Unfortunately, the discovery of novel classes of antibiotics stalled in the 1980s [16]. Over the past 40 years, only a limited number of newly discovered antibiotic classes have been identified and approved by the Food and Drug Administration [11]. New types of antimicrobial agents available in the market are either based on the modification or optimization of known scaffolds/leads for the treatment of infectious diseases [25]. The development of novel drug-leads to approved drugs on the market is both costly and time-consuming, often spanning several years of extensive research and clinical trials [11,12]. In addition, pharmaceutical companies have been focusing on non-antimicrobial drug discovery, mostly due to economic benefits [16].

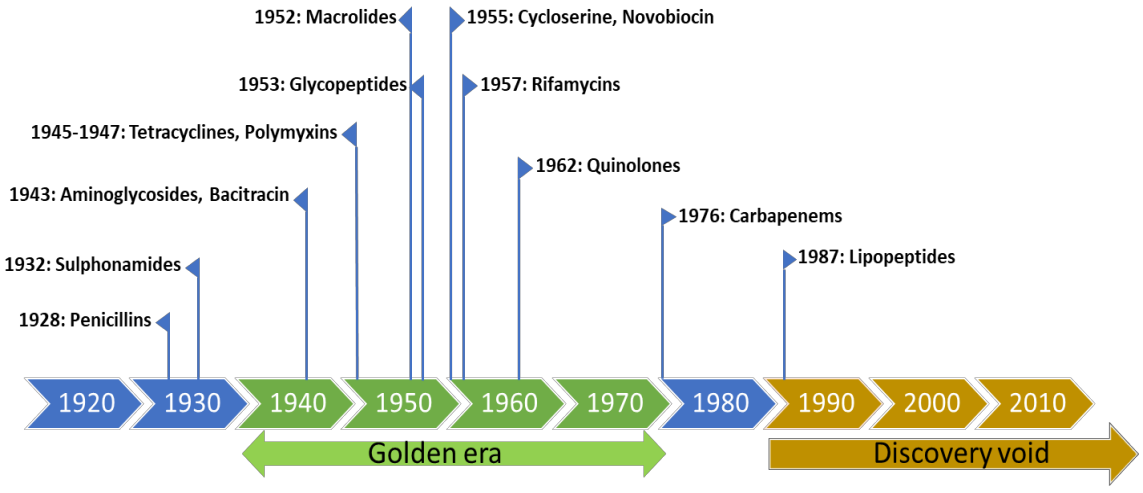

***Figure 2**. Timeline showing the decade when most new antibiotic classes were discovered, followed by discovery void. Based on Silver et al. (2012) [26].*

Considering these issues, alternatives to antibiotics in the market are urgently needed. This urgent demand for new antimicrobials with distinctive unique structures and novel modes-of-action (MoA) is compelling scientists to revisit the exploration of natural product [11]. However, one group of natural

products, antimicrobial peptides (AMPs), is still short of living up to the expectations. As small bioactive molecules, they are increasingly attracting interest due to their seeming abundance in all domains of life and diverse mechanisms of action [27,28]. Utilizing AMPs derived from nature as templates for the development of new synthetic derivatives with improved antimicrobial activity and selectivity represents one of the innovative strategies in drug development [29]. AMPs with antimicrobial, antibiofilm and sensitizing/synergistic potential to restore old antibiotics could contribute to tackle AMR.

1.2 Antimicrobial peptides (AMPs)

As part of our innate immunity, AMPs have been with us to protect us and our ancestors against microbial diseases throughout evolution. AMPs are short polypeptides composed of 10-50 amino acids that are active against a wide range of microorganisms, including bacteria, viruses, fungi, and parasites [30,31]. More than 3500 AMPs have been discovered from various natural sources, including prokaryotes, insects, amphibians, mammals, plants, and invertebrates. [32,33]. They have also been isolated and characterized from marine invertebrates, including sponges, mollusks, crustaceans, and tunicates (**Table 1**). AMPs are structurally diverse and predominantly cationic with a preference for permeabilizing microbial membranes [27]. The expression of natural host defense peptides primarily increases when adapting to microbial challenges in a changing environment [27,34,35]. However, our current understanding of the coevolution of microbial communities and the biological environment that contributes to the emergence of a wide range of AMPs with multifunctionality remains limited [27,35]. Although AMP research started in the early 1920s during the pre-antibiotic era when Alexander Fleming discovered lysozyme (1922) [31], most research has been discontinued due to toxicity and hemolytic activity of the isolated and purified AMPs [27]. Therefore, the marine environment is providing a useful resource for the discovery of novel scaffolds which can be utilized as templates for designing new peptide-based antibiotics with broad-spectrum antimicrobial activities and low toxicities [36].

1.2.1 Biosynthesis

Nature elegantly utilizes the available peptide space by ribosomally and non-ribosomally synthesizing diverse groups of peptides with different amino-acid signatures and structures [27]. Most AMPs in eukaryotes are synthesized using the conventional way of ribosomal protein synthesis as translation products from mRNA templates (ribosomally synthesized AMPs) followed by post-translational modifications [37]. In prokaryotes, a common type of ribosomally synthesized AMPs are the bacteriocins, that provide the host bacteria with a competitive advantage over other microorganisms present in the surroundings [27]. However, some peptide-based antibiotics, such as the glycopeptide vancomycin and lipopeptide daptomycin, are products of non-ribosomal peptide synthetases (NRPs), in a process involving multiple enzymes [35,37]. AMP expression can be constitutive or inducible in response to microbial virulence, metabolites, or other external stimuli [25,38,39]. Their constitutive expression has been observed for example in the lymphocytes and epithelial tissues in mammals.

***Table 1**. Natural antimicrobial peptides from various sources.*

Peptide name	Source	Structure	Activity	References
	Mammals			
Defensin: hBD1	Human monocytes	β-sheet	Antibacterial	[40]
Cathelicidin: LL-37	Human granulocytes	α-helical	Antibacterial	[41]
Lactoferricin	Human	Mixed/distorted antiparallel β-sheet	Antibacterial, anti-inflammatory	[42]
Histatin	Human saliva	Extended/flexible	Antifungal	[43]
Protegrin 1	Pig leukocytes	β-hairpin, cystine-cystine	Antibacterial	[44]
	Insects			
Cecropin: CecA	*Hyalophora cecropia* (moth)	α-helical	Antibacterial, antifungal	[45]
Melittin	Honeybee venom	α-helical	Antibacterial, anti-inflammatory	[46]
	Amphibians			
Buforin II	Toad	α-helical	Antibacterial and non-membranolytic	[47]
Magainins, Temporins	Frog skin	α-helical	Anticancer, antibacterial (Gram-positive)	[48]
	Marine invertebrates			
Aurelin	*Aurelia aurita,* (jellyfish)	Defensin like, cystine-rich	Antibacterial	[49]
Arasin 1	*Hyas araneus* (spider crab)	Proline-rich	Antibacterial and non-membranolytic	[50]
Centrocin 1	*Strongylocentrotus droebachiensis* (green sea urchin)	α-helical	Antibacterial	[51]
Dicynthaurin	*Halocynthia aurantium* (sea squirt)	α-helical, homodimeric	Antibacterial	[52]
	Bacteria			
Nisin	*Lactococcus lactis*	Polycyclic	Antibacterial	[53]
Gramicidin	*Bacillus brevis*	Polycationic and cyclic	Antibacterial	[54]
Polymyxin	*Paenibacillus polymyxa*	Polycationic and cyclic	Antibacterial (Gram-negative)	[55]

1.2.2 Characteristics

AMPs are classified into several categories based on their amino acid composition, size, charge, structure, mechanism, and source. Most natural AMPs are cationic and possess a net charge of +2 to +9 [56]. Anionic AMPs are less frequent and contain 5-70 amino acids, and have a net charge of -1 to -8 [57]. Cationic AMPs often contain arginine, proline, tryptophan, phenylalanine, glycine, and cysteine [33]. Their secondary structures are commonly used to classify AMPs as α-helical, β-sheet, a mixture of αβ, or non-αβ random coils, as illustrated in **Figure 3**. AMPs remain unstructured or exhibit a random coil structure in solution; however, upon interaction with bacterial membranes, they undergo conformational changes [27,58-60].

Cecropins and magainins have been extensively studied as α-helical peptides with antimicrobial activities [39]. Common human cationic AMPs with helical structures and β-strands belong to the cathelicidin and α-defensin families, respectively, while members of the β-defensin family contain both a helical structure and β-strands [39,61]. Similar to human defensins, plant and insect defensins are cysteine-rich and are characterized by a β-sheet conformation with several disulfide bonds [62]. An example of a non-αβ extended structure is the proline-rich peptide indolicidin [63].

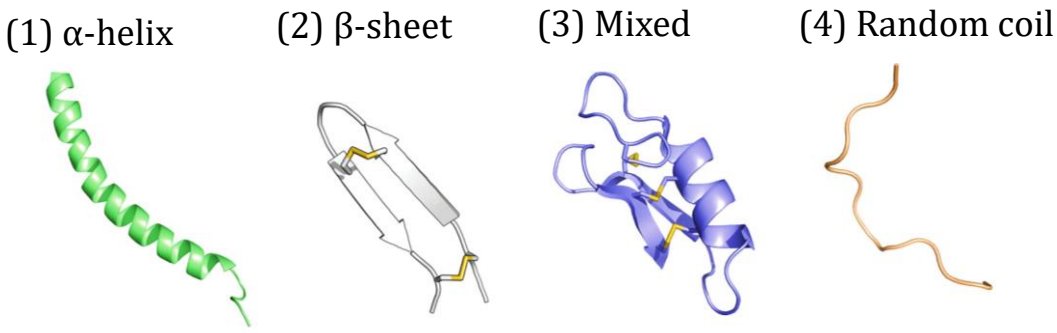

***Figure 3**. Representative common secondary structures of (1) LL-37 containing α-helix, (2) tachyplesin I containing β-hairpin, (3) plectasin containing a combined α-helix and β-sheet, and (4) indolicidin-containing random coil. Adapted with permission from Amiss et al. (2022) [64].*

Despite classification based on different folding patterns, the amphipathic secondary structure of AMPs is primarily determined by their cationic properties and hydrophobicity [39,65]. However, optimal functionality requires a balanced net positive charge and hydrophobicity, as an excess of either can lead to undesirable outcomes such as poor selectivity and antimicrobial activity. For example, excessive hydrophobicity may prompt peptide self-association or aggregation. On the other hand, peptide self-assembly has also been shown to result in antimicrobial activity [27]. Achieving an appropriate cationicity to hydrophobicity ratio is crucial for enhanced activity.

1.2.3 AMP modifications for therapeutic efficacy

Despite extensive studies and promising *in vitro* results, the impact of AMPs on human medicine beyond topical application has been limited [66]. Owing to their inherent susceptibility to proteolysis and low stability, the development of natural AMPs into therapeutics is challenging [30]. These drawbacks can be compensated by modifications in synthetic cationic peptides, which remain active and stable under physiological conditions [67]. Small synthetic peptides could make the synthesis less

time-consuming and more cost-effective [68-71]. Natural AMPs are commonly used as templates to modulate their native structures. Several strategies have been applied to modify and develop novel peptide sequences. For example, peptide truncation, amino acid replacement, and alanine scanning are common ways to distinguish the antimicrobial motif from the original larger peptide [70,71]. Besides, several structural parameters, such as sequence, length, cationicity, and amphipathic potential, are within the scope of understanding the structure-activity landscape. In addition, *C*-terminal amidation [72], *N*-terminal acylation, and cyclization have also been applied to stabilize amphipathic helices against protease attacks. Structural modifications have been shown to improve antibacterial properties and reduce problems related to drug resistance, proteolytic instability, biofilms, and non-growing persister cells [73]. Moreover, any minor changes can result in a unique novel peptide with novel mechanisms, where tuning with both hydrophobic and hydrophilic amino acids influences the amphipathic balance and net charge associated with antimicrobial properties [68].

Furthermore, studying synthetic mimics of antimicrobial peptides (SMAMPs) that structurally and functionally mimic natural AMPs allows us to understand the physicochemical activity relationship of AMPs [74,75]. Therefore, the rational design of novel SMAMPs with improved activity and toxicity, as well as novel modes of action, is gaining interest.

1.2.4 Bacterial resistance against AMPs

As previously mentioned, bacteria use different mechanisms to confer AMR depending on several classes of antibiotics (14, 15). AMPs were falsely assumed not to be prone to bacterial resistance development [76,77]. However, recent studies have demonstrated that bacteria can also withstand AMP action, emphasizing the importance of considering bacterial resistance in AMP research [78]. Virulence genes associated with acquired and intrinsic resistance to AMPs are evident in microorganisms. Various mechanisms by which bacteria resist the action of AMPs include degradation by extracellular and intracellular proteases, exclusion by efflux pumps, alteration of surface charge and cytoplasmic membrane, sequestration/trapping, and biofilm formation [78]. The most common resistance mechanisms to AMPs in both Gram-positive and Gram-negative bacteria are summarized in **Figure 4**. Some examples of the important mechanisms and fate of AMPs are discussed below.

The degradation of AMPs by bacterial enzymes, specifically proteases, is a defense strategy that bacteria follow in the fight against AMPs. Gram-positive staphylococci, streptococci, and enterococci secrete various proteases, including the metalloproteases aureolysin and SepA, cysteine protease SpeB, and other serine proteases [79]. Due to their broad substrate range, SpeB and SepA are known to inactivate many host defense peptides, including LL-37 and an anionic AMP constitutively expressed in the human sweat gland called dermcidin [80,81]. SpeB not only degrades LL-37 but also indirectly inactivates human α-defensin HNP-1 by releasing a degradation product of proteoglycan dermatan sulfate, which binds α-defensin HNP-1 [82]. It is important to note that inactivation of AMPs by proteases is highly dependent on the sequence and structure of the target peptide [77,83]. The omptin family proteases in Gram-negative bacteria, such as OmpT in *Escherichia coli*, PgtE in *Salmonella enterica* serovar Typhimurium (*S.* Typhimurium), and Pla in *Yersinia pestis*, have been demonstrated to cleave AMPs, including LL-37, the homologous murine cathelicidin-related antimicrobial peptide (CRAMP), and protamine [77,84]. Another important contributor to bacterial resistance to antimicrobials and toxic molecules is multi-drug transporters or efflux pumps. Multidrug transporters

are bacterial integral membrane proteins that provide protection by transporting harmful substances to the outside environment once they enter cells [85]. This type of mechanism is responsible for intrinsic and acquired resistance induced by exposure to toxic agents that leads to the overexpression of transporters [86]. Although the expression of the resistance-nodulation-cell division (RND) family transporter AcrAB-TolC in *E. coli* and MexAB in *P. aeruginosa* did not evoke resistance against AMPs [87], efflux pumps in other bacterial strains associated with resistance mechanisms showed decreased susceptibility to AMPs. For example, AcrAB-TolC efflux pumps in *Klebsiella pneumoniae* and VexAB-TolC in *Vibrio cholerae* have been shown to confer resistance to defensins and polymyxin B, respectively [88,89], whereas MtrCDE from *Neisseria gonorrhoeae* and *N. meningitis* confer resistance to LL-37 and protegrin-1 [77,88-91].

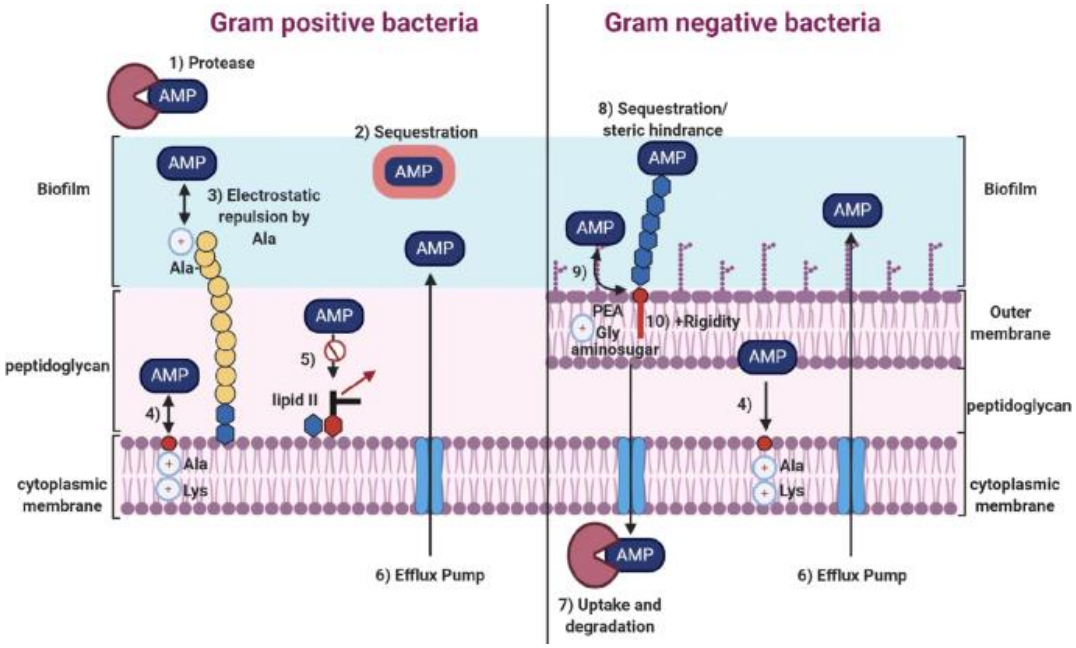

***Figure 4**. Common resistance mechanisms to AMPs in Gram-positive and Gram-negative bacteria. Reproduced with permission by Springer Nature from Cardoso et al. (2021) [78].*

However, the evolution of AMP resistance is driven by other factors, such as the mutation supply rate, fitness of the resistant mutant at different AMP concentrations, and strength of selective pressure (16). These factors are related to the fact that clinically relevant microbial strains associated with complicated infections are more prone to developing AMP resistance [92]. To confer selective pressure for resistance development against membrane-active AMPs, bacteria need fundamental changes in the membrane structure, and the window of selection is much narrower for membrane-active AMPs than for conventional antibiotics [34].

Nature also provides ways to evade proteolytic degradation of certain classes of AMPs. For instance, certain bacteriocins/lantibiotics contain multiple disulfide bonds or complicated post-translational modifications, highlighting the multifaceted evolutionary dynamics between AMP producers and resistant microorganisms [83,93]. To overcome resistance caused by proteolysis, scientists have experimented with replacing natural L-amino acids with all D-amino acids that retain their antimicrobial potency [94]. The replacement of L-amino acids with D enantiomers at the enzyme

recognition site, as well as employing β-amino acids as their primary constituents, can alter the activity, specificity, and proteolytic stability of AMPs [95-97].

1.3 Mechanism of action of AMPs

A significant aspect of AMP research is the early identification of its mechanisms of action in essential pathways. The mechanisms of action of AMPs have been extensively studied using *in vitro* model membranes that provide information on peptide self-assembly and accumulation, pore formation, and leakage of intracellular components and ions. Selectivity and specificity towards bacterial membranes are important for the application of AMPs as therapeutics; however, nonspecific membrane interactions sometimes reflect their broad-spectrum bactericidal mechanisms [98,99]. The diverse composition of the hydrophobic and hydrophilic amino acids in the peptide sequence is also the underlying basis for nonspecific physical charge–charge interactions.

1.3.1 Membrane selective activity

The selective and specific interaction of AMPs with bacterial membranes is largely attributed to their dynamic behavior and the structural disparities between prokaryotic and eukaryotic membranes. Understanding membrane biology is important, as the complex structure of the microbial cell envelope affects the AMP entry strategy [100]. The bacterial and fungal cell envelope is the primary barrier against external threats as it maintains shape and stability, molecular signaling, and selective cell permeability [59,100]. The structures of different cell envelopes are shown in **Figure 5**. Gram-positive, and Gram-negative bacteria differ significantly in their cell envelope. The envelope of Gram-positive bacterial cells consists of an outermost layer of a thick peptidoglycan cell wall that is rich in the acidic polysaccharide lipoteichoic acid (LTA) and a plasma membrane (PM) that is rich in negatively charged phospholipids [101]. In the cell envelope of Gram-negative bacteria, a thin peptidoglycan layer is located between the PM and the outer membrane (OM), also known as the periplasmic space [59]. The outer leaflet of Gram-negative bacterial OM contains lipopolysaccharides (LPS), which consist of hydrophobic and negatively charged lipid A, connected to O-antigen polysaccharides through an oligosaccharide core [102]. The stability of LPS in the OM is maintained by bridging with divalent cations such as Mg^{2+} and Ca^{2+}. The structural composition of the fungal cell envelope is unique as well. Its cell wall components, characterized by glucan, chitin and mannoprotein provide a resilient barrier. Additionally, the fungal PM is more rigid than the bacterial membrane due to the presence of zwitterionic phospholipids and ergosterol, although the presence of phosphatidylinositol, phosphatidylserine (PS), and diphosphatidylglycerol provides negative charges to the surface of the membranes. In addition to their interaction with the negatively charged membrane, AMPs can inhibit functional cell wall components to exert antifungal activity [59]. Unlike bacterial membranes, mammalian cell membranes contain asymmetric phospholipid distributions. The presence of zwitterionic phosphatidylcholine (PC), together with sphingomyelin phospholipids in the outer leaflet, and negatively charged PS in the inner leaflet, makes the surface of the mammalian membrane neutral in charge [59].

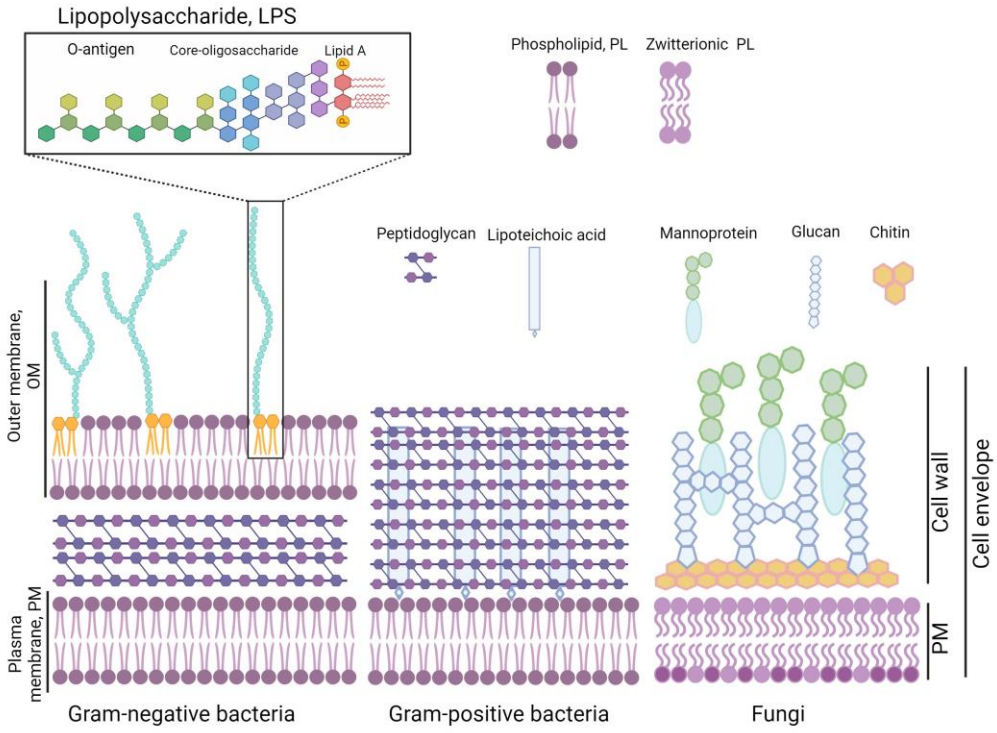

***Figure 5**. Cell envelope structures of various microbial families. Image was created with BioRender.com. Adapted and modified from Malanovic et al. (2016) [59].*

It has been suggested that AMP-mediated surface interaction is the initial step before AMPs can diffuse through nano-sized pores in the peptidoglycan layers (Gram-positives) and translocate or traverse through the OM of Gram negative bacteria by dislocating divalent cations [103]. This indicates that there must be an electrostatic interaction between the anionic bacterial surface and the cationic AMPs. Notably, this interaction is not directly related to their ability to kill bacteria; however, this attachment is usually employed by AMPs to interact with other targets, for example the cytoplasmic membrane [104]. At a critical bactericidal concentration, AMPs act via membrane integration or pore formation [58,60]. As a result, the electrochemical gradient across the membrane collapses and microorganisms tend to lose energy and eventually die [58]. However, at low AMP concentrations, they can change the structural dynamics and stability of bacteria, leading to the emergence of a heterogeneous bacterial population [105]. Several pore-forming models have been suggested as summarized in **Figure 6**; notably the barrel stave model, the carpet model and the toroidal pore model [103]. The barrel stave model describes how perpendicular insertion of AMPs generates channels in the membrane. Here, amphipathic peptides are usually lined up by each other around the outer/aqueous layer of the channel, interacting with both the lipid head groups and the hydrophobic acyl chains. The carpet model explains that the binding of peptides to the surface of the lipid bilayer causes a detergent-like effect that ultimately disintegrates the membrane. The toroidal pore model, on the other hand, proposes that peptides are inserted into the lipid bilayer when part of the pore is lined by (only) lipid headgroups [106]. Peptides can then self-assemble to generate larger pores.

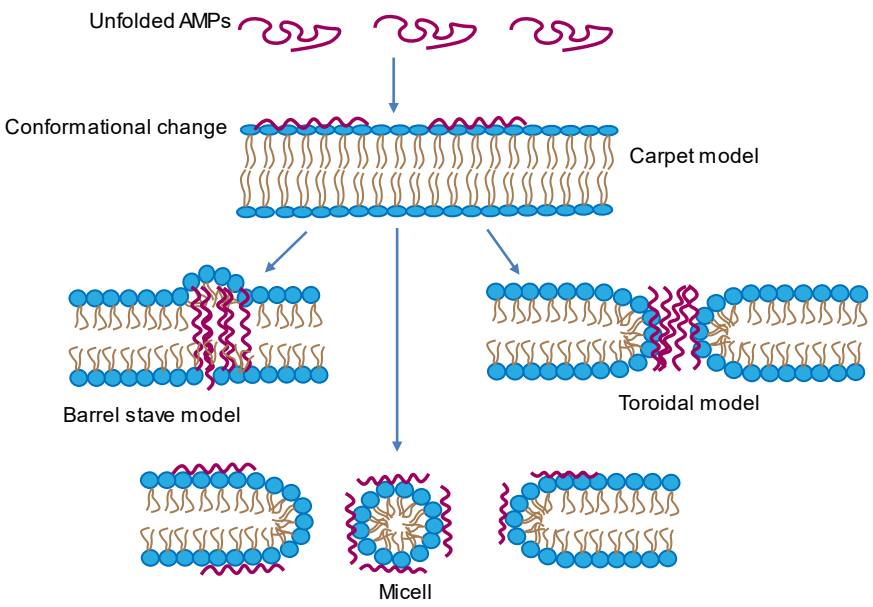

***Figure 6**. Models of the mechanism of AMPs. Once AMPs interact with bacterial cells, they bind to phospholipids on plasma membranes, forming cavities and destroying or permeabilizing the membranes, leading to bacterial cell lysis and death. Adapted and modified from Dijksteel et al. (2021) [66].*

1.3.2 Non-membrane dependent mechanism

Other mechanisms by which AMP works without forming pores have been described in the literature. Although the initial interaction between cationic AMPs and the cytoplasmic membrane could be the first step, several studies have provided evidence that some AMPs possess the ability to cross bacterial cell membranes without forming pores and causing membrane damage and instead interact with intracellular targets such as DNA and RNA [30,104]. This, in turn, can result in disturbances of bacterial metabolic activity by inhibiting protein and cell wall biosynthesis, enzymatic activity, and DNA and RNA synthesis [103]. Bac7 and other proline-rich peptides of the same family, including PR-39, seem to be transported into gram-negative bacteria by a membrane transporter called SbmA. Thus, they do not need to perturb the membrane to enter the cells but can inhibit cell growth by blocking protein synthesis. Omiganan, a derivative of indolicidin and buforin II, was reported to be able to translocate through the membrane without causing any damage and act by crosslinking with DNA [30,59,107]. The lantibiotics nisin and HNP1 have been reported to kill bacteria by targeting lipid II [30,108]. Increased antimicrobial activity has been observed for the D-form AMP KLKLLLLLKLK-NH_2 compared to the L-form, mainly due to its higher affinity for cell wall components [109].

1.4 Approaches to analyze the activity of AMPs

1.4.1 *In vitro* bioactivity studies

A common approach to assess the potency of an antimicrobial agent is to determine its minimum inhibitory concentration (MIC). The MIC is the lowest concentration required to inhibit planktonic bacterial growth. AMPs exhibit bacteriostatic or bactericidal activity depending on the size of the inoculum, their MoA, and their concentration. The inoculum size refers to the number of bacterial cells in the liquid medium incubated with a 2-fold dilution series of the antimicrobial agent. Turbidity or sedimentation represents bacterial growth and is measured after a defined incubation time, often 24

h or the time necessary for the untreated control to reach the stationary phase. Turbidity above 10% of the untreated control is interpreted as growth whereas lack of turbidity in the drug-containing media is interpreted as antimicrobial activity or inhibition. Several other methods are also used, such as agar dilution, disk/agar diffusion, E test, and spot test. The disadvantages of these methods are the need for high concentrations of the compounds, which increases the manufacturing cost. Therefore, these methods are no longer used for high-throughput peptide screening (6). Broth microdilution can also be used to determine the minimum bactericidal concentration (MBC). The bacteria that survived after a defined exposure period can be counted as colony-forming units (CFUs) by plating dilutions of the culture on nutrient agar to determine the MBC, which is defined as the minimum concentration for an antimicrobial agent to kill 99.9% of a bacterial inoculum at a certain time point (6).

Despite being a standardized method, the MIC test has considerable limitations. The MIC value does not represent the effectiveness of new compounds *in vivo*. Most importantly, MoA information cannot be elucidated simply by determining an MIC value [110]. In addition, to gain a more comprehensive understanding of the mechanism(s) involved, various biotechnology approaches can be used to genetically modify bacteria to express a sensitive or resistant phenotype. Including these modified strains together with other representative candidates of pathogenic bacteria in the screening process of novel compounds can help identifying or confirming mechanisms of action. Furthermore, testing of novel compounds against anaerobic bacteria can yield more physiologically relevant data for treatment of infections [111].

1.4.2 Bacterial whole-cell biosensors as tools in AMP optimization

Biosensors are devices that can detect changes in biological systems and translate these changes into measurable signals. They can be used for different applications, such as the detection of pollutants, microorganisms, and disease markers, but also in drug discovery [112]. Biosensors can be based on cell-free systems or on bioengineered self-propagating organisms, often bacteria, called whole-cell biosensors. Whole cell biosensors detect specific biochemical changes in response to known environmental variations experienced by the cell and represent these changes as reporter protein activity [113]. For example, coupling a stress responsive promotor to a luciferase operon will induce bioluminescence in presence of the stressor/analyte. The biosensor response is then measurable and quantifiable as light emission by electronic devices such as photodiodes or photomultiplier tubes in microplate readers. The main advantage of whole-cell biosensors in drug discovery compared to alternative approaches are cost benefits, specificity, throughput, and often close to real-time feedback [113,114]. As described in the previous chapter, AMPs are known to interfere with bacterial membrane integrity and thereby kill the bacteria. When optimizing AMPs by sequence and structure modifications, whole-cell biosensors can help to quantify and evaluate changes in peptide activity more rapidly than biochemical assays and cell-based MIC or MBC assays [114]. Here, three ways of using biosensors as tools in studying mechanisms of action of AMPs are described in the following.

A) Visualizing the killing kinetics of AMPs

AMPs with strong membrane activity often kill bacteria rapidly, with most of the bacteria dead in a matter of minutes [115]. It is difficult to record such rapid killing kinetics with classical growth-based assays relying on optical density or viable cell count alone, as the response time is a matter of hours at best, rather than minutes. Other assays are hampered by the necessity of adding viability responsive

fluorophores or dyes for visualization of bactericidal effects, which add cost and complexity to the assay, while the response time does not necessarily improve.

A rapid and cost-effective assay of cell viability is achieved by employing bacterial whole-cell biosensors constitutively expressing a *lux* operon with light emission as a proxy of cell viability [113,116]. The *lux* operon encodes the bacterial luciferase subunits (*luxAB*) and a multienzyme fatty acid reductase (*luxCDE*) involved in recycling long-chain fatty aldehydes, which are the substrate. While the light-emitting reaction itself depends on long-chain fatty aldehydes, $FMNH_2$, and oxygen, the regeneration of the substrate by the fatty acid reductase complex requires NADPH and ATP, thus integrating important indicators of active metabolism in the intensity of light emission [117,118]. *Lux* operons can be expressed in both Gram-positive and Gram-negative bacteria (**Figure 7**). Although not specific for membrane activity, these biosensors can be used to record the rapid killing kinetics of bacterial populations with a resolution of a few seconds, if necessary, where loss of light emission resembles loss of viability. Thus, bacterial luciferase-based biosensors can be used to evaluate the changes in activity of AMP derivatives.

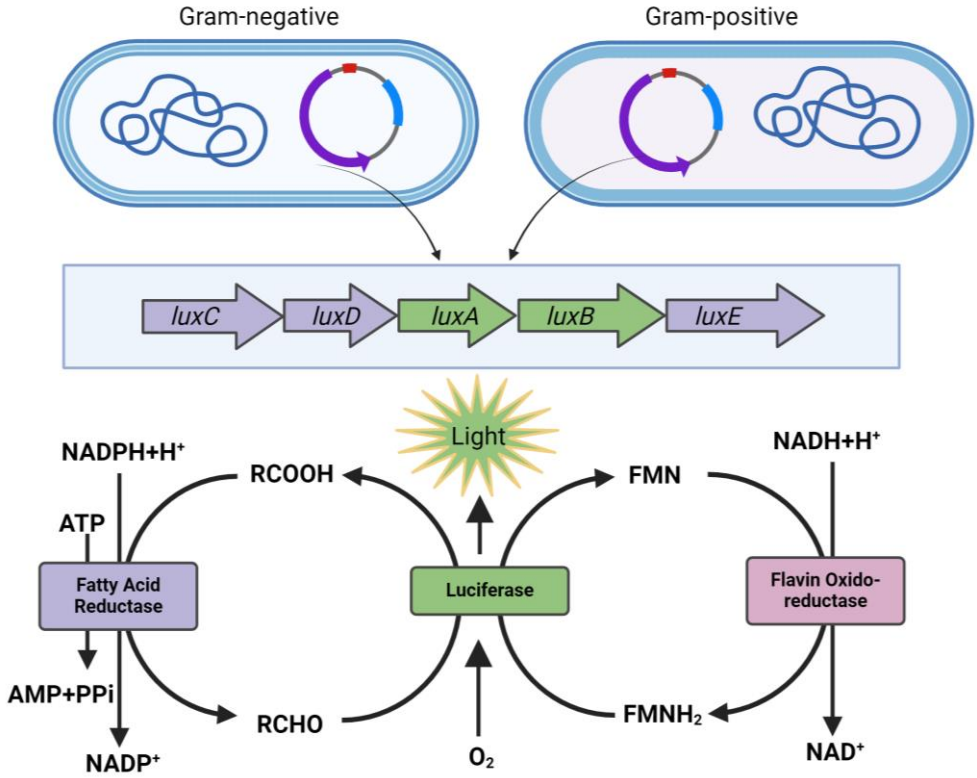

***Figure 7**. The lux operon consists of genes encoding proteins to produce luminescence (LuxCDABE) and the enzymatic process to regenerate the substrate pool. Image was created with BioRender.com. Adapted from Miyashiro et al. [118] (modified).*

B) Measuring the loss of plasma membrane integrity

One major function of the PM is its selective separation of the cytoplasm from the outside environment, preventing the free diffusion of charged and/or large molecules. This membrane feature

can be an obstacle when trying to use reporter genes dependent on externally added ligands or substrates to measure promoter activity. An increase in permeability of the PM for substrates on the other hand, can be used as an indicator of loss of membrane integrity. The same principle is also used for membrane integrity assays based on fluorophores, resulting in cell fluorescence only when the plasma membrane is damaged.

Eukaryotic luciferases depend on substrates called luciferins. For luminescence to occur in recombinant bacteria expressing these luciferases, only the ATP required for the light reaction is provided by the cell, while luciferins must be added externally. At neutral pH, the bacterial plasma membrane is mostly impermeable to the D-luciferin substrate of the click-beetle luciferase *lucGR* [119]. Thus, light emission of constitutively expressed *lucGR* is primarily dependent on membrane permeabilization. However, as the plasma membrane loses its integrity and allows for diffusion of D-luciferin, bacteria immediately lose their primary source of ATP, as respiration is essentially short-circuited, with protons and hydroxide freely diffusing through the compromised membrane. Meanwhile existing ATP is either diffusing from the cell or hydrolyzed by the action of the luciferase and other metabolic processes. Consequently, strongly membranolytic compounds will induce a peak of light emission followed by a drop in luminescence below the background luminescence of the sensor bacteria (summarized in **Figure 8**). Although more complex than the previously described viability biosensor, this membrane integrity biosensor links rapid bactericidal activity to the membrane as the primary target and can be used to evaluate the kinetics of membrane permeabilization caused by AMPs [115,116,120].

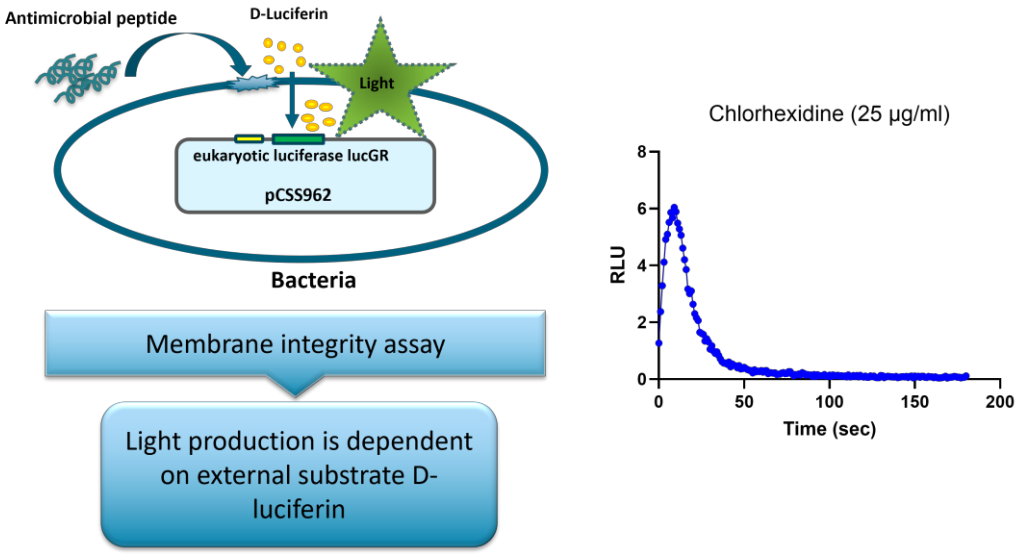

***Figure 8**. Overview of the membrane integrity assay. The light emission of lucGR is dependent on membrane permeabilization and diffusion of the substrate D-luciferin.*

C) Mode of action specific biosensors based on promotor-reporter gene fusions

The co-evolution of microorganisms and their biochemical warfare has resulted in intricate regulatory responses to stress caused by antimicrobial molecules. Some of these responses are rather specific for the modes of action and are already induced at sub-MIC concentrations. They can therefore be used to categorize unknown antimicrobial molecules according to the stress they cause and hence their mode

of action [114]. The easiest and most cost-effective way to interrogate the activity of a set of known promoters in a bacterial strain is to construct a panel of biosensors, which each can be used on an unlimited number of molecules to identify if they induce its specific stress response. To construct such biosensors, reporter genes, for example the previously mentioned bacterial *lux* operon, can be fused to the specific stress responsive promoters, which must be known through for example transcriptomic studies [114,121,122]. Thus, promoter induction is reported as light emission by the bacterial biosensor strains harboring these fusions. To assay for all available modes of action an AMP must be tested against all the sensor strains in the panel. In contrast to the previously described sensor constructs for viability and membrane integrity, stress responsive promoter based biosensing elements cannot easily be transferred between bacterial genera as the underlying regulatory networks and promoter sequences are not necessarily conserved [122,123].

1.4.3 Synergistic potential

A eukaryotic organism produces a wide variety of natural AMPs, however, not all peptides have the same activity and specificity to combat an infection. AMPs with different mechanisms of action and structural diversity induce varying defense strategies in bacteria and thus contribute to diverse sensitivity profiles [28]. Antimicrobials in nature are the result of billions of years of co-evolution, and it is surprising that they are still effective despite simultaneous bacterial adaptations to survive these natural defenses [124]. It is rational to accept that there is a trade-off between different antibiotic resistance mechanisms where the presence of a resistance mechanism to one antibiotic can increase the sensitivity to another [124,125]. Therefore, induced collateral sensitivity and low tendency to develop cross-resistance between AMPs with different mechanism of actions, explain partly how the combination of several different AMPs are adopted by immune systems [124]. For example, the amphibian peptide magainin-2 and PGLa are reported to act synergistically to inhibit *E. coli* growth. They exert stronger antimicrobial activity by binding to each other to form a "supramolecular complex" [126,127]. The molecular mechanism of membrane disintegration depends on both membrane composition and the AMP structure, therefore, the synergism between two AMPs might also be a consequence of a stable pore formation through heterodimerization [126-128]. Moreover, increased collateral sensitivity in resistant populations through changes in OM integrity provides knowledge about AMP-antibiotic combinations, which enhance antimicrobial activity [129]. At the same time, several publications report AMPs facilitating the delivery of antibiotics to their targets in the periplasm or cytoplasm by disrupting bacterial membranes [125,128,130,131].

To supplement and increase the therapeutic potential against multi-resistant pathogens, synergistic interaction between AMPs and conventional antibiotics are providing advantages for adjunctive strategies [131]. This is exemplified in **Figure 9**, where AMP based OM disruption facilitates the access of antibiotics usually only active in Gram-positive bacteria. In Gram-negative bacteria, the asymmetric OM is a permeability barrier, protecting the bacteria from toxic materials. Therefore, targeting the OM by AMPs and resensitizing Gram-negative bacteria to existing antibiotics is an effective approach to reverse AMR phenotypes [125,130].

Extensive research has been conducted in the field of combination therapy, specifically in investigating the effectiveness of various membrane targeting compounds to enhance the entry of intracellularly targeted compounds. This inquiry has been ongoing for a considerable period, resulting in an abundance of research data available. Nonetheless, there is still a vast amount of knowledge yet

to be acquired to fully comprehend the fundamental biology leading bacterial responses to a novel membrane active substance, as well as its interactions with other molecules [102].

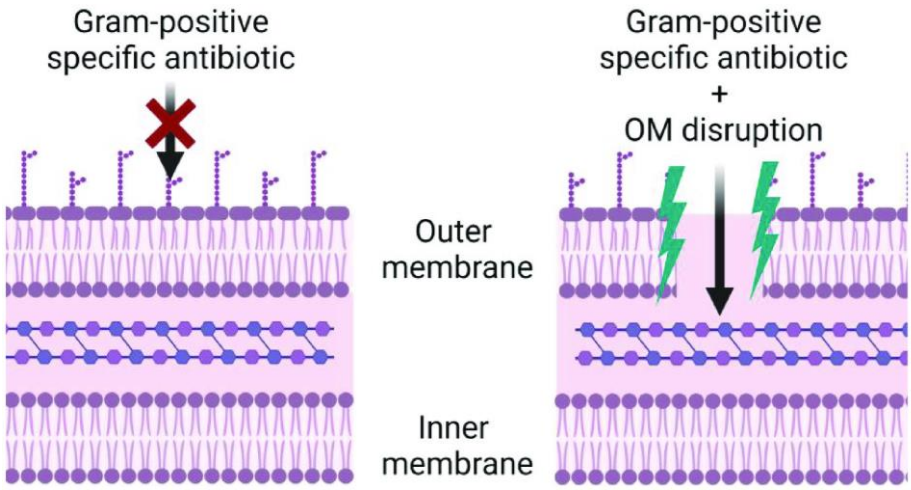

***Figure 9**. Outer membrane disruption facilitates the entry of antibiotics and restore the sensitivity against Gram-negative bacteria. Adapted with permission from Wesseling et al. (2022) [132]*

1.4.4 Antibiofilm activity

Bacteria protect themselves from toxic molecules with different physical barriers such as cell envelope, biofilm production, and efflux mechanisms that render many antibiotics ineffective. Most studies on antimicrobial activity are traditionally conducted with planktonic bacteria, however the predominant lifestyles of bacteria in their natural environment are in biofilms. Interestingly, the biofilm lifestyle also prevails among pathogens infecting bodies of host organisms. Biofilms are commonly surface associated aggregates surrounded by cell secreted extracellular polymeric substances (EPS), consisting of polysaccharides, lipids, proteins, DNA, ions, etc [7,17,18], however, free floating biofilms such as pellicles have also been described [133]. Biofilm associated infections are challenging to treat because the bacteria in the biofilm can often withstand high concentrations of antimicrobial agents [134]. An inherent problem with traditional antibiotics is their dependence on active cell metabolism and growth. Cells in the biofilm are not only protected by the EPS but are often dormant and therefore less susceptible to traditional antibiotic treatment [19,135]. The structure of LPS and biofilm EPS has structural similarities in Gram-negative bacteria. EPS protects bacteria by creating a physical barrier that hinders larger molecules to diffuse and penetrate as well as provide a microenvironment that is disadvantageous to their activity [17]. It was previously reported that sub-inhibitory concentrations of antibiotics, including polymyxin B, stimulate biofilm formation. To compensate for cell envelope stress, the transition from a planktonic to a biofilm lifestyle may be a strategy applied by bacteria [22].

AMPs might hold significant promise to be developed into antibiofilm agents as they are able to attack non-growing heterogenous bacterial populations in biofilms e.g. through PM disruption. PM disruption will kill both actively metabolizing and dormant cells. AMPs can also induce bacterial twitching motility and downregulate various genes involved in biofilm formation [136]. Several potential ways for use of AMPs against biofilm associated infections are illustrated in **Figure 10**. The

peptides could be used to inhibit biofilm formation in the first place. Here the ideal mode of action would not be to kill potential biofilm formers, but to manipulate them not to settle and form biofilm (**Figure 10A**). AMPs could be used to kill bacteria in already present biofilms and clear already formed biofilms (**Figure 10B**). Therefore, it is important to investigate the effects of novel antimicrobial compounds on biofilms.

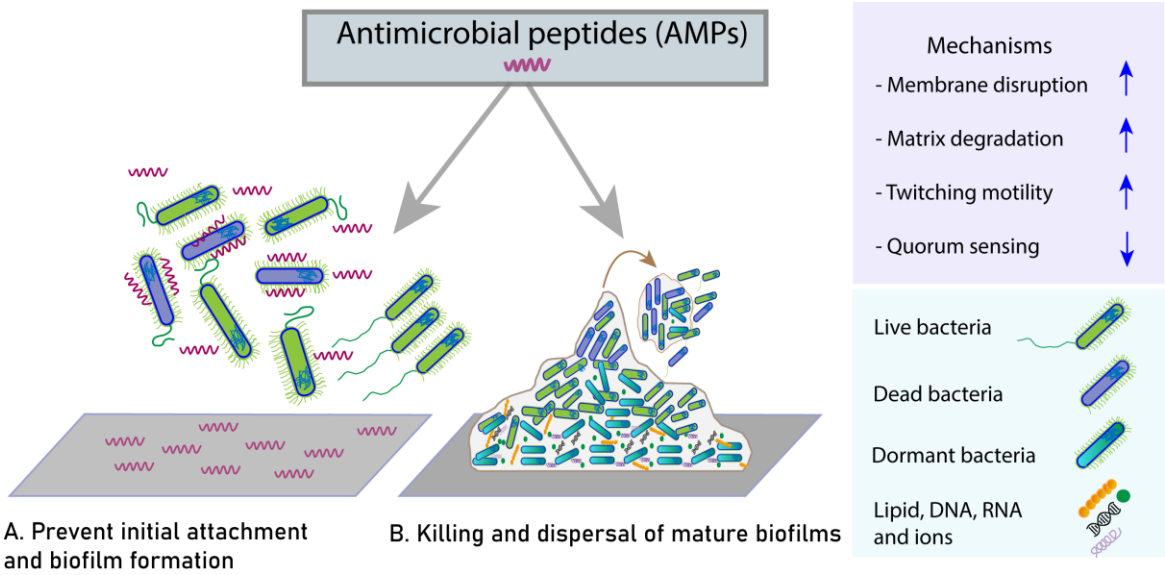

***Figure 10**. Schematic diagram of anti-biofilm activity and mechanism of action of antimicrobial peptides (AMPs). AMPs effect mainly involve A. prevention of initial bacterial attachment and inhibition of biofilm formation or B. disruption of pre-formed/mature biofilms. Activation (upward arrow), Inhibition (downward arrow). Based on Yasir et al. (2018) and Vishwakarma et. Al (2021) [136,137]*

2 Aims of the thesis

The project partners have identified amphipathic synthetic peptide analogues derived from marine origin as a class of antimicrobials that exhibit potent antimicrobial activity against both Gram-positive and Gram-negative bacteria. The structural design of these compounds is inspired by linear amphipathic AMPs and other peptide-like marine natural products. The main objectives of this PhD project include:

1. Determination of the activity spectrum, structure activity relationship (SAR) and selectivity (antimicrobial *versus* hemolytic activities) of novel synthetic marine peptide analogues, screened against a panel of Gram-positive and Gram-negative bacteria.

2. Determination of activity and stability of synthetic marine peptide analogues against endoprotease OmpT-producers.

3. Perform MoA studies on promising derivatives using a panel of MoA specific Gram-negative and Gram-positive bacterial biosensors, together with traditional assays, like killing experiments and membrane permeability assays.

4. Determination of antibiofilm activity against different Gram-positive and Gram-negative biofilm forming bacterial strains.

5. Determination of potential synergies, and adjuvant effects of novel synthetic analogues in combination with commercially available antibiotics.

3 Summary of papers

Paper I - Synthesis and antimicrobial activity of short analogues of the marine antimicrobial peptide Turgencin A: Effects of SAR optimisations, Cys-Cys cyclisation and lipopeptide modifications.

Hymonti Dey[#], Danijela Simonovic[#], Ingrid Norberg-Schulz Hagen, Terje Vasskog, Elizabeth G. Aarag Fredheim, Hans-Matti Blencke, Trude Anderssen, Morten B. Strøm, and Tor Haug

([#]shared first authorship)

In this study, a cationic loop region of Turgencin A, consisting of 12 amino acids, encompassing two intramolecular cystine residues forming a disulphide bond were explored. The sequence was selected for designing and synthesizing a series of modified peptides for structure-activity-relationship (SAR) and MoA studies. The reason for choosing these modifications is to focus on several key attributes such as cationicity, hydrophobicity and cyclization to improve the antimicrobial effects and to increase the selectivity and stability of the synthetic analogues (**Figure 11A**). In this regard, the effects of lysine to arginine substitution, proline/glycine to tryptophan substitution, cystine-cystine cyclisation and *N*-terminal acylation using octanoic acid (C_8), decanoic acid (C_{10}) or dodecanoic acid (C_{12}) were investigated (**Figure 11B**). *C*-terminal amidation was performed for all the peptides. Substitution of lysine with arginine, generated potent analogues with improved activity against both Gram-positive and Gram-negative bacteria in comparison with the lysine-containing analogues. The highest antimicrobial activity was, however, achieved for the cyclic lipopeptides C_{12}-cTurg-1 and C_8-cTurg-2 indicating the importance of acylation and cyclization for improving activity and stability. Mode of action studies confirmed that these lipopeptides are bactericidal with rapid membranolytic properties against Gram-positive bacteria (**Figure 11C**). However, a delayed effect on the *E. coli* membrane was observed. Analysis using an *E. coli* mutant with impaired outer membrane indicate that the outer membrane is no barrier for the arginine-modified peptides but has some protective effect for the other peptides tested. The presence of an outer membrane seems to render Gram-negative bacteria less susceptible to these peptides.

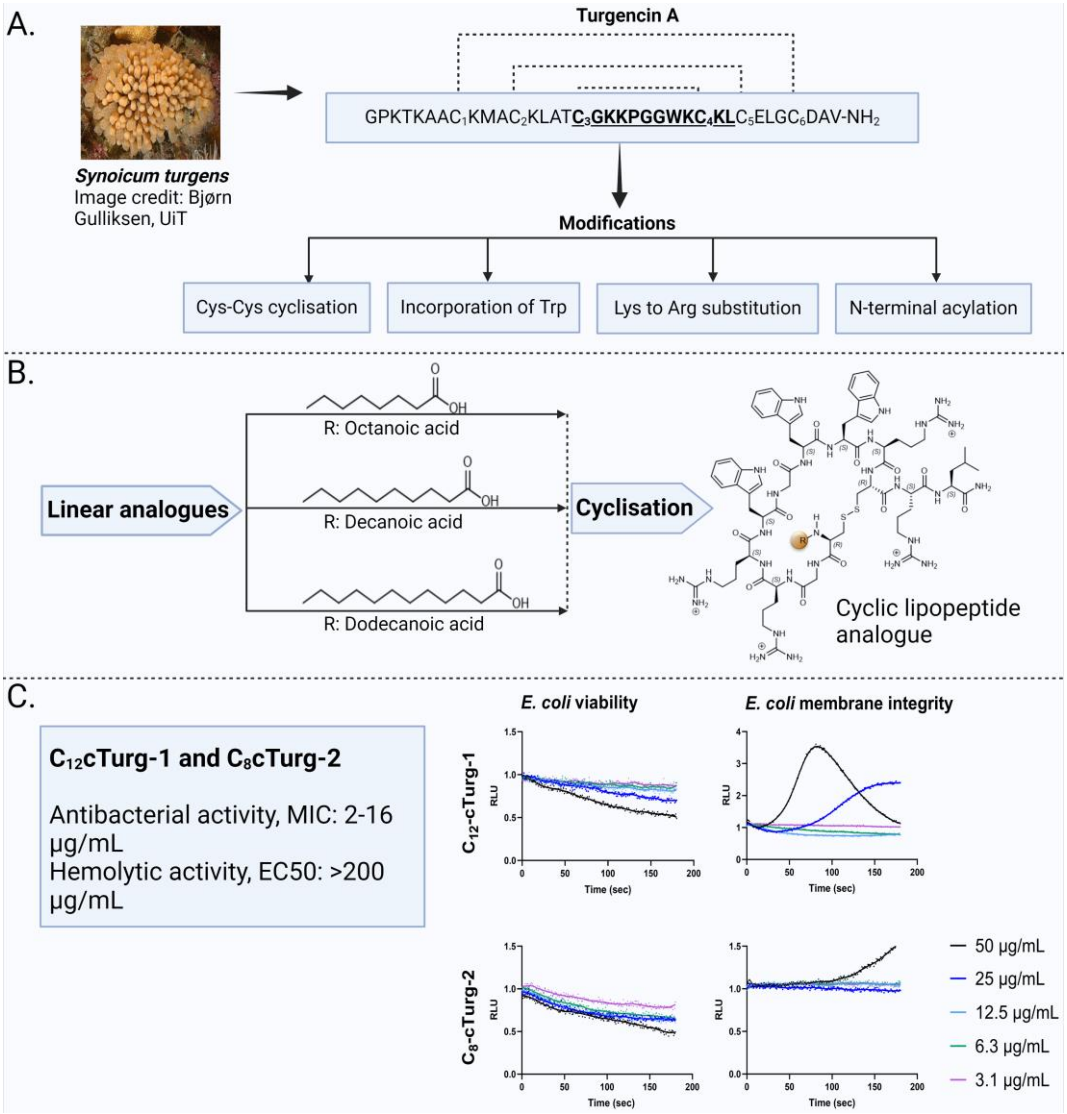

***Figure 11**. Overview of optimization strategies for SAR and MoA investigation (Paper I).*

Paper II – Antimicrobial activity of short analogues of the marine peptide EeCentrocin 1: Synthesis of lipopeptides and head-to-tail cyclic peptides and mechanism of action studies

Danijela Simonovic[#], Hymonti Dey[#], Natascha Johansen, Trude Anderssen, Ida K. Ø. Hansen, Hege Devold, Terje Vasskog, Hans-Matti Blencke, Frode Øyen, Elizabeth G. Aarag Fredheim, Tor Haug, Morten B. Strøm

([#]shared first authorship)

A heterodimeric marine antimicrobial peptide EeCentrocin 1 was previously isolated from red sea urchin *Echinus esculentus*. In this study, the modified lead peptide P6, derived from the *N*-terminal segment of the heavy chain (HC) of EeCentrocin 1 was selected for synthesizing a series of 12-residue analogues with the following modifications: amino-acid substitutions (introduction of tryptophan, lysine or arginine), *N*-terminal acylation and head-to-tail cyclisation (**Figure 12**). The antibacterial, antifungal and the haemolytic activity against human red blood cells were evaluated and SAR analyses were conducted. Initial screening results indicate that substitution of alanine to lysine/arginine, and threonine to tryptophan increases the potency and membrane activity of the lead peptide P6. Extensive MoA studies of the two most potent analogues, the linear peptide, P6-W6R8 and its head-to-tail cyclic counterpart cP6-W6R8 revealed a cell wall/membrane targeting profile. At the same time, the activity and proteolytic stability of these peptides was investigated when exposed to different *E. coli* strains with/without expressing the outer membrane protease OmpT. The results indicate that the OmpT protease degrades both peptides, but the degradation has only a minor effect on their antibacterial activity.

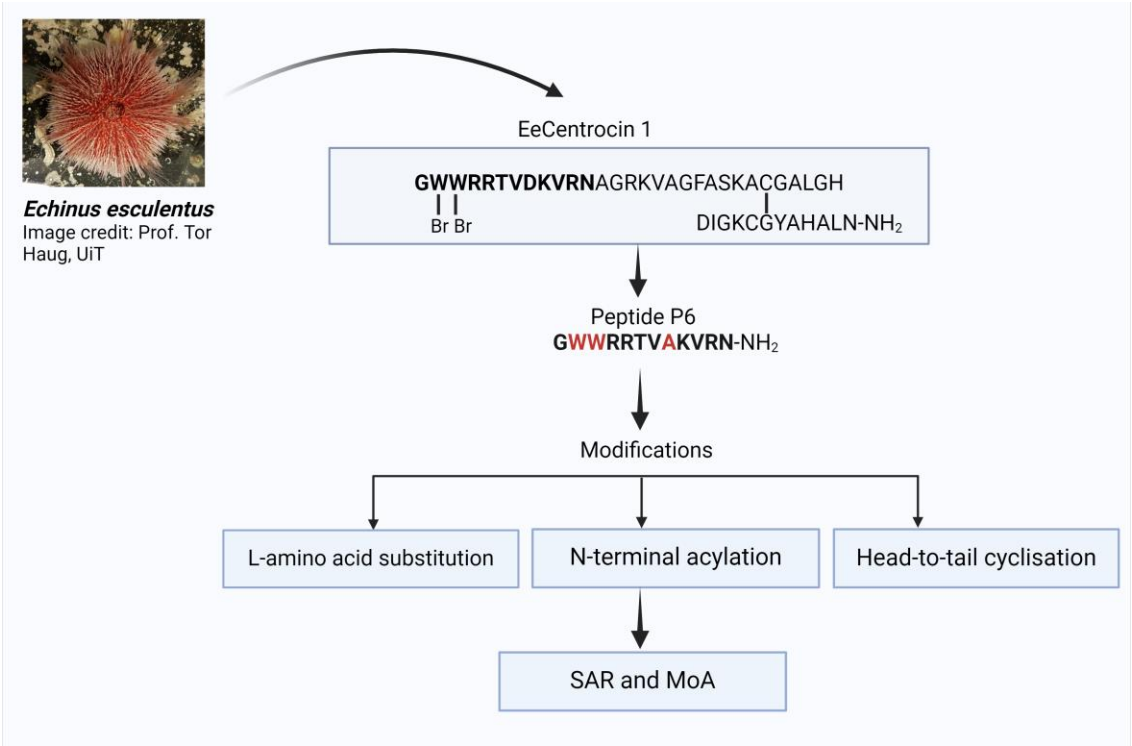

***Figure 12**. Overview of optimization strategies for SAR and MoA investigation (Paper II).*

Paper III - Outer Membrane Integrity-Dependent Fluorescence of the Japanese Eel UnaG Protein in Live *Escherichia coli* Cells

Céline S. M. Richard, Hymonti Dey, Frode Øyen, Munazza Maqsood and Hans-Matti Blencke

The bilirubin-dependent fluorescent protein UnaG from the Japanese eel (*Anguilla japonica*) was utilized to develop a novel biosensor based on live *E. coli* cells. Using the *E. coli* wild-type strain MC4100 and its isogenic OM-deficient mutant strain NR698, the outer membrane related MoA of several OM-active compounds and two different synthetic analogues of marine antimicrobial peptide Turgencin A were evaluated. Fluorescence signals emitted from both UnaG-billirubin based assay and an established assay using the hydrophobic probe 1-*N*-phenylnaphthylamine (NPN) were compared in response to the OM-integrity of MC4100 cells in the presence of polymyxin B, polymyxin B nonapeptide (PMBN), chlorhexidine and synthetic Turgencin A analogues cTurg-2 and C_{12}-cTurg-1(**Figure 13**). This study confirmed that the ligand-based fluorescence response is solely dependent on the disruption of OM integrity at low bilirubin (BR) concentrations. High membrane disruptive concentrations of the membranolytic compounds including TurgencinA analogues result in low fluorescence most likely due to loss of viability resulting from plasma membrane disruption and arrested UnaG synthesis.

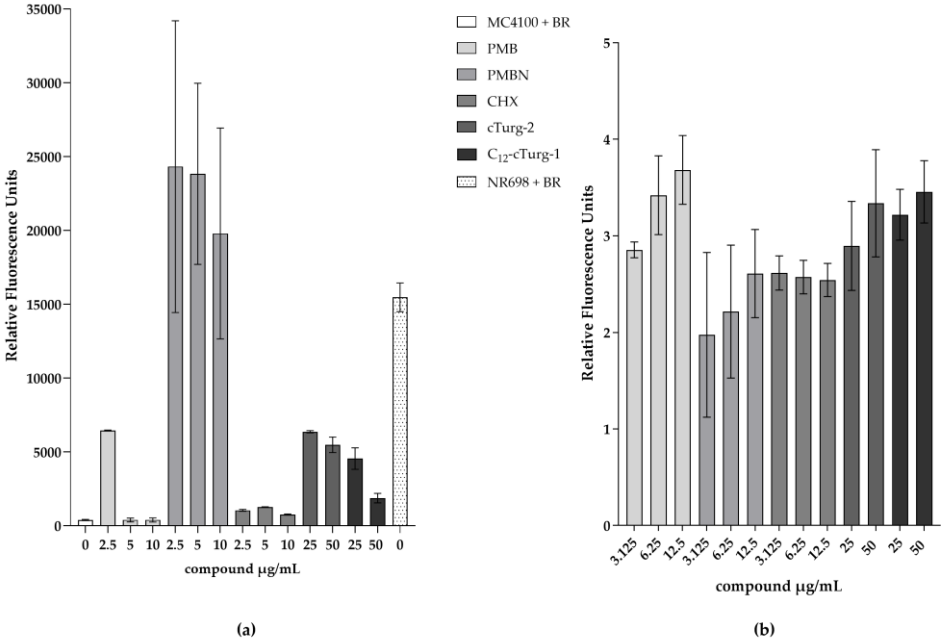

***Figure 13**. Comparison of a) BR dependent relative fluorescence units of the UnaG-based OM integrity biosensor and b) the traditional NPN assay in response to membrane damage.*

Paper IV – Combining outer membrane active synthetic antimicrobial peptides with vancomycin or erythromycin increases antibacterial and antibiofilm activity

Hymonti Dey, Danijela Simonovic, Céline S. M. Richard, Ingrid Norberg-Schulz Hagen, Natascha Johansen, Frode Øyen, Elizabeth G. Aarag Fredheim, Morten B. Strøm, Roger Simm, Tor Haug, Hans-Matti Blencke

Synthetic derivatives of Turgencin A and EeCentrocin 1 were screened for antimicrobial and antibiofilm activity against three biofilm forming bacterial strains and the Gram-positive facultative anaerobic *Clostridium difficile*. The minimum inhibitory concentrations (MIC) and the antibiofilm effects of the selected peptides were determined using the broth microdilution method and Crystal violet staining assay. Additionally, putative synergy was evaluated by the checkerboard assay, calculating the fractional inhibitory concentration index for each analogue in combination with either erythromycin or vancomycin. According to our results, only the lipopeptide analogues C_{12}-cTurg-1 and C_8-cTurg-2 showed activity against *C. difficile*. In combination studies with erythromycin or vancomycin, synergistic interaction was most frequently observed in *E. coli* for the OM active analogues whereas no synergy was observed in Gram-positive bacteria. In antibiofilm assays, linear and cyclic derivatives (P6-W6R8, cP6-W6R8, C_{12}-cTurg-1 and C_8-cTurg-2) showed stronger effects on the early stages of biofilm development, although significant biofilm inhibition was generally not observed below 0.5x MIC. Moreover, Synergistic combinations effectively inhibited biofilm formation of both *S.* Typhimurium UMR1 and *P. aeruginosa* PA01. These findings support previous research regarding outer membrane specific synergism of AMPs which potentiate ineffective antibiotics by facilitating target access. The data from our study provide knowledge about the antimicrobial and antibiofilm activity of several derivatives that can serve as a template for studying the application of AMPs for potential synergism and biofilm inhibition.

4 Discussion

The PhD project is a part of the multi-faculty and interdisciplinary research project *Lead-to-drug development of amphipathic scaffolds targeting multi-resistant bacteria – LEADScAMR*.

Identification of new antimicrobial hit-molecules is inspired by the abundance of unique and diverse groups of bioactive metabolites or host defense peptides found in a variety of species. However, to go from hit molecules to lead compounds, it is a great advantage to study compounds that possess "bioactive motifs" which can be used for lead validation and optimization for future development into potential drug candidates. Based on the prerequisite optimization strategies, this work focused on the biological perspective as supported by initial bioactivity screening and SAR-studies of synthetic truncated versions of Turgencin A and EeCentrocin 1 as lead peptides. The antimicrobial efficacy, hemolytic activity and MoA studies of several amino acid substituted versions of cyclic, and cyclic lipopeptide derivatives with different *N*-terminal fatty acid linkages and their corresponding linear counterparts are discussed in **paper I-IV**.

4.1 Peptide modifications to improve antimicrobial activity and selectivity

In the face of the lead optimization process, it is important to monitor if the new compound class is active. Due to the unique physical and chemical properties of AMPs, various optimization strategies can be applied to enhance the desired performance for their therapeutic application [138].

4.1.1 Effects of amino acid replacement

Previous studies have demonstrated that amphipathic properties, due to the presence of both hydrophobic and cationic residues, are important for the antimicrobial effect of small cationic AMPs [139]. The presence of cationic amino acids provides the electrostatic interaction between AMPs and the anionic microbial membrane surface. Therefore, the incorporation of positively charged amino acids Lys and Arg, are a common strategy to improve the cationicity of AMPs and their selectivity for microbial membranes [140]. Although the human cathelicidin peptide with its primary sequence of 37 amino acid residues possesses *in vitro* antimicrobial activity, a truncated C-terminal region of this peptide has been used as a template to produce many other variants with antimicrobial activity [141-143]. For example, synthesis of several potent analogues through random substitution as well as specific amino acid replacement showed efficacy against Gram-positive and Gram-negative multidrug-resistant pathogens, biofilm-producers and persister cells.

In our study, incorporation of tryptophan in place of proline and/or glycine residues in the core PGG sequence of cTurg-1, resulted in cyclic peptides with improved antimicrobial activity against both Gram-positive and Gram-negative bacteria **(Paper I)**. However, in the modified peptides, cTurg-2 – cTurg-4, the positioning of tryptophan residues in the core sequence did not have a major impact on the antimicrobial potency. These tryptophan -derivatives showed similar activities against clinically relevant Gram-positive and Gram-negative strains, including *S. aureus*, *E. coli* and *P. aeruginosa* although the activities against Gram-negatives were poor. When we utilized an OM deficient *E. coli*

strain (NR698), it was confirmed that the presence of the OM in the wild-type strains limits the activity of these lysine- and tryptophan-containing derivatives. However, substitution of lysine with arginine residues in cTurg-5 – cTurg-7 improved the activity against Gram-negative bacteria. Increased antimicrobial activity by changing the lysine residues to arginine is consistent with previous studies implying the influence of the guanidine groups in arginine being responsible for stronger membrane interaction and permeabilization [144]. In paper II, similar effects were observed for EeCentrocin 1 analogues when both charge and amphipathicity were increased. The resulting α-helical linear peptides P6-R8, P6-W6K8 and P6-W6R8 with lysine/arginine and tryptophan substitutions showed improved activity against *S. aureus* and *E. coli* compared to the parent peptide P6. All the above-mentioned synthetic peptides, derived from both Turgencin A and EeCentrocin 1, were non-hemolytic. Therefore, stepwise replacement with hydrophobic tryptophan and cationic arginine residues provided us with fundamental insights into the basic rules governing the activity of the short AMP sequences.

4.1.2 Effects of cyclization and acylation

Different forms of cyclization are common in natural AMPs, such as head-to-tail-cyclization, disulphide bond formation, or internal linkage between side chains [141,145]. Cyclic peptides, such as defensins, commonly occur in mammals, plants, and insects, and highlight the importance of cyclization for antimicrobial activity and stability. Other AMPs, isolated from bacteria, also known as bacteriocins contain a charged complex cyclic structure, for example, gramicidin S, polymyxin B, and bactenecin [146]. The synthesis of cyclic bonds sometimes complicates the development process of synthetic AMPs. However, cyclic AMPs have been shown to have considerable advantages over linear peptides in terms of the stability of the peptides due to the presence of conformational rigidity and proteolytic stability [138]. In recent studies, cyclic analogues have been shown to have improved stability and reduced hemolytic profile compared to their parent peptides isolated from horseshoe crabs [147]. Mwangi et al.; [148] also found that the cystine-cystine link is correlated with its stability *in vitro* and *in vivo*, resistance to proteolysis and increased antimicrobial activity against MDR pathogens.

In our studies, both cystine-cystine side-chain cyclization and head-to-tail cyclization have been applied (**Paper I** and **Paper II**). For Turgencin A analogues, cystine-cystine cyclization gave rise to slightly increased antimicrobial activity which might be due to the structural stabilization compared to those of their linear counterparts. Also, head-to-tail cyclization of the highly potent linear analogue P6-W6R8 resulted in the cyclic derivative cP6-W6R8 with comparative antimicrobial activity. Although all the peptides in this series were non-hemolytic, slightly lower antimicrobial activity of the cyclic derivatives might be due to the formation of different secondary structures or decrease in overall net positive charge.

Like the optimization effects of cyclization, acylation is another way of increasing hydrophobicity and creating a stable secondary structure formation of peptides and to increase their degree of insertion into the bacterial membranes. Several lipopeptide antibiotics isolated from Gram-positive and Gram-negative bacteria, with varying fatty acid composition and conjugated to cyclic/linear oligo peptides, have been extensively studied [149,150]. Most studies demonstrated that *N*-terminal lipidation with different carbon chain lengths is correlated with both increased antimicrobial activity and cell selectivity due to the fact that increased hydrophobicity increases their membrane interaction and

insertion [151]. For example, the *N*-terminal acyl chain in polymyxin B is known to be involved in Gram-negative membrane interaction and bactericidal activity, whereas removal of the lipid tail resulted in an inactive derivative (polymyxin B nonapeptide) with only OM activity [58,152]. However, it is recognized that increased hydrophobicity of the α-helical structure of a lipopeptide is proportional to its increased hemolytic activity [153-155]. Moreover, lipopeptides with longer acyl chains tend to form aggregation and self-assembly, which may lead to a decrease in their activity [155]. In **paper I,** C_8-, C_{10}-, or C_{12}- carbon acyl chains in both linear and cyclic peptides (cTurg-1, cTurg-2 and cTurg-6) were investigated. *N*-terminal acylation and cystine-cystine cyclization of the inactive lead peptide cTurg-1 and Lys substituted analogue cTurg-2 resulted in two highly potent broad-spectrum lipopeptides, C_{12}-cTurg-1 and C_8-cTurg-2, with MIC values of 2-4 μg/mL against *S. aureus* and *E. coli*. It is worth noting that the linear Turg-1 and the cyclic cTurg-1 with lower intrinsic hydrophobicity showed increased antimicrobial activity with increased length of the acyl chain whereas C_{10} and C_{12} acylation did not further improve the antimicrobial activity of the tryptophan containing analogues Turg-2/cTurg-2 and Turg-6/cTurg-6. Besides, acylation influenced their selectivity with the highest hemolytic activity for the C_{12} conjugated analogues. In **paper II**, the introduction of C_8-, C_{10}-, or C_{12}- acyl chains in the arginine-modified peptide P6-R8 generated acylated analogues C_8-P6-R8, C_{10}-P6-R8 and C_{12}-P6-R8 with no major changes in antimicrobial activity. However, the hemolytic activity was gradually increased for the acylated lipopeptides C_{10}-P6-R8 and C_{12}-P6-R8. Overall, our data support previous research that intrinsic hydrophobicity of the parent peptide is an important determinant to achieve the optimal hydrophobic or amphipathic nature required for improved activity with elongated hydrocarbon chain.

4.2 Disruption of bacterial membranes and the effects on viability

4.2.1 Membrane disruptive activity

The bactericidal activity of AMPs against both Gram-negative and Gram-positive bacteria is based on their ability to accumulate or partition near the cytosolic interface to interact with anionic phospholipid head groups and fatty acyl chains in the PM [59,156-158]. An interplay between the AMP structure and concentration, as well as the composition of the microbial membrane, influences their effect on membrane integrity [59,106,159]. It is important to mention that the ratio between peptides and lipids represents a crucial aspect that impacts the interaction between AMPs and cell membranes [104,160]. Furthermore, depending on the variable affinity for the membrane, not all AMPs show the same level of permeation. Partial membrane permeation by AMPs is sometimes enough to critically affect bacterial growth and metabolism [161,162]. There is evidence that cationic amino acid arginine plays a vital role for the initial binding of AMPs to the bacterial membranes, while the presence of hydrophobic amino acid tryptophan mainly facilitates membrane internalization and ultimately perturbation [59,68,106]. It was previously demonstrated that a cyclic magainin 2 analogue is less membrane active than its linear counterpart, indicating that linear AMPs can reach the cytoplasmic membrane faster, while the cyclic peptide may have less flexibility making it difficult to cross several barriers to reach its target [163]. In **Paper I** & **Paper II**, the effects of amino acid substitution, acylation, and cyclization of Turgencin A and EeCentrocin 1 analogues on OM and PM activity were investigated. Optimization of the peptide structure resulted in several variants with variable membrane permeabilizing abilities against the Gram-positive and Gram-negative biosensor strains. A strong and

immediate membranolytic effect of modified and active analogues was observed against the Gram-positive *B. subtilis* compared to the Gram-negative *E. coli*. For some analogues this delayed effect was attributed to the barrier function of the cell envelope in *E. coli*. Furthermore, differences in the rate of both OM and PM disruption were observed across varying test concentrations, with higher concentrations leading to more rapid lysis demonstrating a concentration-dependent effect. Using MoA specific biosensors, we wanted to investigate the secondary and hidden activities of the analogues and possibly confirm the membrane activity through adequate stress response. As it was described in the introduction, these biosensors can detect several MoA-specific stressors, resulting in increased light output indicative of cellular stress reported through each promoter-lux-operon fusion such as P_{liaI} responds to cell envelope and membrane damage by cationic AMPs, P_{yorB} to inhibition of DNA replication, P_{yvgS} to transcription inhibition, P_{yheI} to translation inhibition and P_{fabHB} to inhibition of fatty acid synthesis [121,123]. Of the five sensors used in this study, only the biosensor with the P_{liaI} fusion responded positively to peptide addition, indicating membrane damage caused by P6, P6-W6R8, and cP6-W6R8.

However, there was a delayed response compared to the vancomycin and bacitracin antibiotic control which coincided with the growth of the bacterial population that survived after the first attack of the peptide. This late effect suggests that membrane-active compounds may interfere with the detection of secondary activities, potentially leading to false negatives, if the induction range surpasses the minimal concentration required for membrane activity. Although primary mechanism of action of the active analogues analysed in this study appears to be the disruption of membrane integrity, we still cannot rule out the possibility that linear and cyclic analogues might have additional targets.

4.2.2 UnaG as a suitable sensor for outer membrane damage

In Gram-negative bacteria, membrane-active cationic AMPs first permeabilize the OM before interfering with the PM or other intracellular targets [162]. Analyses of OM activity using the hydrophobic probe 1-*N*-phenylnapthylamine (NPN), which is normally excluded by Gram-negative OM, gave us the idea of the immediate effects on OM permeability in the presence of peptides in a concentration-dependent manner [164]. In our studies, the active analogues also influenced the kinetics and achievement of steady-state levels, suggesting their initial interaction and disorientation of the OM before they reached the PM. However, this assay fails to distinguish between the molecules, which solely exert their effects on OM permeability from the other active membrane disruptive analogues. Therefore, a better model for identifying the OM barrier function was needed. During initial trials of using UnaG as a reporter gene (**Paper III**), little or no fluorescence was observed at bilirubin (BR) concentrations around 5 μM. Due to the relatively high molecular weight of BR, we hypothesized that OM might be responsible for the lack of fluorescence by excluding BR from accessing the cells. The interesting aspect of using this UnaG assay is the sustained stability for a duration of several hours, which benefits a potential utilization of the system in experiments involving live *E. coli* cells (**Figure 14**). This allows for continuous monitoring of the integrity of the OM in real-time. When the concentration of membranolytic compounds reaches a threshold that severely impacts the membrane, unlike the NPN assay, there is a noticeable decrease in fluorescence. This decline can be attributed to a loss of viability caused by disruption of the PM, as well as halting of UnaG synthesis.

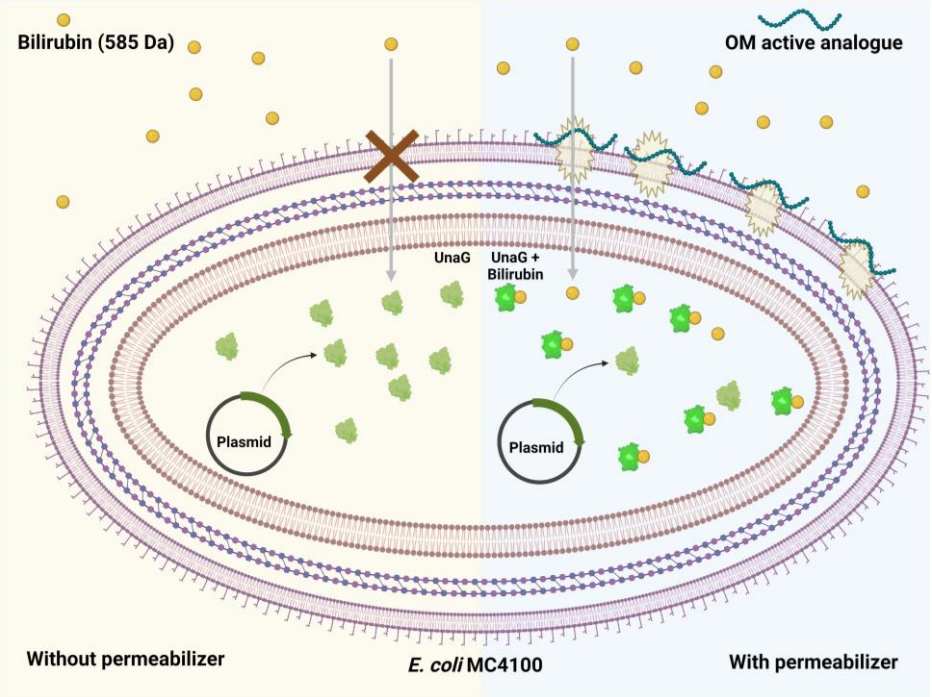

***Figure 14**. Schematic overview of the application of the UnaG-bilirubin whole-cell biosensor as a tool for analyzing OM permeabilization. Created with BioRender.com.*

In **paper IV**, we applied the dual biosensor to decipher their membrane related mechanisms of action of AMPs. This biosensor was based on the constitutive expression of UnaG and LucGR in an artificial operon where fluorescence and luminescence are dependent on the intake of the respective fluorogen/substrate through the compromised OM and PM, respectively. OM integrity sensing depends on the uptake of BR, which acts as a fluorogen of UnaG, whereas PM integrity sensing depends on the uptake of the luciferase substrate D-luciferin. In all our assays, the membranolytic effect of the CHX control was much stronger than that of our peptides. This is because AMPs have a higher molecular weight and are unable to diffuse through porins, whereas CHX, being a broad-spectrum antiseptic with a low molecular weight, can exert the MoA by passive diffusion through the cell wall, rapid binding, and adsorption to the negatively charged plasma membrane [165]. Importantly, our approach to test promising peptides in novel OM-specific biosensors enables us to distinguish between stronger and weaker membrane-disruptive mechanisms of synthetic peptides.

4.2.3 Activity spectrum and effects on viability

Synthetic analogues were screened against a panel of clinically relevant human pathogens and laboratory strains of bacteria and fungi. We found that all tested strains exhibited increased sensitivity to the active modified analogues, suggesting a broad-spectrum antimicrobial effect. While MIC values ranged between 2-16 µg/mL (ca. 1-8 µM) for the most potent analogues, various factors including growth media, inoculum size, and anaerobic growth conditions influenced the activity. In the biosensor-based viability assay, the rate and concentration required for the decrease in viability correlated with the rapid effects on membrane integrity in *B. subtilis*, whereas, in *E. coli* the effect was less pronounced. In this case higher concentration of the peptides (25 - 50 µg/mL) were required to

observe an effect while at lower analogue concentrations, there was no change in light emission. This might be due to the use of a 1000-fold higher bacterial inoculum than that usually used for MIC assays (3×10^4 – 5×10^5 CFU/mL) to detect a reliable signal in both luminescence and fluorescence-based assays. As described in the introduction, the viability assay integrates ATP and reduction equivalents for light production and substrate regeneration while the membrane assay is based on ATP as energy source and externally added D-luciferin. It was observed for some analogues that within the 3 min. measurement window, there was an increase in light production indicating effects on membrane integrity without substantial effects on viability. This might indicate the presence of different subpopulations of bacterial cells, with partial membrane damage or different susceptibility to the analogues, resulting in an average light emission. Therefore, it is important to assess whether the slow decrease in light emission is result of membrane damage.

4.3 Proteolytic degradation of synthetic analogues

In addition to the increased expression of efflux pump or the surface modification of Gram-negative LPS, secretion of proteases is another defense strategy that bacteria employ. Sometimes these proteases influence the activity of several AMPs. Clinically resistant bacteria have been shown to have profound effects on reducing the antimicrobial activity of AMPs [166]. Previous studies reported that chronic ulcers infected with various pathogenic bacteria are the key producers of proteinases that degrade and inactivate LL-37/hCAP18 as well as downregulate the expression of AMPs [166]. Stumpe et al. [167] reported for the first time that the cationic peptide protamine is degraded by OmpT protease. Later, many other publications reported that cationic AMPs including LL-37 and synthetic peptide derivatives containing dibasic amino acids in their primary sequences are substrates for proteolytic degradation by OmpT. The observation of these reports suggested that overexpression of OmpT was sufficient to protect Gram-negative *E. coli* from cationic AMPs. Since OmpT is an extracytoplasmic endoprotease, peptides that are internalized inside the membrane might be safe from degradation [167,168].

In our study (**Paper II**) two selected peptides were tested for relative activity and proteolytic stability against different *E. coli* wild type and mutant strains. In the matrix-assisted laser desorpion/ionization (MALDI-TOF) analyses, no fragmentation was detected in the mutant *E. coli* strain without the expression of OmpT protease, although there was not a significant difference in MICs against the wild type and mutant strains (with or without OmpT protease). Since we only detected the fragments which were the cleavage products between the dibasic residues of the synthetic analogues, these results indicate that degradation of peptides by OmpT protease is a common virulence mechanism in *E. coli* that degrades both natural and synthetic AMPs (**Figure 15**). Furthermore, cyclization was not found to be sufficient to decrease the susceptibility to proteolytic degradation. Analyses of concentration dependent fragmentation pattern was difficult to achieve as there was a large variation in the m/z intensity of peaks between experimental replicates. The reason for using the BL-21 strain with plasmid containing OmpT was that we could control the induction of the expression right before peptide exposure. Continuous expression of OmpT could therefore give rise to fragmentation and inactivation of AMPs even at higher peptide concentrations. However, only a twofold increase in MIC of both the linear and cyclic analogues against this strain compared to the parent strain without OmpT and Lon proteases were observed. This could be due to the low inoculum size used in our experiments (2.5×10^4 CFU/mL), which represents a relatively low proportion of cells that express OmpT in both wild-

type strains as well as the OmpT plasmid-complemented BL-21 strain. This study gave us valuable information on nature's strategy regarding bacterial defence towards various structural constraints of peptide analogues.

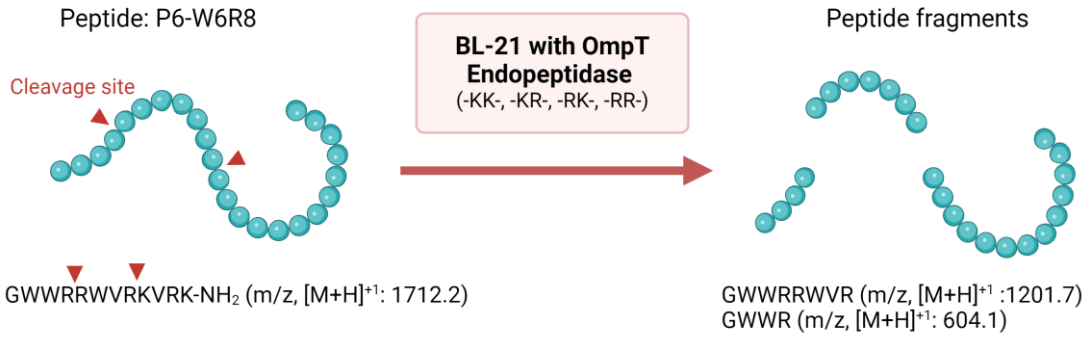

***Figure 15**. Effects of OmpT protease on degradation of the linear P6-W6R8. Image was created with Biorender.com.*

Taking proteolytic degradation into consideration, designing new AMPs could improve their potential as future drugs. Papo et al. showed already more than 2 decades ago that replacement of 35% L-amino acids with D-amino acids in α-helical synthetic AMPs reduces sensitivity to proteolytic degradation [169]. Therefore, utilizing the information of degradation profiles might be beneficial for new drug development strategies including structural modification, development of protease inhibitors or masking specific cleavage sites.

4.4 Enhanced antibacterial and antibiofilm activity

4.4.1 Antibiotic potentiation by outer membrane disruption

The development of antibiotics that are effective against Gram-negative bacteria has lagged due to the structural complexity of Gram-negative bacteria compared to Gram-positive bacteria [170,171]. This lack of progress is attributed to the presence of the OM that limits the entry of toxic compounds, thus renders Gram-negative bacteria intrinsically resistant to many antibiotics and AMPs [170]. The OM functions as a barrier with an exclusion threshold of 500-600 Da, which is close to the size of bilirubin (585 Da) but seemingly big enough to efficiently prevent it from entering the cell [172]. Higher molecular weight antibiotics, such as vancomycin, rifampicin, erythromycin, and novobiocin, are effectively excluded by OM and can therefore not be applied against infections caused by Gram-negative pathogens [22,172,173]. One possibility to circumvent the permeability barrier could be molecules specifically affecting OM integrity, thereby allowing for the free diffusion of higher molecular weight antibiotics to their targets in the periplasm or cytoplasm [22]. Furthermore, beta-lactam antibiotics affecting peptidoglycan synthesis might be potentiated if the resistance is based on drug efflux pumps or beta-lactamases. Drug efflux pumps only work efficiently if there is a diffusion barrier separating the environment from the transpeptidases in the periplasm and thereby allowing to establish an energy dependent gradient across the OM [174]. Loss of integrity will allow free diffusion of the antibiotic to its target and thereby potentiate its activity [172]. In addition, OM disruption might also diminish the effect of beta-lactamases, which are exported to the periplasm to degrade the antibiotics before they can interact with the transpeptidases responsible for crosslinking new

peptidoglycan layers. OM disruption would allow for diffusion of the beta-lactamases from the periplasm and therefore reduce their efficacy [174,175]. Moreover, synergistic interaction between AMPs and other antimicrobials reflects the combined effects that is higher than the sum of the individual effects. A lowered effective dose increases the therapeutic index and thus the risk for toxic side effects. Among the earlier approaches, derivatives of polymyxin and colistin were promising [175]. PMBN is one of the derivatives with strong OM activity that has been used to sensitize Gram-negative bacteria and shown to potentiate other antibiotics. The chelator EDTA (ethylenediaminetetraacetic acid) and the AMPs magainin II, polymyxin B, PMBN, and a recent PMBN derivative SPR74, are all known to bind to OM LPS and trigger permeability changes by displacing divalent cations and destabilizing the LPS layer [15,175]. These membrane targeting peptides were found to act in synergy with various hydrophobic and large molecular weight antibiotics including vancomycin, rifampicin, erythromycin as well as β-lactam antibiotics [125,130,131,175,176]. In **paper IV**, several OM active cyclic and linear derivatives were screened for synergistic interactions with erythromycin and/or vancomycin. As mentioned earlier we thought that these molecules might act synergistically with antibiotics mostly excluded by the OM. Therefore, we tested the synergistic effects of nine synthetic analogues of the marine antimicrobial peptide Turgencin A and two EeCentrocin 1 analogues in combination with either erythromycin or vancomycin and calculated the fractional inhibitory concentration index (FICI). We chose erythromycin and vancomycin although they differ in their mode of action, as they both are excluded by the OM and therefore are mostly active against Gram-positives. The results revealed that the membrane active lipopeptides and both tryptophan and arginine containing peptides lost the synergistic potential (especially with vancomycin) compared to their moderately active but OM disruptive counterparts. This might be due to the modifications that helped the analogues anchor more firmly into the membrane leading to membrane disintegration instead of pore formation.

4.4.2 Antibiofilm activity of synthetic analogues

AMPs of various classes have been reported as antibiofilm agents [177]. Synthetic derivatives based on human cathelicidin LL-37 and smaller designed fragments were among the previously reported AMPs to show antibiofilm properties against *P. aeruginosa* without affecting planktonic growth [178]. Interestingly, the antibiofilm peptide 1018 and its derivatives were later shown to have even stronger effects on biofilm inhibition and eradication that are independent of antibacterial effects against clinical isolates of *P. aeruginosa* from patients with CF [179]. This peptide also displayed potential synergy and synergistic antibiofilm effects with conventional antibiotics [180]. In our study, the synthetic derivatives were investigated for antibiofilm activities to explore if some of the peptides could work as potential biofilm inhibitors, without having a direct killing effect. Here, we screened several potent analogues for activity against the formation of *P. aeruginosa*, *S.* Typhimurium and *Staphylococcus epidermidis* biofilms where the mechanism could be the inhibition of initial attachment and maturation of biofilms (**Paper IV**). The reduction of biofilm biomass observed for analogues with high antimicrobial activity were probably due to combination of bactericidal and antibiofilm activities. One interesting characteristic of the OM active analogues, however, was that some of them did not display any growth inhibition of the planktonic cells but were able to inhibit the biofilm formation at concentrations below their MIC.

5 Conclusions

In this thesis, we have focused on the investigation of the antimicrobial activity and mechanism of action of synthetic derivatives of marine antimicrobial peptides Turgencin A and EeCentrocin 1. In **paper I** and **II**, we have shown that various optimization strategies for example, amino acid substitution, cyclization, and lipopeptide modifications can be applied to enhance the desired performance. Our SAR results are in line with previous research showing that structural modification are useful tools for fine-tuning antimicrobial and hemolytic activity of marine derived peptides. The biosensor-based membrane integrity and viability studies indicated their concentration-dependent rapid effects primarily on the Gram-positive and Gram-negative bacterial membranes. Analyzing the MALDI-Tof fragmentation patterns of the two potent analogues of EeCentrocin 1 helped to identify the cleavage products generated by *E. coli* OmpT protease confirming the stability of the analogues (**Paper II**). The investigation of OM activity of the Turgencin A analogues using a novel *E. coli* biosensor as a tool revealed their in-detail membrane-related mechanisms (**Paper III**). However, interesting derivatives were also found to be effective with their antibiofilm property at the concentrations that did not affect the bacterial growth. Finally, considering the OM related MoA of the synthetic analogues, synergistic interaction with relatively high molecular weight antibiotics (vancomycin and erythromycin) opens their future application as adjuvant against Gram negative pathogens (**paper IV**). This current thesis demonstrates how the mutually beneficial principle of close collaboration between chemistry- and biology-oriented projects can serve as a fundament for effective development of potential alternatives drug candidates with improved antimicrobial and mechanism of action.

6 Perspectives

AMPs are a promising class of bioactive compounds. At the same time, short synthetic mimics of AMPs, derived from a larger lead sequence, can circumvent the labor and cost of synthesizing a complex original peptide to generate a series of peptides for SAR and MoA studies. Furthermore, the synthesis of novel short analogues with significant potency against Gram-negative and Gram-positive bacterial isolates will have a larger drug potential, as the number of potential proteolytic cleavage sites are reduced.

The activity of many natural AMPs is hampered by proteolytic degradation under physiological conditions. Taken knowledge from the peptide's stability and fate in bacterial cultures, we can explore newly designed truncated peptides with D-amino acids instead of L-amino acids. This could further reduce the number of cleavage sites as well as increase selectivity. More comprehensive studies in the future using advanced MALDI-TOF-MS can help to quantitatively determine the amount of cell-bound and internalized peptide analogs to elucidate further molecular mechanisms. Other major applications of AMPs are their immunomodulatory and anticancer properties. The investigation of novel analogues with these potential properties would be beneficial for future peptide-based drug development.

Although this study confirmed the membrane related MoA of promising analogues, exploring the possibility that the peptides can have other secondary mechanisms than membrane disruption could give us a complete picture of their antibacterial mechanisms. As we have utilized the *E. coli* OM-defective mutant NR698 (MC4100 lptD4213) to verify the OM active analogues, it would be interesting to use this strain to test gene expression and morphological changes in biofilm condition and in combination with OM active analogues. Investigating these synthetic analogues at sub-MIC level might illuminate how OM stress can be connected to biofilm formation. A similar effect has been reported for LPS transport protein LptD depletion in combination with colistin, which had an impact on carbohydrate metabolism, motility, and biofilm formation [181].

It would also be of interest to check whether membrane active peptides combined with other antibiotics that are affected by resistance elements such as efflux pump, enzymatic inactivation, or target modification can mitigate the problems associated with AMR. In parallel, a serial passage experiments to test whether OM perturbation can reduce the development of resistance to different high molecular weight antibiotics would provide important knowledge regarding the potential of AMPs as future antibiotics.

7 References

1. Murray, C.J.; Ikuta, K.S.; Sharara, F.; Swetschinski, L.; Aguilar, G.R.; Gray, A.; Han, C.; Bisignano, C.; Rao, P.; Wool, E. Global burden of bacterial antimicrobial resistance in 2019: a systematic analysis. *The Lancet* **2022**, *399*, 629-655, doi:10.1016/S0140-6736(21)02724-0.
2. Lewis, K. The Science of Antibiotic Discovery. *Cell* **2020**, *181*, 29-45, doi:10.1016/j.cell.2020.02.056.
3. Tiwari, P.; Srivastava, Y.; Sharma, A.; Vinayagam, R. Antimicrobial Peptides: The Production of Novel Peptide-Based Therapeutics in Plant Systems. *Life (Basel)* **2023**, *13*, doi:10.3390/life13091875.
4. Adebisi, Y.A.; Ogunkola, I.O. The global antimicrobial resistance response effort must not exclude marginalised populations. *Tropical medicine and health* **2023**, *51*, 33, doi:10.1186/s41182-023-00524-w.
5. O'neill, J. Antimicrobial resistance: tackling a crisis for the health and wealth of nations. *The Review on Antimicrobial Resistance* **2014**.
6. Walesch, S.; Birkelbach, J.; Jézéquel, G.; Haeckl, F.P.J.; Hegemann, J.D.; Hesterkamp, T.; Hirsch, A.K.H.; Hammann, P.; Müller, R. Fighting antibiotic resistance—strategies and (pre)clinical developments to find new antibacterials. *EMBO reports* **2023**, *24*, e56033, doi:10.15252/embr.202256033.
7. Uruén, C.; Chopo-Escuin, G.; Tommassen, J.; Mainar-Jaime, R.C.; Arenas, J. Biofilms as Promoters of Bacterial Antibiotic Resistance and Tolerance. *Antibiotics (Basel)* **2020**, *10*, doi:10.3390/antibiotics10010003.
8. C, S.; G. R, R.; L. F, L.; M.C.G, d.R.; N.B, C.; S.C, D.; O. L, F. Advances and perspectives for antimicrobial peptide and combinatory therapies. *Frontiers in Bioengineering and Biotechnology* **2022**, *10*, doi:10.3389/fbioe.2022.1051456.
9. Durand, G.A.; Raoult, D.; Dubourg, G. Antibiotic discovery: history, methods and perspectives. *International journal of antimicrobial agents* **2019**, *53*, 371-382, doi:10.1016/j.ijantimicag.2018.11.010.
10. Davies, J.; Davies, D. Origins and evolution of antibiotic resistance. *Microbiology and molecular biology reviews* **2010**, *74*, 417-433, doi:10.1128/MMBR.00016-10.
11. Miethke, M.; Pieroni, M.; Weber, T.; Brönstrup, M.; Hammann, P.; Halby, L.; Arimondo, P.B.; Glaser, P.; Aigle, B.; Bode, H.B.; et al. Towards the sustainable discovery and development of new antibiotics. *Nature Reviews Chemistry* **2021**, *5*, 726-749, doi:10.1038/s41570-021-00313-1.
12. Collier, R. Rapidly rising clinical trial costs worry researchers. *Canadian Medical Association journal* **2009**, *180*, 277-278, doi:10.1503/cmaj.082041.
13. Steinbuch, K.B.; Fridman, M. Mechanisms of resistance to membrane-disrupting antibiotics in Gram-positive and Gram-negative bacteria. *RSC Medicinal Chemistry* **2016**, *7*, 86-102, doi:10.1039/C5MD00389J.
14. Munita, J.M.; Arias, C.A. Mechanisms of Antibiotic Resistance. *Microbiology Spectrum* **2016**, *4*, doi:10.1128/microbiolspec.VMBF-0016-2015.
15. Dhanda, G.; Acharya, Y.; Haldar, J. Antibiotic Adjuvants: A Versatile Approach to Combat Antibiotic Resistance. *ACS omega* **2023**, *8*, 10757-10783, doi:10.1021/acsomega.3c00312.
16. Gould, I.M., & Bal, A. M. . New antibiotic agents in the pipeline and how they can help overcome microbial resistance. *Virulence* **2013**, *4*, 185-191, doi:10.4161/viru.22507.
17. Sharma, D.; Misba, L.; Khan, A.U. Antibiotics versus biofilm: an emerging battleground in microbial communities. *Antimicrobial resistance and infection control* **2019**, *8*, 76, doi:10.1186/s13756-019-0533-3.
18. Costerton, J.W.; Stewart, P.S.; Greenberg, E.P. Bacterial biofilms: a common cause of persistent infections. *Science (New York, N.Y.)* **1999**, *284*, 1318-1322, doi:10.1126/science.284.5418.1318.
19. Vestby, L.K.; Grønseth, T.; Simm, R.; Nesse, L.L. Bacterial Biofilm and its Role in the Pathogenesis of Disease. *Antibiotics* **2020**, *9*, 59, doi:10.3390/antibiotics9020059.

20. Panda, S.K.; Buroni, S.; Swain, S.S.; Bonacorsi, A.; da Fonseca Amorim, E.A.; Kulshrestha, M.; da Silva, L.C.N.; Tiwari, V. Recent advances to combat ESKAPE pathogens with special reference to essential oils. *Frontiers in microbiology* **2022**, *13*, 1029098, doi:10.3389/fmicb.2022.1029098.
21. Breijyeh, Z.; Jubeh, B.; Karaman, R. Resistance of Gram-Negative Bacteria to Current Antibacterial Agents and Approaches to Resolve It. *Molecules* **2020**, *25*, 1340, doi:10.3390/molecules25061340.
22. MacNair, C.R.; Brown, E.D. Outer Membrane Disruption Overcomes Intrinsic, Acquired, and Spontaneous Antibiotic Resistance. *mBio* **2020**, *11*, doi:10.1128/mBio.01615-20.
23. Emmerson, A.M.; Jones, A.M. The quinolones: decades of development and use. *Journal of antimicrobial chemotherapy* **2003**, *51 Suppl 1*, 13-20, doi:10.1093/jac/dkg20.
24. Butler, M.S.; Henderson, I.R.; Capon, R.J.; Blaskovich, M.A.T. Antibiotics in the clinical pipeline as of December 2022. *The Journal of Antibiotics* **2023**, *76*, 431-473, doi:10.1038/s41429-023-00629-8.
25. Lei, J.; Sun, L.; Huang, S.; Zhu, C.; Li, P.; He, J.; Mackey, V.; Coy, D.H.; He, Q. The antimicrobial peptides and their potential clinical applications. *American journal of translational research* **2019**, *11*, 3919-3931.
26. Silver, L.L. Challenges of antibacterial discovery. *Clinical microbiology reviews* **2011**, *24*, 71-109, doi:10.1128/CMR.00030-10.
27. Chakraborty, S.; Chatterjee, R.; Chakravortty, D. Evolving and assembling to pierce through: Evolutionary and structural aspects of antimicrobial peptides. *Computational and structural biotechnology journal* **2022**, *20*, 2247-2258, doi:10.1016/j.csbj.2022.05.002.
28. Hollmann, A., Martinez, M., Maturana, P., Semorile, L. C., & Maffia, P. C. . Antimicrobial Peptides: Interaction With Model and Biological Membranes and Synergism With Chemical Antibiotics. *Frontiers in Chemistry* **2018**, *6*, doi:10.3389/fchem.2018.00204.
29. Torres, M.D.T.; de la Fuente-Nunez, C. Reprogramming biological peptides to combat infectious diseases. *Chemical Communications* **2019**, *55*, 15020-15032, doi:10.1039/C9CC07898C.
30. Zhang, Q.-Y.; Yan, Z.-B.; Meng, Y.-M.; Hong, X.-Y.; Shao, G.; Ma, J.-J.; Cheng, X.-R.; Liu, J.; Kang, J.; Fu, C.-Y. Antimicrobial peptides: mechanism of action, activity and clinical potential. *Military Medical Research* **2021**, *8*, 48, doi:10.1186/s40779-021-00343-2.
31. Nakatsuji, T.; Gallo, R.L. Antimicrobial peptides: old molecules with new ideas. *The Journal of investigative dermatology* **2012**, *132*, 887-895, doi:10.1038/jid.2011.387.
32. Zong, X.; Fu, J.; Xu, B.; Wang, Y.; Jin, M. Interplay between gut microbiota and antimicrobial peptides. *Animal Nutrition* **2020**, *6*, 389-396, doi:10.1016/j.aninu.2020.09.002.
33. Singh, N.; Abraham, J. Ribosomally synthesized peptides from natural sources. *The Journal of Antibiotics* **2014**, *67*, 277-289, doi:10.1038/ja.2013.138.
34. Lazzaro, B.P.; Zasloff, M.; Rolff, J. Antimicrobial peptides: Application informed by evolution. *Science* **2020**, *368*, doi:10.1126/science.aau5480.
35. Zasloff, M. Antimicrobial peptides of multicellular organisms. *Nature* **2002**, *415*, 389-395, doi:10.1038/415389a.
36. Ovchinnikova, T.V.; Balandin, S.V.; Aleshina, G.M.; Tagaev, A.A.; Leonova, Y.F.; Krasnodembsky, E.D.; Men'shenin, A.V.; Kokryakov, V.N. Aurelin, a novel antimicrobial peptide from jellyfish Aurelia aurita with structural features of defensins and channel-blocking toxins. *Biochemical and biophysical research communications* **2006**, *348*, 514-523, doi:10.1016/j.bbrc.2006.07.078.
37. Nolan, E.M.; Walsh, C.T. How nature morphs peptide scaffolds into antibiotics. *Chembiochem* **2009**, *10*, 34-53, doi:10.1002/cbic.200800438.
38. Morio, K.A.; Sternowski, R.H.; Brogden, K.A. Induction of Endogenous Antimicrobial Peptides to Prevent or Treat Oral Infection and Inflammation. *Antibiotics (Basel)* **2023**, *12*, doi:10.3390/antibiotics12020361.
39. Hancock, R.E.; Lehrer, R. Cationic peptides: a new source of antibiotics. *Trends in biotechnology* **1998**, *16*, 82-88, doi:10.1016/s0167-7799(97)01156-6.

40. Zhang, G.; Hiraiwa, H.; Yasue, H.; Wu, H.; Ross, C.R.; Troyer, D.; Blecha, F. Cloning and characterization of the gene for a new epithelial beta-defensin. Genomic structure, chromosomal localization, and evidence for its constitutive expression. *The Journal of biological chemistry* **1999**, *274*, 24031-24037, doi:10.1074/jbc.274.34.24031.
41. Sørensen, O.E.; Follin, P.; Johnsen, A.H.; Calafat, J.; Tjabringa, G.S., Hiemstra, P. S., Borregaard, N. Human cathelicidin, hCAP-18, is processed to the antimicrobial peptide LL-37 by extracellular cleavage with proteinase 3. *Blood* **2001**, *97*, 3951-3959, doi:10.1182/blood.v97.12.3951.
42. Hwang, P.M.; Zhou, N.; Shan, X.; Arrowsmith, C.H.; Vogel, H.J. Three-dimensional solution structure of lactoferricin B, an antimicrobial peptide derived from bovine lactoferrin. *Biochemistry* **1998**, *37*, 4288-4298, doi:10.1021/bi972323m.
43. Takahashi, D.; Shukla, S.K.; Prakash, O.; Zhang, G. Structural determinants of host defense peptides for antimicrobial activity and target cell selectivity. *Biochimie* **2010**, *92*, 1236-1241, doi:10.1016/j.biochi.2010.02.023.
44. Zeng, F.; Zhao, C.; Wu, X.; Dong, R.; Li, G.; Zhu, Q.; Zheng, E.; Liu, D.; Yang, J.; Moisyadi, S.; et al. Bacteria-induced expression of the pig-derived protegrin-1 transgene specifically in the respiratory tract of mice enhances resistance to airway bacterial infection. *Scientific Reports* **2020**, *10*, 16020, doi:10.1038/s41598-020-73084-2.
45. Steiner, H.; Hultmark, D.; Engström, A.; Bennich, H.; Boman, H.G. Sequence and specificity of two antibacterial proteins involved in insect immunity. *Nature* **1981**, *292*, 246-248, doi:10.1038/292246a0.
46. Choi, J.H.; Jang, A.Y.; Lin, S.; Lim, S.; Kim, D.; Park, K.; Han, S.M.; Yeo, J.H.; Seo, H.S. Melittin, a honeybee venom-derived antimicrobial peptide, may target methicillin-resistant Staphylococcus aureus. *Molecular medicine reports* **2015**, *12*, 6483-6490, doi:10.3892/mmr.2015.4275.
47. Park, C.B.; Kim, H.S.; Kim, S.C. Mechanism of action of the antimicrobial peptide buforin II: buforin II kills microorganisms by penetrating the cell membrane and inhibiting cellular functions. *Biochemical and biophysical research communications* **1998**, *244*, 253-257, doi:10.1006/bbrc.1998.8159.
48. Casciaro, B.; Cappiello, F.; Loffredo, M.R.; Ghirga, F.; Mangoni, M.L. The Potential of frog skin peptides for anti-Infective therapies: the Case of Esculentin-1a (1-21) NH2. *Current medicinal chemistry* **2020**, *27*, 1405-1419, doi:10.2174/0929867326666190722095408.
49. Ovchinnikova, T.V.; Balandin, S.V.; Aleshina, G.M.; Tagaev, A.A.; Leonova, Y.F.; Krasnodembsky, E.D.; Men'shenin, A.V.; Kokryakov, V.N. Aurelin, a novel antimicrobial peptide from jellyfish Aurelia aurita with structural features of defensins and channel-blocking toxins. *Biochemical and biophysical research communications* **2006**, *348*, 514-523, doi:10.1016/j.bbrc.2006.07.078.
50. Stensvåg, K.; Haug, T.; Sperstad, S.V.; Rekdal, Ø.; Indrevoll, B.; Styrvold, O.B. Arasin 1, a proline–arginine-rich antimicrobial peptide isolated from the spider crab, Hyas araneus. *Developmental and comparative immunology* **2008**, *32*, 275-285, doi:10.1016/j.dci.2007.06.002.
51. Li, C.; Haug, T.; Moe, M.K.; Styrvold, O.B.; Stensvåg, K. Centrocins: Isolation and characterization of novel dimeric antimicrobial peptides from the green sea urchin, Strongylocentrotus droebachiensis. *Developmental and Comparative Immunology* **2010**, *34*, 959-968, doi:10.1016/j.dci.2010.04.004.
52. Lee, I.H.; Lee, Y.S.; Kim, C.H.; Kim, C.R.; Hong, T.; Menzel, L.; Boo, L.M.; Pohl, J.; Sherman, M.A.; Waring, A. Dicynthaurin: an antimicrobial peptide from hemocytes of the solitary tunicate, Halocynthia aurantium. *Biochimica et Biophysica Acta (BBA)-General Subjects* **2001**, *1527*, 141-148, doi:10.1016/s0304-4165(01)00156-8.
53. De Kwaadsteniet, M.; Doeschate, K.T.; Dicks, L.M. Nisin F in the treatment of respiratory tract infections caused by Staphylococcus aureus. *Letters in applied microbiology* **2009**, *48*, 65-70, doi:10.1111/j.1472-765X.2008.02488.x.

54. David, J.M.; Rajasekaran, A.K. Gramicidin A: A New Mission for an Old Antibiotic. *Journal of kidney cancer and VHL* **2015**, *2*, 15-24, doi:10.15586/jkcvhl.2015.21.
55. Storm, D.R., Rosenthal, K. S., & Swanson, P. E. Polymyxin and Related Peptide Antibiotics. *Annual Review of Biochemistry* **1977**, *46*, 723-763, doi:10.1146/annurev.bi.46.070177.003451.
56. Mohammed, E.H.M.; Lohan, S.; Ghaffari, T.; Gupta, S.; Tiwari, R.K.; Parang, K. Membrane-Active Cyclic Amphiphilic Peptides: Broad-Spectrum Antibacterial Activity Alone and in Combination with Antibiotics. *Journal of Medicinal Chemistry* **2022**, *65*, 15819-15839, doi:10.1021/acs.jmedchem.2c01469.
57. Dennison, S.R.; Harris, F.; Mura, M.; Phoenix, D.A. An atlas of anionic antimicrobial peptides from amphibians. *Current Protein and Peptide Science* **2018**, *19*, 823-838, doi:10.2174/1389203719666180226155035.
58. Li, J.; Koh, J.-J.; Liu, S.; Lakshminarayanan, R.; Verma, C.S.; Beuerman, R.W. Membrane Active Antimicrobial Peptides: Translating Mechanistic Insights to Design. *Frontiers in Neuroscience* **2017**, *11*, doi:10.3389/fnins.2017.00073.
59. Malanovic, N.; Lohner, K. Gram-positive bacterial cell envelopes: The impact on the activity of antimicrobial peptides. *Biochimica et Biophysica Acta (BBA) - Biomembranes* **2016**, *1858*, 936-946, doi:10.1016/j.bbamem.2015.11.004.
60. Melo, M.N.; Ferre, R.; Castanho, M.A.R.B. Antimicrobial peptides: linking partition, activity and high membrane-bound concentrations. *Nature Reviews Microbiology* **2009**, *7*, 245-250, doi:10.1038/nrmicro2095.
61. Dürr, U.H.; Sudheendra, U.; Ramamoorthy, A. LL-37, the only human member of the cathelicidin family of antimicrobial peptides. *Biochimica et Biophysica Acta (BBA)-Biomembranes* **2006**, *1758*, 1408-1425, doi:10.1016/j.bbamem.2006.03.030.
62. Lyu, Z.; Yang, P.; Lei, J.; Zhao, J. Biological Function of Antimicrobial Peptides on Suppressing Pathogens and Improving Host Immunity. *Antibiotics* **2023**, *12*, 1037.
63. Hancock, R.E.; Scott, M.G. The role of antimicrobial peptides in animal defenses. *Proceedings of the National Academy of Sciences of the United States of America* **2000**, *97*, 8856-8861, doi:10.1073/pnas.97.16.8856.
64. Amiss, A.S.; Henriques, S.T.; Lawrence, N. Antimicrobial peptides provide wider coverage for targeting drug-resistant bacterial pathogens. *Peptide Science* **2022**, *114*, e24246, doi:10.1002/pep2.24246.
65. Hancock, R.E.W.; Scott, M.G. The role of antimicrobial peptides in animal defenses. *Proceedings of the National Academy of Sciences* **2000**, *97*, 8856-8861.
66. Dijksteel, G.S.; Ulrich, M.M.W.; Middelkoop, E.; Boekema, B. Review: Lessons Learned From Clinical Trials Using Antimicrobial Peptides (AMPs). *Front Microbiol* **2021**, *12*, 616979, doi:10.3389/fmicb.2021.616979.
67. Fjell, C.D.; Hiss, J.A.; Hancock, R.E.W.; Schneider, G. Designing antimicrobial peptides: form follows function. *Nature Reviews Drug Discovery* **2012**, *11*, 37-51, doi:10.1038/nrd3591.
68. Scheinpflug, K.; Nikolenko, H.; Komarov, I.V.; Rautenbach, M.; Dathe, M. What Goes around Comes around-A Comparative Study of the Influence of Chemical Modifications on the Antimicrobial Properties of Small Cyclic Peptides. *Pharmaceuticals (Basel)* **2013**, *6*, 1130-1144, doi:10.3390/ph6091130.
69. Junkes, C.; Harvey, R.D.; Bruce, K.D.; Dölling, R.; Bagheri, M.; Dathe, M. Cyclic antimicrobial R-, W-rich peptides: the role of peptide structure and E. coli outer and inner membranes in activity and the mode of action. *European biophysics journal* **2011**, *40*, 515-528, doi:10.1007/s00249-011-0671-x.
70. Fjell, C.D.; Hiss, J.A.; Hancock, R.E.W.; Schneider, G. Designing antimicrobial peptides: form follows function. *Nature reviews Drug discovery* **2011**, *11*, 37-51, doi:10.1038/nrd3591.
71. Hilpert, K.; Volkmer-Engert, R.; Walter, T.; Hancock, R.E. High-throughput generation of small antibacterial peptides with improved activity. *Nature biotechnology* **2005**, *23*, 1008-1012, doi:10.1038/nbt1113.

72. Amorim-Carmo, B.; Parente, A.M.S.; Souza, E.S.; Silva-Junior, A.A.; Araújo, R.M.; Fernandes-Pedrosa, M.F. Antimicrobial Peptide Analogs From Scorpions: Modifications and Structure-Activity. *Frontiers in Molecular Biosciences* **2022**, *9*, doi:10.3389/fmolb.2022.887763.
73. Riahifard, N.; Mozaffari, S.; Aldakhil, T.; Nunez, F.; Alshammari, Q.; Alshammari, S.; Yamaki, J.; Parang, K.; Tiwari, R.K. Design, Synthesis, and Evaluation of Amphiphilic Cyclic and Linear Peptides Composed of Hydrophobic and Positively-Charged Amino Acids as Antibacterial Agents. *Molecules (Basel)* **2018**, *23*, doi:10.3390/molecules23102722.
74. Michael Henderson, J.; Lee, K.Y.C. Promising antimicrobial agents designed from natural peptide templates. *Current Opinion in Solid State and Materials Science* **2013**, *17*, 175-192, doi:10.1016/j.cossms.2013.08.003.
75. Méndez-Samperio, P. Peptidomimetics as a new generation of antimicrobial agents: current progress. *Infection and drug resistance* **2014**, *7*, 229-237, doi:10.2147/IDR.S49229.
76. Hancock, R.E.; Sahl, H.-G. Antimicrobial and host-defense peptides as new anti-infective therapeutic strategies. *Nature biotechnology* **2006**, *24*, 1551-1557, doi:10.1038/nbt1267.
77. Joo, H.S.; Fu, C.I.; Otto, M. Bacterial strategies of resistance to antimicrobial peptides. *Philos Trans R Soc Lond B Biol Sci* **2016**, *371*, doi:10.1098/rstb.2015.0292.
78. Cardoso, P.; Glossop, H.; Meikle, T.G.; Aburto-Medina, A.; Conn, C.E.; Sarojini, V.; Valery, C. Molecular engineering of antimicrobial peptides: microbial targets, peptide motifs and translation opportunities. *Biophysical Reviews* **2021**, *13*, 35-69, doi:10.1007/s12551-021-00784-y.
79. Lai, Y.; Villaruz, A.E.; Li, M.; Cha, D.J.; Sturdevant, D.E.; Otto, M. The human anionic antimicrobial peptide dermcidin induces proteolytic defence mechanisms in staphylococci. *Molecular microbiology* **2007**, *63*, 497-506, doi:10.1111/j.1365-2958.2006.05540.x.
80. Sieprawska-Lupa, M.; Mydel, P.; Krawczyk, K.; Wójcik, K.; Puklo, M.; Lupa, B.; Suder, P.; Silberring, J.; Reed, M.; Pohl, J.; et al. Degradation of human antimicrobial peptide LL-37 by Staphylococcus aureus-derived proteinases. *Antimicrobial agents and chemotherapy* **2004**, *48*, 4673-4679, doi:10.1128/AAC.48.12.4673-4679.2004.
81. Hytönen, J.; Haataja, S.; Gerlach, D.; Podbielski, A.; Finne, J. The SpeB virulence factor of Streptococcus pyogenes, a multifunctional secreted and cell surface molecule with strepadhesin, laminin-binding and cysteine protease activity. *Molecular microbiology* **2001**, *39*, 512-519, doi:10.1046/j.1365-2958.2001.02269.x.
82. Schmidtchen, A.; Frick, I.M.; Björck, L. Dermatan sulphate is released by proteinases of common pathogenic bacteria and inactivates antibacterial alpha-defensin. *Molecular microbiology* **2001**, *39*, 708-713, doi:10.1046/j.1365-2958.2001.02251.x.
83. Peschel, A.; Sahl, H.-G. The co-evolution of host cationic antimicrobial peptides and microbial resistance. *Nature Reviews Microbiology* **2006**, *4*, 529-536, doi:10.1038/nrmicro1441.
84. Haiko, J.; Suomalainen, M.; Ojala, T.; Lähteenmäki, K.; Korhonen, T.K. Invited review: Breaking barriers--attack on innate immune defences by omptin surface proteases of enterobacterial pathogens. *Innate immunity* **2009**, *15*, 67-80, doi:10.1177/1753425909102559.
85. Santos Costa, S.; Viveiros, M.; Rosato, A.E.; Melo-Cristino, J.; Couto, I. Impact of efflux in the development of multidrug resistance phenotypes in Staphylococcus aureus. *BMC Microbiology* **2015**, *15*, 232, doi:10.1186/s12866-015-0572-8.
86. Kobylka, J.; Kuth, M.S.; Müller, R.T.; Geertsma, E.R.; Pos, K.M. AcrB: a mean, keen, drug efflux machine. *Annals of the New York Academy of Sciences* **2020**, *1459*, 38-68, doi:10.1111/nyas.14239.
87. Rieg, S.; Huth, A.; Kalbacher, H.; Kern, W.V. Resistance against antimicrobial peptides is independent of Escherichia coli AcrAB, Pseudomonas aeruginosa MexAB and Staphylococcus aureus NorA efflux pumps. *International journal of antimicrobial agents* **2009**, *33*, 174-176, doi:10.1016/j.ijantimicag.2008.07.032.
88. Padilla, E.; Llobet, E.; Doménech-Sánchez, A.; Martínez-Martínez, L.; Bengoechea, J.A.; Albertí, S. Klebsiella pneumoniae AcrAB efflux pump contributes to antimicrobial resistance

and virulence. *Antimicrobial agents and chemotherapy* **2010**, *54*, 177-183, doi:10.1128/AAC.00715-09.
89. Bina, X.R.; Provenzano, D.; Nguyen, N.; Bina, J.E. Vibrio cholerae RND family efflux systems are required for antimicrobial resistance, optimal virulence factor production, and colonization of the infant mouse small intestine. *Infection and immunity* **2008**, *76*, 3595-3605, doi:10.1128/IAI.01620-07.
90. Shafer, W.M.; Qu, X.; Waring, A.J.; Lehrer, R.I. Modulation of Neisseria gonorrhoeae susceptibility to vertebrate antibacterial peptides due to a member of the resistance/nodulation/division efflux pump family. *Proceedings of the National Academy of Sciences of the United States of America* **1998**, *95*, 1829-1833, doi:10.1073/pnas.95.4.1829.
91. Tzeng, Y.L.; Ambrose, K.D.; Zughaier, S.; Zhou, X.; Miller, Y.K.; Shafer, W.M.; Stephens, D.S. Cationic antimicrobial peptide resistance in Neisseria meningitidis. *Journal of bacteriology* **2005**, *187*, 5387-5396, doi:10.1128/JB.187.15.5387-5396.2005.
92. Chromek, M.; Slamová, Z.; Bergman, P.; Kovács, L.; Podracká, L.u.; Ehrén, I.; Hökfelt, T.; Gudmundsson, G.H.; Gallo, R.L.; Agerberth, B.; et al. The antimicrobial peptide cathelicidin protects the urinary tract against invasive bacterial infection. *Nature Medicine* **2006**, *12*, 636-641, doi:10.1038/nm1407.
93. Bierbaum, G.; Sahl, H.-G. Lantibiotics: mode of action, biosynthesis and bioengineering. *Current pharmaceutical biotechnology* **2009**, *10*, 2-18, doi:10.2174/138920109787048616.
94. Maloy, W.L.; Kari, U.P. Structure-activity studies on magainins and other host defense peptides. *Biopolymers* **1995**, *37*, 105-122, doi:10.1002/bip.360370206.
95. Fernandez-Lopez, S.; Kim, H.S.; Choi, E.C.; Delgado, M.; Granja, J.R.; Khasanov, A.; Kraehenbuehl, K.; Long, G.; Weinberger, D.A.; Wilcoxen, K.M.; et al. Antibacterial agents based on the cyclic D,L-alpha-peptide architecture. *Nature* **2001**, *412*, 452-455, doi:10.1038/35086601.
96. Oren, Z.; Shai, Y. Cyclization of a Cytolytic Amphipathic α-Helical Peptide and Its Diastereomer: Effect on Structure, Interaction with Model Membranes, and Biological Function. *Biochemistry* **2000**, *39*, 6103-6114, doi:10.1021/bi992408i.
97. Porter, E.A.; Wang, X.; Lee, H.-S.; Weisblum, B.; Gellman, S.H. Non-haemolytic β-amino-acid oligomers. *Nature* **2000**, *404*, 565-565, doi:10.1038/35007145.
98. Lyu, Z.; Yang, P.; Lei, J.; Zhao, J. Biological Function of Antimicrobial Peptides on Suppressing Pathogens and Improving Host Immunity. *Antibiotics (Basel)* **2023**, *12*, doi:10.3390/antibiotics12061037.
99. Giuliani, A., Pirri, G. & Nicoletto, S.F. Antimicrobial peptides: an overview of a promising class of therapeutics. *Open Life Sciences* **2007**, *2*, 1-33, doi:10.2478/s11535-007-0010-5.
100. Pasupuleti, M.; Schmidtchen, A.; Malmsten, M. Antimicrobial peptides: key components of the innate immune system. *Critical reviews in biotechnology* **2012**, *32*, 143-171, doi:10.3109/07388551.2011.594423.
101. Meroueh, S.O.; Bencze, K.Z.; Hesek, D.; Lee, M.; Fisher, J.F.; Stemmler, T.L.; Mobashery, S. Three-dimensional structure of the bacterial cell wall peptidoglycan. *Proceedings of the National Academy of Sciences of the United States of America* **2006**, *103*, 4404-4409, doi:10.1073/pnas.0510182103.
102. Zimmerman, S.M.; Lafontaine, A.J.; Herrera, C.M.; McLean, A.B.; Trent, M.S. A Whole-Cell Screen Identifies Small Bioactives That Synergize with Polymyxin and Exhibit Antimicrobial Activities against Multidrug-Resistant Bacteria. *Antimicrobial agents and chemotherapy* **2020**, *64*, doi:10.1128/AAC.01677-19.
103. Tanu, S.; Princy, C.; Sangeeta, S. Antimicrobial Peptides: Mechanism of Action. In *Insights on Antimicrobial Peptides*, Shymaa, E., Jorge, M.-S., Anna, S., Eds.; IntechOpen: Rijeka, 2022; p. Ch. 3.
104. Brogden, K.A. Antimicrobial peptides: pore formers or metabolic inhibitors in bacteria? *Nature Reviews Microbiology* **2005**, *3*, 238-250, doi:10.1038/nrmicro1098.

105. Snoussi, M., Talledo, J. P., Del Rosario, N. A., Mohammadi, S., Ha, B. Y., Košmrlj, A., & Taheri-Araghi, S. Heterogeneous absorption of antimicrobial peptide LL37 in Escherichia coli cells enhances population survivability. *eLife* **2018**, *7*, 313536, doi:10.7554/eLife.38174.
106. Gong, H., Hu, X., Liao, M., Fa, K., Ciumac, D., Clifton, L. A., Sani, M. A., King, S. M., Maestro, A., Separovic, F., Waigh, T. A., Xu, H., McBain, A. J., & Lu, J. R. Structural Disruptions of the Outer Membranes of Gram-Negative Bacteria by Rationally Designed Amphiphilic Antimicrobial Peptides. *ACS Applied Materials & Interfaces* **2021**, *13*, 16062-16074, doi:10.1021/acsami.1c01643.
107. Marchand, C.; Krajewski, K.; Lee, H.-F.; Antony, S.; Johnson, A.A.; Amin, R.; Roller, P.; Kvaratskhelia, M.; Pommier, Y. Covalent binding of the natural antimicrobial peptide indolicidin to DNA abasic sites. *Nucleic Acids Research* **2006**, *34*, 5157-5165, doi:10.1093/nar/gkl667.
108. Hale, J.D.; Hancock, R.E. Alternative mechanisms of action of cationic antimicrobial peptides on bacteria. *Expert review of anti-infective therapy* **2007**, *5*, 951-959, doi:10.1586/14787210.5.6.951.
109. Manabe, T.; Kawasaki, K. D-form KLKLLLLLKLK-NH2 peptide exerts higher antimicrobial properties than its L-form counterpart via an association with bacterial cell wall components. *Scientific Reports* **2017**, *7*, 43384, doi:10.1038/srep43384.
110. Mouton, J.W.; Muller, A.E.; Canton, R.; Giske, C.G.; Kahlmeter, G.; Turnidge, J. MIC-based dose adjustment: facts and fables. *The Journal of antimicrobial chemotherapy* **2018**, *73*, 564-568, doi:10.1093/jac/dkx427.
111. Kowalska-Krochmal, B.; Dudek-Wicher, R. The Minimum Inhibitory Concentration of Antibiotics: Methods, Interpretation, Clinical Relevance. *Pathogens (Basel, Switzerland)* **2021**, *10*, doi:10.3390/pathogens10020165.
112. Bhalla, N.; Jolly, P.; Formisano, N.; Estrela, P. Introduction to biosensors. *Essays in biochemistry* **2016**, *60*, 1-8, doi:10.1042/EBC20150001.
113. Moraskie, M.; Roshid, M.H.O.; O'Connor, G.; Dikici, E.; Zingg, J.-M.; Deo, S.; Daunert, S. Microbial whole-cell biosensors: Current applications, challenges, and future perspectives. *Biosensors and Bioelectronics* **2021**, *191*, 113359, doi:10.1016/j.bios.2021.113359.
114. Urban, A.; Eckermann, S.; Fast, B.; Metzger, S.; Gehling, M.; Ziegelbauer, K.; Rübsamen-Waigmann, H.; Freiberg, C. Novel whole-cell antibiotic biosensors for compound discovery. *Applied and environmental microbiology* **2007**, *73*, 6436-6443, doi:10.1128/AEM.00586-07.
115. Hansen, I.; Isaksson, J.; Poth, A.G.; Hansen, K.; Andersen, A.J.C.; Richard, C.S.M.; Blencke, H.M.; Stensvåg, K.; Craik, D.J.; Haug, T. Isolation and Characterization of Antimicrobial Peptides with Unusual Disulfide Connectivity from the Colonial Ascidian Synoicum turgens. *Marine drugs* **2020**, *18*, doi:10.3390/md18010051.
116. Hansen, I.; Lövdahl, T.; Simonovic, D.; Hansen, K.; Andersen, A.J.C.; Devold, H.; Richard, C.S.M.; Andersen, J.H.; Strøm, M.B.; Haug, T. Antimicrobial Activity of Small Synthetic Peptides Based on the Marine Peptide Turgencin A: Prediction of Antimicrobial Peptide Sequences in a Natural Peptide and Strategy for Optimization of Potency. *International Journal of Molecular Sciences* **2020**, *21*, doi:10.3390/ijms21155460.
117. Meighen, E.A. Molecular biology of bacterial bioluminescence. *Microbiol Rev* **1991**, *55*, 123-142, doi:10.1128/mr.55.1.123-142.1991.
118. Miyashiro, T.; Ruby, E.G. Shedding light on bioluminescence regulation in Vibrio fischeri. *Molecular Microbiology* **2012**, *84*, 795-806, doi:10.1111/j.1365-2958.2012.08065.x.
119. Virta, M.; Åkerman, K.E.O.; Saviranta, P.; Oker-Blom, C.; Karp, M.T. Real-time measurement of cell permeabilization with low-molecular-weight membranolytic agents. *Journal of Antimicrobial Chemotherapy* **1995**, *36*, 303-315, doi:10.1093/jac/36.2.303.
120. Dey, H.; Simonovic, D.; Norberg-Schulz Hagen, I.; Vasskog, T.; Fredheim, E.G.A.; Blencke, H.-M.; Anderssen, T.; Strøm, M.B.; Haug, T. Synthesis and Antimicrobial Activity of Short Analogues of the Marine Antimicrobial Peptide Turgencin A: Effects of SAR Optimizations, Cys-Cys Cyclization and Lipopeptide Modifications. *International Journal of Molecular Sciences* **2022**, *23*, 13844, doi:10.3390/ijms232213844.

121. Radeck, J.; Kraft, K.; Bartels, J.; Cikovic, T.; Dürr, F.; Emenegger, J.; Kelterborn, S.; Sauer, C.; Fritz, G.; Gebhard, S.; et al. The Bacillus BioBrick Box: generation and evaluation of essential genetic building blocks for standardized work with Bacillus subtilis. *Journal of Biological Engineering* **2013**, *7*, 29, doi:10.1186/1754-1611-7-29.
122. Juskewitz, E.; Mishchenko, E.; Dubey, V.K.; Jenssen, M.; Jakubec, M.; Rainsford, P.; Isaksson, J.; Andersen, J.H.; Ericson, J.U. Lulworthinone: In Vitro Mode of Action Investigation of an Antibacterial Dimeric Naphthopyrone Isolated from a Marine Fungus. *Marine Drugs* **2022**, *20*, doi:10.3390/md20050277.
123. Radeck, J.; Fritz, G.; Mascher, T. The cell envelope stress response of Bacillus subtilis: from static signaling devices to dynamic regulatory network. *Current Genetics* **2017**, *63*, 79-90, doi:10.1007/s00294-016-0624-0.
124. Kintses, B.; Jangir, P.K.; Fekete, G.; Számel, M.; Méhi, O.; Spohn, R.; Daruka, L.; Martins, A.; Hosseinnia, A.; Gagarinova, A.; et al. Chemical-genetic profiling reveals limited cross-resistance between antimicrobial peptides with different modes of action. *Nature Communications* **2019**, *10*, 5731, doi:10.1038/s41467-019-13618-z.
125. Naghmouchi, K.; Le Lay, C.; Baah, J.; Drider, D. Antibiotic and antimicrobial peptide combinations: synergistic inhibition of Pseudomonas fluorescens and antibiotic-resistant variants. *Research in Microbiology* **2012**, *163*, 101-108, doi:10.1016/j.resmic.2011.11.002.
126. Lohner, K. New strategies for novel antibiotics: peptides targeting bacterial cell membranes. *General physiology and biophysics* **2009**, *28*, 105-116, doi:10.4149/gpb_2009_02_105.
127. Patel, H.; Huynh, Q.; Bärlehner, D.; Heerklotz, H. Additive and Synergistic Membrane Permeabilization by Antimicrobial (Lipo)Peptides and Detergents. *Biophysical journal* **2014**, *106*, 2115-2125, doi:10.1016/j.bpj.2014.04.006.
128. Duong, L.; Gross, S.P.; Siryaporn, A. Developing Antimicrobial Synergy With AMPs. *Frontiers in medical technology* **2021**, *3*, 640981, doi:10.3389/fmedt.2021.640981.
129. Lázár, V.; Martins, A.; Spohn, R.; Daruka, L.; Grézal, G.; Fekete, G.; Számel, M.; Jangir, P.K.; Kintses, B.; Csörgő, B.; et al. Antibiotic-resistant bacteria show widespread collateral sensitivity to antimicrobial peptides. *Nature microbiology* **2018**, *3*, 718-731, doi:10.1038/s41564-018-0164-0.
130. Ruden, S.; Rieder, A.; Chis Ster, I.; Schwartz, T.; Mikut, R.; Hilpert, K. Synergy Pattern of Short Cationic Antimicrobial Peptides Against Multidrug-Resistant Pseudomonas aeruginosa. *Frontiers in Microbiology* **2019**, *10*, doi:10.3389/fmicb.2019.02740.
131. Choi, H.; Lee, D.G. Synergistic effect of antimicrobial peptide arenicin-1 in combination with antibiotics against pathogenic bacteria. *Research in Microbiology* **2012**, *163*, 479-486, doi:10.1016/j.resmic.2012.06.001.
132. Wesseling, C.M.J.; Martin, N.I. Synergy by Perturbing the Gram-Negative Outer Membrane: Opening the Door for Gram-Positive Specific Antibiotics. *ACS infectious diseases* **2022**, *8*, 1731-1757, doi:10.1021/acsinfecdis.2c00193.
133. Ng, H.K.; Puah, S.M.; Teh, C.S.J.; Idris, N.; Chua, K.H. Characterisation of pellicle-forming ability in clinical carbapenem-resistant Acinetobacter baumannii. *PeerJ* **2023**, *11*, e15304, doi:10.7717/peerj.15304.
134. Hall, C.W.; Mah, T.-F. Molecular mechanisms of biofilm-based antibiotic resistance and tolerance in pathogenic bacteria. *FEMS Microbiology Reviews* **2017**, *41*, 276-301, doi:10.1093/femsre/fux010.
135. Gebreyohannes, G.; Nyerere, A.; Bii, C.; Sbhatu, D.B. Challenges of intervention, treatment, and antibiotic resistance of biofilm-forming microorganisms. *Heliyon* **2019**, *5*, doi:10.1016/j.heliyon.2019.e02192.
136. Yasir, M.; Willcox, M.D.P.; Dutta, D. Action of Antimicrobial Peptides against Bacterial Biofilms. *Materials (Basel)* **2018**, *11*, doi:10.3390/ma11122468.
137. Vishwakarma, A.; Dang, F.; Ferrell, A.; Barton, H.A.; Joy, A. Peptidomimetic Polyurethanes Inhibit Bacterial Biofilm Formation and Disrupt Surface Established Biofilms. *Journal of the American Chemical Society* **2021**, doi:10.1021/jacs.1c02324.

138. Huan, Y.; Kong, Q.; Mou, H.; Yi, H. Antimicrobial Peptides: Classification, Design, Application and Research Progress in Multiple Fields. *Frontiers in microbiology* **2020**, *11*, 582779, doi:10.3389/fmicb.2020.582779.
139. Pirtskhalava, M.; Vishnepolsky, B.; Grigolava, M.; Managadze, G. Physicochemical Features and Peculiarities of Interaction of AMP with the Membrane. *Pharmaceuticals* **2021**, *14*, 471, doi:10.3390/ph14050471.
140. Jin, L.; Bai, X.; Luan, N.; Yao, H.; Zhang, Z.; Liu, W.; Chen, Y.; Yan, X.; Rong, M.; Lai, R.; et al. A Designed Tryptophan- and Lysine/Arginine-Rich Antimicrobial Peptide with Therapeutic Potential for Clinical Antibiotic-Resistant Candida albicans Vaginitis. *Journal of Medicinal Chemistry* **2016**, *59*, 1791-1799, doi:10.1021/acs.jmedchem.5b01264.
141. Mwangi, J.; Kamau, P.M.; Thuku, R.C.; Lai, R. Design methods for antimicrobial peptides with improved performance. *Zoological research* **2023**, *44*, 1095-1114, doi:10.24272/j.issn.2095-8137.2023.246.
142. de Breij, A.; Riool, M.; Cordfunke, R.A.; Malanovic, N.; de Boer, L.; Koning, R.I.; Ravensbergen, E.; Franken, M.; van der Heijde, T.; Boekema, B.K.; et al. The antimicrobial peptide SAAP-148 combats drug-resistant bacteria and biofilms. *Science Translational Medicine* **2018**, *10*, eaan4044, doi:10.1126/scitranslmed.aan4044.
143. Rajasekaran, G.; Kim, E.Y.; Shin, S.Y. LL-37-derived membrane-active FK-13 analogs possessing cell selectivity, anti-biofilm activity and synergy with chloramphenicol and anti-inflammatory activity. *Biochimica et Biophysica Acta (BBA) - Biomembranes* **2017**, *1859*, 722-733, doi:10.1016/j.bbamem.2017.01.037.
144. Cutrona, K.J.; Kaufman, B.A.; Figueroa, D.M.; Elmore, D.E. Role of arginine and lysine in the antimicrobial mechanism of histone-derived antimicrobial peptides. *FEBS letters* **2015**, *589*, 3915-3920, doi:10.1016/j.febslet.2015.11.002.
145. Huan, Y.; Kong, Q.; Mou, H.; Yi, H. Antimicrobial Peptides: Classification, Design, Application and Research Progress in Multiple Fields. *Frontiers in Microbiology* **2020**, *11*, doi:10.3389/fmicb.2020.582779.
146. Sarkar, T.; Chetia, M.; Chatterjee, S. Antimicrobial Peptides and Proteins: From Nature's Reservoir to the Laboratory and Beyond. *Frontiers in Chemistry* **2021**, *9*, doi:10.3389/fchem.2021.691532.
147. Vernen, F.; Harvey, P.J.; Dias, S.A.; Veiga, A.S.; Huang, Y.-H.; Craik, D.J.; Lawrence, N.; Troeira Henriques, S. Characterization of Tachyplesin Peptides and Their Cyclized Analogues to Improve Antimicrobial and Anticancer Properties. *International Journal of Molecular Sciences* **2019**, *20*, 4184, doi:10.3390/ijms20174184.
148. Mwangi, J.; Yin, Y.; Wang, G.; Yang, M.; Li, Y.; Zhang, Z.; Lai, R. The antimicrobial peptide ZY4 combats multidrug-resistant Pseudomonas aeruginosa and Acinetobacter baumannii infection. *Proceedings of the National Academy of Sciences of the United States of America* **2019**, *116*, 26516-26522, doi:10.1073/pnas.1909585117.
149. Meena, K.R.; Kanwar, S.S. Lipopeptides as the Antifungal and Antibacterial Agents: Applications in Food Safety and Therapeutics. *BioMed Research International* **2015**, *2015*, 473050, doi:10.1155/2015/473050.
150. Mandal, S.M.; Sharma, S.; Pinnaka, A.K.; Kumari, A.; Korpole, S. Isolation and characterization of diverse antimicrobial lipopeptides produced by Citrobacter and Enterobacter. *BMC Microbiology* **2013**, *13*, 152, doi:10.1186/1471-2180-13-152.
151. Datta, A.; Kundu, P.; Bhunia, A. Designing potent antimicrobial peptides by disulphide linked dimerization and N-terminal lipidation to increase antimicrobial activity and membrane perturbation: Structural insights into lipopolysaccharide binding. *Journal of Colloid and Interface Science* **2016**, *461*, 335-345, doi:10.1016/j.jcis.2015.09.036.
152. Tsubery, H.; Ofek, I.; Cohen, S.; Fridkin, M. Structure− function studies of polymyxin B nonapeptide: implications to sensitization of gram-negative bacteria. *Journal of medicinal chemistry* **2000**, *43*, 3085-3092, doi:10.1021/jm0000057.

153. Jensen, S.K.; Thomsen, T.T.; Oddo, A.; Franzyk, H.; Løbner-Olesen, A.; Hansen, P.R. Novel Cyclic Lipopeptide Antibiotics: Effects of Acyl Chain Length and Position. *Int J Mol Sci* **2020**, *21*, doi:10.3390/ijms21165829.
154. Grimsey, E.; Collis, D.W.P.; Mikut, R.; Hilpert, K. The effect of lipidation and glycosylation on short cationic antimicrobial peptides. *Biochimica et Biophysica Acta (BBA) - Biomembranes* **2020**, *1862*, 183195, doi:10.1016/j.bbamem.2020.183195.
155. Rounds, T.; Straus, S.K. Lipidation of Antimicrobial Peptides as a Design Strategy for Future Alternatives to Antibiotics. *International journal of molecular sciences* **2020**, *21*, 9692, doi:10.3390/ijms21249692.
156. Sani, M.A.; Separovic, F. How Membrane-Active Peptides Get into Lipid Membranes. *Accounts of chemical research* **2016**, *49*, 1130-1138, doi:10.1021/acs.accounts.6b00074.
157. Wu, M.; Maier, E.; Benz, R.; Hancock, R.E.W. Mechanism of Interaction of Different Classes of Cationic Antimicrobial Peptides with Planar Bilayers and with the Cytoplasmic Membrane of Escherichia coli. *Biochemistry* **1999**, *38*, 7235-7242, doi:10.1021/bi9826299.
158. Wenzel, M.; Chiriac, A.I.; Otto, A.; Zweytick, D.; May, C.; Schumacher, C.; Gust, R.; Albada, H.B.; Penkova, M.; Krämer, U.; et al. Small cationic antimicrobial peptides delocalize peripheral membrane proteins. *Proceedings of the National Academy of Sciences* **2014**, *111*, E1409-E1418, doi:10.1073/pnas.1319900111.
159. Maturana, P.; Gonçalves, S.; Martinez, M.; Espeche, J.C.; Santos, N.C.; Semorile, L.; Maffia, P.C.; Hollmann, A. Interactions of "de novo" designed peptides with bacterial membranes: Implications in the antimicrobial activity. *Biochimica et Biophysica Acta (BBA) - Biomembranes* **2020**, *1862*, 183443, doi:10.1016/j.bbamem.2020.183443.
160. Li, X.; Zuo, S.; Wang, B.; Zhang, K.; Wang, Y. Antimicrobial Mechanisms and Clinical Application Prospects of Antimicrobial Peptides. *Molecules* **2022**, *27*, doi:10.3390/molecules27092675.
161. Choi, H.; Yang, Z.; Weisshaar, J.C. Single-cell, real-time detection of oxidative stress induced in Escherichia coli by the antimicrobial peptide CM15. *Proceedings of the National Academy of Sciences of the United States of America* **2015**, *112*, E303-310, doi:10.1073/pnas.1417703112.
162. Kim, S.; Lee, J.; Lee, S.; Kim, H.; Sim, J.-Y.; Pak, B.; Kim, K.; Il Kim, J. Matching amino acids membrane preference profile to improve activity of antimicrobial peptides. *Communications Biology* **2022**, *5*, 1199, doi:10.1038/s42003-022-04164-4.
163. Unger, T.; Oren, Z.; Shai, Y. The Effect of Cyclization of Magainin 2 and Melittin Analogues on Structure, Function, and Model Membrane Interactions: Implication to Their Mode of Action. *Biochemistry* **2001**, *40*, 6388-6397, doi:10.1021/bi0026066.
164. Loh, B.; Grant, C.; Hancock, R.E. Use of the fluorescent probe 1-N-phenylnaphthylamine to study the interactions of aminoglycoside antibiotics with the outer membrane of Pseudomonas aeruginosa. *Antimicrobial agents and chemotherapy* **1984**, *26*, 546-551, doi:10.1128/AAC.26.4.546.
165. Poppolo Deus, F.; Ouanounou, A. Chlorhexidine in Dentistry: Pharmacology, Uses, and Adverse Effects. *International dental journal* **2022**, *72*, 269-277, doi:10.1016/j.identj.2022.01.005.
166. Schmidtchen, A.; Frick, I.-M.; Andersson, E.; Tapper, H.; Björck, L. Proteinases of common pathogenic bacteria degrade and inactivate the antibacterial peptide LL-37. *Molecular Microbiology* **2002**, *46*, 157-168, doi:10.1046/j.1365-2958.2002.03146.x.
167. Stumpe, S.; Schmid, R.; Stephens, D.L.; Georgiou, G.; Bakker, E.P. Identification of OmpT as the protease that hydrolyzes the antimicrobial peptide protamine before it enters growing cells of Escherichia coli. *Journal of Bacteriology* **1998**, *180*, 4002-4006, doi:10.1128/jb.180.15.4002-4006.1998.
168. Wu, F.; Tan, C. Dead bacterial absorption of antimicrobial peptides underlies collective tolerance. *Journal of The Royal Society Interface* **2019**, *16*, 20180701, doi:10.1098/rsif.2018.0701.

169. Papo, N.; Oren, Z.; Pag, U.; Sahl, H.-G.; Shai, Y. The consequence of sequence alteration of an amphipathic α-helical antimicrobial peptide and its diastereomers. *The Journal of biological chemistry* **2002**, *277*, 33913-33921, doi:10.1074/jbc.M204928200.
170. Ghai, I.; Ghai, S. Understanding antibiotic resistance via outer membrane permeability. *Infection and drug resistance* **2018**, *11*, 523-530, doi:10.2147/IDR.S156995.
171. Barreto-Santamaría, A.; Arévalo-Pinzón, G.; Patarroyo, M.A.; Patarroyo, M.E. How to Combat Gram-Negative Bacteria Using Antimicrobial Peptides: A Challenge or an Unattainable Goal? *Antibiotics (Basel)* **2021**, *10*, doi:10.3390/antibiotics10121499.
172. Zgurskaya, H.I.; Löpez, C.A.; Gnanakaran, S. Permeability Barrier of Gram-Negative Cell Envelopes and Approaches To Bypass It. *ACS infectious diseases* **2015**, *1*, 512-522, doi:10.1021/acsinfecdis.5b00097.
173. Krüger, M.; Richter, P.; Strauch, S.M.; Nasir, A.; Burkovski, A.; Antunes, C.A.; Meißgeier, T.; Schlücker, E.; Schwab, S.; Lebert, M. What an Escherichia coli Mutant Can Teach Us About the Antibacterial Effect of Chlorophyllin. *Microorganisms* **2019**, *7*, doi:10.3390/microorganisms7020059.
174. Zheng, M.; Lupoli, T.J. Counteracting antibiotic resistance enzymes and efflux pumps. *Current Opinion in Microbiology* **2023**, *75*, 102334, doi:10.1016/j.mib.2023.102334.
175. Vaara, M. Polymyxin Derivatives that Sensitize Gram-Negative Bacteria to Other Antibiotics. *Molecules* **2019**, *24*, 249, doi:10.3390/molecules24020249.
176. Narendrakumar, L.; Chakraborty, M.; Kumari, S.; Paul, D.; Das, B. β-Lactam potentiators to re-sensitize resistant pathogens: Discovery, development, clinical use and the way forward. *Frontiers in Microbiology* **2023**, *13*, doi:10.3389/fmicb.2022.1092556.
177. Galdiero, E.; Lombardi, L.; Falanga, A.; Libralato, G.; Guida, M.; Carotenuto, R. Biofilms: Novel Strategies Based on Antimicrobial Peptides. *Pharmaceutics* **2019**, *11*, doi:10.3390/pharmaceutics11070322.
178. Fuente-Núñez, C.d.l.; Korolik, V.; Bains, M.; Nguyen, U.; Breidenstein, E.B.M.; Horsman, S.; Lewenza, S.; Burrows, L.; Hancock, R.E.W. Inhibition of Bacterial Biofilm Formation and Swarming Motility by a Small Synthetic Cationic Peptide. *Antimicrobial Agents and Chemotherapy* **2012**, *56*, 2696-2704, doi:10.1128/AAC.00064-12.
179. De la Fuente-Núñez, C.; Mansour, S.C.; Wang, Z.; Jiang, L.; Breidenstein, E.B.M.; Elliott, M.; Reffuveille, F.; Speert, D.P.; Reckseidler-Zenteno, S.L.; Shen, Y.; et al. Anti-Biofilm and Immunomodulatory Activities of Peptides That Inhibit Biofilms Formed by Pathogens Isolated from Cystic Fibrosis Patients. *Antibiotics (Basel, Switzerland)* **2014**, *3*, 509-526, doi:10.3390/antibiotics3040509.
180. Reffuveille, F.; Fuente-Núñez, C.d.l.; Mansour, S.; Hancock, R.E.W. A Broad-Spectrum Antibiofilm Peptide Enhances Antibiotic Action against Bacterial Biofilms. *Antimicrobial Agents and Chemotherapy* **2014**, *58*, 5363-5371, doi:10.1128/AAC.03163-14.
181. Frisinger, F.S.; Jana, B.; Ortiz-Marquez, J.C.; van Opijnen, T.; Donadio, S.; Guardabassi, L. LptD depletion disrupts morphological homeostasis and upregulates carbohydrate metabolism in Escherichia coli. *FEMS Microbes* **2023**, *4*, xtad013, doi:10.1093/femsmc/xtad013.

Paper I

International Journal of
Molecular Sciences

MDPI

Article

Synthesis and Antimicrobial Activity of Short Analogues of the Marine Antimicrobial Peptide Turgencin A: Effects of SAR Optimizations, Cys-Cys Cyclization and Lipopeptide Modifications

Hymonti Dey [1,†], Danijela Simonovic [2,†], Ingrid Norberg-Schulz Hagen [2], Terje Vasskog [2], Elizabeth G. Aarag Fredheim [2], Hans-Matti Blencke [1], Trude Anderssen [2], Morten B. Strøm [2,*] and Tor Haug [1,*]

[1] The Norwegian College of Fishery Science, Faculty of Biosciences, Fisheries and Economics, UiT The Arctic University of Norway, NO-9037 Tromsø, Norway
[2] Department of Pharmacy, Faculty of Health Sciences, UiT The Arctic University of Norway, NO-9037 Tromsø, Norway
* Correspondence: morten.strom@uit.no (M.B.S.); tor.haug@uit.no (T.H.)
† These authors contributed equally to this work.

Abstract: We have synthesised short analogues of the marine antimicrobial peptide Turgencin A from the colonial Arctic ascidian *Synoicum turgens*. In this study, we focused on a central, cationic 12-residue Cys-Cys loop region within the sequence. Modified (tryptophan- and arginine-enriched) linear peptides were compared with Cys-Cys cyclic derivatives, and both linear and Cys-cyclic peptides were N-terminally acylated with octanoic acid (C_8), decanoic acid (C_{10}) or dodecanoic acid (C_{12}). The highest antimicrobial potency was achieved by introducing dodecanoic acid to a cyclic Turgencin A analogue with low intrinsic hydrophobicity, and by introducing octanoic acid to a cyclic analogue displaying a higher intrinsic hydrophobicity. Among all tested synthetic Turgencin A lipopeptide analogues, the most promising candidates regarding both antimicrobial and haemolytic activity were **C_{12}-cTurg-1** and **C_8-cTurg-2**. These optimized cyclic lipopeptides displayed minimum inhibitory concentrations of 4 µg/mL against *Staphylococcus aureus*, *Escherichia coli* and the fungus *Rhodothorula* sp. Mode of action studies on bacteria showed a rapid membrane disruption and bactericidal effect of the cyclic lipopeptides. Haemolytic activity against human erythrocytes was low, indicating favorable selective targeting of bacterial cells.

Keywords: AMPs; Cys-Cys cyclic peptides; lipopeptides; short antibacterial peptides; structure–activity relationship; mechanism of action

check for updates

Citation: Dey, H.; Simonovic, D.; Norberg-Schulz Hagen, I.; Vasskog, T.; Fredheim, E.G.A.; Blencke, H.-M.; Anderssen, T.; Strøm, M.B.; Haug, T. Synthesis and Antimicrobial Activity of Short Analogues of the Marine Antimicrobial Peptide Turgencin A: Effects of SAR Optimizations, Cys-Cys Cyclization and Lipopeptide Modifications. *Int. J. Mol. Sci.* **2022**, *23*, 13844. https://doi.org/10.3390/ijms232213844

Academic Editor: Oxana V. Galzitskaya

Received: 19 October 2022
Accepted: 8 November 2022
Published: 10 November 2022

Publisher's Note: MDPI stays neutral with regard to jurisdictional claims in published maps and institutional affiliations.

1. Introduction

Antimicrobial resistance (AMR) poses a serious threat to human health worldwide. According to a recent study, an estimated 4.95 million deaths were associated with AMR globally in 2019, out of which 1.27 million deaths were directly attributable to it [1]. Due to increasing AMR, treatment of infectious diseases has become one of the greatest challenges in modern medicine [2]. One of the efforts to mitigate this threat includes the development of new antibacterial agents, which could circumvent existing resistance mechanisms by attacking new targets (i.e., having novel mechanisms of action). Although efforts have been made in this direction, progress remains rather slow [3].

Natural products have historically played an invaluable role in drug discovery and development, and most antibiotics currently in commercial use, and those being developed, are of natural origin [4]. Gene-encoded, ribosomal synthesized antimicrobial peptides (AMPs) are widespread in nature and have been identified in various species ranging from bacteria and fungi to plants, invertebrates and vertebrates (including fish, birds and

mammals) [5]. In eukaryotes, they are involved in the innate immunity as a first line of defense against infectious microorganisms. These compounds, generally small, cationic, amphipathic peptides, hold promise in the fight against AMR. Due to their non-specific mechanism of action, targeting the fundamental structure of the bacterial membrane, AMPs are thought to delay the emergence of bacterial resistance [6]. Many AMPs are shown to possess selective toxicity for microbes and a broad spectrum of antimicrobial activity, acting against both Gram-positive and Gram-negative bacteria [7]. Moreover, several studies have shown a synergistic and/or adjuvant effect of AMPs with conventional antibiotics [8,9]. Due to their favorable properties, AMPs have been successfully used as templates for the development of drug candidates with improved potency and selectivity, and several natural and synthetic peptides are currently in clinical trials [10].

The marine environment, with its vast biological diversity, is shown to be a promising source for future antibiotic discoveries, including novel AMPs [11]. We have previously isolated and characterized a 36-residue long AMP, named Turgencin A, from the Arctic marine colonial ascidian *Synoicum turgens* [12], and investigated the antimicrobial activity of its shortened linear 10-residue sequence rich in cationic residues (residues 18–27 of Turgencin A) [13] (Figure 1). In the native Turgencin A peptide, this 10-residue sequence is part of a loop region in which two cysteine residues (Cys^{17}-Cys^{26}) are crosslinked by a disulphide bond.

$$G^{1}PKTK^{5}AACKM^{10}ACKLA^{15}T\underline{C}\mathbf{GKK^{20}PGGWK^{25}}\underline{C}\mathbf{KL}CE^{30}LGCDA^{35}V\text{-}NH_2$$

Figure 1. Amino acid sequence of Turgencin A with the 12-residue loop region in bold (residues 17–28). Cys-Cys connectivity in the loop region is underlined. Disulphide connectivity in the native Turgencin A peptide is Cys8-Cys33, Cys12-Cys29 and Cys17-Cys26 [12].

In the present study, we prepared a series of 12-residue peptides (residues 17–28) encompassing this loop region. The Lys^{27} and Leu^{28} residues belonging to the original Turgencin A sequence were also included as additional cationic and lipophilic residues, respectively. Our aim was to investigate the structure–activity relationship (SAR) of a variety of modifications to the antimicrobial activity and selectivity: (1) increasing lipophilicity (by including two tryptophan residues in the PGG core sequence), (2) Lys to Arg substitutions, (3) N-terminal acylation and (4) Cys-Cys cyclization. In doing so, we wanted to gain insight into how these modifications could be best utilized to fine-tune the properties of potential novel AMP leads, increasing both their antimicrobial activity and selectivity. All peptides, like the originally isolated Turgencin A, were C-terminally amidated in order to increase the overall positive charge. Minimal inhibitory concentrations (MIC) were determined against selected Gram-positive and Gram-negative bacterial strains and fungi. Haemolytic activity (EC_{50}) was tested against human red blood cells (RBCs) and a bacterial selectivity index (SI) was calculated for each peptide. Selected peptides were investigated for their antibacterial mode of action (MoA) using luciferase and fluorescence-based assays to assess the viability and integrity of the cytoplasmic inner and outer membrane of bacterial cells.

2. Results and Discussion

2.1. Peptide Design and Synthesis

All analogues of the 12-residue loop region of Turgencin A were synthesized by Fmoc solid phase peptide synthesis (SPPS) on a fully automated microwave assisted peptide synthesizer. Standard conditions were used and coupling was completed with O-(1H-6-chlorobenzotriazole-1-yl)-1,1,3,3-tetramethyluronium hexafluorophosphate (HCTU) and *N,N*-diisopropylethylamine (DIEA) as a base. A double coupling strategy was employed to ensure efficient N-terminal acylation with octanoic (C_8), decanoic (C_{10}) and dodecanoic acid (C_{12}). Prior to Cys-Cys cyclization, the synthesized peptides were purified by preparative reversed-phase high-performance liquid chromatography (RP-HPLC). Cyclization of the peptides (by disulphide formation) was successfully carried out in distilled water (pH: 6.5) at room temperature with atmospheric O_2, or by bubbling O_2 through the aqueous solution

for one to four days. The progress of cyclization was monitored by liquid chromatography–mass spectrometry (LC–MS). The mass of the final products, obtained after lyophilization, were verified by high resolution–mass spectrometry (HR–MS) (Table S1) and the purity (>90% for all peptides) was determined by ultra-performance liquid chromatography with UV detection (UPLC-UV) (Table S2 and Figures S1–S25).

2.2. Structure–Activity Relationship (SAR) of Cyclic Trp- and Arg-Modified Peptides

The first series of Cys-Cys cyclic peptides (**cTurg-1–7**) were synthesized to investigate the effects of increasing the lipophilicity of the 12-residue loop region of Turgencin A (residues 17–28) by incorporating Trp-residues, and by replacing Lys-residues with Arg-residues (Table 1). The model peptides for these modifications were based on a previously reported series of short linear Turgencin A peptides (StAMP-peptides) demonstrating improved antimicrobial activity by introducing two additional Trp-residues [13].

The first peptide in the cTurg-series, **cTurg-1**, which contained the original Turgencin A (17–28) loop sequence was, however, inactive against all tested bacterial strains (MIC $\geq$ 256 μg/mL), except against the sensitive strain *Corynebacterium glutamicum* (MIC: 16 μg/mL). The Trp-modified peptides, **cTurg-2**, **cTurg-3** and **cTurg-4** were derived from **cTurg-1** by substituting amino acids present in the central PGG core of Turgencin A. The central PGG sequence of **cTurg-1** was modified as follows: WWG for **cTurg-2**, WGW for **cTurg-3** and PWW for **cTurg-4** (Table 1). Compared to **cTurg-1,** the Trp-enriched cyclic peptides showed considerable improvement in activity against all bacterial strains, except for **cTurg-4** against *Pseudomonas aeruginosa* (Table 1). The highest antibacterial activity was achieved against the Gram-positive strains *Bacillus subtilis* and *C. glutamicum* (MIC: 4–8 μg/mL), as well as improved potency against *Staphylococcus aureus* and *Staphylococcus epidermidis* (MIC: 16–64 μg/mL). However, the potency against the Gram-negative strains (*Escherichia coli* and *P. aeruginosa*), though better than that of **cTurg-1**, was low (MIC: 32–256 μg/mL). This reduced activity of AMPs is most likely due to the presence of a lipopolysaccharide (LPS) layer, which is the main constituent of the outer membrane of Gram-negative bacteria and which binds to AMPs, thereby inhibiting their effect [14].

The next modification included substitution of the Lys- with Arg-residues in **cTurg-2**, **cTurg-3** and **cTurg-4**, resulting in the Arg-modified peptides **cTurg-5** (WWG), **cTurg-6** (WGW) and **cTurg-7** (PWW). These modifications led to a considerable increase in antimicrobial activity for the arginine-modified peptides against the Gram-positive bacteria, *S. aureus* and *S. epidermidis* (MIC: 8–16 μg/mL), and also against the Gram-negative bacteria *E. coli* and *P. aeruginosa* (MIC: 8–32 μg/mL) (Table 1). The most potent peptide was **cTurg-6** (WGW) with a MIC of 4–16 μg/mL against the Gram-positive bacterial strains and a MIC of 8–16 μg/mL against the Gram-negative bacterial strains. Of note, **cTurg-3** (WGW), with the same central core as **cTurg-6,** was the most potent peptide among the Lys-containing peptides, except against *P. aeruginosa*. The lowest overall antimicrobial activity for both the Lys- and Arg-containing analogues was observed for the two peptides with a PWW central core and three adjacent tryptophan residues in their sequences (**cTurg-4** and **cTurg-7**). All peptides were non-haemolytic (EC_{50}: $\geq$ 849 μg/mL) except for **cTurg-7**, which had an EC_{50} value of 197 μg/mL against human RBCs.

2.3. Structure–Activity Relationship of Linear Lipopeptides

A well-established strategy for generating peptides with increased efficacy is N-terminal conjugation with aliphatic fatty acids [15,16] (Figure 2). To investigate the effects of acylation on antimicrobial activity, we decided to synthesise both linear and cyclic lipopeptide analogues of three selected peptides. Our choice of peptides for acylation was driven by the observed potencies of the previously synthesised cyclic analogues. We chose **cTurg-1** for being a mostly inactive peptide, **cTurg-2** for being the most potent peptide against *P. aeruginosa* among the Lys-containing peptides, and finally the Arg-modified peptide **cTurg-6**, which exerted the overall highest antimicrobial activity against all strains. **cTurg-2** and **cTurg-6** were also non-haemolytic (EC_{50}: >1045 μg/mL).

Table 1. Antimicrobial activity (MIC in μg/mL), haemolytic activity against human RBC (EC_{50} in μg/mL) and selectivity index (SI). Sequence modifications (Trp and Arg replacements) compared to Turgencin A are shown in bold, and sequences in parentheses denote Cys-Cys cyclic peptides. SI was calculated as the ratio between haemolytic activity (EC_{50}) and the geometric mean (GM) of the MIC values against all bacterial strains, i.e., SI = EC_{50}/GM.

		Peptide	Sequence	Mw [2]	Net Charge [3]	Rt [4]	Antimicrobial Activity (MIC) [1]										RBC Tox. (EC_{50})	SI
							Gram +				Gram −		GM	Fungi				
							Bs	Cg	Sa	Se	Ec	Pa		Ap	Ca	Rh		
Cyclic peptides		cTurg-1	(CGKKPGGWKC)KL-NH_2	1301.6	+5	3.11	256	16	>256	>256	>256	>256	161	32	128	64	nt [5]	nt
	W	cTurg-2	(CGKK**WW**GWKC)KL-NH_2	1519.9	+5	3.87	8	4	32	16	64	64	20	32	32	32	>1045	>52
		cTurg-3	(CGKK**W**G**W**WKC)KL-NH_2	1519.9	+5	3.92	4	4	32	16	32	128	18	32	32	32	849	47
		cTurg-4	(CGKKP**WW**WKC)KL-NH_2	1560.0	+5	3.97	8	4	64	32	64	256	32	32	64	32	>1065	>33
	R/W	cTurg-5	(CG**RRWW**G**W**R**R**C)**R**L-NH_2	1632.0	+5	3.98	8	4	16	8	8	16	9	32	32	32	>1101	>123
		cTurg-6	(CG**RRW**G**WW**R**R**C)**R**L-NH_2	1632.0	+5	4.02	4	4	16	8	8	16	8	32	32	32	1101	138
		cTurg-7	(CG**RRPWWW**R**R**C)**R**L-NH_2	1672.0	+5	4.09	4	4	16	8	16	32	10	32	32	32	197	20
Linear lipopeptides		C_8-Turg-1	C_8-CGKKPGGWKC KL-NH_2	1429.8	+4	4.38	8	4	128	32	32	128	29	32	128	16	>943	>33
		C_{10}-Turg-1	C_{10}-CGKKPGGWKC KL-NH_2	1457.9	+4	4.89	4	4	16	8	16	32	10	32	64	8	>957	>95
		C_{12}-Turg-1	C_{12}-CGKKPGGWKC KL-NH_2	1486.0	+4	5.44	4	4	8	4	8	16	6	32	64	8	>971	>153
	W	C_8-Turg-2	C_8-CGKK**WW**GWKC KL-NH_2	1648.1	+4	4.97	8	4	8	8	16	16	9	32	64	32	198	22
		C_{10}-Turg-2	C_{10}-CGKK**WW**GWKC KL-NH_2	1676.2	+4	5.41	8	4	8	8	8	16	8	32	64	32	64	8
		C_{12}-Turg-2	C_{12}-CGKK**WW**GWKC KL-NH_2	1704.2	+4	5.89	8	16	16	8	16	32	14	32	64	32	55	4
	R/W	C_8-Turg-6	C_8-CG**RRW**G**WW**R**R** **R**L-NH_2	1760.2	+4	5.07	4	4	16	8	8	32	9	128	64	128	54	6
		C_{10}-Turg-6	C_{10}-CG**RRW**G**WW**R**R** **R**L-NH_2	1788.2	+4	5.51	8	16	32	16	32	64	23	128	64	128	21	1
		C_{12}-Turg-6	C_{12}-CG**RRW**G**WW**R**R** **R**L-NH_2	1816.3	+4	5.98	16	16	32	16	64	128	32	128	64	>128	39	1
Cyclic lipopeptides		C_8-cTurg-1	C_8-(CGKKPGGWKC)KL-NH_2	1427.8	+4	4.27	4	4	128	32	32	128	25	64	64	8	>942	>37
		C_{10}-cTurg-1	C_{10}-(CGKKPGGWKC)KL-NH_2	1455.9	+4	4.74	2	2	16	4	8	32	6	32	64	4	>956	>151
		C_{12}-cTurg-1	C_{12}-(CGKKPGGWKC)KL-NH_2	1483.9	+4	5.22	2	2	4	4	4	16	4	32	64	4	219	55
	W	C_8-cTurg-2	C_8-(CGKK**WW**GWKC)KL-NH_2	1646.1	+4	4.70	2	2	4	4	4	8	4	16	32	4	439	123
		C_{10}-cTurg-2	C_{10}-(CGKK**WW**GWKC)KL-NH_2	1674.1	+4	5.11	2	4	4	4	8	8	5	32	64	16	106	24
		C_{12}-cTurg-2	C_{12}-(CGKK**WW**GWKC)KL-NH_2	1702.2	+4	5.55	4	8	8	8	16	16	9	32	64	32	32	4
	R/W	C_8-cTurg-6	C_8-(CG**RRW**G**WW**R**R**C)**R**L-NH_2	1758.2	+4	4.85	4	4	8	4	8	16	6	64	64	32	30	5
		C_{10}-cTurg-6	C_{10}-(CG**RRW**G**WW**R**R**C)**R**L-NH_2	1786.2	+4	5.28	4	4	8	8	16	16	8	64	64	32	16	2
		C_{12}-cTurg-6	C_{12}-(CG**RRW**G**WW**R**R**C)**R**L-NH_2	1814.3	+4	5.72	8	8	16	8	32	32	14	64	128	64	9	1
		Polymyxin B		1301.6	+5		3.1	3.1	12.5	6.3	3.1	3.1	161	3.1	12.5	3.1	nt	nt
		Chlorhexidine		505.5	+2		1.6	0.8	1.6	1.6	1.6	6.3	20	1.0	7.8	1.0	nt	nt

[1] Microbial strains; Bs—*Bacillus subtilis*, Cg—*Corynebacterium glutamicum*, Sa—*Staphylococcus aureus*, Se—*Staphylococcus epidermidis*, Ec—*Escherichia coli*, Pa—*Pseudomonas aeruginosa*, Ap—*Aurobasidium pollulans*, Ca—*Candida albicans*, Rh—*Rhodotorula* sp. [2] Average molecular mass without including a TFA salt for each cationic charge. [3] Net charge at physiological pH (7.4). [4] Hydrophobicity measured as retention time (Rt; min) on a RP-UPLC C_{18} column using a linear acetonitrile/water gradient. [5] nt: not tested.

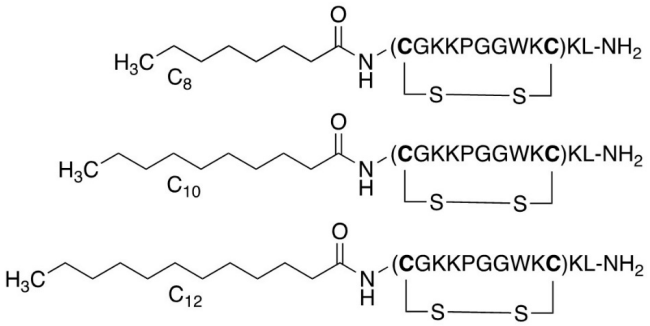

Figure 2. Lipopeptide modifications exemplified for **cTurg-1** lipopeptides containing C_8, C_{10} and C_{12} fatty acids.

Acylation was done with three aliphatic fatty acids: octanoic acid (C_8), decanoic acid (C_{10}) and dodecanoic acid (C_{12}), since these fatty acid were previously found to improve the antibacterial activity of various peptides [17]. Of note, similar, but two-residues shorter linear analogues of these peptides (based on Turgencin A residues 18–27) have been previously reported in literature, e.g., non-acylated peptides and those without the Cys-residues [13]. For the linear peptides **C_8-Turg-1**, **C_{10}-Turg-1** and **C_{12}-Turg-1** elongation of the lipid chain from 8 to 12 carbons resulted in an overall increase in antimicrobial activity (Table 1). The most potent linear lipopeptide was the longest acylated peptide **C_{12}-Turg-1** with a MIC of 4–16 μg/mL against all bacterial strains. The highest increase in antimicrobial activity following acyl chain elongation was observed against *S. aureus* with improvement in MIC from 128 to 8 μg/mL, and *P. aeruginosa* with improvement in MIC from 128 to 16 μg/mL. All three peptides **C_8-Turg-1**, **C_{10}-Turg-1** and **C_{12}-Turg-1** were non-haemolytic (EC_{50}: >943 μg/mL).

Regarding the more lipophilic peptide, **cTurg-2** (having a central WWG region), elongation of the N-terminal acyl chain of linear analogues had an opposite effect than that observed for the linear lipopeptides based on **cTurg-1** (PGG). In other words, for the lipopeptides **C_8-Turg-2**, **C_{10}-Turg-2** and **C_{12}-Turg-2**, increasing the length of the acyl chain resulted in peptides having the same or slightly reduced antimicrobial activity. One exception in this regard was the activity of **C_{10}-Turg-2** against *E. coli*, with a two-fold increased potency (MIC: 8 μg/mL) compared to **C_8-Turg-2** and **C_{12}-Turg-2** (MIC: 16 μg/mL). Thus, among the linear **Turg-2** lipopeptides, **C_8-Turg-2** and **C_{10}-Turg-2** showed the highest potency against both the Gram-positive (MIC: 4–8 μg/mL) and Gram-negative bacteria (MIC: 8–16 μg/mL). Of note, all three lipopeptides **C_8-Turg-2**, **C_{10}-Turg-2** and **C_{12}-Turg-2** showed the same antimicrobial activity against *B. subtilis* and *S. epidermidis* (MIC: 8 μg/mL). Compared to **C_8-Turg-1** and **C_{10}-Turg-1** (PGG core sequence), we observed improved antimicrobial activity for **C_8-Turg-2** and **C_{10}-Turg-2** (WWG core sequence) against *S. aureus*, *E. coli* and *P. aeruginosa*. However, **C_8-Turg-2**, **C_{10}-Turg-2** and **C_{12}-Turg-2** displayed increasingly higher haemolytic activity from EC_{50}: 198 to 55 μg/mL.

The linear lipopeptides based on the **cTurg-6** (WGW) sequence resulted in an even more noticeable reduction in antimicrobial activity following acyl chain elongation than that observed for the **C_8-Turg-2**, **C_{10}-Turg-2** and **C_{12}-Turg-2** lipopeptides. Compared to **cTurg-6**, the linear lipopeptide **C_8-Turg-6** showed a similar antibacterial effect. Further acyl chain elongation in **C_{10}-Turg-6** and **C_{12}-Turg-6** resulted in a significant decrease in potency, which was especially noticeable against *S. aureus* and the Gram-negative bacteria, *E. coli* and *P. aeruginosa* (MIC: 32–128 μg/mL). Additionally, **C_8-Turg-6**, **C_{10}-Turg-6** and **C_{12}-Turg-6** were all rather haemolytic (EC_{50}: 21–54 μg/mL). As expected, acyl chain elongation led to increased hydrophobicity for all three lipopeptide series, as monitored by their retention time on an RP-HPLC C_{18} column (Table 1).

2.4. Structure–Activity Relationship of Cyclic Lipopeptides

Our final modification included peptide cyclization of the previous series of lipopeptides by sidechain disulphide formation. In general, cyclization of the acylated peptides

resulted in some of the most potent peptides prepared and it had some unexpected effects on their haemolytic activity (Table 1). The antimicrobial activity of the cyclic lipopeptides **C_8-cTurg-1**, **C_{10}-cTurg-1** and **C_{12}-cTurg-1** was improved by increasing the acyl chain length. The latter lipopeptide, **C_{12}-cTurg-1,** was the most potent in this series with a two-fold increased antimicrobial activity against four out of six strains, compared to its linear analogue **C_{12}-Turg-1**. However, as opposed to **C_{12}-Turg-1**, the cyclic analogue **C_{12}-cTurg-1** displayed detectable haemolytic activity (EC_{50}: 219 μg/mL).

Similar to the linear lipopeptides, we observed a small reduction in antimicrobial activity following the increase in the acyl chain length for the cyclic analogues **C_8-cTurg-2**, **C_{10}-cTurg-2** and **C_{12}-cTurg-2**. Importantly, the cyclic lipopeptides in this series were more potent than their linear analogues. Moreover, this series included the overall most potent peptide prepared in this study, **C_8-cTurg-2,** with a MIC of 2–4 μg/mL against all Gram-positive bacterial test strains and *E. coli*, and a MIC of 8 μg/mL against *P. aeruginosa*. Cys-Cys sidechain cyclization had a positive effect on the overall antimicrobial activity, most likely due to the formation of a more rigid cyclic structure. Somewhat surprisingly, **C_8-cTurg-2** was considerably less haemolytic (EC_{50}: 439 μg/mL) than the linear precursor lipopeptides **C_8-, C_{10}- and C_{12}-Turg-2** (EC_{50}: 55–198 μg/mL)**.**

Cyclic lipopeptides **C_8-cTurg-6**, **C_{10}-cTurg-6** and **C_{12}-cTurg-6** were more potent than their linear analogues, but we also noticed a reduction in antimicrobial activity following the increase in the acyl chain length. Moreover, we observed an undesirable increase in haemolytic activity for this series of cyclic lipopeptides (EC_{50}: 9–30 μg/mL), which, in contrast to antimicrobial activity, increased following acyl chain elongation. These results clearly demonstrate that optimization of the peptide's activity involves a trade-off between achieving desired antimicrobial potency and minimizing unwanted toxicity against human RBCs.

2.5. SAR Summary

Our first series of cyclic peptides **cTurg-1**–**cTurg-7** demonstrated that substitution of Lys to Arg results in peptides with higher antimicrobial activity (Table 1). The cyclic Arg-modified peptides **cTurg-5**–**cTurg-7** were generally more potent than their Lys-containing counterparts **cTurg-2**–**cTurg-4**. The awareness of changes in haemolytic activity following Lys to Arg substitution is important, as shown for the Arg-modified cyclic peptide **cTurg-7** displaying weak haemolytic activity (EC_{50}: 197 μg/mL), whereas its Lys analogue, **cTurg-4,** as well as other Trp and Arg modified cyclic peptides were non-haemolytic (EC_{50}: $\geq$ 849 μg/mL).

For the linear lipopeptides **C_8-**, **C_{10}-** and **C_{12}-Turg-1**, as well as the cyclic lipopeptides **C_8-**, **C_{10}-** and **C_{12}-cTurg-1**, an increase in the number of carbons in the acyl chain resulted in increased potency of the corresponding analogues. A reverse trend was observed for both linear **C_8-**, **C_{10}-**, **C_{12}-Turg-2** and cyclic **C_8-**, **C_{10}-**, **C_{12}-cTurg-2** lipopeptides, as chain elongation beyond C_8 resulted in analogues with mostly unchanged potency (C_{10}-analogues), or even a two- to four-fold decrease in potency (C_{12}-analogues). A similar observation was made for the linear **C_8-**, **C_{10}-**, **C_{12}-Turg-6** and cyclic **C_8-**, **C_{10}-**, **C_{12}-cTurg-6** lipopeptides, where the greatest decrease in potency was observed against *E. coli* (MIC: from 8 μg/mL to 64 μg/mL). The sequences of the linear and cyclic **C_8-**, **C_{10}-**, **C_{12}-Turg-2/c-Turg-2** and **C_8-**, **C_{10}-**, **C_{12}-Turg-6/c-Turg-6** lipopeptides were more hydrophobic than that of **C_8-**, **C_{10}-**, **C_{12}-Turg-1/c-Turg-1**, due to their tryptophan-rich core sequence, which could, in part, explain the observed trend. As for the **C_8-**, **C_{10}-**, **C_{12}- Turg-1/c-Turg-1** lipopeptides, it remains unclear whether the C_{12}-chain conferred the threshold hydrophobicity, or whether this threshold could have been achieved by acylation with fatty acids containing more than 12 carbons. These results suggest that there might be an upper limit regarding hydrophobicity (threshold hydrophobicity) and that its further increase could have an unfavourable effect on antimicrobial activity, and in some cases even abrogate it entirely. This may occur, as proposed in a study done by Chu-Kung et al., when the minimal bactericidal concentration of the peptide is higher than its critical miscelle concentration [18]. Furthermore, studies have demonstrated that lipopeptides containing long fatty acid chains

tend to self-assemble, resulting in reduced antimicrobial activity [19,20]. Our findings give further credence to the assumption that hydrophobicity, easily tuned by lipidation, is an important factor influencing antimicrobial activity of peptides.

The direct correlation between haemolytic activity and hydrophobicity (mirrored in the acyl chain length) of the peptides was especially prominent for the linear **C_8-, C_{10}-, C_{12}-Turg-2** and **C_8-, C_{10}-Turg 6** lipopeptides, except for **C_{12}-Turg-6,** which had a slightly reduced haemolytic activity than its analogue with **C_{10}** fatty acid chain (Table 1). This trend was not observed for **C_8-, C_{10}-Turg-1**, and its cyclic analogues, as they were all non-haemolytic. In general, cyclic lipopeptides were more haemolytic compared to their linear analogues. These results support previous findings that lipopeptides with longer acyl chains have higher haemolytic activity, most likely due to their lower membrane selectivity [21,22].

While the effect of lipidation is shown to be bidirectional, depending on the initial hydrophobicity of the peptides, among other things, intramolecular cyclization led to increased antimicrobial activity of linear lipopeptides regardless of their primary sequence. For all cyclic lipopeptides synthesized in this work, the potency was either unchanged or improved four-fold, compared to their corresponding linear analogues. It should be noted that changes in the position of the acylation may also have bearing on the potency of lipopeptides, as well as head-to-tail cyclization, two strategies that remain to be explored. Our results are in line with previous research showing that acylation and intramolecular cyclization are useful tools important for fine-tuning antimicrobial and haemolytic activity of AMPs [17].

2.6. Antifungal Activity

The synthesised peptides were screened for antifungal activity against the molds *Aurobasidium pollulans* and *Rhodotorula* sp., and the yeast *Candida albicans*. All cyclic peptides of the **cTurg-1**–**cTurg-7** series displayed almost equal antifungal activity (MIC: 32–128 μg/mL) against all three fungi tested (Table 1). Even **cTurg-1,** containing the original Turgencin A core sequence, displayed antifungal activity against all strains at concentrations below the MIC against bacteria (except for *C. glutamicum*). None of the peptides of this series stood out as more potent than the others, indicating that the amino acid substitutions in the central core sequence are not important for antifungal activity.

All linear and cyclic lipopeptides prepared in this study displayed antifungal activity. In general, their MIC values ranged from 32 to 128 μg/mL against *A. pullulans* and *C. albicans*, making it difficult to conclude any structure–activity relationship for the peptides against these strains. The activity against *Rhodothorula* sp. varied more between the different peptides with MIC values from 4 to >128 μg/mL. The cyclic lipopeptides **C_8-, C_{10}-** and **C_{12}-cTurg-1** were somewhat more potent against *Rhodothorula* sp. compared to the linear lipopeptides **C_8-, C_{10}-** and **C_{12}-Turg-1**, while the longer C_{10}/C_{12} analogues (MIC: 4 μg/mL) were slightly more potent compared to the corresponding C_8 analogues. The linear lipopeptides **C_8-, C_{10}-** and **C_{12}-Turg-2** were equally potent (MIC: 32 μg/mL) against *Rhodothorula* sp. However, among the cyclic lipopeptides, **C_8-cTurg-2** was the most potent peptide (MIC: 4 μg/mL), followed by **C_{10}-cTurg-2** (MIC: 16 μg/mL) and **C_{12}-cTurg-2** (MIC: 32 μg/mL). These results support the antibacterial data, indicating an upper limit regarding lipophilicity. Among all lipopeptides tested, **C_8-cTurg-2** was the most potent peptide against *A. pullulans* (MIC: 16 μg/mL). The linear lipopeptides **C_8-, C_{10}-** and **C_{12}-Turg-6** were overall the least potent with MIC-values of 64 to >128 μg/mL against all test strains, but with a two- to four-fold increase in potency for their cyclic versions (**C_8-, C_{10}-** and **C_{12}-cTurg-6**) against *A. pullulans* and *Rhodothorula* sp.

2.7. Selectivity Index

The selectivity index (SI) of the peptides towards bacteria over eukaryotic cells was calculated using the geometric mean (GM) of the MIC values against all bacterial test strains, according to the method by Orlov et al. [23]. The SI for each peptide was determined as the ratio of the RBC-EC_{50} value by the corresponding GM value. Larger SI values indicate greater

selectivity for microbial cells [24]. As shown in Table 1, **cTurg-6** had the highest selectivity of the cyclic peptides (**cTurg-1** to **cTurg-7**), with an SI value of 138 for all bacterial strains tested. Interestingly, two of the lipopeptides, **C_{10}-cTurg-1 and C_{12}-Turg-1,** emerged as a promising candidates for further optimization, both having SI values for bacteria above 150. In addition, **C_8-cTurg-2** showed the best selectivity profile among both cyclic and linear lipopeptides derived from the **cTurg-2** series. In general, the SI was higher against the Gram-positive bacteral strains than the Gram-negative strains. (Table S3). Overall, peptides displaying EC_{50} < 100 μg/mL were considered too haemolytic to be of interest for further exploration.

2.8. Effects on Bacterial Viability and Membrane Integrity

We used two luciferase-based assays to investigate whether the synthesized peptides had an immediate effect on bacterial viability and membrane integrity. Changes in light emission of sensor bacteria constitutively expressing the bacterial lux operon or a eukaryotic luciferase can be used as a proxy for viability and membrane integrity, respectively [25]. Light production of the viability biosensors represents metabolic activity of the bacteria. For the membrane integrity assay on the other hand, light production depends on the influx of the externally added D-luciferin, which at neural pH will not readily pass the intact plasma membrane. An initial increase in light production therefore corresponds with damage to the plasma membrane and a concomitant influx of D-luciferin, while a subsequent drop in light emission indicates diminishing ATP reserves of the dying sensor bacteria.

Here we present the results for the two most potent cyclic lipopeptides, **C_{12}-cTurg-1** and **C_8-cTurg-2,** as well as for the membrane active agent chlorhexidine (CHX) that was used for comparison (Figures 3 and 4). The results for the remaining peptides can be found in the Supporting information, Figures S26–S33. The overall results for **C_{12}-cTurg-1** and **C_8-cTurg-2** in *B. subtilis* 168 show that increasing concentrations resulted in a decrease in light emisssion (and in increasing rates), suggesting a dose-dependent effect on viability (Figure 3).

In order to confirm that the observed decrease in viability was the result of membrane damage, we used the membrane integrity assay [13,25]. The results of the membrane integrity assay for *B. subtilis* 168 show that increasing lipophilicity of the cyclic lipopeptides **C_8-, C_{10}-,** and **C_{12}-cTurg-1** caused increased membranolytic activity. A rapid and strong membrane disruptive effect was observed for the highly potent **C_{12}-cTurg-1** peptide (Figures 3 and S27). When analysing the membrane integrity effects of the cyclic lipopeptides **C_8-, C_{10}-** and **C_{12}-cTurg-2**, increasing lipophilicity was also concordant with increased membrane activity, but not to a greater extent than for the **C_8-, C_{10}-** and **C_{12}-cTurg-1** peptides. We observed a minor effect on increased lipophilicity on the membrane activity of **C_8-, C_{10}-** and **C_{12}-cTurg-2** and **C_8-, C_{10}-** and **C_{12}-cTurg-6** cyclic lipopetides, as they showed somewhat similar activity, showing a rapid decrease in light production, from concentrations 50 to 12.5 μg/mL (Figures 3 and S29). At the lowest concentration, close to the MIC value of 2 μg/mL for all tested peptides, we observed minor changes in membrane activity and viability, most likely due to the high concentration of bacterial inoculum (1000-fold greater than that used for the MIC assay). This could explain why higher concentrations of the peptides were needed to see a more pronounced effect. However, at higher concentrations, the membranolytic action for some lipopeptides was so rapid (< 3 s) that the luminescence peak could not be detected, as the signal started declining even before the first measurement was made. This phenomenon was observed for **C_{12}-cTurg-1** and **C_8-cTurg-2** (at the highest test concentrations of 25 μg/mL and 50 μg/mL), indicating a more rapid or even different mechanism for disruption of membrane integrity than that of chlorhexidine (Figure 3).

The viability and membrane integrity assay results for *E. coli* K12 were quite different from what was observed for *B. subtilis*. For both **C_{12}-cTurg-1** and **C_8-cTurg-2,** we observed a gradual, dose-dependent reduction in viability in *E. coli*, although not as prominent as for *B. subtilis*. In the membrane integrity assay, **C_{12}-cTurg-1** showed a delayed, 3.5-fold rise in luminescence at the highest test concentration (50 μg/mL) compared to chlorhexidine, with a subsequent decline in luminescence during the assay timeframe (Figure 4). A

further delayed response was observed for **C_{12}-cTurg-1** at 25 µg/mL, whereas no effect was observed at lower concentrations. **C_8-cTurg-2** gave an even further delayed rise in peak luminescence in the membrane integrity assay, but only at the highest test concentration of 50 µg/mL (Figure 4). Although **C_{12}-cTurg-1** and **C_8-cTurg-2** displayed similar MIC values of 4 µg/mL against *E. coli* (ATCC 25922) in the screening assay run for 24 h, the results from the membrane integrity assay with *E. coli* K12 indicate a different mode of membrane disruption. This might suggest that the peptides were acting on the outer LPS and inner cytoplasmic membranes of *E. coli* at different rates, resulting in their delayed action observed in both the viability and membrane integrity assays.

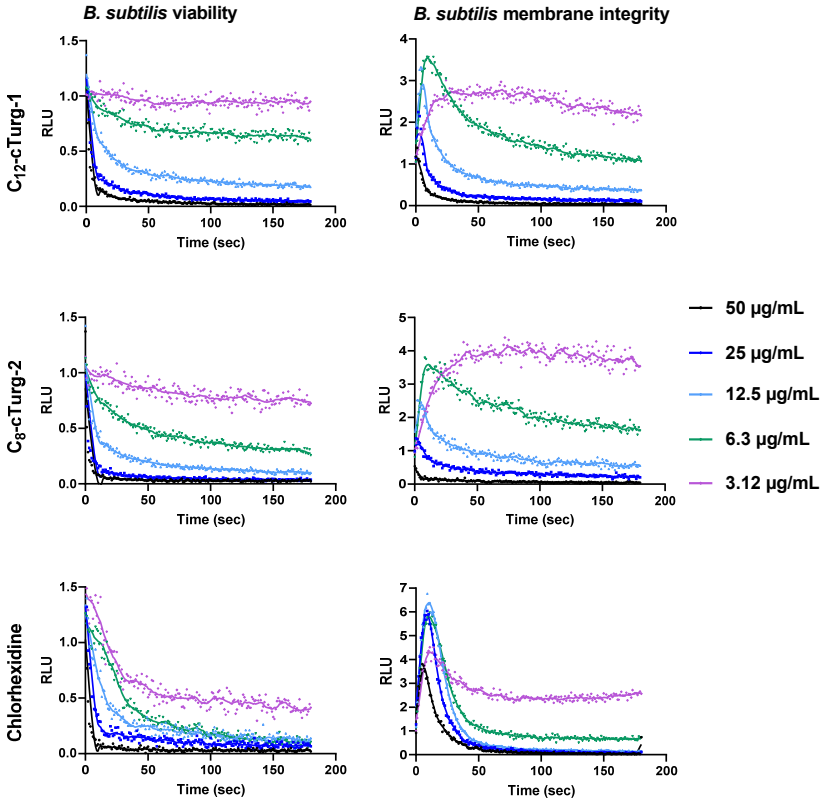

Figure 3. Effects of **C_{12}-cTurg-1**, **C_8-cTurg-2** and chlorhexidine on the kinetics of viability (**left**) and membrane integrity (**right**) in *B. subtilis* 168. Light emission normalized to the untreated water control is plotted as relative luminescence emission (RLU) over time (seconds). Kinetics of the immediate effect (within 3 min) on bacterial viability and membrane integrity, as measured by relative luminescence emission in *B. subtilis* 168 treated with increasing concentrations of the lipopeptides. Chlorhexidine served as a positive (membranolytic) control and water as a negative (untreated) control. All the graphs of this figure show a representative data set where each experiment was run at least three times independently.

2.9. Effects on E. coli Mutant Strain with an Impaired Outer Membrane

Antimicrobial activity of all synthesised cyclic peptides were determined against two additional *E. coli* strains: the hyperpermeable mutant strain NR698, and its isogenic wild type (WT) MC4100 (Table 2). The outer membrane deficiency of the mutant strain *E. coli* NR698 is based on the allele *imp*4213/*lptD*4213 constituting an in-frame deletion of the *imp* (increased membrane permeability) gene in *E. coli* [26]. It has been shown that *imp* mutations make the outer membrane more permeable to antibiotics like vancomycin, which normally does not readily cross the outer membrane barrier of *E. coli*. In addition, this mutation is also suggested to cause defects in LPS assembly [27,28]. The results from the previous screening against the laboratory strain *E. coli* ATCC 25922 are included in Table 2 for comparison and show that both the WT and mutant NR698 strains were in many cases more sensitive to the cyclic peptides than the *E. coli* ATCC 25922 laboratory strain.

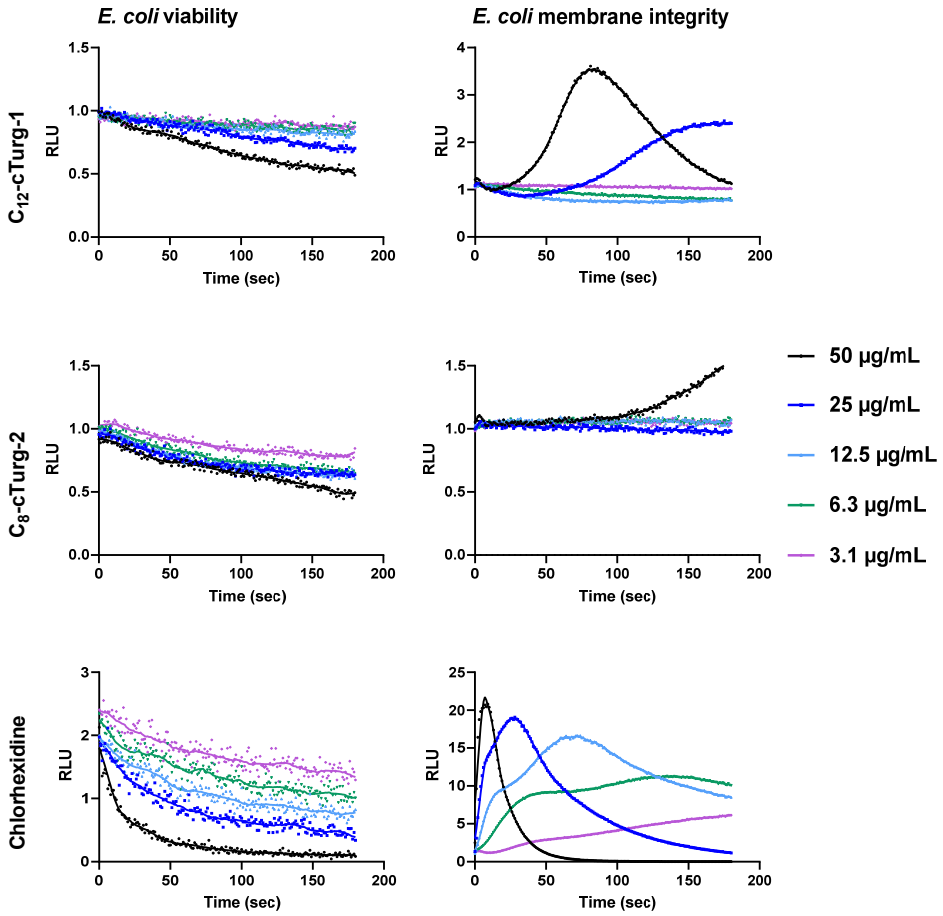

Figure 4. Effects of **C_{12}-cTurg-1**, **C_8-cTurg-2** and chlorhexidine on the kinetics of viability (**left**) and membrane integrity (**right**) in *E. coli* K12. Light emission normalized to the untreated water control is plotted as relative luminescence emission (RLU) over time (seconds). After addition of the bacterial inoculum (mixed with 1 mM D-luciferin in the membrane assay) to the wells, preloaded with lipopeptides, the light emission was measured each second for three min. Each colored line represents the total 180 s data points (mean of three independent measurements) from the assay at different concentration of the lipopeptides.

The cyclic peptide **cTurg-1,** containing the native Turgencin A core sequence, was found to be active against the mutant NR698 strain (MIC: 64 µg/mL). However, against the WT strain and the *E. coli* ATCC 25922 laboratory strain it showed no activity (Table 2). In contrast to **cTurg-1,** Trp-modified cyclic peptides **cTurg-2** to **cTurg-4** displayed increased antimicrobial activity against all three *E. coli* strains, among which the mutant NR698 was most sensitive. Thus, for these peptides, the outer membrane appeared to hinder their antimicrobial effect. For the analogous, Arg-modified cyclic peptides **cTurg-5** to **cTurg-7**, no major differences in antimicrobial activity were observed against the three *E. coli* strains (MIC: 8–16 µg/mL), making these peptides seemingly less affected by the outer LPS membrane.

With regard to the cyclic lipopeptides (Table 2), the potency against the mutant strain NR698 showed the same trend as previously described (SAR section), although with lower MIC values. In brief, according to SAR, improved potency was achieved by increasing the acyl chain length for the cyclic lipopeptides **C_8-**, **C_{10}-** and **C_{12}-cTurg-1**, while the opposite trend was observed for **C_8-**, **C_{10}-** and **C_{12}-cTurg-2** and **C_8-**, **C_{10}-** and **C_{12}-cTurg-6**. The results for the WT MC4100 strain are also in accordance with our previous SAR observations, but to a lesser degree than for the other two strains. These results clearly demonstrate that structural modifications can optimize target interactions and antibacterial potency as seen for example in **C_{12}-cTurg-1, which** displays similar high potency against all three strains (MIC: 2–4 µg/mL).

Table 2. Antimicrobial activity (MIC in μg/mL) of cyclic peptides and selected antibiotics against three strains of *E. coli* for investigation of effects concerning outer membrane permeability. In addition to the laboratory strain *E. coli* ATCC 25922, the activity against *E. coli* MC4100 (wild type, WT) and the outer membrane permeable mutant *E. coli* NR698 was measured and compared.

			***E. coli* Strains**		
		Peptide	**ATCC 25922 (from Table 1)**	**MC4100 (WT)**	**NR698 [1] (mutant)**
Cyclic peptides		cTurg-1	>256	>256	64
	W	cTurg-2	64	16	8
		cTurg-3	32	16	8
		cTurg-4	64	16	8
	R/W	cTurg-5	8	8	8
		cTurg-6	8	8	8
		cTurg-7	16	8	8
Cyclic lipopeptides		C_8-cTurg-1	32	16	8
		C_{10}-cTurg-1	8	8	4
		C_{12}-cTurg-1	4	4	2
	W	C_8-cTurg-2	4	8	2
		C_{10}-cTurg-2	8	8	4
		C_{12}-cTurg-2	16	8	8
	R/W	C_8-cTurg-6	8	8	8
		C_{10}-cTurg-6	16	8	8
		C_{12}-cTurg-6	32	16	16
Antibiotics		Polymyxin B	3.1	0.8	0.2
		Chlorhexidine	1.6	0.3	0.3
		Vancomycin	125	64	0.3
		Ampicillin	8	8	0.3
		Chloramphenicol	1.8	12.5	3.1

[1] *E. coli* MC4100 NR698 *imp*4213 (with deficient outer membrane).

In order to more closely evaluate the effect of an outer membrane on antimicrobial activity of synthesised peptides, we tested several commercially available antibiotics. Major improvement in antimicrobial activity was achieved against the mutant NR698 strain compared to the WT strain when treated with polymyxin B, vancomycin, ampicillin and chloramphenicol (Table 2). Compared to these antibiotics, several of the present cyclic peptides, such as **C_{12}-cTurg-1** and **C_8-cTurg-2**, showed similar or higher antibacterial activity against the *E. coli* ATCC 25922 and WT strains. In summary, the overall higher antibacterial activity against the mutant NR698 strain supports the hypothesis that the outer LPS membrane present in the WT strains could act as a barrier, limiting the effect of the synthesised peptides. This, in turn, may have affected the rate of bacterial membrane disruption as observed in the viability and membrane integrity studies.

2.10. Permeabilization of the Outer Membrane of E. coli

The outer membrane of Gram-negative bacteria acts as a barrier for many hydrophobic and larger hydrophilic substances (>600 Da) [29]. However, some peptides can sensitize the outer membrane and thus facilitate the entry of various hydrophobic molecules. To explore if the peptides affect the outer membrane of *E. coli* MC4100, **C_{12}-cTurg-1** and **C_8-cTurg-2** were tested for their ability to enable the entry of the hydrophobic fluorescent probe 1-*N*-phenylnapthylamine (NPN, MW of 219 Da) (Figure 5). In aqueous solutions, NPN shows very low fluorescence, which greatly increases upon interaction with the hydrophobic environment of biological membranes. Normally, the hydrophobic NPN is excluded by *E. coli* bacteria, but it can enter the bacteria once the integrity of the outer membrane is compromised. In this assay, both cyclic lipopeptides, **C_{12}-cTurg-1** and **C_8-cTurg-2**, as well as chlorhexidine, were found to increase the NPN fluorescence in a concentration-dependent manner (Figure 5), but at a slightly different rate, via membrane permeabilization. The stronger effect for **C_{12}-cTurg-1**, with almost a four-fold increase in both fluorescence and

luminescence for the concentrations of 25 to 50 µg/mL, suggests that **C_{12}-cTurg-1** disrupts both the outer and the inner membrane at a similar rate at higher concentrations (6.3–12.5 × MIC). In contrast, **C_8-cTurg-2** was found to alter the outer membrane permeability at concentrations that did not initially give any increase in luminescence in the inner membrane integrity assay (Figures 4 and 5). Thus, the observed effects indicate that the outer membrane passage of **C_8-cTurg-2** was a rate-limiting step that was most likely preventing the peptide from reaching and accumulating in the inner membrane.

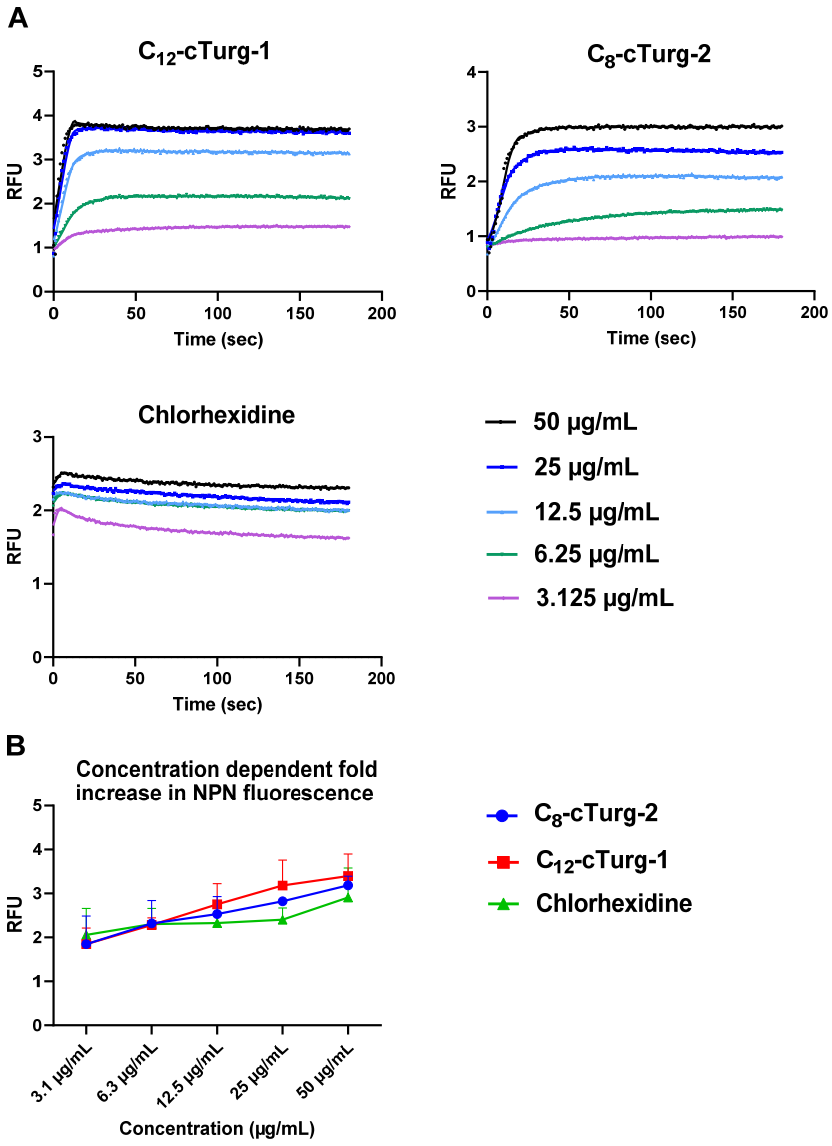

Figure 5. (**A**) Comparison of the effects of **C_{12}-cTurg-1**, **C_8-cTurg-2** and chlorhexidine on the kinetics of NPN fluorescence in *E. coli* MC4100 (WT). After addition of the bacterial inoculum (mixed with 20 µM NPN) to the wells (preloaded with lipopeptides), light emission was measured each second for 3 min. Each colored line represents the total 180 s data points from the assay at different concentrations. Each figure shows a representative data set. (**B**) *E. coli* MC4100 grown in MH media were treated with different concentrations of **C_{12}-cTurg-1**, **C_8-cTurg-2** and chlorhexidine. The permeability of the outer membrane was assessed by measuring the fluorescence of NPN after 3 min (mean of three independent measurements). In all data sets, fluorescence values were compared to bacterial cells treated with the same amount of Mill-Q water control.

2.11. Bacterial Killing Experiments

The two most potent lipopeptides (**C_{12}-cTurg-1** and **C_8-cTurg-2**) were selected for bacterial killing experiments to see whether the peptides displayed bacteriostatic or bactericidal effects on the bacterial inoculum used in the MIC assay. In this experiment, 10 µL aliquots from the wells containing peptide-treated bacteria were harvested after the MIC assay (24 h incubation), and 10-fold serially diluted and spotted on MH agar plates for colony counting. At their half-MIC concentration, slightly less colony-forming units (CFU) were formed for both *S. aureus* (ATCC 9144) and *E. coli* (ATCC 25922) in the presence of **C_{12}-cTurg-1** and **C_8-cTurg-2**, compared to the growth control (Figure 6). No CFU were observed at their MIC (or concentrations above MIC). These results show that the peptides displayed a bactericidal action on the bacterial strains tested.

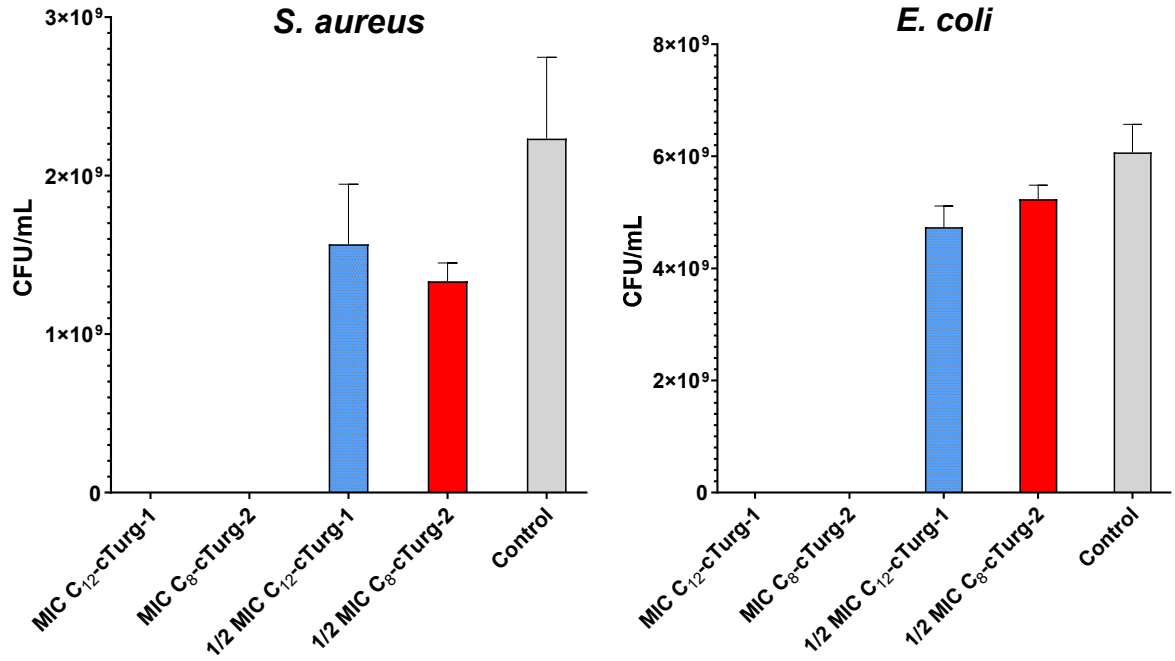

Figure 6. Bactericidal activity of **C_{12}-cTurg-1** and **C_8-cTurg-2** against *S. aureus* and *E. coli.* Colony-forming units (CFU) per mL bacterial inoculum were counted after treatment with MIC (4 µg/mL), 1/2 × MIC and no treatment (Control). Each bar presents the mean of three replicates ± SD.

3. Materials and Methods

3.1. Peptide Synthesis

All reagents and solvents were purchased from commercial sources and used as supplied. All peptides were synthesized using standard Fmoc-solid phase methodology using a Rink Amide ChemMatrix resin (loading 0.50 mmol/g). The resin was pre-swelled in *N*,*N*-dimethylformamide (DMF, 4.5 mL) for 20 min at 70 °C. The Fmoc-protected amino acids (4.0 eq.), saturated fatty acids (4.0 eq.) and O-(6-chlorobenzotriazol-1-yl)*N*,*N*,*N*′,*N*′-tetramethyl-uroniumhexafluorophosphate (HCTU, 4 eq.) were dissolved in DMF to a concentration of 0.5 M, 0.5 M and 0.6 M, respectively. *N*,*N*-Diisopropylethylamine (DIEA, 8 eq.) was dissolved in *N*-methyl-2-pyrrolidone (NMP) to a concentration of 2.0 M. Coupling steps for all amino acids except cysteine were performed under microwave conditions at 75 °C, for 10 min. To avoid racemization of Cys and Arg side-reaction due to microwave heating, Fmoc-Cys(Trt)-OH and Fmoc-Arg(Pbf)-OH were coupled at r.t. for 60 min. For the N-terminally acylated lipopeptides, the coupling reaction with HCTU was performed twice to ensure successful attachment of the acyl chain to the peptides. Following each coupling step, the resin was washed 4 times with DMF (4.5 mL) for 45 s. After the desired linear peptide was assembled, the resin was washed first with dichloromethane (DCM,

4.5 mL) for 45 s (6 times), and then with diethyl ether (3–4 times). The resin was dried on a vacuum manifold and placed in a desiccator overnight.

3.2. Fmoc Deprotection

The peptides were deprotected and cleaved from the resin using a standard cleavage cocktail consisting of trifluoracetic acid (TFA), Milli-Q ultrapure water, 1,2-ethanedithiol (EDT) and triisopropylsilane (TIS) (TFA/water/EDT/TIS; 94/2.5/2.5/1.0 (*v/v/v/v*) at room temperature. The cleavage procedure was repeated twice, each time with 10 mL of the cleavage mixture under occasional stirring. Following the first 3 h cleavage step, the resin was collapsed with a small amount of DCM, and then washed with diethyl ether. The second cleavage step was performed with the same amount of cleavage cocktail (10 mL) for an additional 1 h. After each cleavage step, as well as after addition of DCM and diethyl ether, the resin was dried under a vacuum. The collected filtrates containing the desired peptide were pooled into a round bottom flask and the solvents were evaporated, resulting in a thin, glassy film covering the walls of the flask. Precipitation of the peptides was induced by the addition of ice-cold diethyl ether, which was decanted after 24 h. This procedure was repeated twice, and the residual diethyl ether was evaporated before purification.

3.3. Peptide Purification by Preparative Reversed-Phase High-Performance Liquid Chromatography (RP-HPLC)

Crude peptide purification was performed by RP-HPLC using a preparative SunFire C_{18} OBD, 5 µm, 19 × 250 mm column (Waters, Milford, MA, USA at room temperature. The HPLC system (Waters) was equipped with a 2702 autosampler, a 2998 photodiode array (PDA) detector and an automated fraction collector. The lipopeptides were purified using a linear gradient of eluent A (water with 0.1% TFA) and eluent B (acetonitrile with 0.1% TFA), ranging from 20–60% B, over 25 min, at a flow rate of 10 mL/min. Purified fractions were collected and freeze-dried prior to further characterization.

3.4. Peptide Characterization by High-Resolution Mass Spectrometry (HRMS)

The purified peptides were characterized by HRMS using an Orbitrap Id-X Tribrid mass analyser equipped with an electrospray ionization (ESI) source (Thermo Fischer Scientific, Waltham, MA, USA), with a Vanquish UHPLC system (Waters), coupled to an Acquity Premier BEH C_{18}, 1.7 µm, 2.1 × 100 mm column (Waters). The ESI mass spectra were obtained in positive ion mode. Prior to analysis, all samples were dissolved in 1 mL of Milli-Q water. The lipopeptides were eluted with a 0.5–95.0% linear gradient of the eluent B (A: water with 0.1% formic acid, B: acetonitrile with 0.1% formic acid) over 10 min, with a flow rate of 0.5 mL/min. The injection volume was 2 µL, and the column temperature was set to 60 °C.

3.5. Purity Determination by Ultra-Performance Liquid Chromatography (UPLC)

Purity of the synthetized peptides was determined using an analytical UPLC-PDA H-class system (Waters, Milford, MA, USA). The analysis was conducted on an Acquity UPLC BEH 1.7 µm, 2.1 ×100 mm C_{18} column, using a linear gradient of eluent A (water with 0.1% TFA) and eluent B (acetonitrile with 0.1% TFA), ranging from 0.5–95.0% B, over 10 min. The flow rate was set to 0.5 mL/min and the temperature of the column was set to 60 °C. A 2996 PDA detector with a wavelength ranging from 210–400 nm was used to record the UV absorbance of the purified peptides. Retention times for each peptide were recorded as a measurement of hydrophobicity.

3.6. Cys-Cys Cyclization

The cyclization process included intramolecular disulphide formation between the sulfhydryl (SH) side chains of two cysteine residues, Cys17 and Cys26. This step was performed on a parallel reaction station, either under open air or with a continuous supply of oxygen by careful bubbling. The lipopeptides (5 mg) were dissolved in Milli-Q water

to a concentration of 250 μg/mL. The reaction proceeded at room temperature under continuous magnetic stirring. The progress of the reaction was monitored by UPLC-HRMS. Upon completion of the reaction, peptide solutions were lyophilized, and their purity determined as described above.

3.7. Antibacterial Minimum Inhibitory Concentration (MIC) Assay and Killing Assay

All cyclic and linear peptides were screened for antibacterial activity against four Gram-positive strains: *B. subtilis* (Bs, ATCC 23857), *C. glutamicum* (Cg, ATCC 13032), *S. aureus* (Sa, ATCC 9144) and *S. epidermidis* RP62A (Se, ATCC 35984), and two Gram-negative strains: *E. coli* (Ec, ATCC 25922) and *P. aeruginosa* (Pa, ATCC 27853). The activity was assessed using a broth microdilution assay according to a modified CLSI-based method [30]. Briefly, overnight bacterial cultures were grown in Mueller–Hinton (MH) broth medium (Difco Laboratories, Detroit, MI, USA) for 2 h at room temperature. The optical density (OD_{600}) was measured, and the bacterial suspensions were adjusted to 2.5–3 × 10^4 CFU/mL in MH medium. The bacterial suspension (50 μL) was distributed in 96-well plates (Nunc, Roskilde, Denmark) preloaded with two-fold dilution series (256 to 1 μg/mL) of peptide solutions (50 μL), giving a final well volume of 100 μL. The microplates were incubated in an EnVision 2103 microplate reader (PerkinElmer, Llantrisant, UK) at 35 °C, with OD_{595} recorded every hour for 24 h. MIC was defined as the lowest concentration of peptides showing an optical density less than 10% of the negative (growth) control, consisting of bacterial suspension and water. Polymyxin B sulfate (Sigma-Aldrich, St. Louis, MO, USA) and chlorhexidine acetate (CHX, Fresenius Kabi, Halden, Norway), both with concentrations ranging from 12.5 to 0.09 μg/mL, served as positive (growth inhibition) controls. All peptides were tested in triplicate.

A killing experiment was performed on selected lipopeptides by using actively growing cultures of *S. aureus* (ATCC 9144) and *E. coli* (ATCC 25922). The procedure was performed as previously described [31]. Briefly, after 24 h of peptide treatment (MIC assay, as described above), aliquots (10 μL) of 10-fold serial dilutions (in MH broth) of wells containing 1/2 , 1 and 2 × MIC of the peptides (with bacteria) were plated on MH Agar (Difco) plates. The number of colony-forming units (CFU) was determined after 24 h of incubation at 37 °C. The tests were performed in triplicate.

3.8. Antifungal MIC Assay

The synthesized peptides were screened for antifungal activity against the molds *A. pullulans* (Ap) and *Rhodotorula* sp. (Rh) (both obtained from Professor Arne Tronsmo, The Norwegian University of Life Sciences, Ås, Norway) and the yeast *C. albicans* (Ca, ATCC 10231) as previously described [13]. In short, fungal spores were grown in potato dextrose broth media (Difco) containing 2% D(+)-glucose (Merck, Darmstadt, Germany) at 25–30 °C while shaking at 200 rpm overnight. The cultures were diluted with a dextrose media containing glucose to a concentration of approx. 4 × 10^5 spores/mL. Aliquots of the cultures (50 μL) were transferred to 96 well microtiter plates preloaded with the synthetic peptides (50 μL) in two-fold serial dilutions (256 to 1 μg/mL). Polymyxin B and CHX (both with concentrations ranging from 12.5 to 0.09 μg/mL) served as positive antibiotic controls. The microtiter plates containing the fungal spores and the test peptides were incubated at room temperature for 48 h and OD_{600} was recorded using a Synergy H1 Hybrid microplate reader system (BioTek, Winooski, VT, USA). MIC was defined as the lowest peptide concentration showing an optical density less than 10% of the negative (growth) control. All experiments were performed in triplicate.

3.9. Haemolytic Activity Assay

The synthetized lipopeptides were screened for haemolytic activity against human red blood cells (RBC), in concentrations ranging from 500 to 3.9 μM, following a previously described protocol [32]. In brief, haemolysis was determined using a heparinizied (10 IU/mL) fraction of freshly drawn human blood. A second fraction of blood, which

was collected in test tubes containing ethylenediaminetetraacetic acid (EDTA, Vacutest, KIMA, Arzergrande, Italy), was used for determination of the hematocrit (hct). Plasma was removed from heparinized blood by washing three times with prewarmed phosphate-buffered saline (PBS) before being adjusted to a hematocrit of 4%. Peptides dissolved in dimethyl sulfoxide (DMSO) were further diluted with PBS to a final DMSO content of $\leq$1%. Triton X-100 (Sigma-Aldrich, St. Louis, MO, USA), used at a final concentration of 0.1%, served as a positive control for 100% haemolysis, whereas 1% DMSO in PBS buffer served as a negative control where no toxicity was detected. Duplicates of test solutions and erythrocytes, with 1% hct final concentration, were prepared in a 96-well polypropylene V-bottom plate (Nunc, Fischer scientific, Oslo, Norway). They were incubated under agitation at 37 °C and 800 rpm for 1 h. After centrifugation (5 min, 3000$\times$ *g*), 100 µL from each well were transferred to a flat-bottomed 96-well plate and absorbance was measured at 545 nm with a microplate reader (SpectraMax 190, Molecular Devices, San Jose, CA, USA). After subtracting PBS background, the percentage of haemolysis was calculated as the ratio of the absorbance in the peptide-treated and surfactant-treated samples. Three independent experiments were performed, and EC_{50} (the concentration giving 50% haemolysis) values are presented as averages.

3.10. Bacterial Biosensor Membrane Integrity Assay

A membrane integrity assay was performed using two bacterial biosensors, *B. subtilis* 168 (ATCC 23857) and *E. coli* K12 (ATCC MC1061). Both strains carry the pCSS962 plasmid that contains a eukaryotic luciferase gene (*lucGR*), which originate from the click beetle *Pyrophorus plagiophthalamus* [33]. The assay was performed as described previously [13]. Briefly, overnight cultures grown in MH media in the presence of respective antibiotics such as 5 µg/mL chloramphenicol (Merck, Darmstadt, Germany) for *B. subtilis* and both 20 µg/mL chloramphenicol and 100 µg/mL ampicillin (Sigma-Aldrich) for *E. coli*, were further diluted in fresh MH media without antibiotics and grown until they reached an OD_{600} of 0.1. D-luciferin potassium salt (Synchem Inc., Elk Grove Village, IL, USA) was added to the cell suspension at a final concentration of 1 mM. Two-fold dilutions (final assay concentration of 50–1.56 µg/mL) of peptides dissolved in Milli-Q water were prepared and added (10 µL per well) to black round-bottom 96-well microtiter plates (Nunc). Milli-Q water served as a negative control used for the normalization purpose and CHX, having known membranolytic activity, was used as a positive control. The plates were loaded into a Synergy H1 Hybrid Reader and the background luminescence was monitored before aliquots (90 µL) of the cell suspension with D-luciferin were added, one well at the time, by an automatic injector. Light emission was recorded every second for 3 min. Each study was performed at least three times independently, and the figures show a representative dataset.

3.11. Bacterial Biosensor Viability Assay

Bacterial viability, based on light production by constitutively expressed bacterial luciferase, was measured in real time according to the method described by Hansen et al. [13]. The assay was performed using *B. subtilis* 168 with chromosomally integrated *lux*ABCDE operon and *E. coli* K12 carrying the plasmid pCGLS-11 containing the *lux*CDABE operon. The assay set up was the same as for the membrane integrity assay, with the exception that *B. subtilis* 168 and *E. coli* colonies were grown in MH media supplemented with 5 µg/mL chloramphenicol and 100 µg/mL ampicillin, respectively. No D-luciferin was added to the cell suspension. Each assay was performed at least three times independently, and the figures show a representative dataset.

3.12. Screening for Activity against E. coli Mutants

MIC values were determined for all cyclic peptides against two *E. coli* strains: wild type (WT) MC4100 and the hyperpermeable variant NR698, having a deficient outer membrane. The NR698 strain, containing *lptD*4213/*imp*4213 mutation, was kindly provided by M. Grabowicz (Emory University School of Medicine, Rollins Research Center, Atlanta, GA,

USA) [28]. The assay was performed in the same way as previously described for the antibacterial MIC assay. Vancomycin hydrochloride (Hospira Enterprises BV, Almere, The Netherlands) and ampicillin: inhibitors of peptidoglycan synthesis, chloramphenicol: inhibitor of protein synthesis, and CHX and polymyxin B: membrane active compounds, were used as reference antibiotics to evaluate the permeability defects in *E. coli* NR698.

3.13. Outer Membrane Permeability Assay

The permeability of the *E. coli* outer membrane was analysed by measuring increased fluorescence as kinetics of 1-N-phenylnaphthylamine (NPN, Sigma-Aldrich) uptake following the protocol described by [34], with minor modifications. Briefly, a single colony of *E. coli* MC4100 (WT) was suspended in MH medium and incubated overnight at 37 °C with shaking (225 rpm). The culture was diluted in MH medium and adjusted to OD_{600} = 0.1 and incubated at 37 °C until it reached an OD_{600} of 0.5. The cells were centrifuged and washed twice with an assay buffer (5 mM HEPES, 5 mM glucose, pH 7.2) and resuspended in the same buffer to a final OD_{600} of 1.0. *E. coli* MC4100 cells were mixed with 20 µM NPN. The assay set up was the same as for the membrane integrity and viability assay, using black round-bottom 96-well microtiter plates (Nunc) containing 10 µL of 2-fold dilutions of peptides (500 to 31.2 µg/mL). A volume of 90 µL of cell suspension with NPN was added to each well by the automated injector of the Synergy H1 Hybrid Reader. The fluorescence was immediately measured (well by well) at an excitation wavelength of 350 nm and an emission wavelength of 420 nm every second for 3 min. The relative fluorescence was calculated by normalizing the values from each time point with the negative control (Milli-Q water). CHX was included as a positive control.

Supplementary Materials: The following supporting information can be downloaded at: https://www.mdpi.com/article/10.3390/ijms232213844/s1.

Author Contributions: D.S. and I.N.-S.H. performed the peptide synthesis; M.B.S. and T.H. performed the sequence analysis; H.D. and T.A. performed the biological activity experiments; H.D., T.A., E.G.A.F., H.-M.B., M.B.S. and T.H. conceived the biological experiments and analyzed data; D.S., I.N.-S.H., T.V. and M.B.S. conceived the MS experiments and analyzed data; H.D., D.S., I.N.-S.H., E.G.A.F., H.-M.B., M.B.S. and T.H. wrote the paper. M.B.S. and T.H. contributed to the conception of the work and supervised the project. All authors have read and agreed to the published version of the manuscript.

Funding: This work was supported by a grant (no. 217/6770) from UiT The Arctic University of Norway. The publication charges for this article have been covered by the publication fund of UiT The Arctic University of Norway.

Institutional Review Board Statement: Not applicable.

Informed Consent Statement: Not applicable.

Data Availability Statement: Not applicable.

Conflicts of Interest: The authors declare no conflict of interest.

References

1. Murray, C.J.L.; Ikuta, K.S.; Sharara, F.; Swetschinski, L.; Robles Aguilar, G.; Gray, A.; Han, C.; Bisignano, C.; Rao, P.; Wool, E.; et al. Global burden of bacterial antimicrobial resistance in 2019: A systematic analysis. *Lancet* **2022**, *399*, 629–655. [CrossRef]
2. World Health Organization. Antibiotic Resistance. Available online: https://www.who.int/news-room/fact-sheets/detail/antibiotic-resistance (accessed on 14 December 2018).
3. Boucher, H.W.; Talbot, G.H.; Benjamin, D.K., Jr.; Bradley, J.; Guidos, R.J.; Jones, R.N.; Murray, B.E.; Bonomo, R.A.; Gilbert, D.; Infectious Diseases Society of America. 10 × ′20 Progress—Development of new drugs active against Gram-negative bacilli: An update from the Infectious Diseases Society of America. *Clin. Infect. Dis.* **2013**, *56*, 1685–1694. [CrossRef] [PubMed]
4. Hutchings, M.I.; Truman, A.W.; Wilkinson, B. Antibiotics: Past, present and future. *Curr. Opin. Microbiol.* **2019**, *51*, 72–80. [CrossRef]
5. Bulet, P.; Stöcklin, R.; Menin, L. Anti-microbial peptides: From invertebrates to vertebrates. *Immunol. Rev.* **2004**, *198*, 169–184. [CrossRef]

6. Erdem Büyükkiraz, M.; Kesmen, Z. Antimicrobial peptides (AMPs): A promising class of antimicrobial compounds. *J. Appl. Microbiol.* **2022**, *132*, 1573–1596. [CrossRef] [PubMed]
7. Lei, M.; Jayaraman, A.; Deventer, J.A.V.; Lee, K. Engineering selectively targeting antimicrobial peptides. *Annu. Rev. Biomed. Eng.* **2021**, *23*, 339–357. [CrossRef]
8. Geitani, R.; Ayoub Moubareck, C.; Touqui, L.; Karam Sarkis, D. Cationic antimicrobial peptides: Alternatives and/or adjuvants to antibiotics active against methicillin-resistant *Staphylococcus aureus* and multidrug-resistant *Pseudomonas aeruginosa*. *BMC Microbiol.* **2019**, *19*, 54. [CrossRef]
9. Li, J.; Fernández-Millán, P.; Boix, E. Synergism between host defence peptides and antibiotics against bacterial infections. *Curr. Top. Med. Chem.* **2020**, *20*, 1238–1263. [CrossRef]
10. Dijksteel, G.S.; Ulrich, M.M.W.; Middelkoop, E.; Boekema, B.K.H.L. Review: Lessons learned from clinical trials using antimicrobial peptides (AMPs). *Front. Microbiol.* **2021**, *12*, 616979. [CrossRef]
11. Wu, R.; Patocka, J.; Nepovimova, E.; Oleksak, P.; Valis, M.; Wu, W.; Kuca, K. Marine invertebrate peptides: Antimicrobial peptides. *Front. Microbiol.* **2021**, *12*, 785085. [CrossRef]
12. Hansen, I.; Isaksson, J.; Poth, A.G.; Hansen, K.; Andersen, A.J.C.; Richard, C.S.M.; Blencke, H.M.; Stensvåg, K.; Craik, D.J.; Haug, T. Isolation and characterization of antimicrobial peptides with unusual disulfide connectivity from the colonial ascidian *Synoicum turgens*. *Mar. Drugs* **2020**, *18*, 51. [CrossRef] [PubMed]
13. Hansen, I.K.Ø.; Lövdahl, T.; Simonovic, D.; Hansen, K.Ø.; Andersen, A.J.C.; Devold, H.; Richard, C.S.M.; Andersen, J.H.; Strøm, M.B.; Haug, T. Antimicrobial activity of small synthetic peptides based on the marine peptide Turgencin A: Prediction of antimicrobial peptide sequences in a natural peptide and strategy for optimization of potency. *Int. J. Mol. Sci.* **2020**, *21*, 5460. [CrossRef] [PubMed]
14. Papo, N.; Shai, Y. A molecular mechanism for lipopolysaccharide protection of Gram-negative bacteria from antimicrobial peptides. *J. Biol. Chem.* **2005**, *280*, 10378–10387. [CrossRef]
15. Avrahami, D.; Shai, Y. Conjugation of a magainin analogue with lipophilic acids controls hydrophobicity, solution assembly, and cell selectivity. *Biochemistry* **2002**, *41*, 2254–2263. [CrossRef]
16. Makovitzki, A.; Avrahami, D.; Shai, Y. Ultrashort antibacterial and antifungal lipopeptides. *Proc. Natl. Acad. Sci. USA* **2006**, *103*, 15997–16002. [CrossRef]
17. Rounds, T.; Straus, S.K. Lipidation of antimicrobial peptides as a design strategy for future alternatives to antibiotics. *Int. J. Mol. Sci.* **2020**, *21*, 9692. [CrossRef] [PubMed]
18. Chu-Kung, A.F.; Nguyen, R.; Bozzelli, K.N.; Tirrell, M. Chain length dependence of antimicrobial peptide–fatty acid conjugate activity. *J. Colloid Interface Sci.* **2010**, *345*, 160–167. [CrossRef]
19. Malina, A.; Shai, Y. Conjugation of fatty acids with different lengths modulates the antibacterial and antifungal activity of a cationic biologically inactive peptide. *Biochem. J.* **2005**, *390*, 695–702. [CrossRef]
20. Kamysz, E.; Sikorska, E.; Jaśkiewicz, M.; Bauer, M.; Neubauer, D.; Bartoszewska, S.; Barańska-Rybak, W.; Kamysz, W. Lipidated analogs of the LL-37-derived peptide fragment KR12—structural analysis, surface-active properties and antimicrobial activity. *Int. J. Mol. Sci.* **2020**, *21*, 887. [CrossRef]
21. Grimsey, E.; Collis, D.W.P.; Mikut, R.; Hilpert, K. The effect of lipidation and glycosylation on short cationic antimicrobial peptides. *Biochim. Biophys. Acta* **2020**, *1862*, 183195. [CrossRef]
22. Húmpola, M.V.; Rey, M.C.; Carballeira, N.M.; Simonetta, A.C.; Tonarelli, G.G. Biological and structural effects of the conjugation of an antimicrobial decapeptide with saturated, unsaturated, methoxylated and branched fatty acids. *J. Pept. Sci.* **2017**, *23*, 45–55. [CrossRef] [PubMed]
23. Orlov, D.S.; Shamova, O.V.; Eliseev, I.E.; Zharkova, M.S.; Chakchir, O.B.; Antcheva, N.; Zachariev, S.; Panteleev, P.V.; Kokryakov, V.N.; Ovchinnikova, T.V.; et al. Redesigning Arenicin-1, an antimicrobial peptide from the marine *Polychaeta arenicola marina*, by strand rearrangement or branching, substitution of specific residues, and backbone linearization or cyclization. *Mar. Drugs* **2019**, *17*, 376. [CrossRef] [PubMed]
24. Lyu, Y.; Yang, Y.; Lyu, X.; Dong, N.; Shan, A. Antimicrobial activity, improved cell selectivity and mode of action of short PMAP-36-derived peptides against bacteria and *Candida*. *Sci. Rep.* **2016**, *6*, 27258. [CrossRef] [PubMed]
25. Virta, M.; Åkerman, K.E.O.; Saviranta, P.; Oker-Blom, C.; Karp, M.T. Real-time measurement of cell permeabilization with low-molecular-weight membranolytic agents. *J. Antimicrob. Chemother.* **1995**, *36*, 303–315. [CrossRef] [PubMed]
26. Braun, M.; Silhavy, T.J. Imp/OstA is required for cell envelope biogenesis in *Escherichia coli*. *Mol. Microbiol.* **2002**, *45*, 1289–1302. [CrossRef] [PubMed]
27. Eggert, U.S.; Ruiz, N.; Falcone, B.V.; Branstrom, A.A.; Goldman, R.C.; Silhavy, T.J.; Kahne, D. Genetic basis for activity differences between vancomycin and glycolipid derivatives of vancomycin. *Science* **2001**, *294*, 361–364. [CrossRef]
28. Ruiz, N.; Falcone, B.; Kahne, D.; Silhavy, T.J. Chemical conditionality: A genetic strategy to probe organelle assembly. *Cell* **2005**, *121*, 307–317. [CrossRef]
29. Novikova, O.D.; Solovyeva, T.F. Nonspecific porins of the outer membrane of Gram-negative bacteria: Structure and functions. *Biochem. (Mosc.) Suppl. A Membr. Cell Biol.* **2009**, *3*, 3–15. [CrossRef]
30. Igumnova, E.M.; Mishchenko, E.; Haug, T.; Blencke, H.-M.; Sollid, J.U.E.; Fredheim, E.G.A.; Lauksund, S.; Stensvåg, K.; Strøm, M.B. Synthesis and antimicrobial activity of small cationic amphipathic aminobenzamide marine natural product mimics and

evaluation of relevance against clinical isolates including ESBL–CARBA producing multi-resistant bacteria. *Bioorg. Med. Chem.* **2016**, *24*, 5884–5894. [CrossRef]
31. Solstad, R.G.; Johansen, C.; Stensvåg, K.; Strøm, M.B.; Haug, T. Structure-activity relationship studies of shortened analogues of the antimicrobial peptide EeCentrocin 1 from the sea urchin *Echinus esculentus*. *J. Pept. Sci.* **2020**, *26*, e3233. [CrossRef]
32. Paulsen, M.H.; Ausbacher, D.; Bayer, A.; Engqvist, M.; Hansen, T.; Haug, T.; Anderssen, T.; Andersen, J.H.; Sollid, J.U.E.; Strøm, M.B. Antimicrobial activity of amphipathic α,α-disubstituted β-amino amide derivatives against ESBL—CARBA producing multi-resistant bacteria; effect of halogenation, lipophilicity and cationic character. *Eur. J. Med. Chem.* **2019**, *183*, 111671. [CrossRef] [PubMed]
33. Lampinen, J.; Koivisto, L.; Wahlsten, M.; Mäntsälä, P.; Karp, M. Expression of luciferase genes from different origins in *Bacillus subtilis*. *Mol. Gen. Genet.* **1992**, *232*, 498–504. [CrossRef] [PubMed]
34. Helander, I.M.; Mattila-Sandholm, T. Fluorometric assessment of Gram-negative bacterial permeabilization. *J. Appl. Microbiol.* **2000**, *88*, 213–219. [CrossRef] [PubMed]

Supporting information

Synthesis and Antimicrobial Activity of Short Analogues of the Marine Antimicrobial Peptide Turgencin A: Effects of SAR Optimizations, Cys-Cys Cyclization And lipopeptide Modifications

Hymonti Dey [1,†], Danijela Simonovic [2,†], Ingrid Norberg-Schulz Hagen [2], Terje Vasskog [2], Elizabeth G. Aarag Fredheim [2], Hans-Matti Blencke [1], Trude Anderssen[2], Morten B. Strøm [2,*] and Tor Haug [1,*]

[1] The Norwegian College of Fishery Science, Faculty of Biosciences, Fisheries and Economics, UiT The Arctic University of Norway, NO-9037 Tromsø, Norway
[2] Department of Pharmacy, Faculty of Health Sciences, UiT The Arctic University of Norway, NO-9037 Tromsø, Norway
* Correspondence: morten.strom@uit.no (M.B.S.); tor.haug@uit.no (T.H.)
† These authors contributed equally to this work.

Contents:

Figure S27. Kinetic of the effect on viability as measured by relative luminescence in *B. subtilis* (pCGLS11) treated with different concentrations of **C_8-cTurg-1**, **C_{10}-cTurg-1**, **C_{10}-cTurg-2**, **C_{12}-cTurg-2**, **C_8-cTurg-6**, **C_{10}-cTurg-6**, and **C_{12}-cTurg-6**.

Figure S28. Kinetic of the effect on membrane integrity as measured by relative luminescence in *B. subtilis* (pCSS962) treated with different concentrations **of cTurg-1**, **cTurg-2**, **cTurg-3**, **cTurg-4**, **cTurg-5**, **cTurg-6** and **cTurg-7**.

Figure S29. Kinetic of the effect on membrane integrity as measured by relative luminescence in *B. subtilis* (pCSS962) treated with different concentrations of **C_8-cTurg-1**, **C_{10}-cTurg-1**, **C_{10}-cTurg-2**, **C_{12}-cTurg-2**, **C_8-cTurg-6**, **C_{10}-cTurg-6**, and **C_{12}-cTurg-6**.

Figure S30. Kinetic of the effect on viability as measured by relative luminescence in *E. coli* (pCGLS-11) treated with 50 μg/mL of **cTurg-1-7** and 25 μg/mL of **chlorhexidine**.

Figure S31. Kinetic of the effect on viability as measured by relative luminescence in *E. coli* (pCGLS-11) treated with different concentrations **of C_8-cTurg-1**, **C_{10}-cTurg-1**, **C_{10}-cTurg-2**, **C_{12}-cTurg-2**, **C_8-cTurg-6**, **C_{10}-cTurg-6**, and **C_{12}-cTurg-6**.

Figure S32. Kinetic of the effect on membrane integrity as measured by relative luminescence in *E. coli* (pCSS962) treated with different concentrations of cyclic peptides **cTurg-1**, **cTurg-2**, **cTurg-3**, **cTurg-4**, **cTurg-5**, **cTurg-6** and **cTurg-7**.

Figure S33. Kinetic of the effect on membrane integrity as measured by relative luminescence in *E. coli* (pCSS962) treated with different concentrations of **C_8-cTurg-1**, **C_{10}-cTurg-1**, **C_{10}-cTurg-2**, **C_{12}-cTurg-2**, **C_8-cTurg-6**, **C_{10}-cTurg-6**, and **C_{12}-cTurg-6**.

Table S1. Theoretical and measured monoisotopic mass (Da), and theoretical and observed m/z ions during HRMS of the synthesised peptides.

Table S2. Purity of synthesized peptides (%) and retention time (min), determined by UPLC using a reversed phase column.

Table S3. Selectivity index (SI) calculated as the ration between haemolytic activity (EC_{50}, in μg/mL) and the geometric mean (GM) of the MIC values (in μg/mL) against bacteria and fungi, i.e., SI = EC_{50} / GM.

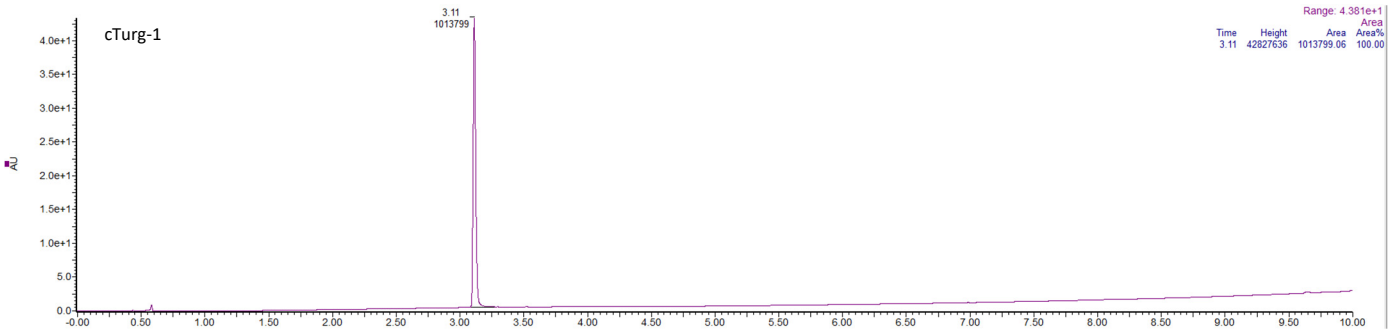

Figure S1. UPLC chromatogram of purified cyclic peptide **cTurg-1**. The peptide purity is 100 % based on the UPLC calculated area under the curves.

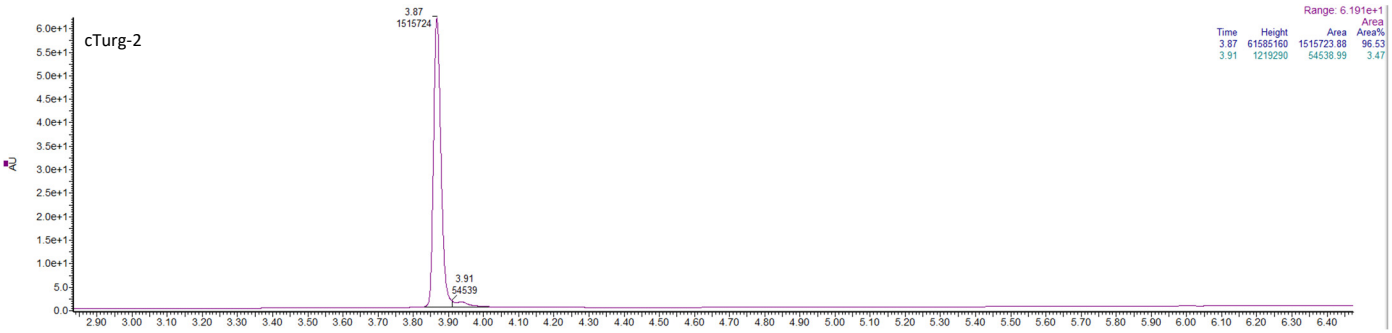

Figure S2. UPLC chromatogram of purified cyclic peptide **cTurg-2**. The peptide purity is 96.53 % based on the UPLC calculated area under the curves.

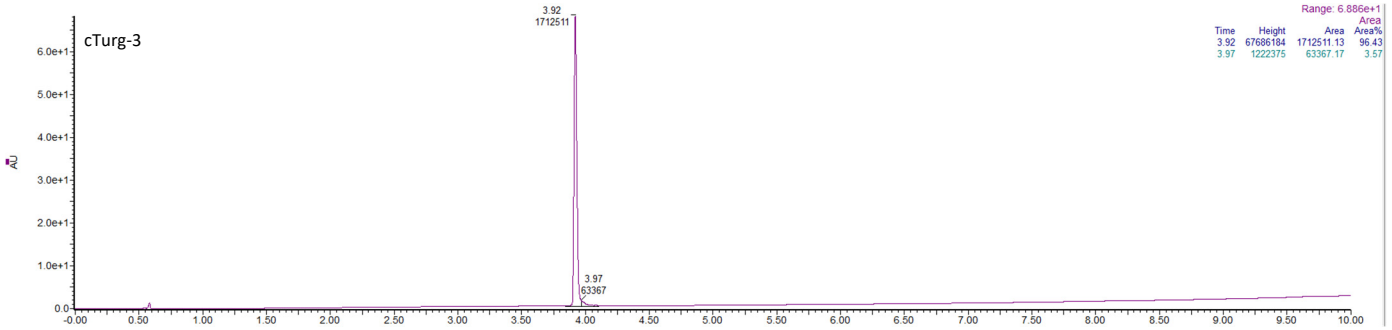

Figure S3. UPLC chromatogram of purified cyclic peptide **cTurg-3**. The peptide purity is 96.43 % based on the UPLC calculated area under the curves.

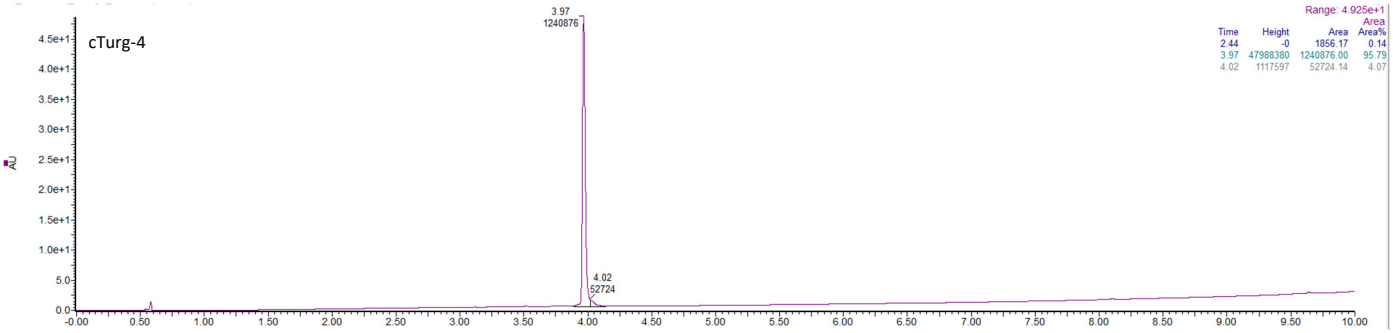

Figure S4. UPLC chromatogram of purified cyclic peptide **cTurg-4**. The peptide purity is 95.79 % based on the UPLC calculated area under the curves.

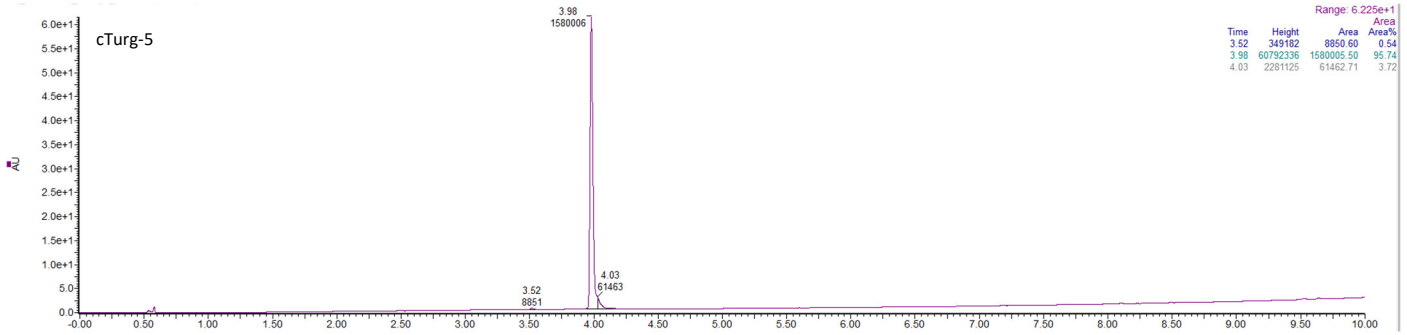

Figure S5. UPLC chromatogram of purified cyclic peptide **cTurg-5**. The peptide purity is 95.74 % based on the UPLC calculated area under the curves.

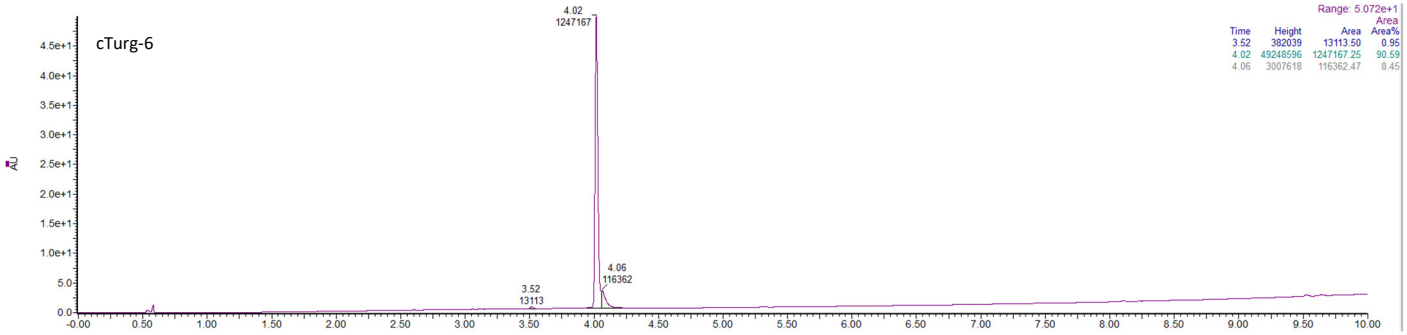

Figure S6. UPLC chromatogram of purified cyclic peptide **cTurg-6**. The peptide purity is 90.59 % based on the UPLC calculated area under the curves.

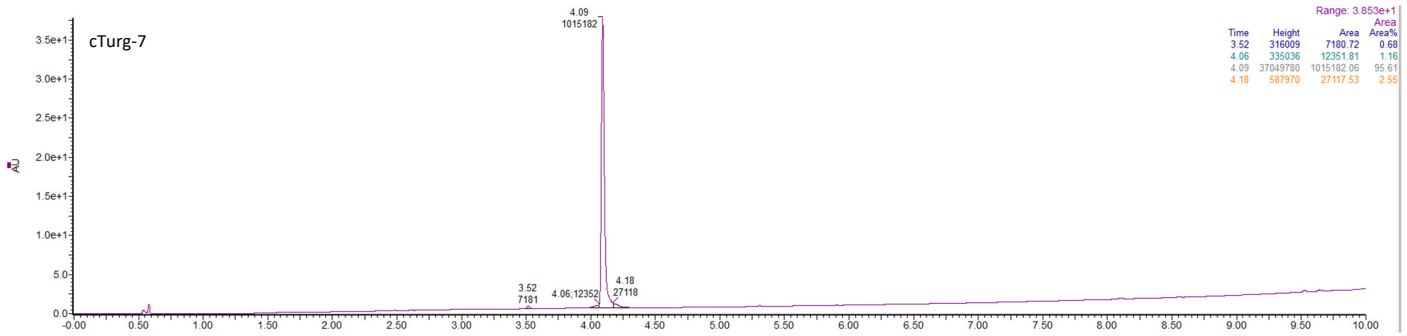

Figure S7. UPLC chromatogram of purified cyclic peptide **cTurg-7**. The peptide purity is 95.61 % based on the UPLC calculated area under the curves.

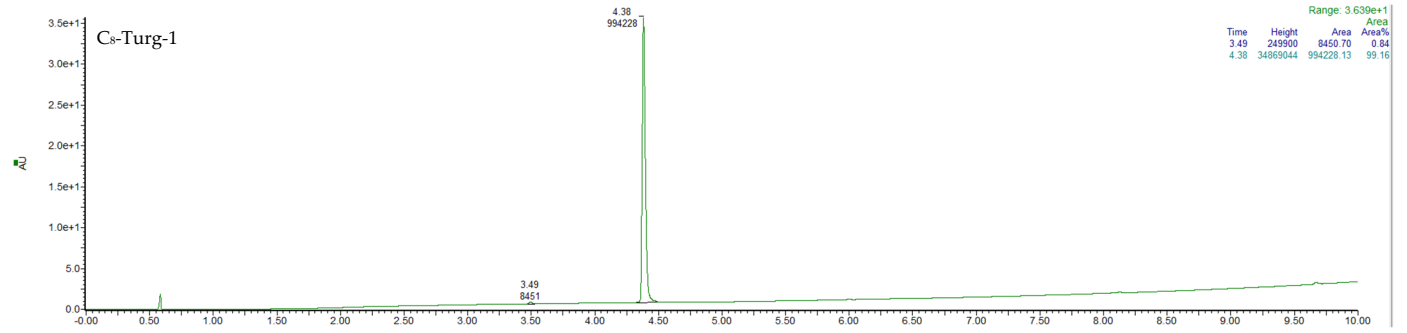

Figure S8. UPLC chromatogram of purified linear lipopeptide **C8-Turg-1**. The peptide purity is 99.16 % based on the UPLC calculated area under the curves.

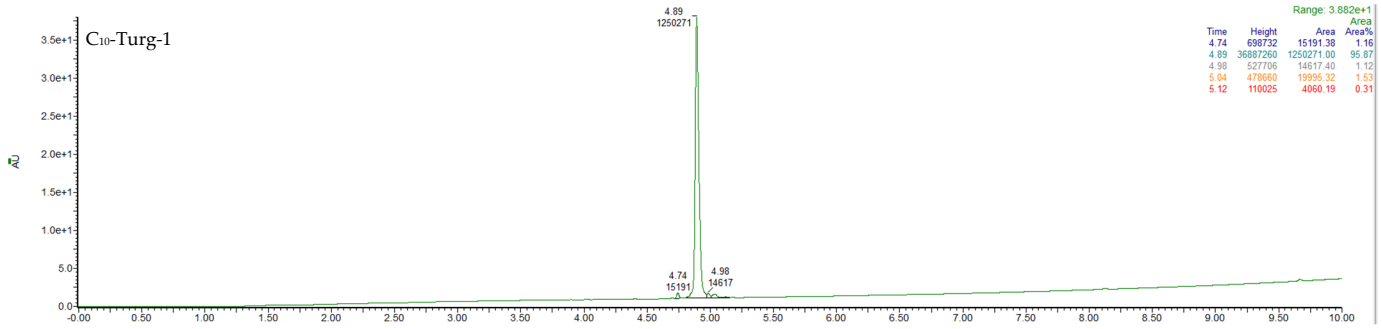

Figure S9. UPLC chromatogram of purified linear lipopeptide **C10-Turg-1**. The peptide purity is 95.87 % based on the UPLC calculated area under the curves.

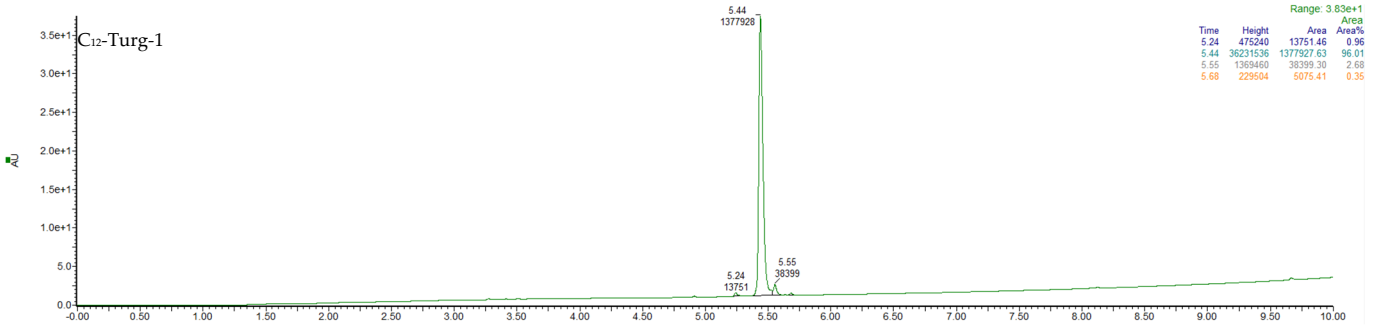

Figure S10. UPLC chromatogram of purified linear lipopeptide **C12-Turg-1**. The peptide purity is 96.01 % based on the UPLC calculated area under the curves.

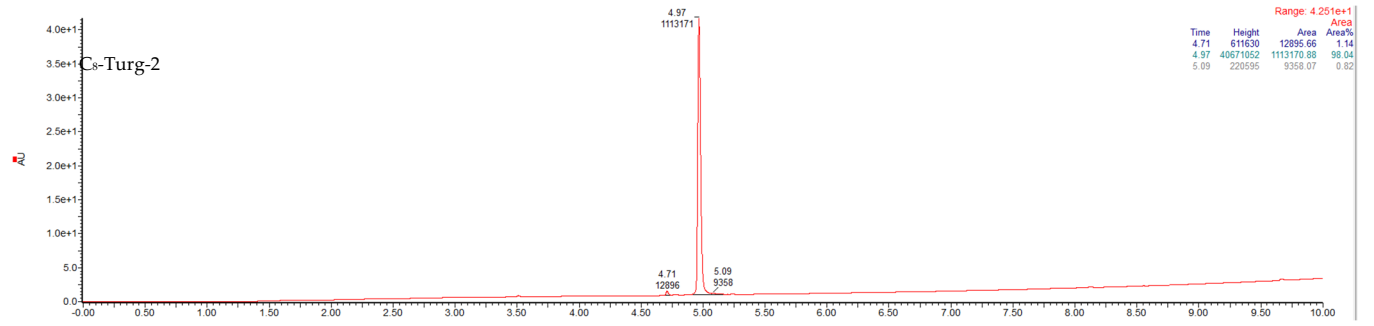

Figure S11. UPLC chromatogram of purified linear lipopeptide **C8-Turg-2**. The peptide purity is 98.04 % based on the UPLC calculated area under the curves.

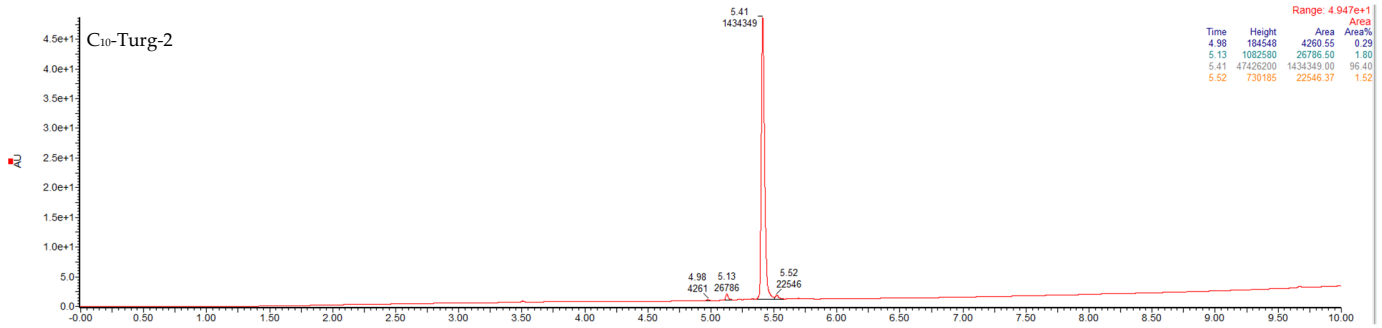

Figure S12. UPLC chromatogram of purified linear lipopeptide **C10-Turg-2**. The peptide purity is 96.40 % based on the UPLC calculated area under the curves.

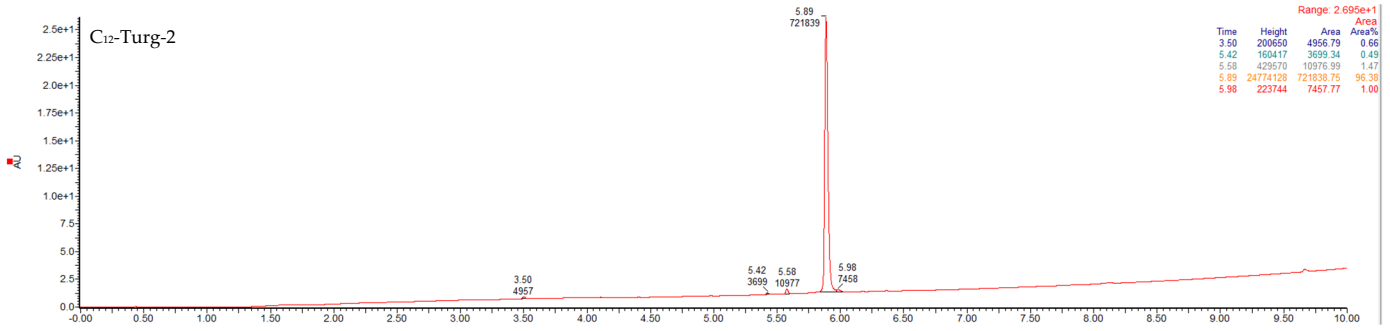

Figure S13. UPLC chromatogram of purified linear lipopeptide **C12-Turg-2**. The peptide purity is 96.38 % based on the UPLC calculated area under the curves.

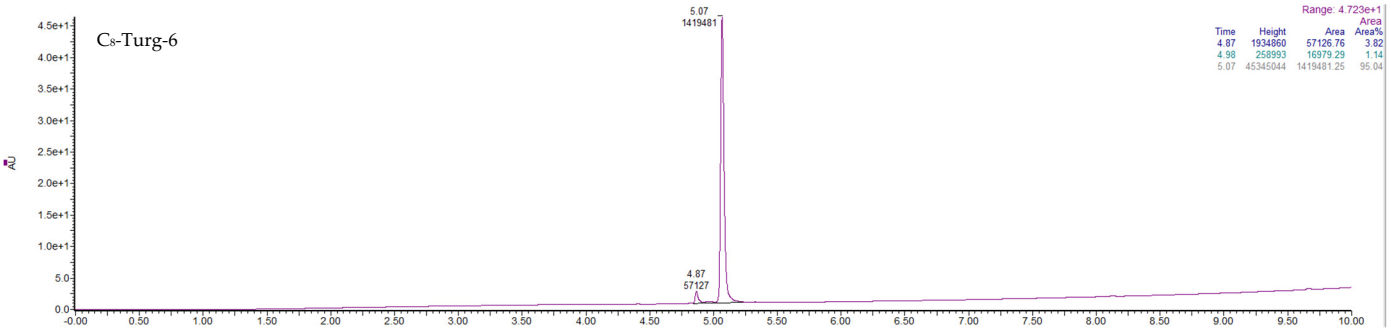

Figure S14. UPLC chromatogram of purified linear lipopeptide **C8-Turg-6**. The peptide purity is 95.04 % based on the UPLC calculated area under the curves.

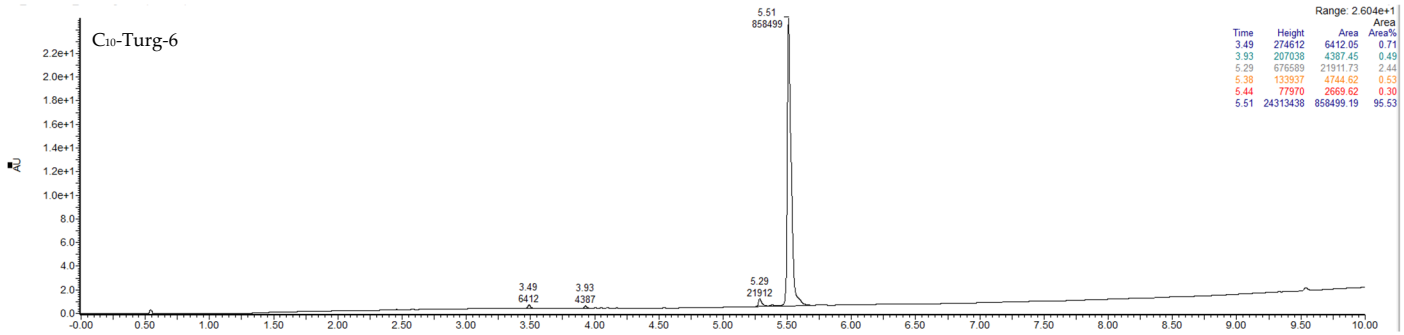

Figure S15. UPLC chromatogram of purified linear lipopeptide **C10-Turg-6**. The peptide purity is 95.53 % based on the UPLC calculated area under the curves.

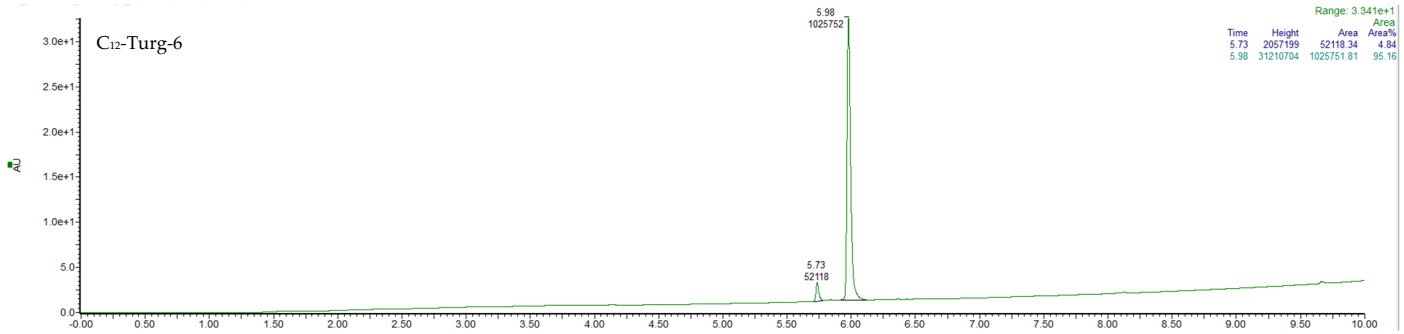

Figure S16. UPLC chromatogram of purified linear lipopeptide **C12-Turg-6**. The peptide purity is 95.16 % based on the UPLC calculated area under the curves.

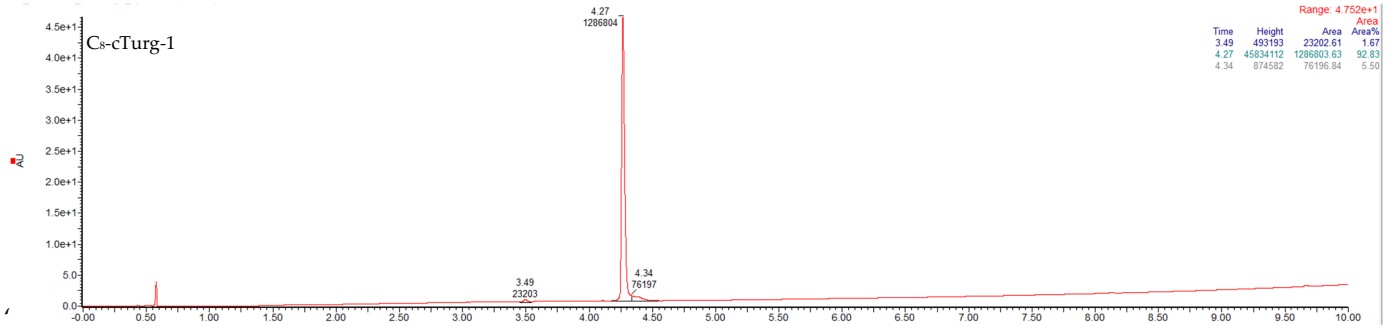

Figure S17. UPLC chromatogram of purified cyclic lipopeptide **C8-cTurg-1**. The peptide purity is 92.83 % based on the UPLC calculated area under the curves.

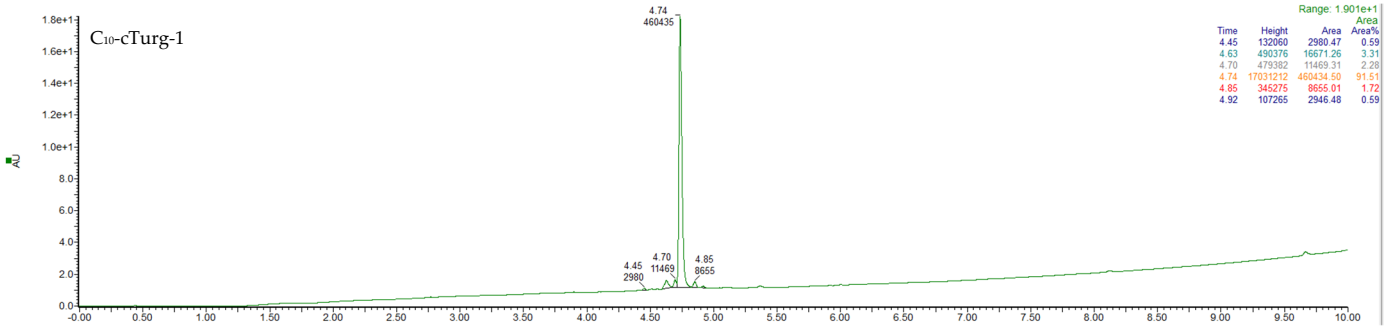

Figure S18. UPLC chromatogram of purified cyclic lipopeptide **C10-cTurg-1**. The peptide purity is 91.51 % based on the UPLC calculated area under the curves.

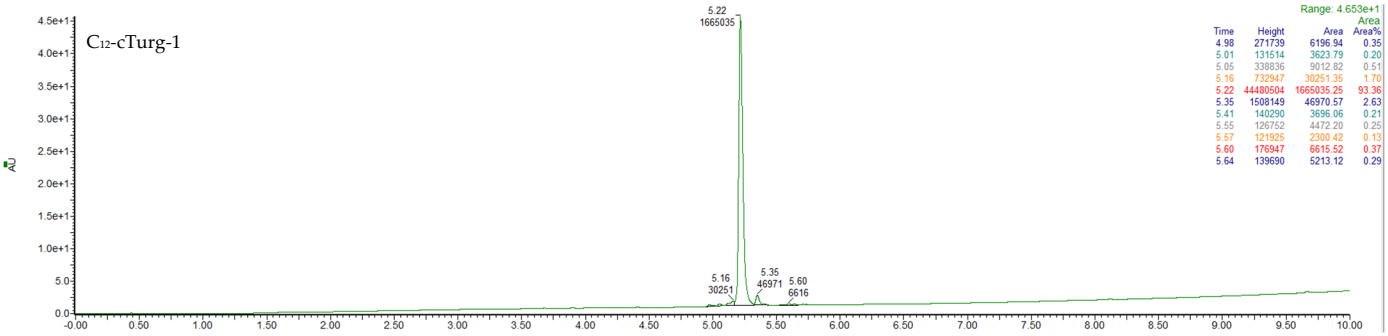

Figure S19. UPLC chromatogram of purified cyclic lipopeptide **C12-cTurg-1**. The peptide purity is 93.36 % based on the UPLC calculated area under the curves.

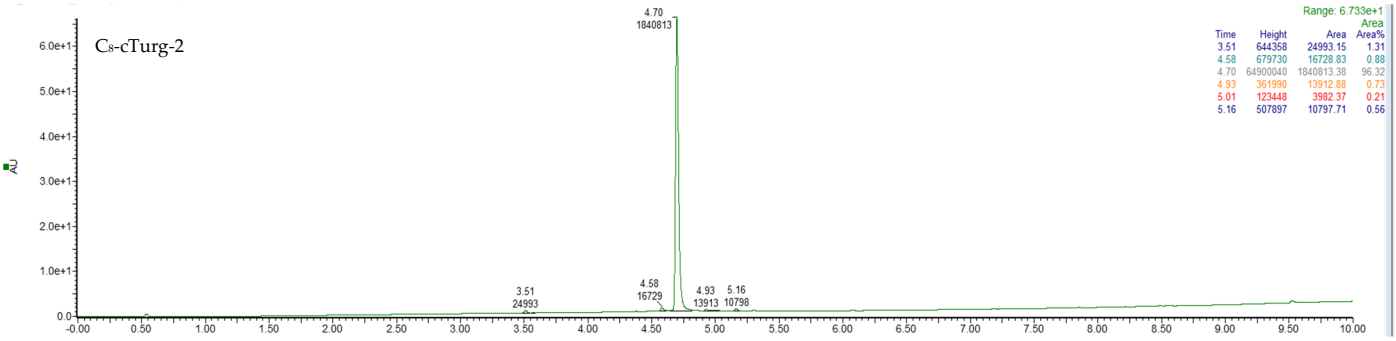

Figure S20. UPLC chromatogram of purified cyclic lipopeptide **C8-cTurg-2**. The peptide purity is 96.32 % based on the UPLC calculated area under the curves.

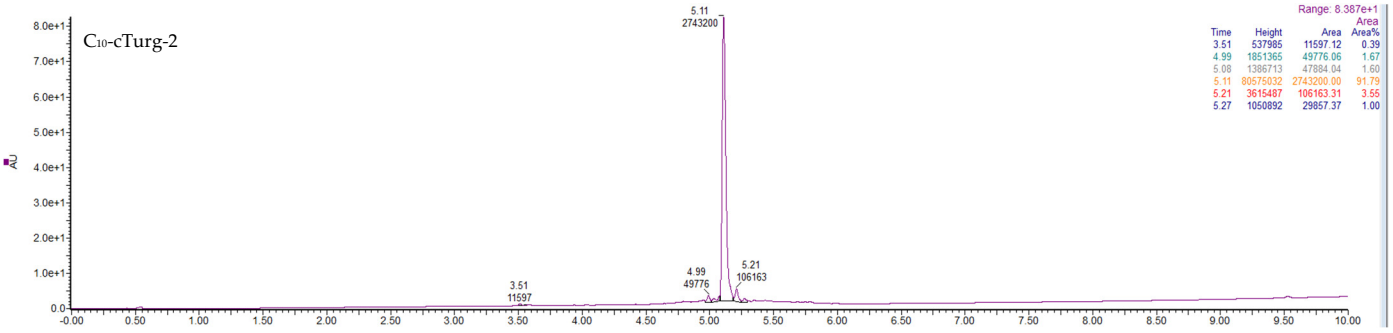

Figure S21. UPLC chromatogram of purified cyclic lipopeptide **C10-cTurg-2**. The peptide purity is 91.79 % based on the UPLC calculated area under the curves.

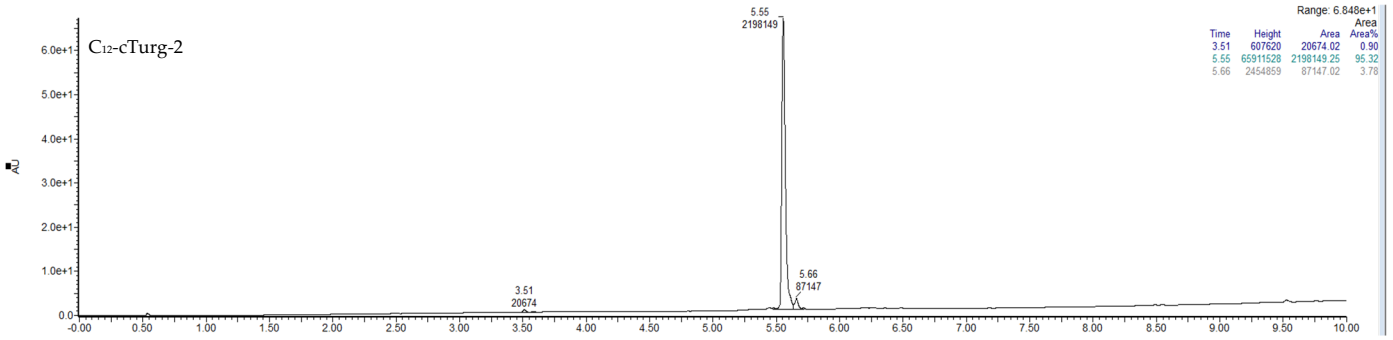

Figure S22. UPLC chromatogram of purified cyclic lipopeptide **C12-cTurg-2**. The peptide purity is 95.32 % based on the UPLC calculated area under the curves.

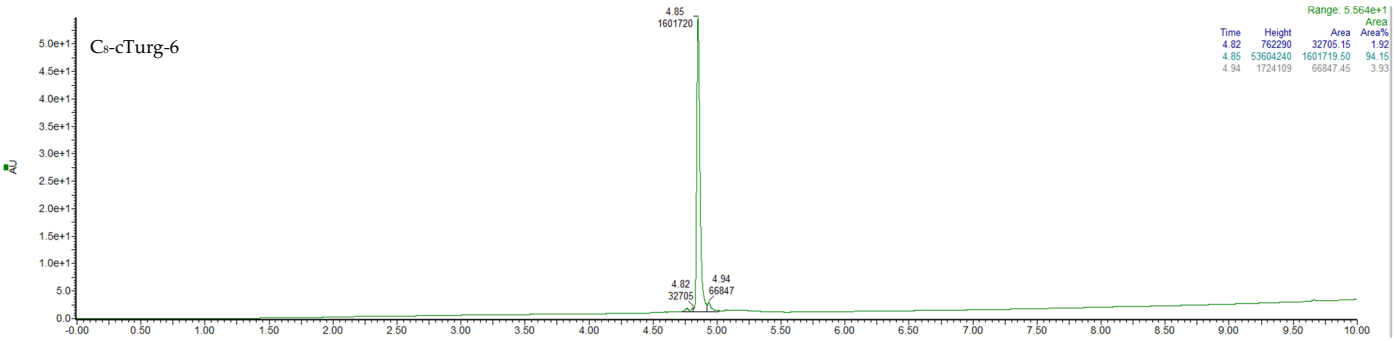

Figure S23. UPLC chromatogram of purified cyclic lipopeptide **C8-cTurg-6**. The peptide purity is 94.15 % based on the UPLC calculated area under the curves.

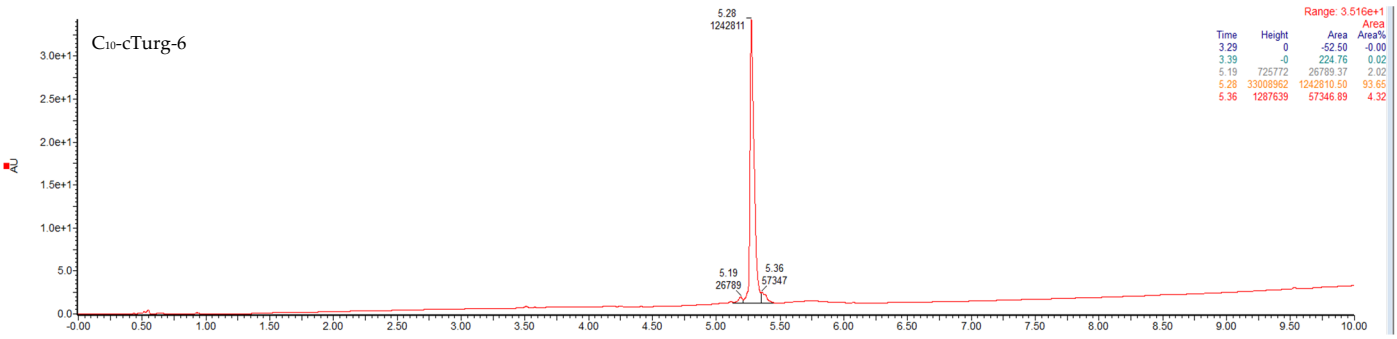

Figure S24. UPLC chromatogram of purified cyclic lipopeptide **C10-cTurg-6**. The peptide purity is 93.65 % based on the UPLC calculated area under the curves.

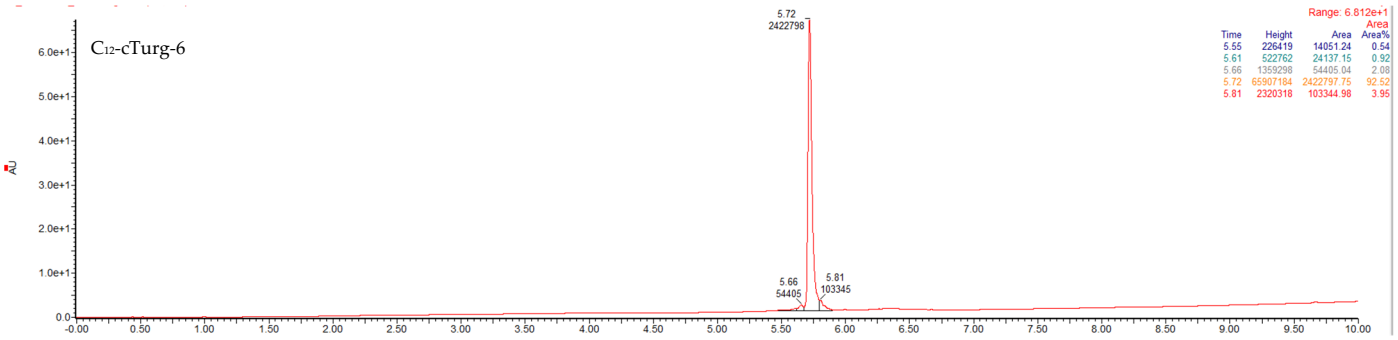

Figure S25. UPLC chromatogram of purified cyclic lipopeptide **C12-cTurg-6**. The peptide purity is 92.52 % based on the UPLC calculated area under the curves.

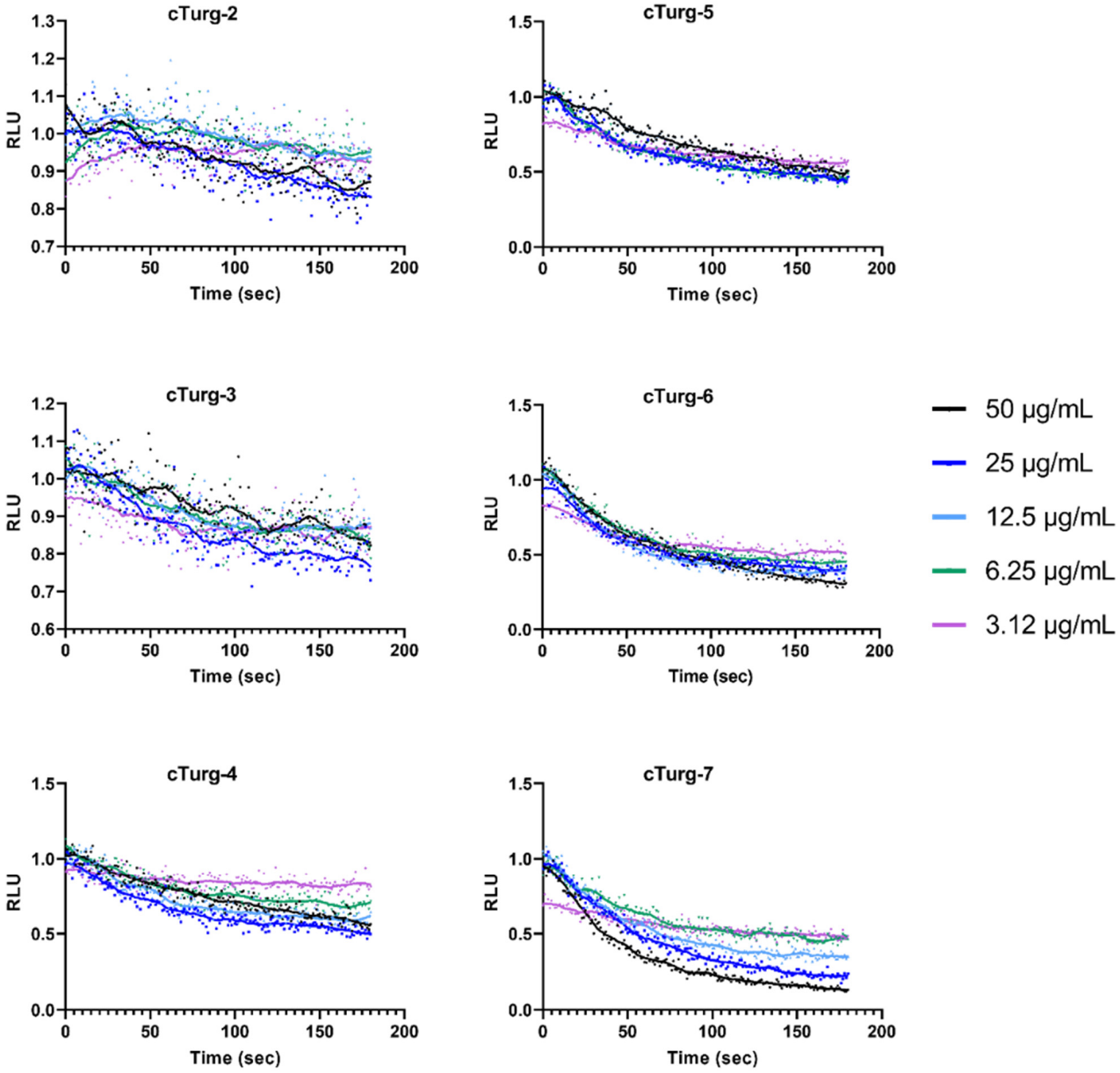

Figure S26. Kinetic of the effect on viability as measured by relative luminescence in *B. subtilis* (pCGLS11) treated with different concentrations of **cTurg-2**, **cTurg-3**, **cTurg-4**, **cTurg-5**, **cTurg-6** and **cTurg-7**.

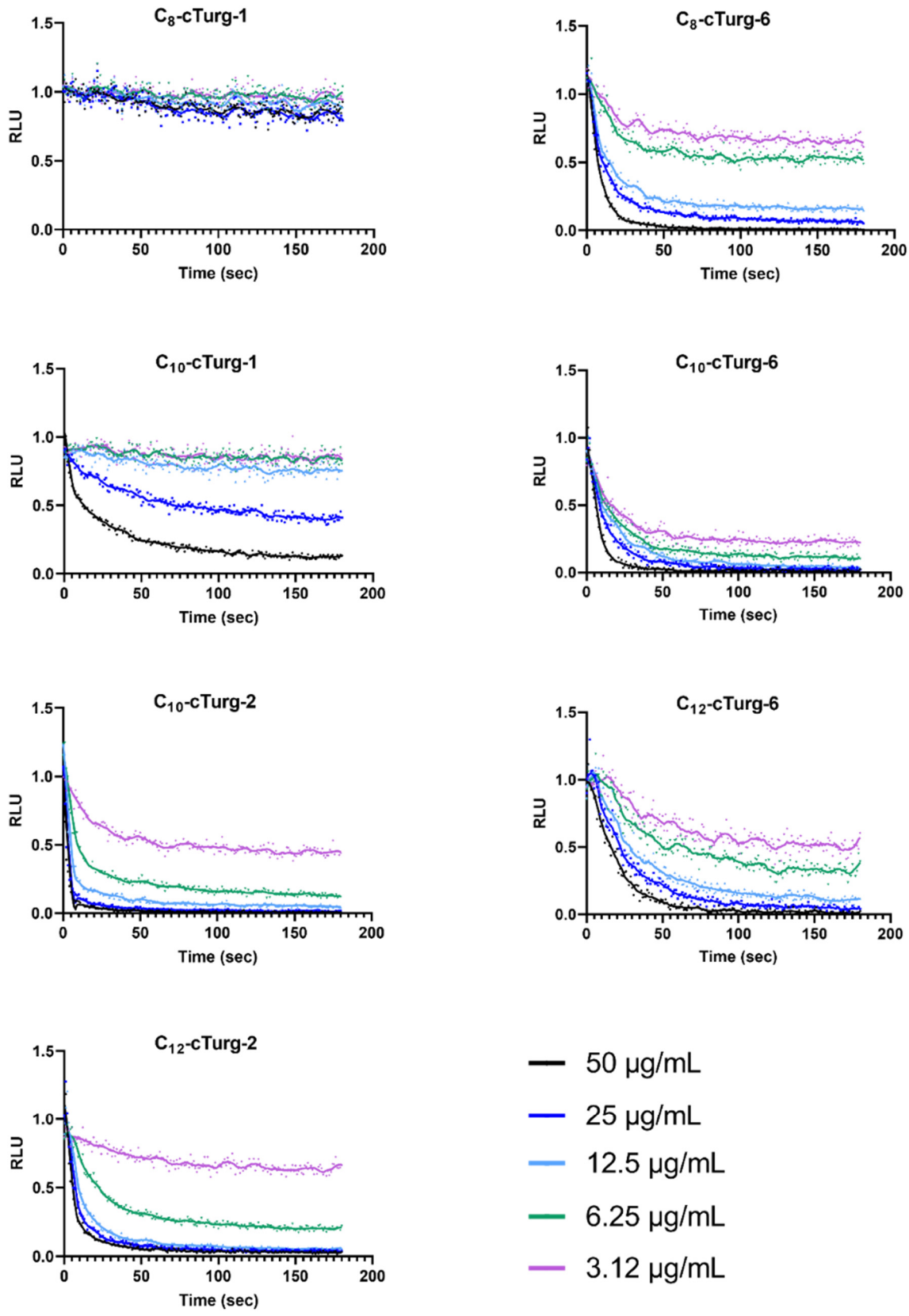

Figure S27. Kinetic of the effect on viability as measured by relative luminescence in *B. subtilis* (pCGLS11) treated with different concentrations of **C_8-cTurg-1**, **C_{10}-cTurg-1**, **C_{10}-cTurg-2**, **C_{12}-cTurg-2**, **C_8-cTurg-6**, **C_{10}-cTurg-6**, and **C_{12}-cTurg-6**.

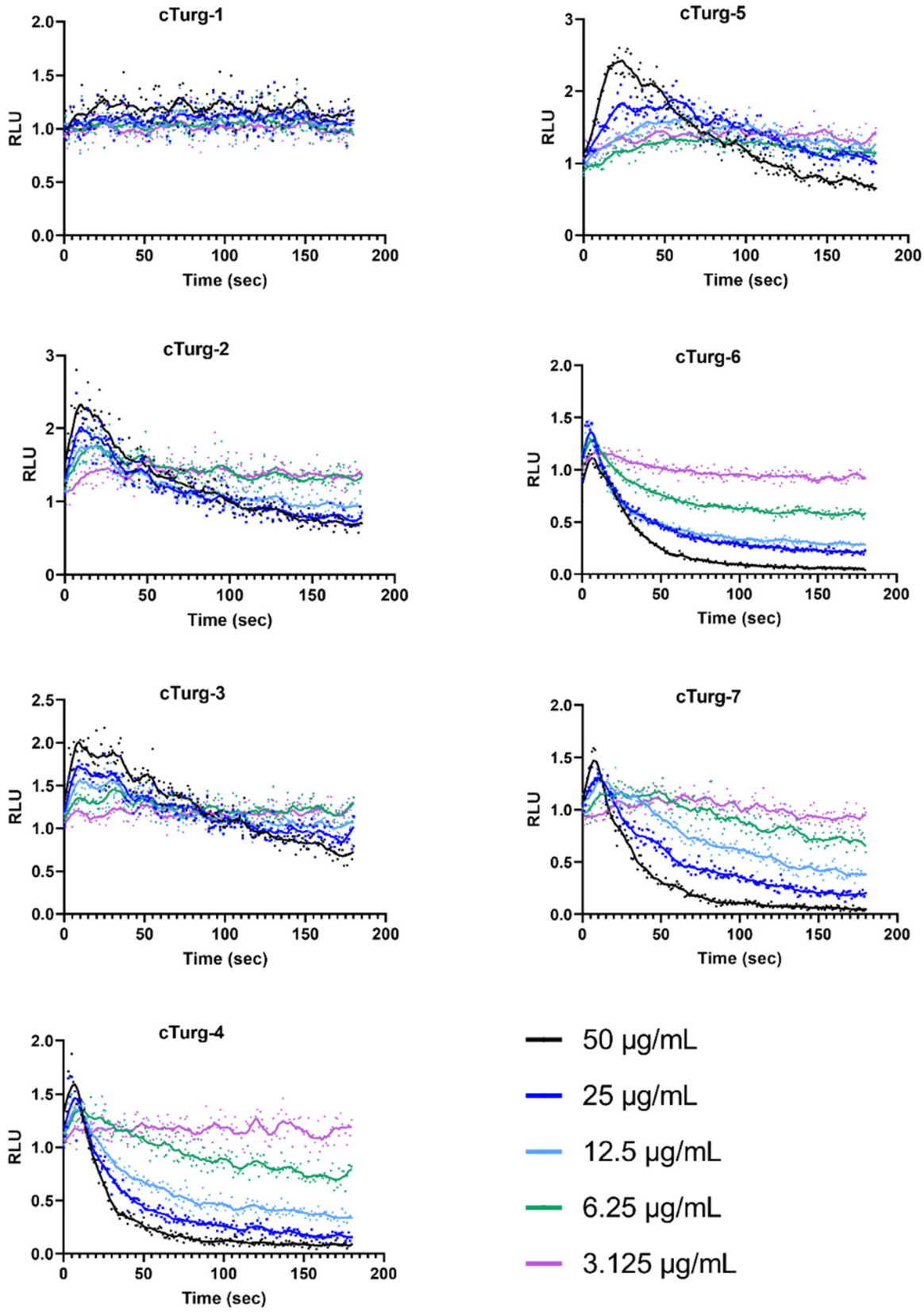

Figure S28. Kinetic of the effect on membrane integrity as measured by relative luminescence in *B. subtilis* (pCSS962) treated with different concentrations of **cTurg-1**, **cTurg-2**, **cTurg-3**, **cTurg-4**, **cTurg-5**, **cTurg-6** and **cTurg-7**.

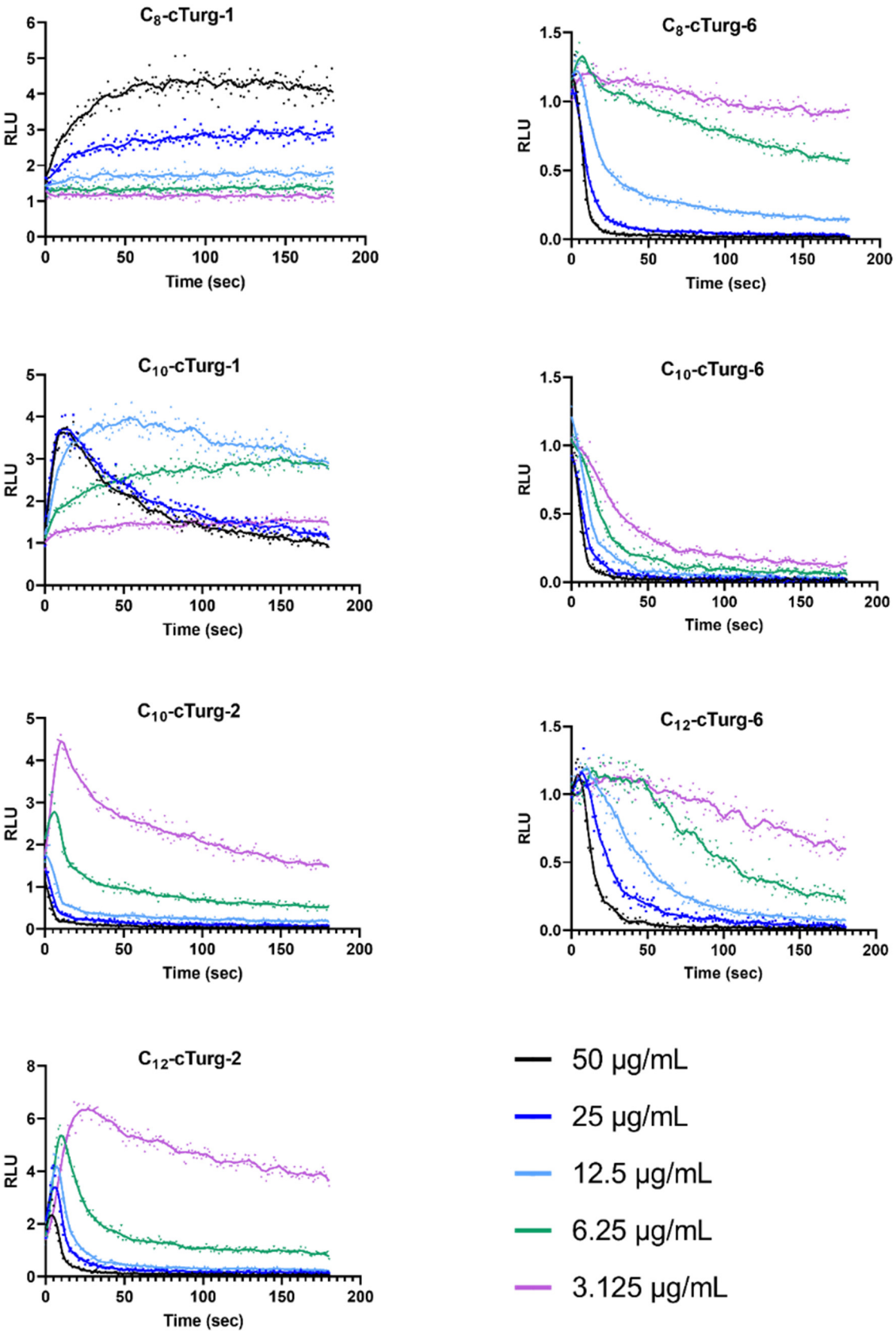

Figure S29. Kinetic of the effect on membrane integrity as measured by relative luminescence in *B. subtilis* (pCSS962) treated with different concentrations of **C8-cTurg-1**, **C10-cTurg-1**, **C10-cTurg-2**, **C12-cTurg-2**, **C8-cTurg-6**, **C10-cTurg-6**, and **C12-cTurg-6**.

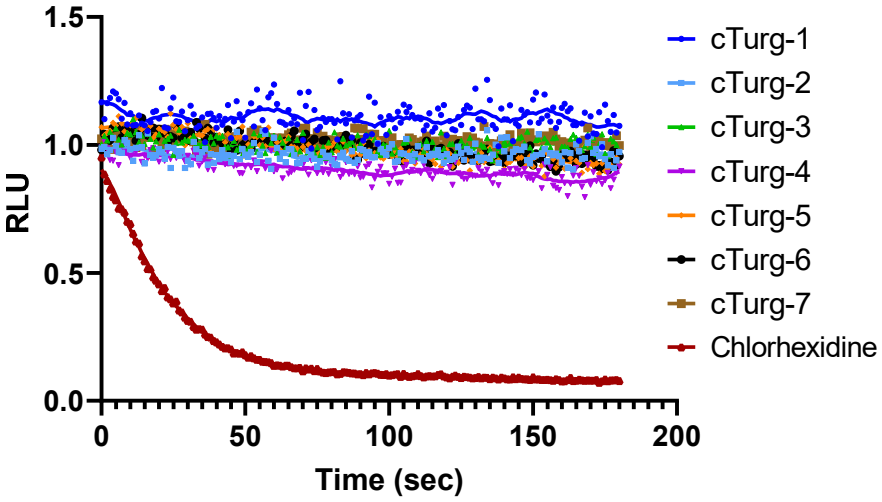

Figure S30. Kinetic of the effect on viability as measured by relative luminescence in *E. coli* (pCGLS-11) treated with 50 μg/mL of **cTurg-1-7** or 25 μg/mL of **chlorhexidine**.

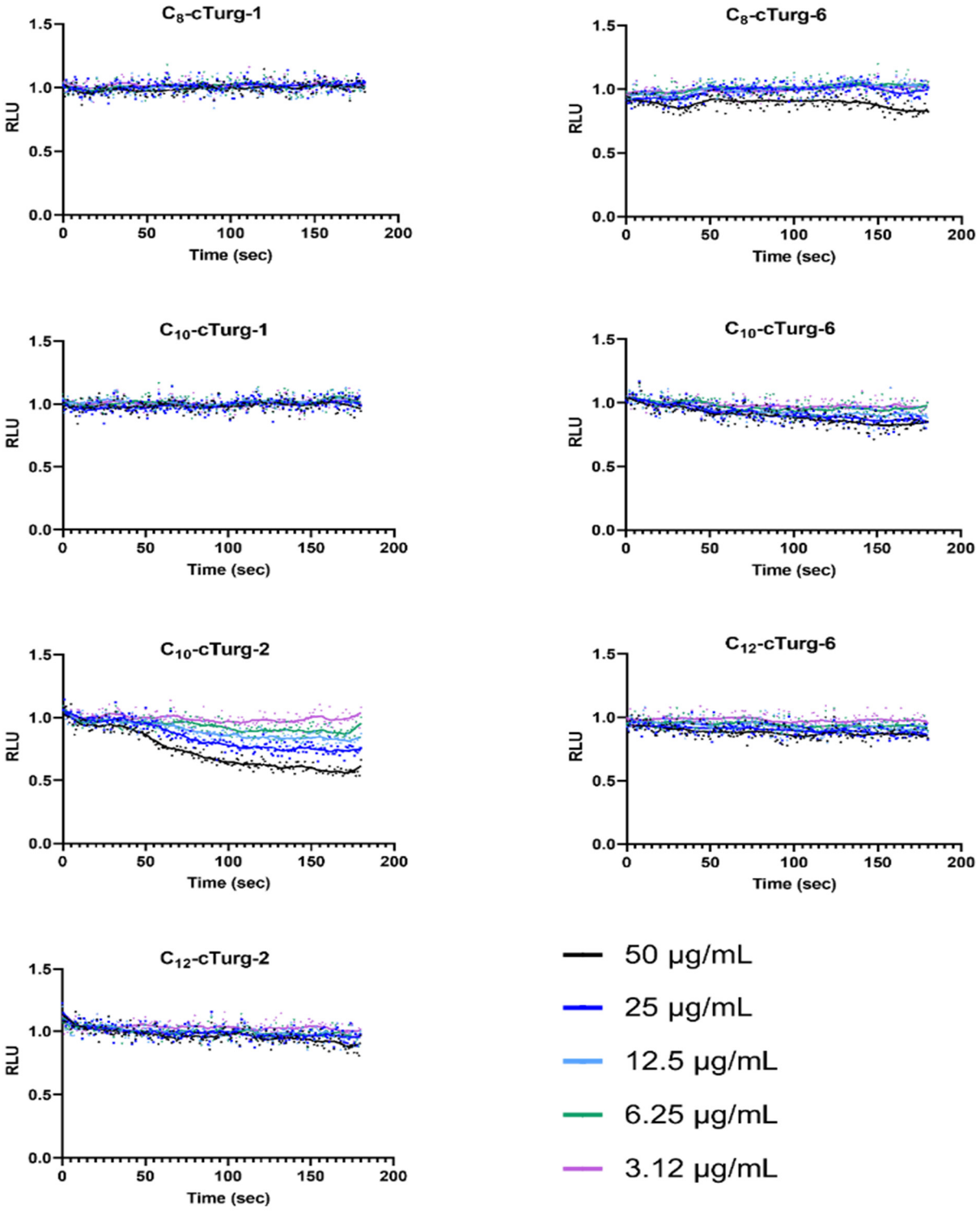

Figure S31. Kinetic of the effect on viability as measured by relative luminescence in *E. coli* (pCGLS-11) treated with different concentrations of **C8-cTurg-1**, **C10-cTurg-1**, **C10-cTurg-2**, **C12-cTurg-2**, **C8-cTurg-6**, **C10-cTurg-6**, and **C12-cTurg-6**.

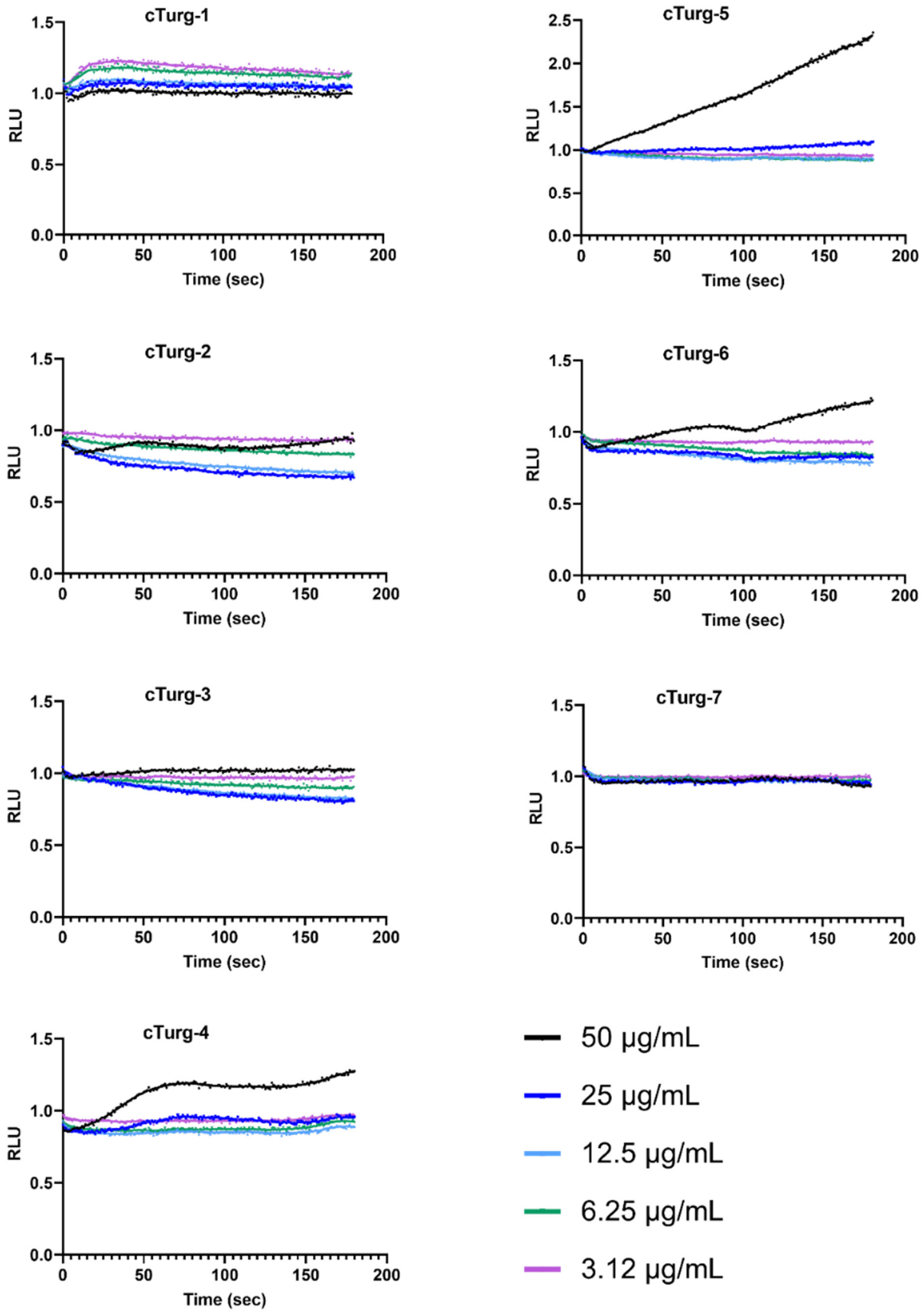

Figure S32. Kinetic of the effect on membrane integrity as measured by relative luminescence in *E. coli* (pCSS962) treated with different concentrations of cyclic peptides **cTurg-1**, **cTurg-2**, **cTurg-3**, **cTurg-4**, **cTurg-5**, **cTurg-6** and **cTurg-7**.

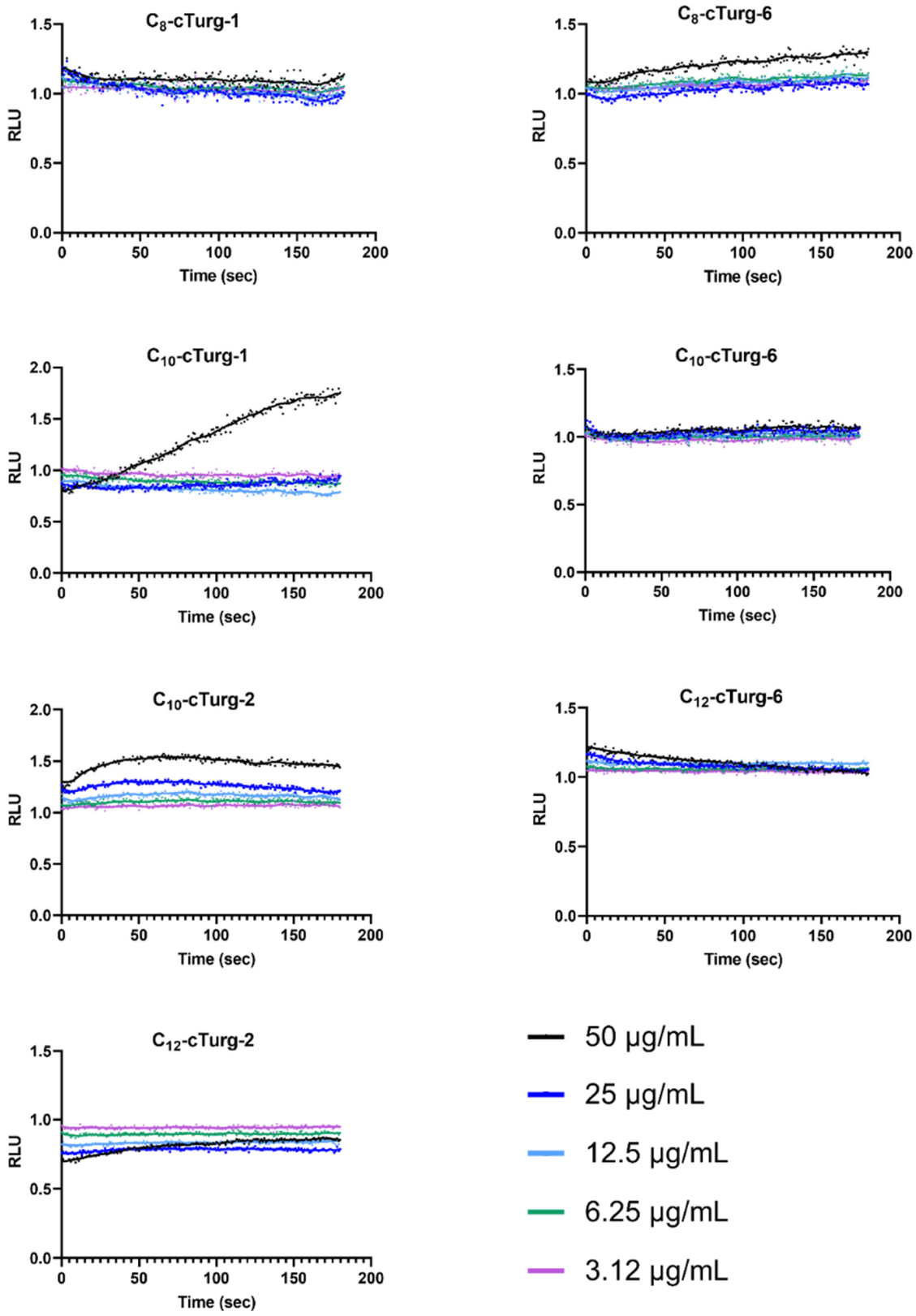

Figure S33. Kinetic of the effect on membrane integrity as measured by relative luminescence in *E. coli* (pCSS962) treated with different concentrations of **C_8-cTurg-1**, **C_{10}-cTurg-1**, **C_{10}-cTurg-2**, **C_{12}-cTurg-2**, **C_8-cTurg-6**, **C_{10}-cTurg-6**, **and C_{12}-cTurg-6**.

Table S1. Theoretical and measured monoisotopic mass (Da), and theoretical and observed m/z ions during HRMS of the synthesised peptides.

	Monoisotopic mass (Da)		$[M+2H]^{2+}$		$[M+3H]^{3+}$		$[M+4H]^{4+}$	
Peptide	Theoretical	Measured	Theoretical	Measured	Theoretical	Measured	Theoretical	Measured
cTurg-1	1300.6897	1300.6915	651.3521	651.3525	434.5705	434.5713	326.1797	326.1803
cTurg-2	1518.7741	1518.7746	760.3943	760.3944	507.2653	507.2656	380.7008	380.7009
cTurg-3	1518.7741	1518.7746	760.3943	760.3944	507.2653	507.2656	380.7008	380.7009
cTurg-4	1558.8054	1558.8061	780.4100	780.4102	520.6091	520.6094	390.7086	390.7088
cTurg-5	1630.7986	1630.7993	816.4066	816.4068	544.6068	544.6071	408.7069	408.7071
cTurg-6	1630.7987	1630.7999	816.4066	816.4068	544.6068	544.6073	408.7069	408.7074
cTurg-7	1670.8299	1670.8308	836.4222	836.4222	557.9506	557.9509	418.7148	418.7152
C_8-Turg-1	1428.8098	1428.8104	715.4122	715.4123	477.2772	477.2775	358.2097	358.2099
C_{10}-Turg-1	1456.8411	1456.8415	729.4278	729.4279	486.6210	486.6211	365.2176	365.2177
C_{12}-Turg-1	1484.8724	1484.8732	743.4435	743.4437	495.9647	495.9651	372.2254	372.2256
C_8-Turg-2	1646.8942	1646.8950	824.4544	824.4544	549.9720	549.9724	412.7308	412.7311
C_{10}-Turg-2	1674.9255	1674.9254	838.4700	838.4695	559.3158	559.3158	419.7387	419.7388
C_{12}-Turg-2	1702.9568	1702.9566	852.4857	852.4851	568.6595	568.6597	426.7465	426.7465
C_8-Turg-6	1758.9188	1758.9195	880.4667	880.4666	587.3135	587.3139	440.7370	440.7373
C_{10}-Turg-6	1786.9501	1786.9515	894.4823	894.4827	596.6573	596.6579	447.7448	447.7452
C_{12}-Turg-6	1814.9814	1814.9829	908.4980	908.4981	606.0011	606.0019	454.7526	454.7531
C_8-cTurg-1	1426.7941	1426.7948	714.4043	714.4045	476.6053	476.6056	357.7058	357.7060
C_{10}-cTurg-1	1454.8254	1454.8257	728.4200	728.4200	485.9491	485.9493	364.7136	364.7137
C_{12}-cTurg-1	1482.8567	1482.8573	742.4356	742.4358	495.2928	495.2931	371.7215	371.7216
C_8-cTurg-2	1644.8785	1644.8805	823.4465	823.4470	549.3001	549.3013	412.2269	412.2273
C_{10}-cTurg-2	1672.9098	1672.9107	837.4622	837.4621	558.6439	558.6446	419.2347	419.2349
C_{12}-cTurg-2	1700.9411	1700.9422	851.4778	851.4775	567.9876	567.9888	426.2426	426.2427
C_8-cTurg-6	1756.9031	1756.9036	879.4588	879.4586	586.6416	586.6420	440.2331	440.2333
C_{10}-cTurg-6	1784.9344	1784.9351	893.4745	893.4743	595.9854	595.9860	447.2409	447.2411
C_{12}-cTurg-6	1812.9657	1812.9685	907.4901	907.4905	605.3292	605.3303	454.2487	454.2498

Table S2. Purity of synthesized peptides (%) and retention time (min), determined by UPLC using a reversed phase column.

Peptide	Sequence	Purity [%]	Retention time [min]
cTurg-1	cyclic	100.00	3.11
cTurg-2	cyclic	96.53	3.87
cTurg-3	cyclic	96.43	3.92
cTurg-4	cyclic	95.79	3.97
cTurg-5	cyclic	95.74	3.98
cTurg-6	cyclic	90.59	4.02
cTurg-7	cyclic	95.61	4.09
C_8-Turg-1	linear	99.16	4.38
C_{10}-Turg-1	linear	95.87	4.89
C_{12}-Turg-1	linear	96.01	5.44
C_8-Turg-2	linear	98.04	4.97
C_{10}-Turg-2	linear	96.40	5.41
C_{12}-Turg-2	linear	96.38	5.89
C_8-Turg-6	linear	95.04	5.07
C_{10}-Turg-6	linear	95.53	5.51
C_{12}-Turg-6	linear	95.16	5.98
C_8-cTurg-1	cyclic	92.83	4.27
C_{10}-cTurg-1	cyclic	91.51	4.74
C_{12}-cTurg-1	cyclic	93.36	5.22
C_8-cTurg-2	cyclic	96.32	4.70
C_{10}-cTurg-2	cyclic	91.79	5.11
C_{12}-cTurg-2	cyclic	95.32	5.55
C_8-cTurg-6	cyclic	94.15	4.85
C_{10}-cTurg-6	cyclic	93.65	5.28
C_{12}-cTurg-6	cyclic	92.52	5.72

Table S3. Selectivity index (SI) calculated as the ration between haemolytic activity (EC_{50}, in µg/mL) and the geometric mean (GM) of the MIC values (in µg/mL) against bacteria and fungi, i.e., SI = EC_{50} / GM. MIC >256 were set to 256 for bacteria, MIC >128 were set to 128 for fungi, and the values for the highest tested concentration was used for haemolytic activity when calculating the SI.

		Peptide	GM of MIC				Selectivity index (SI)			
			G+	G-	Tot. bact.[1]	Fungi	G+	G-	Tot. bact.	Fungi
Cyclic peptides		**cTurg-1**	128	256	161	64	nd[2]	nd	nd	nd
	W	**cTurg-2**	11	64	20	32	92	16	52	33
		cTurg-3	10	64	18	32	89	13	47	27
		cTurg-4	16	128	32	40	67	8	33	26
	R / W	**cTurg-5**	8	11	9	32	138	97	123	34
		cTurg-6	7	11	8	32	164	97	138	34
		cTurg-7	7	23	10	32	29	9	20	6
Linear lipopeptides		**C_8-Turg-1**	19	64	29	40	50	15	33	23
		C_{10}-Turg-1	7	23	10	25	142	42	95	38
		C_{12}-Turg-1	5	11	6	25	204	86	153	38
	W	**C_8-Turg-2**	7	16	9	40	29	12	22	5
		C_{10}-Turg-2	7	11	8	40	10	6	8	2
		C_{12}-Turg-2	11	23	14	40	5	2	4	1
	R / W	**C_8-Turg-6**	7	16	9	102	8	3	6	1
		C_{10}-Turg-6	16	45	23	102	1	0	1	0
		C_{12}-Turg-6	19	91	32	91	2	0	1	0
Cyclic lipopeptides		**C_8-cTurg-1**	16	64	25	32	59	15	37	29
		C_{10}-cTurg-1	4	16	6	20	239	60	151	47
		C_{12}-cTurg-1	3	8	4	20	77	27	55	11
	W	**C_8-cTurg-2**	3	6	4	13	155	78	123	35
		C_{10}-cTurg-2	3	8	5	32	32	13	24	3
		C_{12}-cTurg-2	7	16	9	40	5	2	4	1
	R / W	**C_8-cTurg-6**	5	11	6	51	6	3	5	1
		C_{10}-cTurg-6	6	16	8	51	3	1	2	0
		C_{12}-cTurg-6	10	32	14	81	1	0	1	0

[1] GM of all bacterial test strains, [2] nd: not determined.

Paper II

Antimicrobial activity of short analogues of the marine peptide EeCentrocin 1: Synthesis of lipopeptides and head-to-tail cyclic peptides and mechanism of action studies

Danijela Simonovic[1#], Hymonti Dey[2#], Natascha Johansen[1], Trude Anderssen[1], Ida K. Ø. Hansen[2], Hege Devold[2], Terje Vasskog[1], Hans-Matti Blencke[2], Frode Jacobsen Øyen[2], Elizabeth G. Aarag Fredheim[1], Tor Haug[2*], Morten B. Strøm[1*]

[1] Department of Pharmacy, Faculty of Health Sciences, UiT the Arctic University of Norway, NO-9037 Tromsø, NORWAY.

[2] The Norwegian College of Fishery Science, Faculty of Biosciences, Fisheries and Economics, UiT the Arctic University of Norway, NO-9037 Tromsø, NORWAY.

[#] Authors contributed equally.

* Corresponding authors. Correspondence: tor.haug@uit.no and morten.strom@uit.no

ABSTRACT

Keywords:
Antifungal peptides
Antimicrobial peptides
Head to tail cyclization
Lipopeptides
Pseudo-dilution cyclization
Mechanism of action
Bacterial biosensors

We have synthesised a series of 12-residue analogues of a previously reported lead peptide (**P6**) developed from the heavy chain of the marine peptide EeCentrocin 1, isolated from the sea urchin *Echinus esculentus*. We have explored ways to optimise the lead peptide by increasing its net positive charge, its lipophilicity through *N*-terminal fatty acid acylation or incorporation of a Trp residue, and by synthesising head-to-tail cyclic peptides under *pseudo-high dilution* conditions. All peptides were screened for antimicrobial and antifungal activity, and toxicity was determined against human red blood cells. The two most potent peptide analogues were the linear peptide **P6-W6R8** and its head-to-tail cyclic analogue **cP6-W6R8** displaying minimum inhibitory concentrations of 0.4 – 6.6 µM against Gram-positive and Gram-negative bacteria, and 6.2 – 13 µM against fungi. All peptides were non-haemolytic (EC_{50} > 500 µM) except for two of the lipopeptides, in which haemolytic toxicity correlated with increasing acyl chain length. Mode of action studies using bacterial biosensor strains revealed a membrane disruptive effect of both the linear and the cyclic peptide. The presence of the outer membrane protease OmpT in *Escherichia coli* slightly reduced the effect of both peptides, as demonstrated by bioactivity measurements and detection of proteolytic fragments by mass spectrometry. Overall, the results of our study demonstrated that relatively simple structural modifications could be successfully employed in the development of potent antimicrobial lead peptides derived from marine natural products.

(GRAPHICAL ABSTRACT):

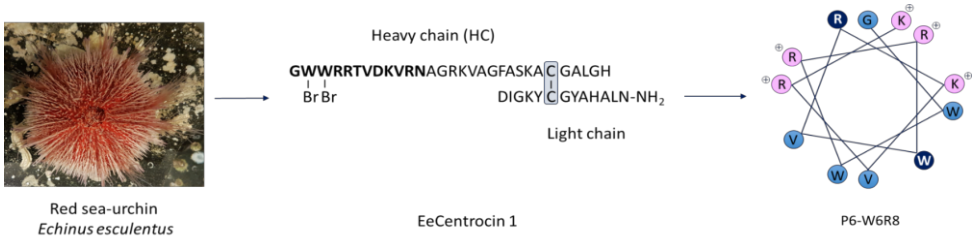

1. Introduction

Emergence and spread of antimicrobial resistance (AMR) pose a serious threat to human health worldwide [1,2]. Infections caused by multidrug resistant bacteria have a significant impact on both morbidity and mortality, creating additional economic burden [3]. Time consuming drug discovery pipeline and lack of development of new antimicrobials further exacerbate the problems associated with AMR. To solve this crisis, new therapeutic alternatives are urgently needed. Natural products play a key role in drug discovery and development [4]. Antimicrobial peptides (AMPs) are ubiquitous natural products present in all domains of life. They are also known as host defense peptides and act as an integral part of innate immunity playing a key role in protecting the host organism against invading pathogens [5]. Due to their rapid bactericidal effect and multifunctionality, they are promising candidates offering alternative treatment options to fight AMR [6]. AMPs with diverse structures and

functions have been derived from various organisms, including bacteria, fungi, plants, and animals [7]. In nature, AMP synthesis follows two distinct pathways, ribosomal and non-ribosomal. The first pathway generates AMPs which are gene encoded and follow ribosome-mediated translation [5,7]. AMPs from the non-ribosomal pathway, on the other hand, are usually the end products assembled by multi-enzyme complexes [7,8]. Most AMPs possess a net positive charge and an amphiphilic structure, enabling them to interact strongly with anionic membranes [9,10]. They have various mechanisms of actions, such as intracellular penetration, pore formation, inhibition of cellular pathways and immunomodulation [5,10], and they often exhibit potent broad-spectrum activity against a wide range of microorganisms, including bacteria, viruses, fungi, and other pathogens. Due to these unique characteristics many natural and synthetic AMPs and their derivatives have been employed as templates for AMP-based drug development [10,11]. However, the effectiveness of AMPs as therapeutics is hampered due to their toxicity and poor selectivity to eukaryotic cells [10,12]. Therefore, rational design aiming to improve their antimicrobial activity, stability, and selectivity is an active area of research [11].

Although most of the natural AMPs are isolated from terrestrial ecosystems, increasing number of research is also focusing on AMPs from marine organisms [13,14]. The antimicrobial peptide EeCentrocin 1, isolated from the marine sea urchin *Echinus esculentus,* consists of a hetero-dimeric structure with a heavy chain (HC) essential for antimicrobial activity [15]. To obtain a shorter *lead peptide* derived from the HC of EeCentrocin 1, a recent study explored several modifications, namely peptide truncation, substitution of the 6-bromo-Trp residues in positions 2 and 3 of the natural HC with Trp, and an alanine scan replacement strategy performed on shorter analogues of the HC [16]. The EeCentrocin 1 HC was in this way successfully truncated and modified resulting in the highly potent peptide **P6** (**Figure 1**). The peptide **P6** consists of the 12 *N*-terminal amino acid residues of the original *EeCentrocin 1* HC sequence, and it is further modified by two amino acid replacements, $Asp^{8} \rightarrow Ala^{8}$ and $Asn^{12} \rightarrow Lys^{12}$, as well as *C*-terminal amidation. The orientation of the hydrophilic and hydrophobic amino acid residues, as demonstrated by an α-helical wheel plot, indicates its amphiphilic character (**Figure 1**). The peptide **P6** is non-haemolytic, with minimal inhibitory concentrations (MICs) against bacteria in the low micromolar range and a promising antifungal activity [16].

In the present study we have investigated strategies to further optimise the potency of **P6** by increasing its net positive charge and lipophilicity, and by synthesising lipopeptide- and head-to-tail cyclic analogues (**Figure 2**). The resulting peptides were screened for antibacterial activity against a panel of Gram-positive and Gram-negative bacterial strains, whereas antifungal and haemolytic activities were determined against three fungal strains and human red blood cells (RBCs). Based on the antibacterial and haemolytic activities, the selectivity index of the peptides towards bacteria versus eukaryotic cells were calculated. Mode of action studies using bacterial biosensor strains (*Bacillus subtilis* and *Escherichia coli*) were performed to explore their effects on bacterial viability and membrane integrity. Finally, the proteolytic effect of the outer membrane protease OmpT in *E. coli* was studied.

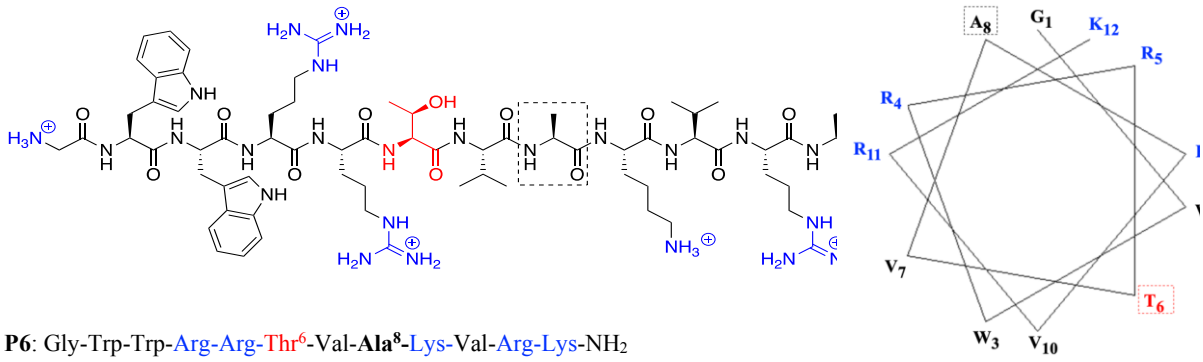

P6: Gly-Trp-Trp-Arg-Arg-Thr[6]-Val-**Ala[8]**-Lys-Val-Arg-Lys-NH_2

Figure 1. Structure and amino acid sequence (left) and α-helical wheel projection (right) of the lead peptide **P6**. The highlighted Thr^{6} residue in the α-helical lipophilic region and the Ala^{8} residue in the cationic region were both targets for the substitutions in the present study [16].

2. Results and Discussion

2.1 Peptide Design and Synthesis

The objective of the present study was to investigate if the antimicrobial potency of the lead peptide **P6** could be further improved by utilising various peptide modification strategies. This was done either by increasing its overall net charge by Ala[8] to Lys[8]/Arg[8] substitution in the α-helical cationic region, or its lipophilicity by Thr[6] to Trp[6] substitution in the α-helical lipophilic region. In addition, we wanted to explore the effects on antimicrobial activity of acylated and head-to-tail cyclic analogues. All peptides were synthesised by Fmoc solid phase peptide synthesis (Fmoc-SPPS) on either a Rink amide ChemMatrix resin, for *N*-terminally amidated peptides, or on a preloaded 2-chlorotrityl resin for the synthesis of cyclic peptides. Head-to-tail cyclisation was performed using a modified *pseudo-high dilution* procedure reported by Malesevic *et al.* [17]. As described in the methods section, cyclisation was performed using two syringes and a mechanical pump (**Figure 3**). This setup allowed for a very slow addition (0.01 mL/min) of the linear protected peptide (contained in syringe 1) and a coupling reagent (contained in syringe 2), thereby creating *pseudo-high dilution* conditions. The method worked nicely in our hands and required relatively low amount of solvent (30 mL DMF in total for cyclisation of 100 µmol of linear protected peptides) [18]. Also, no dimers or polymers of the peptides were isolated after the head-to-tail cyclisation procedures. The total percent yield for the cyclised peptides shown in **Table 1** ranged from 9.8% to 14.5%. Mass and purity measurements of all the synthesised peptides can be found in the Supporting information, **Figures S1-S12** and **Tables S1-S2**.

A) Linear peptide **P6-W6R8** with increased net charge and lipophilicity

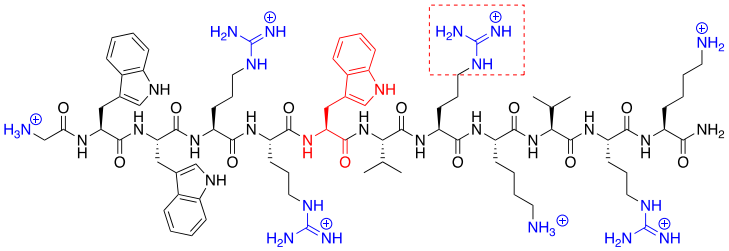

C) Cyclic peptide **cP6-W6R8**

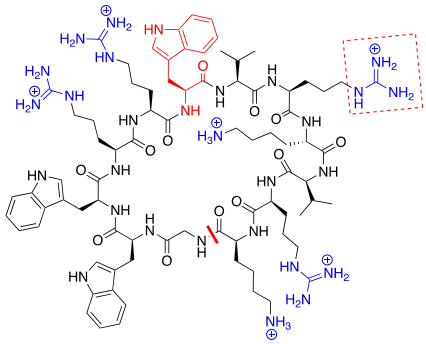

B) Lipopeptide **C8-P6-R8**

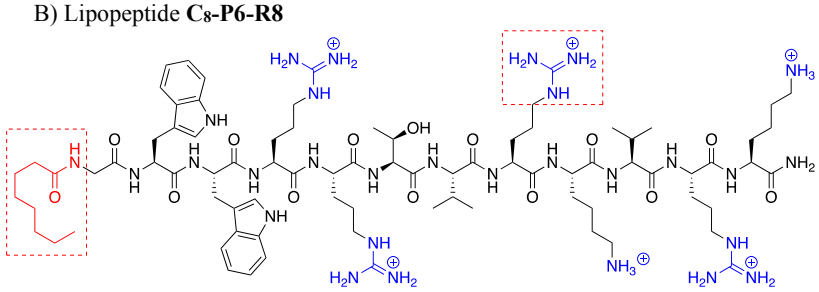

D) Cyclic peptide **cP6-W4R6,8**

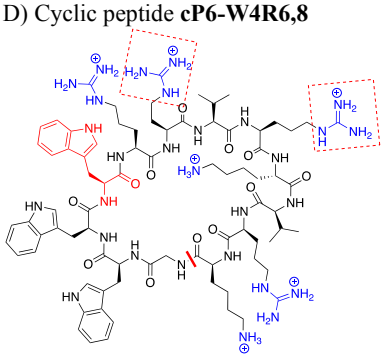

Figure 2. Optimisation strategies investigated for the linear antimicrobial *lead peptide* **P6**. A) Substitution of Ala[8] with Lys[8] or Arg[8] (Arg[8] marked with a red square) in the cationic region of the **P6**-amphiphilic α-helix, and subsequent Thr[6]→Trp[6] (residue in red) substitution in the lipophilic region of the **P6**-amphiphilic α-helix (shown is **P6-W6R8**). B) Synthesis of lipopeptides by *N*-terminal acylation with octanoic acid (shown is **C8-P6-R8**), decanoic acid, and dodecanoic acid. C) Head-to-tail cyclisation of a **P6** analogue (shown is **cP6-W6R8**). D) Formation of a compact lipophilic section in a head-to-tail cyclic **P6** analogue with three consecutive Trp residues (shown is **cP6-W4R6,8**). The red line shows the site of *head-to-tail* cyclisation in C) and D).

2.2 Antimicrobial Activity of Linear Peptides with Increased Net Charge and Lipophilicity

Our previously reported lead peptide **P6** is a potent antimicrobial peptide (AMP), and it is thought to adopt an amphiphilic structure upon interaction with negatively charged bacterial surfaces, as shown in an α-helix projection (**Figure 1**). Apart from being non-haemolytic (EC_{50} >200 μM), it displayed MIC values in the low μM range (MIC: 0.9 – 28 μM) against both Gram-positive and Gram-negative bacteria, and MIC: 7 – 28 μM against fungi (**Table 1**).

Our first strategy was to increase the net positive charge of **P6** by replacing the Ala^8 residue located in the α-helical cationic region with Lys^8, and subsequently with Arg^8 (**Figure 1** and **Table 1**). While both resulting peptides, **P6-K8** and **P6-R8** showed similar antimicrobial activity as observed for **P6**, the Arg modified peptide **P6-R8** displayed two-fold improvement in antimicrobial activity against *Staphylococcus aureus* (**Table 1**). Thus, increasing the net charge from +6 to +7 via Ala^8 to Arg^8 substitution had the greatest impact on antimicrobial activity against *S. aureus*. The observed difference in activity may be due to more favourable electrostatic and H-bond interactions between the guanidine group of Arg^8 and the bacterial membrane, as opposed to those mediated by the amino group of Lys^8.

Next, we wanted to optimise the amphipathicity of these peptides by replacing the Thr^6 residue with Trp^6 in the α-helical lipophilic region. The resulting peptides, **P6-W6K8** and **P6-W6R8** were twice as potent as their Thr-analogues against *Pseudomonas aeruginosa.* A similar improvement in antimicrobial activity was also observed against *Staphylococcus epidermidis* and *E. coli* for the Trp^6/Arg^8 modified peptide **P6-W6R8**. Although major improvement in antimicrobial activity of the already potent lead peptide **P6** was hard to achieve, **P6-W6R8** showed how two strategic amino acid substitutions aimed at increasing overall amphipathicity, resulted in a peptide having superior antimicrobial activity in the very low μM range (MIC: 0.8–1.6 μM) against tested Gram-positive and Gram-negative bacteria (**Table 1**). Moreover, none of the synthesised peptides displayed any measurable haemolytic activity (EC_{50}: >500 μM).

2.3 Antimicrobial Activity of Lipopeptide Analogues

We further wanted to investigate the effects of *N*-terminal acylation on antimicrobial activity and haemolytic toxicity. The peptide **P6-R8** was selected for the *N*-acylation experiments since it was more potent than its lysine analogue, **P6-K8**. As the optimal chain length was found to be between eight and twelve carbon atoms (C_8 to C_{12}), *N*-terminal acylation of **P6-R8** was performed with three aliphatic fatty acids: octanoic acid (C_8), decanoic acid (C_{10}) and dodecanoic acid (C_{12}), resulting in the following lipopeptides: **C_8-P6-R8**, **C_{10}-P6-R8** and **C_{12}-P6-R8** (**Table 1**) [19]. The lipopeptide with shortest acyl chain, **C_8-P6-R8** showed highest antimicrobial activity with MIC of 1.6 μM against all tested Gram-positive strains. It was, however, less potent against *E. coli* (MIC: 6.4 μM) compared to the lipopeptide analogues **C_{10}-P6-R8** and **C_{12}-P6-R8** (MIC: 3.2 μM). A peculiarity was the dramatic increase in haemolytic activity by the stepwise C_2-elongation of the acyl chain in **P6-R8**; starting from **C_8-P6-R8** that was non-haemolytic (EC_{50}: >500 μM), with **C_{10}-P6-R8** causing significant haemolysis (EC_{50}: 173 μM) and ending with the highly haemolytic peptide **C_{12}-P6-R8** (EC_{50}: 26 μM). Thus, *N*-terminal acylation with increasingly longer fatty acids had a greater impact on haemolytic activity than on the antimicrobial activity of the lipopeptides. However, compared to the previous peptides, introducing the Trp^6 residue in **P6-R8** to give **P6-W6R8,** was more beneficial than *N*-terminal acylation, as it resulted in a more potent, non-haemolytic peptide.

2.4 Antimicrobial Activity of Head-to-Tail Cyclic Peptides

Our final investigations involved studying the effects of head-to-tail cyclisation of selected linear peptides on their antimicrobial and haemolytic activity. This modification eliminates an *N*-terminal cationic amino group, thereby reducing the overall positive charge of the cyclised peptide by one unit. Furthermore, head-to-tail cyclisation is most likely to destroy any putative α-helical conformation in the linear **P6** analogues by increasing rigidity and forming a totally new structural arrangement.

To optimise an amphiphilic cyclic structure (**Figure 2**), we synthesised head-to-tail cyclic peptide analogues (given in parentheses) of the starting lead peptide **P6** (**cP6**), the Arg^8 modified peptide **P6-R8** (**cP6-R8**), the highly potent Trp^6/Arg^8 modified peptide **P6-W6R8** (**cP6-W6R8**), and an analogue

of the latter peptide with three consecutive Trp residues (**cP6-W4R6,8**). Our results showed that the cyclic peptide **cP6** had 2- to 17-fold reduced antimicrobial activity compared to the linear lead peptide **P6** (**Table 1**), except against *Corynebacterium glutamicum*. The most dramatic decrease in activity was observed against *P. aeruginosa*. This suggested that cyclisation, and thereby the reduction in overall positive charge of the peptide, along with the loss of a putative amphiphilic α-helical structure, might have contributed to the observed reduction in antimicrobial activity.

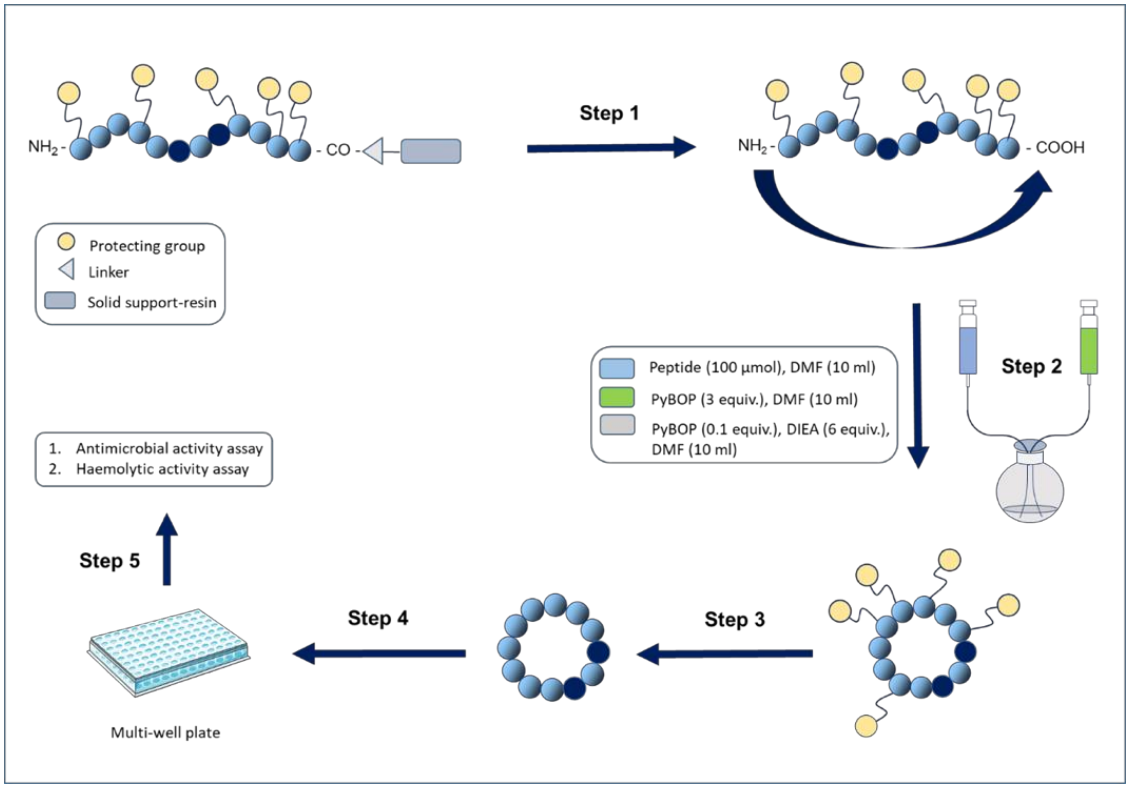

Figure 3. Strategy for preparing head-to-tail cyclic peptides using two syringes attached to a mechanical pump for creating *pseudo-high dilution conditions*[17]. Step 1: Fmoc-SPPS synthesis using a preloaded 2-Cl-Trt resin and subsequent cleavage from the resin with HFIP/DCM. Step 2: Head-to-tail cyclisation. Step 3: Deprotection of side chain protecting groups. Step 4: RP-HPLC peptide purification. Step 5: Bioactivity screening.

By substituting Ala^8 for Arg^8 in **cP6**, we wanted to investigate the effect of increased net charge on antimicrobial activity. The resultant cyclic peptide **cP6-R8** (net charge +6) was more effective against all tested strains compared to **cP6** (net charge +5), with the greatest activity observed against *C. glutamicum* (MIC: 0.1 µM), followed by *B. subtilis* (MIC: 1.7 µM) and *S. epidermidis* (MIC: 1.7 µM). Moreover, the greatest improvement in antimicrobial activity was observed for **cP6-R8** against *S. aureus*. Compared to its linear analogue **P6-R8** (+7), the cyclic peptide **cP6-R8** (+6) was almost equally effective in inhibiting the growth of *S. aureus* (MIC: 6.8 µM), *S. epidermidis* (MIC: 1.7 µM) and *E. c*oli (MIC: 3.4 µM). Against *B. subtilis* **cP6-R8** showed a small decrease in activity compared to **P6-R8**, whereas a more dramatic loss of antimicrobial activity was observed against *P. aeruginosa* (MIC 55 µM for **cP6-R8** compared to MIC: 3.2 µM for **P6-R8**) (**Table 1**). Increasing the lipophilicity by replacing Thr^6 with Trp^6 to give **cP6-W6R8** greatly improved antimicrobial activity compared to **cP6**, with MIC values in the range of 0.4 to 1.6 µM against Gram-positive bacteria and 3.3 to 6.6 µM against Gram-negative bacteria. Compared to its linear analogue **P6-W6R8**, the cyclic peptide **cP6-W6R8** displayed improved potency against *B. subtilis* and *C. glutamicum*, while being equally effective against *S. epidermidis*. Somewhat reduced antimicrobial activity was obtained for **cP6-W6R8** against the Gram-negative strains *E. coli* (MIC: 6.6 µM) and *P. aeruginosa* (MIC: 3.3 µM).

Finally, by switching the positions of Arg^4 and Trp^6 in **cP6-W6R8**, we synthesised a more amphiphilic cyclic analogue **cP6-W4R6,8** (**Figure 2**). The antimicrobial activity of the resultant peptide **cP6-W4R6,8** remained unchanged against *B. subtilis*. It was, however, improved 2-fold against *E. coli* compared to **cP6-W6R8** but was in general reduced 2-fold against the other four bacterial strains: *C. glutamicum*, *S. aureus*, *S. epidermidis* and *P. aeruginosa*. Although significance of having the WWW motif positioned at the *N*-terminus for the antimicrobial and biofilm activity of the linear Trp-rich peptide was reported by Zarena *et al.* [20],our results showed that having three adjacent Trp residues in a cyclic peptide, as in **cP6-W4R6,8**, did not cause additional increase in overall potency.

The strategy of head-to-tail cyclisation revealed that additional sequence optimisations were required to achieve antimicrobial activity in the same μM range as for the linear lead peptide **P6**. Previous research has shown that head-to-tail cyclisation could be effectively used as a tool for reducing haemolysis [21,22]. However, as both the linear peptides and their cyclic analogues were non-haemolytic, this improvement (if present) was not observed. Apart from few exceptions, cyclisation in this study mainly led to 2-fold decrease in antimicrobial activity against tested bacterial strains. It may be that structural constraints conferred by cyclisation, as well as reduction in charge, could have acted unfavourably on the peptide-membrane interactions. All peptides showed high selectivity for bacteria compared to human RBCs except for two of the linear lipopeptides (**C_{10}-P6-R8** and **C_{12}-P6-R8**). A selectivity index (SI) was calculated as the ratio between haemolytic activity (EC_{50}) and the geometric mean (GM) of the MIC values against all bacterial strains, i.e., SI = EC_{50}/GM. When considering the GM, the two most potent and selective peptides could be identified as **P6-W6R8** and its cyclic analogue **cP6-W6R8**, both having a GM of 1.3–1.4 μM and SI > 347. For these two peptides, as our results suggested, the amino acid sequence had much greater influence on antimicrobial activity than a linear vs. cyclic structure. Nevertheless, both peptides are considered amphiphilic, which is most likely to have contributed to their favourable antimicrobial profile (**Figure 1** and **Figure 2).**

2.5 Antifungal Activity

All synthesised peptides were screened for antifungal activity against *Aureobasidium pullulans, Candida albicans*, and *Rhodotorula* sp., out of which *C. albicans* is of greatest medical importance. *A. pullulans* and the *Rhodotorula* sp. can, however, cause severe infections in immunocompromised patients [23-25] and were included in this work for structure-activity relationship purpose (**Table 1**). Previous studies have shown that the EeCentrocin 1 HC peptide had a negligible inhibitory effect against *C. albicans* (MIC: 100 μM) while being active against *Rhodotorula* sp. (MIC: 12.5 μM) [15]. The lead peptide **P6** displays, however, improved antifungal activity especially against *C. albicans* (MIC: 28 μM), and to a lesser degree against *Rhodotorula* sp. (MIC: 7.0 μM) [16]. To our surprise there were only minor variations in antifungal activity with respect to differences in sequence and structure of the synthesised peptides. The linear peptides modified by either the Ala^8 to Lys^8/Arg^8 (**P6-K8** and **P6-R8**) and Thr^6 to Trp^6 substitutions (**P6-W6K8** and **P6-W6R8**) displayed (with one exception) similar antifungal activity against *A. pullulans* and *C. albicans* (MIC: 12-13 μM), but two-fold higher potency against *Rhodotorula* sp. (MIC: 6.2–6.5 μM). These analogues were overall more potent against fungi compared to **P6**. The *N*-acylated **C_8-**, **C_{10}-** and **C_{12}-P6-R8** lipopeptides had antifungal activity comparable to that of **P6** with MIC: 25-26 μM against *A. pullulans* and *C. albicans*, and MIC: 6.3-6.4 μM against *Rhodotorula* sp. Thus, no major variation in antifungal activity was observed by varying the acyl chain length of these lipopeptides.

The head-to-tail cyclic peptides were all equally potent against *A. pullulans* and *C. albicans* (MIC: 13–15 μM). Although still low, the antimicrobial activity of **cP6-R8**, **cP6-W6R8** and **cP6-W4R6,8** was higher against *Rhodotorula* sp. (MIC: 6.6–6.8 μM) than that of **cP6** (MIC: 15 μM). Head-to-tail cyclisation did not seem to have any major effect on antifungal activity since the potencies were comparable to those of their corresponding linear analogues. One exception was improved antifungal activity against *A. pullulans* and *C. albicans* for **cP6** compared to **P6**. However, the opposite effect was observed against *Rhodotorula* sp. in which **P6** was more potent than **cP6**. These findings highlight the need for further research with the aim of identifying the structural modifications necessary for improving the antifungal activity of these peptides.

Table 1. Antimicrobial activity of synthesised peptides against bacteria and fungi (MIC in μM), and toxicity against human RBC (EC_{50} in μM). Sequence modifications (amino acid replacements) compared to the lead peptide **P6** are shown in bold, and sequences in parentheses denote head-to-tail cyclic peptides. The selectivity index (SI) was calculated as the ratio between haemolytic activity (EC_{50}) and the geometric mean (GM) of the MIC values against all bacterial strains, i.e., SI = EC_{50}/GM.

	Peptide	Sequence	Mw[2]	Net Charge[3]	Rt[4]	Antimicrobial activity (MIC)[1]										Tox. (EC_{50})	SI
						Gram +				Gram -		GM	Fungi				
						Bs	Cg	Sa	Se	Ec	Pa		Ap	Ca	Rh	RBC	
Linear peptides	**P6**	GWWRRTVAKVRK-NH_2	1541.9	+6	3.32	0.9	0.9	28	1.8	3.5	3.5	2.8	28	28	7.0	>500	>177
	P6-K8	GWWRRTV**K**KVRK-NH_2	1599.0	+7	3.18	0.8	0.8	13	1.6	3.3	3.3	2.3	13	26	6.5	>500	>217
	P6-R8	GWWRRTV**R**KVRK-NH_2	1627.0	+7	3.20	0.8	0.8	6.4	1.6	3.2	3.2	2.0	13	13	6.4	>500	>248
	P6-W6K8	GWWRR**W**V**K**KVRK-NH_2	1684.1	+7	3.67	1.6	0.8	1.6	1.6	3.1	1.6	1.6	13	13	6.3	>500	>314
	P6-W6R8	GWWRR**W**V**R**KVRK-NH_2	1712.1	+7	3.61	1.6	0.8	1.6	0.8	1.6	1.6	1.3	12	12	6.2	>500	>394
Linear lipo-peptides	**C_8-P6-R8**	C_8-GWWRRTV**R**KVRK-NH_2	1753.2	+6	4.70	1.6	1.6	1.6	1.6	6.4	6.4	2.5	26	26	6.4	>500	>197
	C_{10}-P6-R8	C_{10}-GWWRRTV**R**KVRK-NH_2	1781.2	+6	5.16	3.2	3.2	3.2	1.6	3.2	6.3	3.2	25	26	6.3	173	54
	C_{12}-P6-R8	C_{12}-GWWRRTV**R**KVRK-NH_2	1809.3	+6	5.67	3.1	3.1	3.1	3.1	3.1	6.3	3.5	25	25	6.3	26	7
Cyclic peptides	**cP6**	c(GWWRRTV**A**KVRK)	1524.8	+5	3.36	1.9	0.9	60	15	7.5	60	9.4	15	15	15	>500	>53
	cP6-R8	c(GWWRRTV**R**KVRK)	1610.1	+6	3.20	1.7	0.1	6.8	1.7	3.4	55	2.7	14	14	6.8	>500	>187
	cP6-W6R8	c(GWWRR**W**V**R**KVRK)	1695.1	+6	3.76	0.8	0.4	1.6	0.8	6.6	3.3	1.4	13	13	6.6	>500	>347
	cP6-W4R6,8	c(GWW**W**R**R**V**R**KVRK)	1695.1	+6	3.62	0.8	0.8	3.3	1.6	3.3	6.6	2.0	13	13	6.6	>500	>244
	Oxytetracycline HCl		496.9			40	0.6	0.6	2.5	2.5	40	-[5]	-	-	-	-	-
	Polymyxin B sulfate		1189.3			0.7	0.3	5.3	2.6	0.7	1.3	-	2.6	11	1.3	-	-
	Triclosan		289.5			-	-	-	-	-	-	-	22	22	5.4	-	-

[1] Microbial strains; Bs – *Bacillus subtilis* 168 (ATCC 23857), Cg – *Corynebacterium glutamicum* (ATCC 13032), Sa – *Staphylococcus aureus* (ATCC 9144), Se – *Staphylococcus epidermidis* RP62A (ATCC 35984), Ec – *Escherichia coli* (ATCC 25922), Pa – *Pseudomonas aeruginosa* (ATCC 27853), *Ap – Aureobasidium pullulans, Ca – Candida albicans* (ATCC 10231), *Rh – Rhodotorula* sp. [2] Average molecular mass of synthesised peptides, without including a TFA salt for each cationic charge. [3] Net charge at physiological pH (7.4). [4] Retention time (min) on RP-UPLC. ''-'': not calculated or tested.

2.6 Effects on Bacterial Viability and Membrane Integrity

Two luciferase-based biosensor assays (viability and membrane integrity) were used to investigate the mode of action of all synthesised linear and cyclic analogues on *B. subtilis* 168 and *E. coli* K12 biosensors. Bacterial luciferase is an excellent real-time sensor for bacterial viability, as endogenous production of the substrate pools, such as reduced flavin mononucleotide ($FMNH_2$) and long-chain aliphatic aldehydes, are responsible for the bioluminescence. A decrease in light production indicates loss of metabolic activity and thus viability. In contrast, in the membrane integrity assay the addition of exogenous substrate such as D-luciferin is required for light production by the eukaryotic luciferase gene (*LucGR*). Light emission will peak rapidly when the membrane integrity is compromised, enabling externally added substrate D-luciferin to pass through damaged membrane. The subsequent decrease in light production occurs while ATP in dying cells is being consumed.

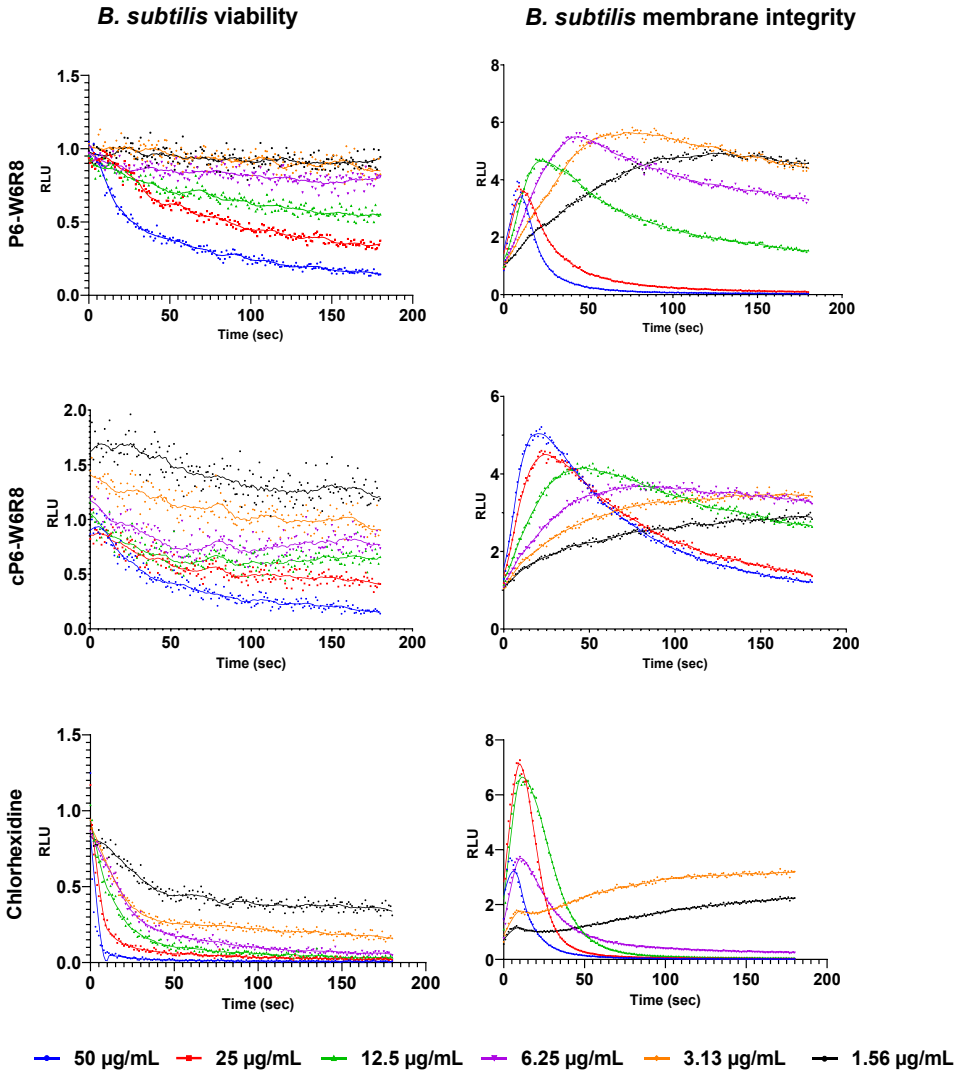

Figure 4. Immediate effects of **P6-W6R8**, **cP6-W6R8** and chlorhexidine (membranolytic control) on the kinetics of viability (left) and membrane integrity (right) in *B. subtilis* 168. Light emission normalized to the untreated water control is plotted as relative luminescence units (RLU) over time (seconds). All the graphs show a representative data set where each experiment was run at least three times independently.

Here we present the results from the mode of actions studies of the linear peptide **P6-W6R8** and its cyclic analogue **cP6-W6R8**. The results for the remaining peptides can be found in the Supporting information, **Figures S13–S20**. As shown in **Figure 4**, both **P6-W6R8** and **cP6-W6R8** clearly affected the viability of *B. subtilis* in a concentration-dependent manner. To further confirm that the rapid decrease in bacterial viability was caused by membrane damage, the membrane integrity assay was performed on the *B. subtilis* biosensor strain. **P6-W6R8** showed a membrane-related mode of action as light emission decreased rapidly at the two highest concentrations. In addition, for the lower concentrations a declining pattern in a dose-dependent manner was also observed (**Figure 4**). For **cP6-**

W6R8, a concentration dependent emission of light was observed, with a subsequent decline at higher concentrations. However, the effect was slightly delayed when compared to the linear peptide **P6-W6R8**. The membranolytic reference control chlorhexidine had a MIC value of 1.6 µg/mL (3.1 µM) against both *B. subtilis* and *E. coli*. While comparing the effects of **P6-W6R8** and **cP6-W6R8** on the viability and membrane integrity of the Gram-negative *E. coli*, we observed a somewhat different mode-of action. As shown in **Figure 5**, the decrease in light emission was substantially slower than that for similar concentrations in *B. subtilis*. The linear analogue **P6-W6R8** affected the membrane integrity of the *E. coli* strain and it shows a concentration-dependent effect on viability. Although **cP6-W6R8** also affected the viability, a much less prominent inner membrane disruptive effect was observed as only concentrations at, or above MIC (≥12.5 µg/mL) gave rise to light emission. This might be due to its lower antimicrobial activity or delayed action on the inner membrane of Gram-negative bacteria.

Results from both the membrane integrity and viability assay at concentrations below 3.13 µg/mL did not seem to reflect the MIC, as light emissions stayed unchanged throughout the assay period. However, these assays are conducted with 1000x higher bacterial concentrations than the MIC assay. In addition, the MIC assay integrates activity over a 24 h time frame, while the luminescence-based assays are only run for 3 min to elucidate immediate activity. At 50 µg/mL **cP6-W6R8** reduced viability by 35% within 3 min, while light emission from the membrane integrity assay stayed at 30x the control. Lower concentrations did not show such a strong membrane effect. This difference in light emission from the two assays is likely based on the different processes for light production. While the membrane assay is solely based on ATP as energy source and externally added D-luciferin, the viability assay integrates both ATP and reduction equivalents for light production and substrate regeneration. In this case the ATP pool does not seem to be limiting.

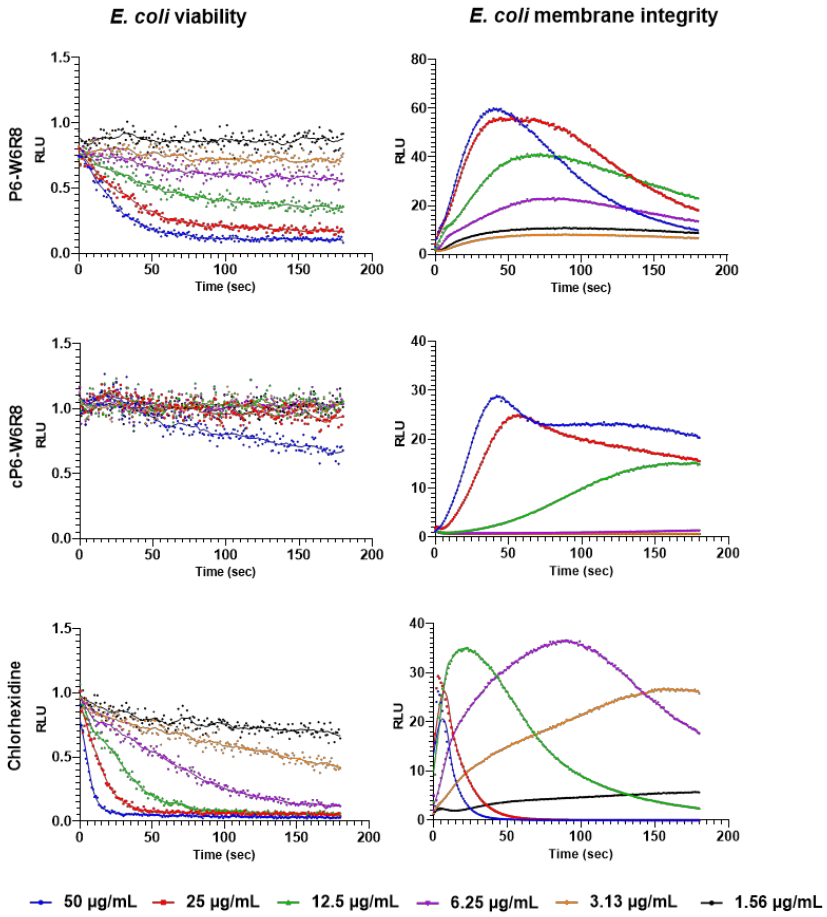

Figure 5. Immediate effects of **P6-W6R8**, **cP6-W6R8** and chlorhexidine (membranolytic control) on the kinetics of viability (left) and membrane integrity (right) in *E. coli* K12. Light emission normalized to the untreated water control is plotted as relative luminescence units (RLU) over time (seconds). All the graphs show a representative data set where each experiment was run at least three times independently.

2.7. Permeabilization of the Outer Membrane of E. coli *and* P. aeruginosa

To investigate whether the delayed and reduced action on the membrane integrity might be due to the presence of the outer membrane of *E. coli* and *P. aeruginosa*, we performed the outer membrane NPN assay [26]. The fluorescence of the lipophilic dye *N*-phenyl-1-napthylamine (NPN) can be utilised to investigate the ability of AMPs to permeabilise the outer membrane of Gram-negative bacteria. NPN emits weak fluorescence in aqueous environment and is highly fluorescent in hydrophobic environment found in lipidic membranes. It cannot insert into intact bacteria membranes. However, upon disruption of the outer membrane of Gram-negative bacteria by AMPs, NPN gains access to lipid layers in the outer membrane and/or in the cytoplasmic membrane resulting in the increase of fluorescence emission. Both **P6-W6R8** and **cP6-W6R8** showed similar concentration-dependent increase in NPN fluorescence at concentrations ranging from 1.56 to 25 µg/mL in *E. coli*, indicating a membrane permeabilising effect (**Figure 6**). However, at lower concentrations, fluorescence intensities were comparatively lower for **cP6-W6R8** than for **P6-W6R8**. Similar effects were observed in *P. aeruginosa* for both **P6-W6R8** and **cP6-W6R8**. Even though both peptides displayed a membrane related (primary) mode of action, there is still possibilities that they have other mechanism at lower concentrations. It has been documented that certain cationic AMPs exhibit a concentration-dependent dual mode of action [27,28].The reference control polymyxin B (PMB), a bactericidal peptide antibiotic known for its membrane disruptive properties, showed a MIC value of 0.78 µg/mL (0.7 µM) against *E. coli* and 1.56 µg/mL (1.3 µM) against *P. aeruginosa* (**Table 1**).

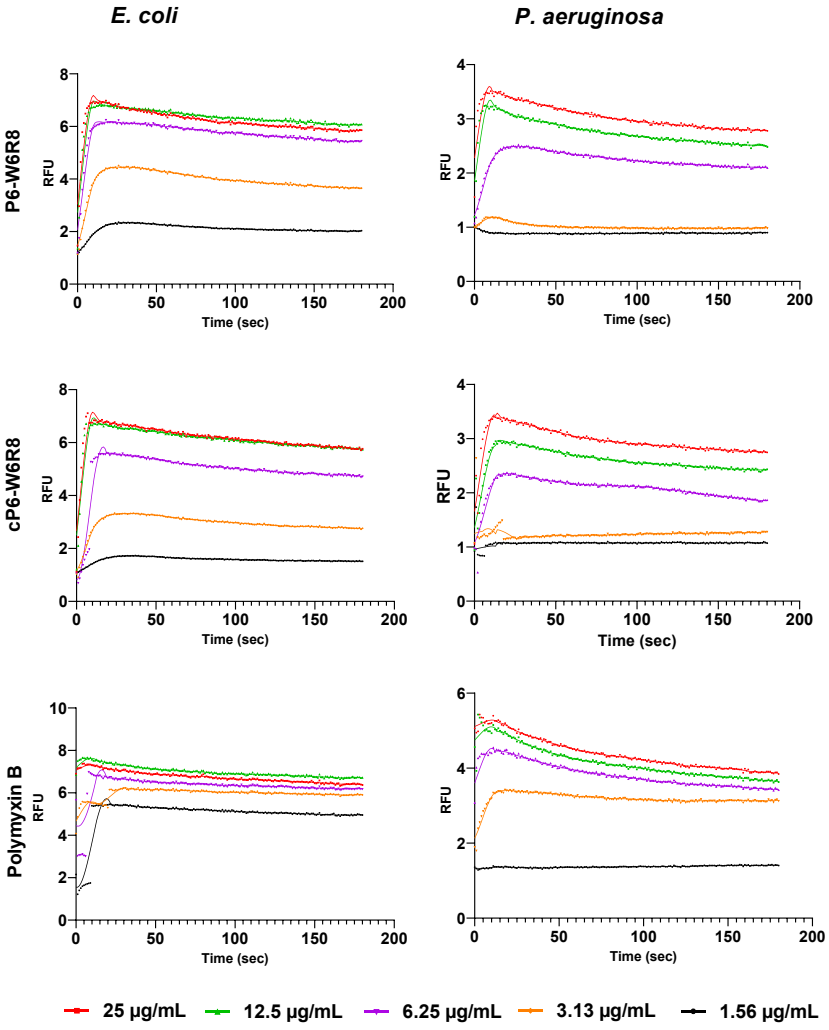

Figure 6. Comparison of the effects of **P6-W6R8**, **cP6-W6R8** and polymyxin B on the kinetics of NPN fluorescence in *E. coli* and *P. aeruginosa*. After addition of the bacterial inoculum (mixed with 20 µM NPN) to the wells (preloaded with lipopeptides), light emission was measured each second for 3 min. Each colored line represents the total 180 s data points from the assay at different concentrations. Each figure shows a representative data set.

2.8. Effects on Cell Envelope related Stress Response in B. subtilis

The assays are based on reporter strains containing chromosomally integrated fusions of different stress inducible promoters from *B. subtilis* to the *luxABCDE* operon, as described by Radeck *et al*. 2013 [29]. The sensors indicate the presence of mode of action specific stressors exhibiting increased light output caused by the specific stress response reported through each promoter-*lux*-operon fusion. P_{liaI} responds to cell envelope perturbations and membrane damage by cationic AMPs, P_{yorB} to inhibition of DNA replication, P_{yvgS} to transcription inhibition, P_{yheI} to translation inhibition and P_{fabHB} to inhibition of fatty acid synthesis (29, 30). Originally, we tested all the synthetic linear and cyclic analogues against the panel of sensor strains. Of the 5 sensors used in this study, only the P_{liaI} fusion, specific for cell envelope stress, responded by increased light output compared to the water control, and where the peptides **P6**, **P6-W6R8** and **cP6-W6R8** reproducibly induced light output. Luminescence kinetics for the first 5.5 h (**Figure S21**). At around 45 minutes after addition, both positive controls, vancomycin and bacitracin, reached their maximal induction levels. On the other hand, the maximal induction rates of the peptides were reached at about 60 minutes. **Table 3** summarizes the average relative luminescence and standard deviations from four measurements as the maximal recorded induction one hour after addition of the peptide and the concentrations corresponding with this maximal activity. Both **P6-W6R8** and **cP6-W6R8** seemed to induce a stress response 4 hours and 5 hours after peptide addition, respectively. This late increase in luminescence coincided with the bacteria beginning to grow.

Table 3. Cell wall stress dependent relative luminescence in *B. subtilis* at 60 minutes after analyte addition.

	P6	**P6-W6R8**	**cP6-W6R8**	**Vancomycin**	**Bacitracin**
Concentration (µg/mL)	25	3.1	6.25	50	100
Relative luminescence	12.0±2.0	2.1±0.3	3.9±0.5	19.7±2.8	197.9±1.9

B. subtilis has been shown to have an intricate network of countermeasures when encountering antibacterial compounds in its environment. To respond in a timely fashion to an antibacterial attack, an intricate response system with built-in failsafes has evolved, enabling *B. subtilis* to survive when encountering antibiotic-producing competitors in their niches [30]. In this study, we used the previously established biosensor strains described by Juskewitz, *et al*., 2022 [31], which tap into a selection of promoters involved in the *B. subtilis* antibiotic stress response. The EeCentrocin-derived lead peptide **P6** and its derivatives had originally been identified as plasma membrane-active and optimized with the goal of increasing this specific activity. We wanted to find out if the peptides had further and hitherto hidden activities and possibly confirm the membrane activity with an adequate stress response.

The only sensor responding to the presence of peptides between 2x and 0.5x MIC was the P_{liaI}-based cell envelope stress sensor, which is known to be part of the defense system against bacitracin but also responds to membrane damage caused by cationic AMPs like LL-37 [32]. Only three peptides, **P6**, **P6-W6R8** and **cP6-W6R8** elicited a consistent response, mostly around the MIC. In contrast, both vancomycin and bacitracin showed a dose-dependent response over at least six dilution steps, including the MIC, which was up to 18 times stronger than that of the peptides (**Figure S21**). At first glance, it seems that the relatively low reported induction of cell envelope stress indicates negligible activity, especially when compared to the high induction rates over a wide range of concentrations observed for vancomycin and bacitracin. However, in contrast to both vancomycin and bacitracin, the peptides immediately affect cell viability by compromising plasma membrane integrity and thereby immediately shut down cell metabolism. Unfortunately, the sensor strains used in this study depend on both translation of the reporter gene and, more importantly, on active metabolism for signal generation, as light emission from *lux*-luciferases directly depends on the presence of FMNH as reducing equivalents - and indirectly on $NADPH_2$ and ATP for regeneration of the long-chain fatty aldehyde substrate and FMNH [33]. Therefore, membrane-active compounds will interfere with the detection of potential secondary activities by camouflaging potential signals as false negatives if the induction range is above

the minimal concentration needed for membrane activity. This is also illustrated by the postponed measurable stress response seen for **P6-W6R8** and **cP6-W6R8**. In contrast, vancomycin and bacitracin do not affect *B. subtilis* viability immediately (if at all in the case of the latter), giving the sensors ample time to generate a response. Reviewing the results considering membrane activity, we can conclude that any potential secondary activity exerted by the peptides against *B. subtilis* is likely secondary in nature and requires higher peptide concentrations than for the membranolytic activity. Further, the results support the conclusion that the peptides are indeed membrane-active, as a membrane-stress-dependent expression of *liaI* has previously been reported [32].

2.9. Antimicrobial Activity against E. coli Strains with or without an Outer Membrane or OmpT Protease

The outer membrane (OM) in Gram-negative bacteria plays a critical role in susceptibility to many antimicrobials since it is a barrier to both hydrophobic and hydrophilic compounds including AMPs [34]. Given the importance to one of the survival strategies that bacteria employ against toxic molecules, several members of the outer membrane Omptin protease family proteins in *Enterobacteriaceae* are reported to act as virulence factors that protect them from cationic AMPs [35,36]. The outer membrane protein T (OmpT), a 33.5 kDa endoprotease found in *E. coli*, has been reported to inactivate endogenous and heterologous AMPs including LL-37, protamine, and the synthetic peptide C18G [35-37]. Overexpressed OmpT is also shown to contribute to virulence of *E. coli* strains in human urinary tract infections [38]. Investigation of OmpT mediated resistance in *E. coli* strains upon peptide exposure can thus be useful for rational design of peptides to improve their proteolytic stability and potency. To investigate if differences in genotype and outer membrane integrity affect the susceptibility to the AMPs, we determined the MIC values of the peptides against different *E. coli* strains including the wild type MC4100 and the isogenic outer membrane deficient NR698 mutant, the wild type BW25113 (from the Keio collection) and its isogenic *ompT* deletion mutant JW0554, and the commercially available strain BL-21(DE3) - lacking genes for Lon and OmpT proteases production, as well as a transformed BL-21(DE3) mutant, containing a plasmid with OmpT overexpressing machinery (**Table 2**).

Table 2. Antimicrobial activity (MIC in μg/mL) of synthesized peptides against different wild type and mutant *E. coli* strains. Dibasic residues in the peptide sequences, putatively susceptible to proteolytic cleavage by OmpT endoprotease, are shaded in grey.

Name	Sequence	MC4100	NR698	BW25113	JW0554 Δ*ompT*	BL-21	BL-21+ *ompT* plasmid
P6	GWWRRTVAKVRK-NH_2	2	2	4	4	4	8
P6-K8	GWWRRTVKKVRK-NH_2	4	4	8	8	8	16
P6-R8	GWWRRTVRKVRK-NH_2	4	4	8	4	4	16
P6-W6K8	GWWRRWVKKVRK-NH_2	4	4	4	4	4	8
P6-W6R8	GWWRRWVRKVRK-NH_2	4	4	8	4	8	16
C_8-P6-R8	C_8-GWWRRTVRKVRK-NH_2	8	4	8	4	8	16
C_{10}-P6-R8	C_{10}-GWWRRTVRKVRK-NH_2	8	4	8	4	8	16
C_{12}-P6-R8	C_{12}-GWWRRTVRKVRK-NH_2	8	8	16	8	8	16
cP6	c(GWWRRTVAKVRK)	16	4	16	8	8	8
cP6-R8	c(GWWRRTVRKVRK)	4	4	8	8	8	8
cP6-W6R8	c(GWWRRWVRKVRK)	4	4	8	8	8	8
cP6-W4R6,8	c(GWWWRRVRKVRK)	4	4	8	16	16	32

We observed similar MIC values against the wild type MC4100 and NR698 for all the linear peptides, as well as the cyclic peptides **cP6-W6R8**, **cP6-R8** and **cP6-W4R6,8**, which may indicate that the presence of an outer membrane does not seem to affect their antimicrobial activity. For cationic peptides with high inner membrane specificity, the antimicrobial potency is unlikely to be dependent on the presence of an outer membrane when the critical threshold concentration reaches a lethal level [39]. However, the outer membrane deficient strain NR698 was slightly more sensitive to the lipopeptides **C_8-P6-R8**, **C_{10}-P6-R8**, and the cyclic **cP6**, indicating that the outer membrane appeared to hinder their antimicrobial effect. The four-fold increase in MIC for **cP6** against the wild type strains, MC4100 and BW25113, compared to NR698 support its slower inner membrane disruption observed in the *E. coli* K-

12 biosensor strain (**Figure 5**). The MIC values against the biosensor strain (**Table S3**) were similar to the MICs against BW25113.

To investigate if the OmpT protease degrades and reduces the effect of the linear peptides in wild type strains and if its absence causes increased susceptibility in the mutant strains, we compared the MIC values against the wild type BW25113 and the Δ*ompT* mutant JW0554, (a knock-out mutant strain from the Keio collection). BW25113 showed a slightly different susceptibility pattern compared to its isogenic Δ*ompT* mutant. It is noteworthy that all the linear peptides containing -R_8K_9- dibasic residues in their sequences (**P6-R8**, **P6-W6R8**, and **C_{8-12}-P6-R8** lipopeptides) showed a 2-fold decrease in MIC in the Δ*ompT* mutant strain whereas the MICs were unchanged for the other linear peptides (**P6**, **P6-K8**, and **P6-W6K8**) (**Table 2**). This might indicate an enzymatic preference for arginine in the P1-position of the cleavage site. However, no apparent difference in MICs were observed for the cyclic peptides, indicating increased proteolytic stability. Another reason for this might be that a single proteolytic cleavage of the cyclic peptides would provide 12 residues linear peptides with equal antibacterial activities.

When we used *E. coli* BL-21(DE3) cells lacking Lon and OmpT proteases, the susceptibility pattern remained unchanged for most of the linear and cyclic peptides compared to the Δ*ompT* mutant (JW0554). To explore the effect of OmpT protease production, we complemented the negative genotype by transforming the BL-21 strain with a plasmid containing an arabinose inducible *ompT* under the control of the P_{BAD} promoter (pHD001). MICs of the BL-21 clone expressing *ompT* in response to the presence of arabinose were compared to its parental strain without the plasmid. Interestingly, complementation of BL-21 with the plasmid-derived OmpT reduced the susceptibility towards all the linear peptides as the MIC increased by two to four-fold while the MICs of the cyclic peptides remained unchanged. Of note, the MICs of both **P6-W6R8** and **cP6-W6R8** against the BL-21 clone expressing *ompT* were 2-fold higher than the MICs against the wild type BW25113. It has been reported that different *E. coli* strains degrade AMPs to different extents due to differential *ompT* expression [36]. We do not exactly know all the factors that are responsible for the differential expressions and optimal catalytic function of OmpT as we did not conduct a quantitative analysis of OmpT expression in the various *E. coli* strains that were used. This might also explain why presence/absence of OmpT does not make the *E. coli* strains hyper-sensitive or hyper-resistant towards the AMPs. It is therefore likely that other proteases or stress related regulatory expression may act synergistically to counteract AMPs. Several other stimuli may account for the resistance mechanism towards AMPs in Gram-negative bacteria, for example the presence of efflux pumps, modification of LPS and other outer membrane components, and secretion of compounds that downregulate host AMP expression [40].

2.10. Proteolytic Stability of AMPs after Exposure to E. coli Strains with or without OmpT Protease

The outer membrane protease OmpT (and its homologue OmpP) possess a membrane bound β-barrel structure facing the active site in the extracellular space of the *E. coli* membrane [38]. The protease cleaves preferentially between two consecutive basic amino acid residues in the scissile peptide sequence [41]. The amino acids involved in the peptide bond (with substrate residues on either side of this bond) is known as P1 and P1′ [42], and for OmpT these are preferably -KK-, -KR-, -RK-, or -RR- [43,44]. To investigate whether OmpT has substrate specificity towards the dibasic residues present in the linear **P6-W6R8** and/or the cyclic **cP6-W6R8**, we used matrix-assisted laser desorption ionization – time of flight (MALDI-TOF) mass spectrometry. By doing so we wanted to detect any peptide fragments produced after exposing the peptides to the *E. coli* wild type BW25113 and its isogenic *ompT* deletion mutant JW0554, and the commercially available strain BL-21(DE3) and the transformed mutant containing a plasmid with *ompT*.

In the wild-type strain BW25113, a proteolytic fragment of m/z 1201.9 were observed when exposed to the linear **P6-W6R8 (Table 3, Figure S22)**. This fragment matches the expected OmpT cleavage site at -R_8-K_9- generating the *N*-terminal fragment P6-W6R8(1-8), representing the sequence GWWRRWVR. No peptide related fragments of **P6-W6R8** were detected in the Δ*ompT* mutant JW0554, which could explain why the MIC against JW0554 was twofold lower than the MIC against the OmpT-producing BW25113. When exposing BW25113 to the cyclic **cP6-W6R8**, two peptide-derived fragments were detected: m/z 1713.1 and m/z 1115.7. The largest fragment (m/z 1713) represents one or more hydrolysis (+18 Da) cleavage products generating linear versions of the peptide. The cyclic peptide has 3 dibasic residues present in its structure, providing three putative linear sequences with a C-terminal hydroxyl-group – all having the same mass (**Table 3**). The observed m/z 1116 fragment is most likely a result of

the internal cleavage between two scissile bonds -R_4-R_5- and -R_8-K_9- in the cyclic peptide (numbering based on the amino acid positions of the linear peptide), resulting in the intermediate fragment cP6-W6R8(9-4) having the sequence KVRKGWWR. As with the linear **P6-W6R8**, no peptide-related fragments of **cP6-W6R8** were identified in the *ompT* knock-out mutant JW0554.

Table 3. Peptides and cleavage fragments detected by MALDI-TOF mass spectrometry after exposing *E. coli* strains with or without OmpT protease production to the linear peptide **P6-W6R8** and the cyclic peptide **cP6-W6R8**. Indication of sequence position of the obtained fragments is based on the amino acid positions of the linear peptide. Suggested cleavage sites by the bacterial OmpT protease are shaded in grey.

Peptide / fragment (and sequence position)	Sequence and proposed cleavage site(s)	Theoretical m/z, $[M+H]^{+1}$	Observed m/z, $[M+H]^{+1}$			
			BW25113	JW0554 Δ*ompT*	BL-21	BL-21 + OmpT
P6-W6R8	GWWRRWVRKVRK-NH_2	1712.0	1712.3	1712.1	1712.1	1712.2
P6-W6R8 (1-8)	GWWRRWVR-K	1201.7	1201.9	-[1]	-	1201.7
P6-W6R8 (1-4)	GWWR-R	604.3	-	-	-	604.1
cP6-W6R8	c(GWWRRWVRKVRK)	1695.0	1695.1	1695.0	1695.2	1695.2
Linear fragments:	Putative sequences:					
cP6-W6R8 (5-4)	R-RWVRKVRKGWWR-R	1713.0				
cP6-W6R8 (8-7)	R-KVRKGWWRRWVR-K	1713.0	1713.1	-	-	1713.1
cP6-W6R8 (12-11)	R-KGWWRRWVRKVR-K	1713.0				
cP6-W6R8 (9-4)	R-KVRKGWWR-R	1115.7	1115.7	-	-	1115.7
cP6-W6R8 (12-4)	R-KGWWR-R	732.4	-	-	-	732.4

[1] Not detected.

To confirm the role of OmpT in the AMP fragmentation, we compared OmpT dependent peptide degradation in *E. coli* BL-21 that lacks the OmpT protease with a BL-21 clone expressing *ompT* in presence of arabinose. As expected, both **P6-W6R8** and **cP6-W6R8** were prone to degradation when exposed to the OmpT-complemented BL-21strain, whereas no cleavage products were observed in the BL-21 strain (lacking genes for OmpT protease production). The previously mentioned peptide fragments (m/z 1201 for the linear peptide and m/z 1115 and m/z 1713 for the cyclic peptide) were all observed when exposed to the OmpT-expressing mutant. We were also able to detect a small fragment with m/z 604.2 from the linear peptide, likely representing the *N*-terminal GWWR - supporting that this protease is also able to cleave the peptide at its dibasic site -R_4-R_5-. In addition, we were able to detect a fragment with m/z 732.4 from the cyclic peptide. This fragment is most likely the internal sequence cP6-W6R8 (12-4), having the sequence KGWWR, supporting cleavage of the peptide also at its dibasic site -R_{11}-K_{12}-(**Table 3, Figure S23**). Cleavage between -R_{11}-K_{12} was, as expected, not observed for the linear peptide since OmpT is an endoprotease.

Altogether, we have verified that both the linear **P6-W6R8** and the cyclic peptide **cP6-W6R8** are, in fact, substrates for OmpT as the protease was able to cleave the peptides at all dibasic sites, producing fragments that were easily detected by MALDI-TOF MS. A single proteolytic cleavage (due to OmpT) of the linear peptides, producing small, putatively inactive fragments of the peptide, might be the reason for the two-fold increase in MIC observed against the OmpT-producing strains (**Table 2**). On the other hand, a single hydrolysis cleavage of the cyclic peptide could in theory produce three linear sequences with equal antibacterial activity (**Table 3**). This might be the explanation for why the MICs of the cyclic peptides remained unchanged between the different strains. The MALDI-TOF data also show that no other proteases than OmpT was involved in the peptide degradation, since no peptide-derived fragments were identified in the MS spectra (in the selected region of m/z 600-2000) of the strains devoid of OmpT.

We were not able to explore any concentration-dependent peptide cleavage, since we observed relatively large variations in the m/z intensity of peptides and fragments between replicates of the different samples, likely due to dependency on bacterial concentrations as well as peptide concentrations around the MIC-values. However, we were able to detect fragments when OmpT-producing strains were exposed to peptide concentrations as low as 4 μg/mL. Below this concentration, the detection of m/z fragments was suppressed by bacterial and matrix components. One should also keep in mind that the intensity of the m/z fragments observed in the BL-21 OmpT-producing mutant only reflects the proportion of cells which expressed OmpT and that the degree of expression was therefore not enough to establish a stable phenotype (with an increased MIC). It is surprising that we observed the intact peptide at concentrations lower than MIC (although the intensities were quite low), which could be

explained by the fact that the peptide substrate concentration below the threshold is not sufficient for a strong electrostatic interaction with the enzyme´s active site. The induced fit theory by Koshland´s explains the basis of enzyme catalysis where substrate binding plays pivotal role in converting an enzyme active site into the proper catalytic arrangement [45,46]. Simulation studies also indicate that strong electrostatic interaction with the substrate can be responsible for modulating the catalytic site of OmpT and thus enhance the activity to a greater extent [46,47]. It has also been reported that if permeabilized dead bacteria sequester or internalize membrane bound peptides - they will no longer be available for proteolytic cleavage [48]. Thus, our results suggest that membrane-bound peptides at low concentration, which are not in direct proximity to the enzyme´s active site, can potentially be concealed from enzymatic cleavage. Overall, these results give valuable information of OmpT substrate specificity that can be used as a stability determinant in future peptide drug development studies. Surprisingly, no proteolytic cleavage products were identified in the OmpT-deficiant strains, indicating that Lon proteases in the wild type strains are not involved in peptide degradation.

3. Materials and Methods

3.1. Synthesis of Linear Peptides

Peptides were synthesised on a Biotage® Initiator+Alstra™ fully automated microwave assisted peptide synthesiser. All Fmoc-amino acids were purchased from Sigma-Aldrich. Solvents were purchased from either VWR chemicals or Sigma-Aldrich. Rink amide ChemMatrix resin was obtained from Biotage (Uppsala, Sweden). Synthesis of the linear peptides and lipopeptides was accomplished by microwave (*mw*) assisted Fmoc solid phase peptide synthesis (Fmoc-SPPS) using Rink amide ChemMatrix resin (loading 0.50 mmol/g, scale 165 mmol). Fmoc-protected amino acids (4 equiv.) were coupled in the presence of O-(1H-6-Chlorobenzotriazole-1-yl)-1,1,3,3-tetramethyluronium-hexafluorophosphate (HCTU, 4 equiv.) and *N,N*-Diisopropylethylamine (DIEA, 8 equiv.) under *mw* irradiation at 70 °C, for 10 min, except for Fmoc-Arg(Pbf)-OH which was coupled at room temperature for 60 min. Prior to synthesis, all amino acids (0.5 M) were dissolved in *N,N*-dimethylformamide (DMF), whereas *N,N*-diisopropylethylamine (DIPEA, 2 M) was dissolved in *N*-methyl-2-pyrrolidone (NMP). A double coupling was used to ensure complete acylation of the *N*-terminal amino group with octanoic-, decanoic- and dodecanoic acid. At each step the Fmoc group was deprotected with 20% piperidine in DMF. After the final step the resin was washed with dichloromethane (DCM) and diethyl ether and dried overnight in a desiccator. The peptide was then cleaved from the resin by two treatments of alternating washes with 10 mL trifluoracetic acid /water/triisopropylsilane (TFA:H_2O:TIS) 95:2.5:2.5 (v/v/v). The mixture was left at room temperature for 1 h with occasional stirring, followed by the second treatment lasting 2-3 h. After each treatment the resin was washed with DCM. The cleavage cocktail was removed by filtration under reduced pressure and the filtrates were combined. Precipitation of the peptide was induced by dropwise addition of ice-cold diethyl ether to the crude product. The suspension was left overnight. The supernatant was removed the following day, and the peptide pellet was resuspended in fresh diethyl ether. After diethyl ether was evaporated under reduced pressure, the final pellet was purified by reversed phase high performance liquid chromatography (RP-HPLC), and pooled fractions were freeze-dried to yield the pure peptide.

3.2. Peptide purification and characterization

Purification and characterization of the synthetized peptides were carried out as described by Dey *et al*. [49]. Briefly, crude peptide purification was performed using an HPLC system (Waters, Milford, MA, USA) equipped with a SunFire Prep C18 OBD (5 μm, 19×250 mm) column, a 2998 photodiode array (PDA) detector and an automated fraction collector. The purity of the peptides was determined by ultra-performance liquid chromatography (UPLC) with PDA detection. The separation was performed using an Acquity™ Premier BEH C18, 1.7 μm, 2.1x100 mm column (Waters) and an acetonitrile/H_2O gradient containing 0.1% TFA. The retention time (Rt) for each peptide was recorded as a measurement of hydrophobicity. The mass of each peptide was determined by RP-HPLC high-resolution mass spectrometry (HRMS) using a Vanquish UHPLC system (Waters), coupled to an Orbitrap Id-X mass analyser with an electrospray ionization (ESI) source (Thermo Fischer Scientific, Waltham, MA, USA). The column used was Acquity™ Premier BEH C18, 1.7 μm, 2.1x100 mm (Waters).

3.3. Head-to-Tail Cyclisation

For the synthesis of the cyclic peptides a preloaded H-Lys(Boc)-2-chlorotrityl resin NovaBiochem (0.75 mmol/g loading, scale 0.2 mmol) was used. Cleavage of the linear protected peptides from the resin was performed with a mixture of hexafluoropropanol-DCM (3:7, v/v, 15 mL). Head-to-tail cyclisation was performed using a modified *microdilution* procedure previously described by Malesevic *et al*. [17]. To maintain microdilution conditions during cyclisation two 10 mL syringes were used. First syringe contained linear protected tetrapeptide (1 eq., 100 µmol) predissolved in DMF (10 mL). The second syringe was filled with a solution containing (benzotriazol-1-yloxy) tripyrrolidinophosphonium hexafluorophosphate (PyBOP, 3 eq., 300 µmol) predissolved in DMF (10 mL). Both syringes were fixed to the dual-syringe programmable pump and the flow rate was set to 0.01 mL/min. This enabled simultaneous, dropwise addition of both solutions into the flask which initially contained DIEA (6 equiv., 600 µmol), PyBOP (0.1 equiv., 10 µmol) and DMF (10 mL). The reaction proceeded under constant stirring. After the cyclisation step, the reaction mixture was diluted with 5% LiCl (approx. 30 mL), prior to extraction with ethyl acetate (3 x 20 mL). The organic phase was washed with 5% LiCl solution (3 x 20 mL) and brine (1 x 20 mL), before drying over Na_2SO_4. The organic phase was filtered and concentrated under vacuum. Global deprotection was achieved using the same cleavage cocktail as previously described and following the same work-up procedure. In the final synthesis step the crude peptide was washed with diethyl ether (3 x 20 mL) and dried under vacuum prior to purification by RP-HPLC. All peptides were >93.6% pure (**Figure S1-S12**, **Table S2**).

3.4. Antibacterial Minimal Inhibitory Concentration (MIC) Assay

All cyclic, linear and lipopeptide analogues of the AMP EeCentrocin-1 were screened for antibacterial activity against four Gram-positive strains; *B. subtilis* 168 (Bs, ATCC 23857), *C. glutamicum* (Cg, ATCC 13032), *S. aureus* (Sa, ATCC 9144) and *S. epidermidis* RP62A (Se, ATCC 35984), and two Gram-negative strains; *E. coli* (Ec, ATCC 25922) and *P. aeruginosa* (Pa, ATCC 27853). All peptides were also tested for antibacterial activity against the wild type *E. coli* strain BW25113 (K12, from the Keio collection) and its isogenic *ompT* deletion mutant JW0554, the commercially available *E. coli* strain BL-21(DE3) (lacking genes for Lon and OmpT proteases production), as well as a transformed BL-21(DE3) strain, containing a plasmid with OmpT overexpressing machinery (see section 3.10). A modified broth microdilution susceptibility assay, based on the CLSI M07-A9 protocol, was used to determine MIC [50]. Briefly, overnight bacterial cultures were grown in Mueller-Hinton (MH) media (Difco Laboratories, USA) for 2 hours at room temperature. The bacterial inoculum was diluted to 2.5 - 3 x 10^4 cells/mL in MH medium and added in 96-well plates (Nunc, Roskilde, Denmark) preloaded with two-fold dilution series of peptide solutions in a ratio of 1:1 giving a final well volume of 100 µL. The microplates were incubated in an EnVision 2103 microplate reader (PerkinElmer, Llantrisant, UK) at 35 °C, with OD_{595} recorded every hour for 24 h. The minimal inhibitory concentration (MIC) value was defined as the lowest concentration of peptides showing an optical density less than 10% of the negative (growth) control, consisting of bacteria and MilliQ-water. Polymyxin B sulfate and oxytetracycline HCl (both from Sigma-Aldrich, St. Louis, MO, USA) served as positive (growth inhibition) controls. All peptides were tested in three technical replicates.

3.5. Antifungal MIC Assay

The synthesised peptides were screened for antifungal activity against the molds *A. pullulans* (Ap) and *Rhodotorula* sp. (Rh) (both obtained from Professor Arne Tronsmo, The Norwegian University of Life Sciences, Ås, Norway) and the yeast *C. albicans* (Ca, ATCC 10231) as previously described [51]. In short, fungal spores were grown in potato dextrose broth media (Difco) containing 2% D(+)-glucose (Merck, Darmstadt, Germany) at 25-30 °C while shaking at 200 rpm overnight. The cultures were diluted with dextrose media containing glucose to a concentration of approx. 4 × 10^5 spores/mL. Aliquots of the cultures (50 µL) were transferred to 96 well microtiter plates preloaded with the synthetic peptides (50 µL) in two-fold serial dilutions. Polymyxin B sulfate and Triclosan (Sigma-Aldrich, Steinheim, Germany) served as positive antibiotic controls. The microtiter plates containing the fungal spores and the test peptides were incubated at room temperature for 48 h and OD_{600} was recorded using a Synergy H1 Hybrid microplate reader system (BioTek, Winooski, VT, USA).

3.6. Haemolytic Activity Assay

The haemolytic activity of the synthesised peptides was determined according to a previously described protocol [52]. Haemolysis was determined using a heparinized fraction (10 IU/mL) of freshly drawn human blood, whereas the haematocrit (hct) was determined using a fraction containing ethylenediaminetetraacetic acid (EDTA, Vacutest®, KIMA, Arzergrande, Italy). In brief, the heparinized fraction was washed 3 times with prewarmed phosphate-buffered saline (PBS) and adjusted to a final hct of 4%. The peptides were screened for activity in a concentration-range from 500 to 3.9 μM. They were initially dissolved in dimethyl sulfoxide (DMSO) and were further diluted with PBS to a final DMSO content of ≤1%. As a positive control for 100% haemolysis, a solution of 1% triton X-100 was used, whereas 1% DMSO in PBS buffer served as a negative control. Duplicates of test solutions and erythrocytes (1% hct final concentration) were prepared in a 96-well polypropylene V-bottom plate (Nunc, Fischer scientific, Oslo, Norway). Following incubation under agitation at 37 °C and 800 rpm for 1 hour, and subsequent centrifugation (5 min, 3000 g), 100 μL from each well were transferred to a flat-bottomed 96-well plate. Absorbance was measured at 545 nm with a microplate reader (SpectraMax 190, Molecular Devices, San Jose, CA, USA). After subtracting PBS background, the percentage of haemolysis was calculated as the ratio of the absorbance in the peptide- and surfactant-treated samples. Three independent experiments were performed, and EC_{50}-values (the concentration giving 50% haemolysis) are presented as averages.

3.7. Bacterial Inner Membrane Integrity Assay

The inner membrane integrity assay was performed in a real-time manner using *B. subtilis* 168 (ATCC 23857) and *E. coli* K12 (ATCC MC1061) biosensor strains, both containing the reporter plasmid pCSS962 constitutively expressing eukaryotic luciferase (*lucGR* gene). Bacterial colonies were grown overnight at RT in MH media supplemented with 5 μg/mL chloramphenicol (Merck KGaA, Darmstadt, Germany) and a mixture of 20 μg/mL chloramphenicol and 100 μg/mL ampicillin (Sigma-Aldrich, USA), respectively. Overnight cultures were further diluted and grown without antibiotics at RT for 2-3 h until they reached OD_{600} = 0.1. D-luciferin potassium salt (Synchem Inc., Elk Grove Village, IL, USA) was added to the bacterial cultures at a final concentration of 1 mM. Black round-bottom 96-well microtiter plates (Nunc, Roskilde, Denmark) were prepared with two-fold dilution series of the compounds (10 μL per well) at final concentrations ranging from 50 to 1.56 μg/mL. Chlorhexidine acetate (CHX, Fresenius Kabi, Halden, Norway) and Milli-Q water were used as positive and negative control, respectively. A Synergy H1 Hybrid Reader (BioTek, Winooski, VT, USA) was primed with bacterial suspension before the assay plate was loaded into the plate reader. Aliquots of 90 μL bacterial inoculum with D-luciferin were successively (well by well) injected into the test wells by an automated injector. The light (luminescence) emission, because of bacterial membrane disruption, was monitored every second for 3 min. Each study was performed at least three times independently, and the figures show a representative dataset.

3.8. Bacterial Viability Assay

The real-time measurement of bacterial viability was performed by using *B. subtilis* 168 and *E. coli* K12, the same strains that were used in the inner membrane integrity assay. However, in this assay *B. subtilis* 168 is carrying a constitutively expressed lux operon as a chromosomal integration in the *sac*A locus (PliaG) and *E. coli* K12 was transformed with the reporter plasmid pCGLS-11 [51]. *B. subtilis* and *E. coli* cultures were prepared the same way as the membrane integrity assay in MH media supplemented with 5 μg/mL chloramphenicol and a mixture of 20 μg/mL chloramphenicol and 100 μg/mL ampicillin, respectively. The continuous light production by these biosensors was monitored in the Synergy H1 Hybrid Reader, and the respective injector was primed with bacterial suspension. Black round-bottom 96-well microtiter plates were prepared with 10 μL of each compound at the final concentration ranging from 50 to 1.56 μg/mL (two-fold dilutions), including chlorhexidine as a positive control and Milli-Q water as a negative control. An aliquot of 90 μL bacterial suspension was subsequently added by the automated injector. As a result of changes in bacterial viability, the decrease in light emission was monitored every second for 3 min. Each study was performed at least three times independently, and the figures show a representative dataset.

3.9. Bacterial Outer Membrane Permeability Assay

The outer membrane integrity assay was performed in a real-time manner using *E. coli* (ATCC 25922) and *P. aeruginosa* (ATCC 27853) as test strains. Externally added *N*-phenyl-1-napthylamine (NPN, Sigma-Aldrich, USA) was used as a substrate for the fluorescence to detect light emission. *E. coli* colonies were suspended in MH media and grown overnight at RT. Overnight cultures were further diluted and grown at RT for 2-3 h until they reached OD_{600} = 0.5. NPN was added to the bacterial cultures at a final concentration of 20 µM in glucose 4-(2-hydroxyethyl)-1-piperazineethanesulfonic acid (HEPES) buffer (5 mM), and the background fluorescence was measured before the actual assay. Black round-bottom 96-well microtiter plates were prepared with two-fold dilution series of the compounds (10 µL per well) at final concentrations ranging from 50 to 1.56 µg/mL. Polymyxin B and Milli-Q water was used as a positive and negative control, respectively. A Synergy H1 Hybrid Reader was primed with bacterial suspension before the assay plate was loaded into the plate reader. Aliquots of 90 µL bacterial inoculum with NPN were successively (well by well) injected into the test wells by an automated injector. The light (fluorescence) emission, observed because of bacterial outer membrane disruption, was monitored every second for 3 min. Each study was performed at least three times independently, and the figures show a representative dataset.

3.10. Induction of Cell Envelope Related Stress Response

Bacterial biosensors strains derived from *B. subtilis* 168 containing selected promoter-luciferase-operon fusions were utilized to analyse whether the synthesized peptides induced a mode of action specific global stress response. Peptides and control antibiotics (bacitracin and vancomycin) in concentrations ranging from 100-1.6 µg/mL were incubated with each biosensor containing the respective reporter gene construct. The assays were performed as described by Juskewitz *et al*. [31]. In short, fresh colonies were used to inoculate MH medium containing 5 mg/mL chloramphenicol and incubated at 37 °C overnight. Overnight cultures were first diluted to an OD_{600} = 0.05 and then grown until the OD_{600} reached 0.2. A 384 well plate was preloaded with 2-fold dilution series of peptides and control antibiotics before adding the cultures of the sensor bacteria. The assay plates were sealed by Breath-Easy sealing membranes (Sigma-Aldrich) to reduce evaporation and incubated in the Envision multi-plate reader at 35 °C. Both luminescence and absorbance were monitored every 30 min for a total of 10 hours. Data was analysed from three individual experiments. Luminescence peaks obtained from control antibiotics and the peptide samples were compared to evaluate if the peptides initiated a similar stress response.

3.11. Cloning and Recombinant Expression of ompT

DNA purification, cloning, and transformation were performed according to standard procedures. All cloning steps were conducted in *E. coli* DH5α. Genomic DNA isolated from a wild type *E. coli* strain (MC4100) was used to amplify *ompT* by the primer pair *ompT*_F (tacaaataattttgtttaagaattcgattgaatggagaacttttatg) and *ompT*_R (gaaggcccatgaggcccagactagtgaaattttagttggcgttct) introducing EcoRI and SpeI restriction enzyme cutting sites. The gene was cloned into the plasmid pCSM0038 under the control of the PBAD promotor. Both, the PCR product, and plasmid pCSM0038 were double digested with EcoRI and SpeI. The restriction digests were purified on an agarose gel electrophoresis and subsequent cutting out and purification of the respective bands prior to ligation. The plasmid construct was verified by restriction digests and Sanger sequencing of the insert. The resulting plasmid was named pHD001. To complement the *ompT*-phenotype, BL-21 DE3 competent cells were transformed with pHD001.Experiments to determine the effect of *ompT* complementation on the MIC and peptide fragmentation were done with the pHD001 complemented BL-21 clones containing *ompT* under the control of the arabinose inducible PBAD promoter. Assays were conducted as described for the MIC assays except for overnight cultures, which were grown in the presence of 100 µg/mL ampicillin. In addition, OmpT expression was induced by the addition of L-arabinose simultaneously with the peptides to a final concentration of 2 mg/mL.

3.12. Matrix-Assisted Laser Desorption/Ionization Time-of-Flight Mass Spectrometry (MALDI-TOF MS)

MALDI-TOF mass spectra of selected *E. coli* strains (with/without OmpT protease) treated with the peptides **P6-W6R8** and **cP6-W6R8** were recorded using an Autoflex Speed instrument (Bruker Daltonics, Germany), containing a 355-nm nitrogen laser for desorption and ionization. Bacterial cells

(2.5-3 x 10^4 cells/mL) were mixed with concentrations around MIC (2-16 µg/mL) of the selected peptides and incubated for 24 h at 37 °C. The matrix for ionization, α-Cyano-4-hydroxycinnamic acid (10 mg/mL), was dissolved in a standard solvent containing 50% aqueous acetonitrile containing 2.5% (v/v) TFA by vigorous vortexing. Aliquots (1 µL) from three individual biological test replicates were mixed with an equal amount of matrix and transferred onto a standard 384 spot MTP target plate. The samples were allowed to dry before loading into the instrument and subjection to MALDI-TOF-MS analysis. The instrument was regularly calibrated with a peptide calibration standard (Bruker, mass range from 700 to 3200 Da) during the analysis. Positive controls (matrix and peptides) and negative controls (matrix and bacteria) were used to identify peptides and proteolytic fragments thereof. The intensity vs. mass-to charge (m/z) spectrum was collected at a laser power of 100 mV in reflectior mode, and other settings were adjusted for the best signal-to-noise ratio. The obtained mass spectra were analyzed using the flexAnalysis software (v.3.3, Bruker Daltonics). Proteolyic fragments identified to derive from the antimicrobial peptides, suggests their susceptibility to undergo degradation by the bacterial OmpT protease.

Acknowledgments: This work was funded by a grant (no. 217/6770) from UiT The Arctic University of Norway.

References

1. Aljeldah, M.M. Antimicrobial Resistance and Its Spread Is a Global Threat. *Antibiotics (Basel)* **2022**, *11*, doi:10.3390/antibiotics11081082.
2. Murray, C.J.; Ikuta, K.S.; Sharara, F.; Swetschinski, L.; Aguilar, G.R.; Gray, A.; Han, C.; Bisignano, C.; Rao, P.; Wool, E. Global burden of bacterial antimicrobial resistance in 2019: a systematic analysis. *The Lancet* **2022**, *399*, 629-655, doi:10.1016/S0140-6736(21)02724-0.
3. Church, N.A.; McKillip, J.L. Antibiotic resistance crisis: challenges and imperatives. *Biologia* **2021**, *76*, 1535-1550, doi:10.1007/s11756-021-00697-x.
4. Atanasov, A.G.; Zotchev, S.B.; Dirsch, V.M.; Orhan, I.E.; Banach, M.; Rollinger, J.M.; Barreca, D.; Weckwerth, W.; Bauer, R.; Bayer, E.A.; et al. Natural products in drug discovery: advances and opportunities. *Nature Reviews Drug Discovery* **2021**, *20*, 200-216, doi:10.1038/s41573-020-00114-z.
5. Pasupuleti, M.; Schmidtchen, A.; Malmsten, M. Antimicrobial peptides: key components of the innate immune system. *Critical reviews in biotechnology* **2012**, *32*, 143-171, doi:10.3109/07388551.2011.594423.
6. Mba, I.E.; Nweze, E.I. Antimicrobial Peptides Therapy: An Emerging Alternative for Treating Drug-Resistant Bacteria. *The Yale journal of biology and medicine* **2022**, *95*, 445-463.
7. Chakraborty, S.; Chatterjee, R.; Chakravortty, D. Evolving and assembling to pierce through: Evolutionary and structural aspects of antimicrobial peptides. *Computational and structural biotechnology journal* **2022**, *20*, 2247-2258, doi:10.1016/j.csbj.2022.05.002.
8. Zasloff, M. Antimicrobial peptides of multicellular organisms. *Nature* **2002**, *415*, 389-395, doi:10.1038/415389a.
9. Pirtskhalava, M.; Vishnepolsky, B.; Grigolava, M.; Managadze, G. Physicochemical Features and Peculiarities of Interaction of AMP with the Membrane. *Pharmaceuticals* **2021**, *14*, 471, doi:10.3390/ph14050471.
10. Kang, H.-K.; Kim, C.; Seo, C.H.; Park, Y. The therapeutic applications of antimicrobial peptides (AMPs): a patent review. *Journal of microbiology* **2017**, *55*, 1-12, doi:10.1007/s12275-017-6452-1.
11. Mwangi, J.; Kamau, P.M.; Thuku, R.C.; Lai, R. Design methods for antimicrobial peptides with improved performance. *Zoological research* **2023**, *44*, 1095-1114, doi:10.24272/j.issn.2095-8137.2023.246.
12. da Cunha, N.B.; Cobacho, N.B.; Viana, J.F.C.; Lima, L.A.; Sampaio, K.B.O.; Dohms, S.S.M.; Ferreira, A.C.R.; de la Fuente-Núñez, C.; Costa, F.F.; Franco, O.L.; et al. The next generation of antimicrobial peptides (AMPs) as molecular therapeutic tools for the treatment of diseases with social and economic impacts. *Drug Discovery Today* **2017**, *22*, 234-248, doi:10.1016/j.drudis.2016.10.017.
13. Huan, Y.; Kong, Q.; Mou, H.; Yi, H. Antimicrobial Peptides: Classification, Design, Application and Research Progress in Multiple Fields. *Frontiers in Microbiology* **2020**, *11*, doi:10.3389/fmicb.2020.582779.
14. Li, X.; Zuo, S.; Wang, B.; Zhang, K.; Wang, Y. Antimicrobial Mechanisms and Clinical Application Prospects of Antimicrobial Peptides. *Molecules* **2022**, *27*, doi:10.3390/molecules27092675.
15. Solstad, R.G.; Li, C.; Isaksson, J.; Johansen, J.; Svenson, J.; Stensvåg, K.; Haug, T. Novel Antimicrobial Peptides EeCentrocins 1, 2 and EeStrongylocin 2 from the Edible Sea Urchin Echinus esculentus Have 6-Br-Trp Post-Translational Modifications. *PLoS One* **2016**, *11*, e0151820, doi:10.1371/journal.pone.0151820.

16. Solstad, R.G.; Johansen, C.; Stensvåg, K.; Strøm, M.B.; Haug, T. Structure-activity relationship studies of shortened analogues of the antimicrobial peptide EeCentrocin 1 from the sea urchin Echinus esculentus. *Journal of peptide science* **2020**, *26*, e3233, doi:10.1002/psc.3233.
17. Malesevic, M.; Strijowski, U.; Bächle, D.; Sewald, N. An improved method for the solution cyclization of peptides under pseudo-high dilution conditions. *Journal of biotechnology* **2004**, *112*, 73-77, doi:10.1016/j.jbiotec.2004.03.015.
18. Paulsen, M.H.; Karlsen, E.A.; Ausbacher, D.; Anderssen, T.; Bayer, A.; Ochtrop, P.; Hedberg, C.; Haug, T.; Ericson Sollid, J.U.; Strøm, M.B. An amphipathic cyclic tetrapeptide scaffold containing halogenated β(2,2) -amino acids with activity against multiresistant bacteria. *Journal of peptide science* **2018**, *24*, e3117, doi:10.1002/psc.3117.
19. Rounds, T.; Straus, S.K. Lipidation of Antimicrobial Peptides as a Design Strategy for Future Alternatives to Antibiotics. *International journal of molecular sciences* **2020**, *21*, 9692, doi:10.3390/ijms21249692.
20. Zarena, D.; Mishra, B.; Lushnikova, T.; Wang, F.; Wang, G. The π Configuration of the WWW Motif of a Short Trp-Rich Peptide Is Critical for Targeting Bacterial Membranes, Disrupting Preformed Biofilms, and Killing Methicillin-Resistant Staphylococcus aureus. *Biochemistry* **2017**, *56*, 4039-4043, doi:10.1021/acs.biochem.7b00456.
21. Vernen, F.; Harvey, P.J.; Dias, S.A.; Veiga, A.S.; Huang, Y.-H.; Craik, D.J.; Lawrence, N.; Troeira Henriques, S. Characterization of Tachyplesin Peptides and Their Cyclized Analogues to Improve Antimicrobial and Anticancer Properties. *International Journal of Molecular Sciences* **2019**, *20*, doi:10.3390/ijms20174184.
22. Tam, J.P.; Lu, Y.-A.; Yang, J.-L. Marked Increase in Membranolytic Selectivity of Novel Cyclic Tachyplesins Constrained with an Antiparallel Two-β Strand Cystine Knot Framework. *Biochemical and biophysical research communications* **2000**, *267*, 783-790, doi:10.1006/bbrc.1999.2035.
23. Wirth, F.; Goldani, L.Z. Epidemiology of Rhodotorula: an emerging pathogen. *Interdisciplinary perspectives on infectious diseases* **2012**, *2012*, 465717, doi:10.1155/2012/465717.
24. Mehta, S.R.; Johns, S.; Stark, P.; Fierer, J. Successful treatment of Aureobasidium pullulans central catheter-related fungemia and septic pulmonary emboli. *IDCases* **2017**, *10*, 65-67, doi:10.1016/j.idcr.2017.08.017.
25. Joshi, A.; Singh, R.; Shah, M.S.; Umesh, S.; Khattry, N. Subcutaneous mycosis and fungemia by Aureobasidium pullulans: a rare pathogenic fungus in a post allogeneic BM transplant patient. *Bone marrow transplantation* **2010**, *45*, 203-204, doi:10.1038/bmt.2009.111.
26. Helander, I.M.; Mattila-Sandholm, T. Fluorometric assessment of gram-negative bacterial permeabilization. *Journal of applied microbiology* **2000**, *88*, 213-219, doi:10.1046/j.1365-2672.2000.00971.x.
27. Paulsen, V.S.; Blencke, H.-M.; Benincasa, M.; Haug, T.; Eksteen, J.J.; Styrvold, O.B.; Scocchi, M.; Stensvåg, K. Structure-Activity Relationships of the Antimicrobial Peptide Arasin 1 — And Mode of Action Studies of the N-Terminal, Proline-Rich Region. *PloS one* **2013**, *8*, e53326, doi:10.1371/journal.pone.0053326.
28. Vasilchenko, A.S.; Rogozhin, E.A. Sub-inhibitory Effects of Antimicrobial Peptides. *Frontiers in microbiology* **2019**, *10*, doi:10.3389/fmicb.2019.01160.
29. Radeck, J.; Kraft, K.; Bartels, J.; Cikovic, T.; Dürr, F.; Emenegger, J.; Kelterborn, S.; Sauer, C.; Fritz, G.; Gebhard, S.; et al. The Bacillus BioBrick Box: generation and evaluation of essential genetic building blocks for standardized work with Bacillus subtilis. *Journal of Biological Engineering* **2013**, *7*, 29, doi:10.1186/1754-1611-7-29.
30. Radeck, J.; Fritz, G.; Mascher, T. The cell envelope stress response of Bacillus subtilis: from static signaling devices to dynamic regulatory network. *Current Genetics* **2017**, *63*, 79-90, doi:10.1007/s00294-016-0624-0.
31. Juskewitz, E.; Mishchenko, E.; Dubey, V.K.; Jenssen, M.; Jakubec, M.; Rainsford, P.; Isaksson, J.; Andersen, J.H.; Ericson, J.U. Lulworthinone: In Vitro Mode of Action Investigation of an Antibacterial Dimeric Naphthopyrone Isolated from a Marine Fungus. *Marine Drugs* **2022**, *20*, doi:10.3390/md20050277.
32. Pietiäinen, M.; Gardemeister, M.; Mecklin, M.; Leskelä, S.; Sarvas, M.; Kontinen, V.P. Cationic antimicrobial peptides elicit a complex stress response in Bacillus subtilis that involves ECF-type sigma factors and two-component signal transduction systems. *Microbiology (Reading)* **2005**, *151*, 1577-1592, doi:10.1099/mic.0.27761-0.
33. Meighen, E.A. Molecular biology of bacterial bioluminescence. *Microbiol Rev* **1991**, *55*, 123-142, doi:10.1128/mr.55.1.123-142.1991.
34. Lewis, K. The Science of Antibiotic Discovery. *Cell* **2020**, *181*, 29-45, doi:10.1016/j.cell.2020.02.056.
35. Stumpe, S.; Schmid, R.; Stephens, D.L.; Georgiou, G.; Bakker, E.P. Identification of OmpT as the protease that hydrolyzes the antimicrobial peptide protamine before it enters growing cells of Escherichia coli. *Journal of Bacteriology* **1998**, *180*, 4002-4006, doi:10.1128/jb.180.15.4002-4006.1998.

36. Thomassin, J.-L.; Brannon, J.R.; Gibbs, B.F.; Gruenheid, S.; Moual, H.L. OmpT Outer Membrane Proteases of Enterohemorrhagic and Enteropathogenic Escherichia coli Contribute Differently to the Degradation of Human LL-37. *Infection and Immunity* **2012**, *80*, 483-492, doi:10.1128/IAI.05674-11.
37. Kohn, E.M.; Shirley, D.J.; Arotsky, L.; Picciano, A.M.; Ridgway, Z.; Urban, M.W.; Carone, B.R.; Caputo, G.A. Role of Cationic Side Chains in the Antimicrobial Activity of C18G. *Molecules* **2018**, *23*, 329, doi:10.3390/molecules23020329.
38. Brannon, J.R.; Thomassin, J.-L.; Desloges, I.; Gruenheid, S.; Le Moual, H. Role of uropathogenic Escherichia coli OmpT in the resistance against human cathelicidin LL-37. *FEMS Microbiology Letters* **2013**, *345*, 64-71, doi:10.1111/1574-6968.12185.
39. Tanu, S.; Princy, C.; Sangeeta, S. Antimicrobial Peptides: Mechanism of Action. In *Insights on Antimicrobial Peptides*, Shymaa, E., Jorge, M.-S., Anna, S., Eds.; IntechOpen: Rijeka, 2022; p. Ch. 3.
40. Gruenheid, S.; Le Moual, H. Resistance to antimicrobial peptides in Gram-negative bacteria. *FEMS Microbiology Letters* **2012**, *330*, 81-89, doi:10.1111/j.1574-6968.2012.02528.x.
41. Kramer, R.A.; Vandeputte-Rutten, L.; de Roon, G.J.; Gros, P.; Dekker, N.; Egmond, M.R. Identification of essential acidic residues of outer membrane protease OmpT supports a novel active site. *FEBS Letters* **2001**, *505*, 426-430, doi:10.1016/s0014-5793(01)02863-0.
42. Schechter, I.; Berger, A. On the size of the active site in proteases. I. Papain. *Biochemical and Biophysical Research Communications* **1967**, *27*, 157-162, doi:10.1016/s0006-291x(67)80055-x.
43. McCarter, J.D.; Stephens, D.; Shoemaker, K.; Rosenberg, S.; Kirsch, J.F.; Georgiou, G. Substrate specificity of the Escherichia coli outer membrane protease OmpT. *Journal of bacteriology* **2004**, *186*, 5919-5925, doi:10.1128/JB.01493-06.
44. Dekker, N.; Cox, R.C.; Kramer, R.A.; Egmond, M.R. Substrate specificity of the integral membrane protease OmpT determined by spatially addressed peptide libraries. *Biochemistry* **2001**, *40*, 1694-1701, doi:10.1021/bi0014195.
45. Koshland, D.E. Application of a Theory of Enzyme Specificity to Protein Synthesis. *Proceedings of the National Academy of Sciences* **1958**, *44*, 98-104, doi:10.1073/pnas.44.2.98.
46. Varadarajan, N.; Gam, J.; Olsen, M.J.; Georgiou, G.; Iverson, B.L. Engineering of protease variants exhibiting high catalytic activity and exquisite substrate selectivity. *Proceedings of the National Academy of Sciences* **2005**, *102*, 6855-6860, doi:10.1073/pnas.0500063102.
47. Zhang, Y.; Baaden, M. Molecular Insights into Substrate Binding of the Outer Membrane Enzyme OmpT. *Catalysts* **2023**, *13*, 214, doi:10.3390/catal13020214.
48. Wu, F.; Tan, C. Dead bacterial absorption of antimicrobial peptides underlies collective tolerance. *Journal of The Royal Society Interface* **2019**, *16*, 20180701, doi:10.1098/rsif.2018.0701.
49. Dey, H.; Simonovic, D.; Norberg-Schulz Hagen, I.; Vasskog, T.; Fredheim, E.G.A.; Blencke, H.-M.; Anderssen, T.; Strøm, M.B.; Haug, T. Synthesis and Antimicrobial Activity of Short Analogues of the Marine Antimicrobial Peptide Turgencin A: Effects of SAR Optimizations, Cys-Cys Cyclization and Lipopeptide Modifications. *International Journal of Molecular Sciences* **2022**, *23*, 13844, doi:10.3390/ijms232213844.
50. Igumnova, E.M.; Mishchenko, E.; Haug, T.; Blencke, H.-M.; Sollid, J.U.E.; Fredheim, E.G.A.; Lauksund, S.; Stensvåg, K.; Strøm, M.B. Synthesis and antimicrobial activity of small cationic amphipathic aminobenzamide marine natural product mimics and evaluation of relevance against clinical isolates including ESBL–CARBA producing multi-resistant bacteria. *Bioorg Med Chem* **2016**, *24*, 5884-5894, doi:10.1016/j.bmc.2016.09.046.
51. Hansen, I.; Lövdahl, T.; Simonovic, D.; Hansen, K.; Andersen, A.J.C.; Devold, H.; Richard, C.S.M.; Andersen, J.H.; Strøm, M.B.; Haug, T. Antimicrobial Activity of Small Synthetic Peptides Based on the Marine Peptide Turgencin A: Prediction of Antimicrobial Peptide Sequences in a Natural Peptide and Strategy for Optimization of Potency. *International Journal of Molecular Sciences* **2020**, *21*, doi:10.3390/ijms21155460.
52. Paulsen, M.H.; Ausbacher, D.; Bayer, A.; Engqvist, M.; Hansen, T.; Haug, T.; Anderssen, T.; Andersen, J.H.; Sollid, J.U.E.; Strøm, M.B. Antimicrobial activity of amphipathic α,α-disubstituted β-amino amide derivatives against ESBL – CARBA producing multi-resistant bacteria; effect of halogenation, lipophilicity and cationic character. *European journal of medicinal chemistry* **2019**, *183*, 111671, doi:10.1016/j.ejmech.2019.111671.

Supporting information

Antimicrobial activity of short analogues of the marine peptide EeCentrocin 1: Synthesis of lipopeptides and head-to-tail cyclic peptides and mechanism of action studies

Danijela Simonovic[1#], Hymonti Dey[2#], Natascha Johansen[1], Trude Anderssen[1], Ida K. Ø. Hansen[2], Hege Devold[2], Terje Vasskog[1], Hans-Matti Blencke[2], Frode Jacobsen Øyen[2], Elizabeth G. Aarag Fredheim[1], Tor Haug[2*], Morten B. Strøm[1*]

[1] Department of Pharmacy, Faculty of Health Sciences, UiT the Arctic University of Norway, NO-9037 Tromsø, NORWAY.

[2] The Norwegian College of Fishery Science, Faculty of Biosciences, Fisheries and Economics, UiT the Arctic University of Norway, NO-9037 Tromsø, NORWAY.

[#] Authors contributed equally.

* Corresponding authors. Correspondence: tor.haug@uit.no and morten.strom@uit.no

Contents:

Figure S20. Kinetics of the effect on membrane integrity as measured by relative luminescence in *E. coli* (pCSS962) treated with different concentrations of **cP6**, **cP6-R8** and **cP6-W4R6,8**.

Figure S21. *B. subtilis* biosensor with P*liaI* fusion, responded by increased light output compared to the water control, and the peptides P6, P6-W6R8 and cP6-W6R8 and the antibiotic controls induced light output.

Figure S22. Selected MALDI-TOF MS spectra of *E. coli* BW25113 and JW0554 ΔOmpT exposed to the linear peptide **P6-W6R8** or the cyclic peptide **cP6-W6R8**, or without exposure to peptides.

Figure S23. Selected MALDI-TOF MS spectra of *E. coli* BL-21 and BL-21+OmpT exposed to the linear peptide **P6-W6R8** or the cyclic peptide **cP6-W6R8**, or without exposure to peptides.

Table S1. Theoretical and measured monoisotopic mass (Da), and theoretical and observed m/z ions during HRMS of the synthesised peptides.

Table S2. Purity of synthesized peptides (%) and retention time (min) determined by UPLC using a reversed phase column.

Table S3. Antimicrobial activity (MIC in μg/mL) of synthesized peptides against the biosensor strain *E. coli* MC1061.

References.

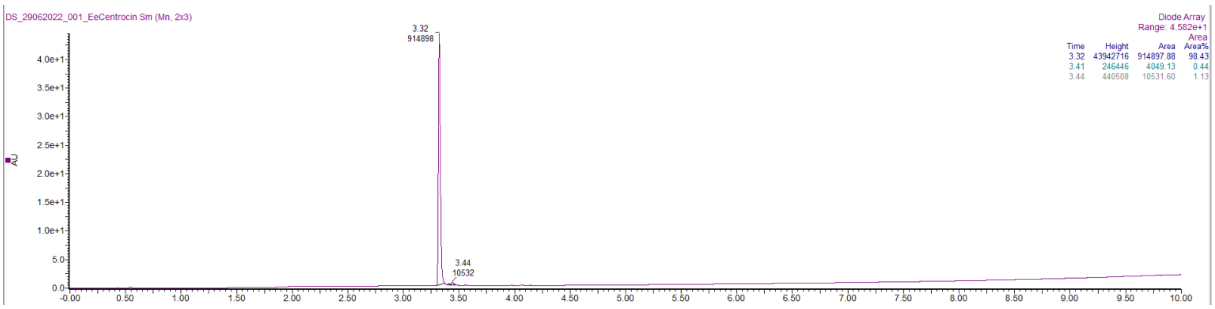

Figure S1. UPLC chromatogram of purified linear peptide **P6**. The peptide purity is 98.43 % based on the UPLC calculated area under the curves.

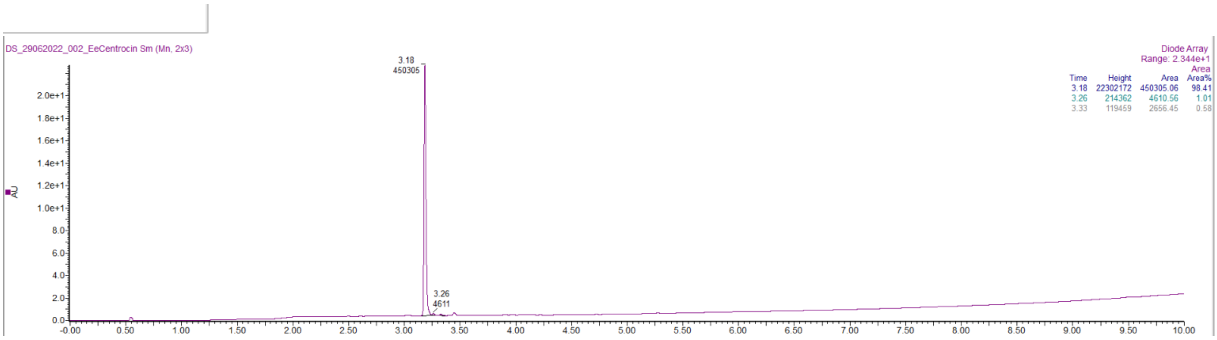

Figure S2. UPLC chromatogram of purified linear peptide **P6-K8**. The peptide purity is 98.41 % based on the UPLC calculated area under the curves.

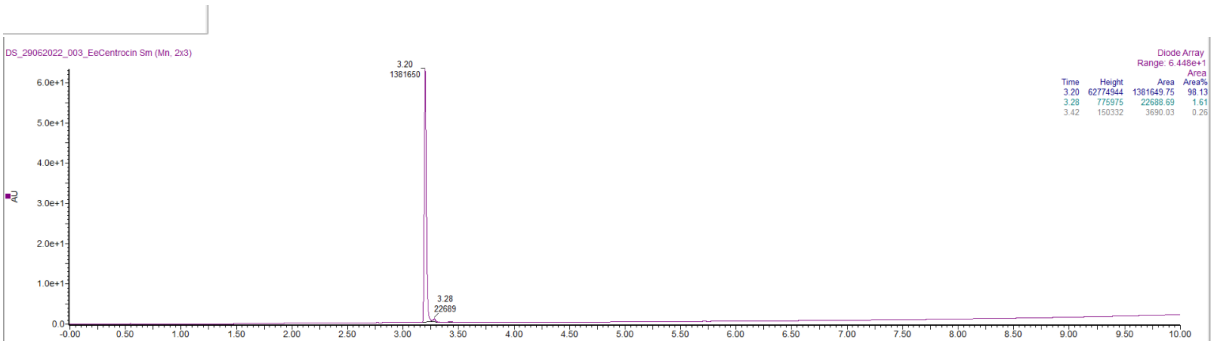

Figure S3. UPLC chromatogram of purified linear peptide **P6-R8**. The peptide purity is 98.13 % based on the UPLC calculated area under the curves.

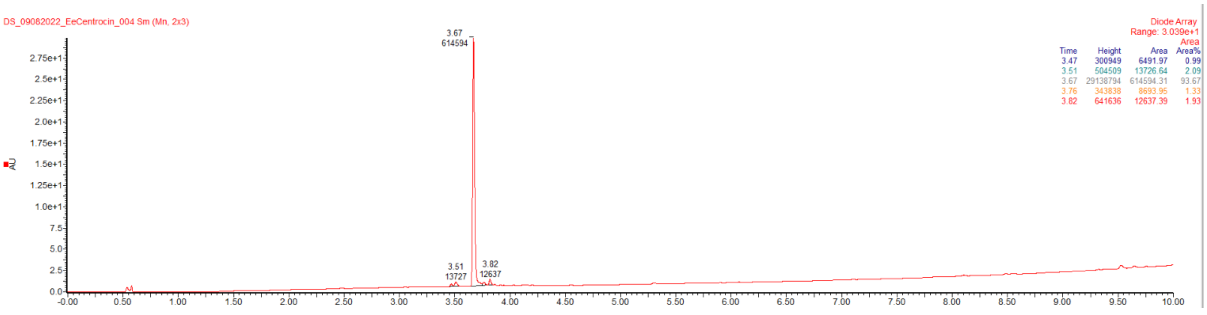

Figure S4. UPLC chromatogram of purified linear peptide **P6-W6K8**. The peptide purity is 93.67 % based on the UPLC calculated area under the curves.

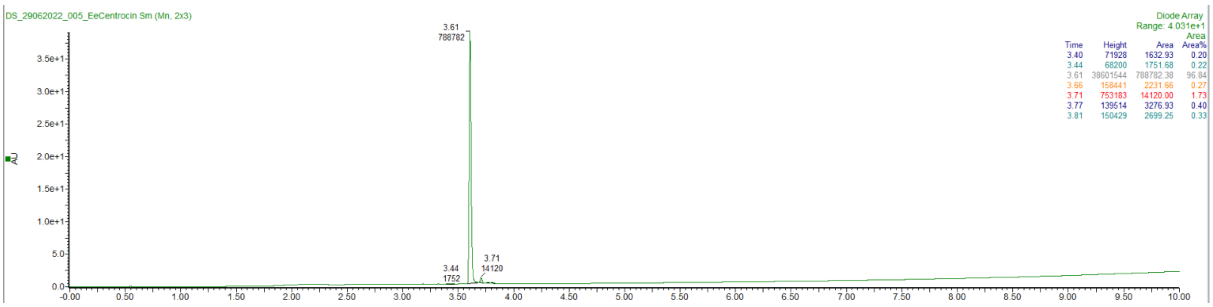

Figure S5. UPLC chromatogram of purified linear peptide **P6-W6R8**. The peptide purity is 96.84 % based on the UPLC calculated area under the curves.

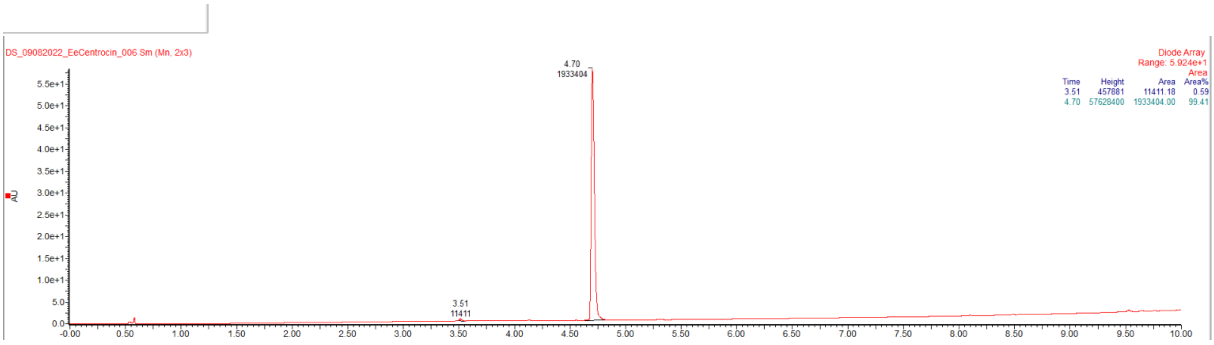

Figure S6. UPLC chromatogram of purified linear lipopeptide **C_8-P6-R8**. The peptide purity is 99.41 % based on the UPLC calculated area under the curves.

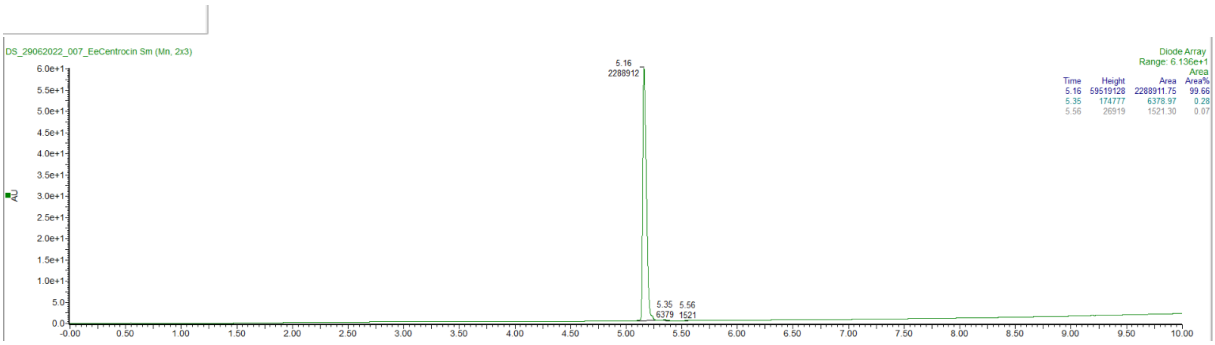

Figure S7. UPLC chromatogram of purified linear lipopeptide **C_{10}-P6-R8**. The peptide purity is 99.66 % based on the UPLC calculated area under the curves.

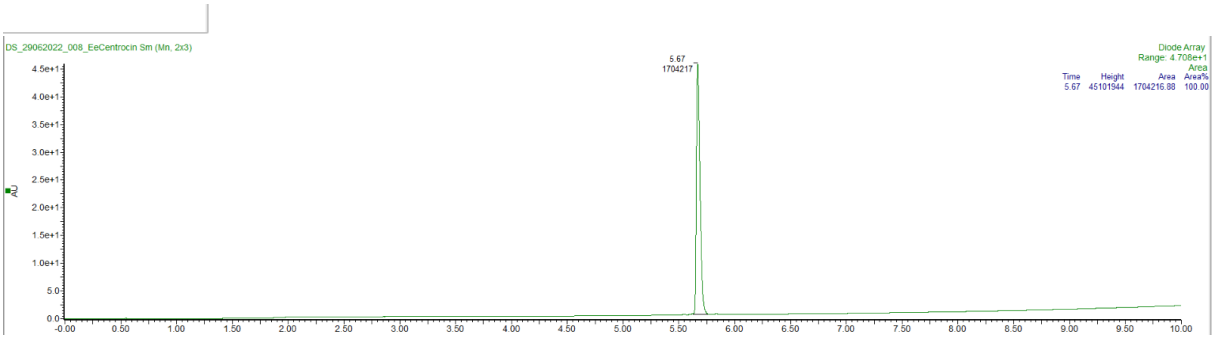

Figure S8. UPLC chromatogram of purified linear lipopeptide **C_{12}-P6-R8**. The peptide purity is 100 % based on the UPLC calculated area under the curves.

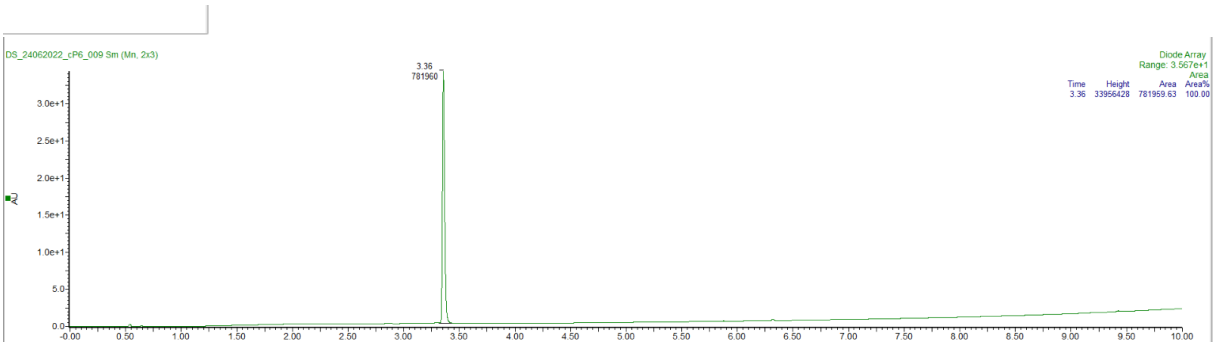

Figure S9. UPLC chromatogram of purified cyclic peptide **cP6**. The peptide purity is 100 % based on the UPLC calculated area under the curves.

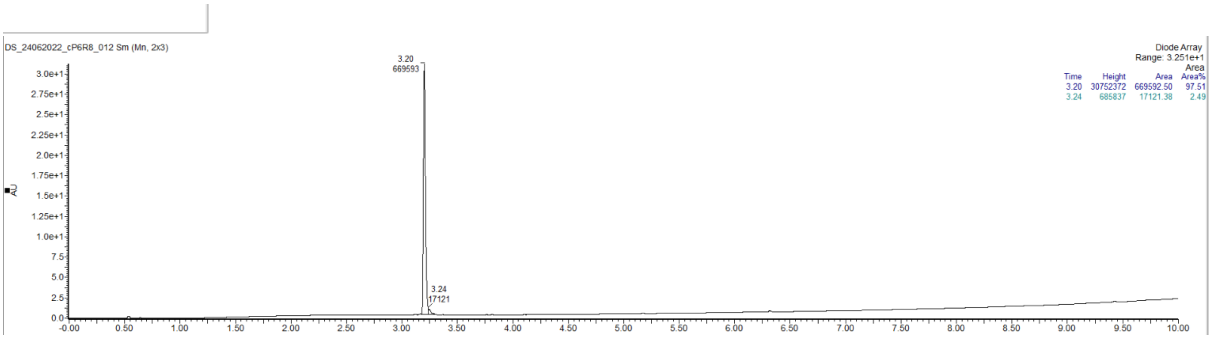

Figure S10. UPLC chromatogram of purified cyclic peptide **cP6-R8**. The peptide purity is 97.51 % based on the UPLC calculated area under the curves.

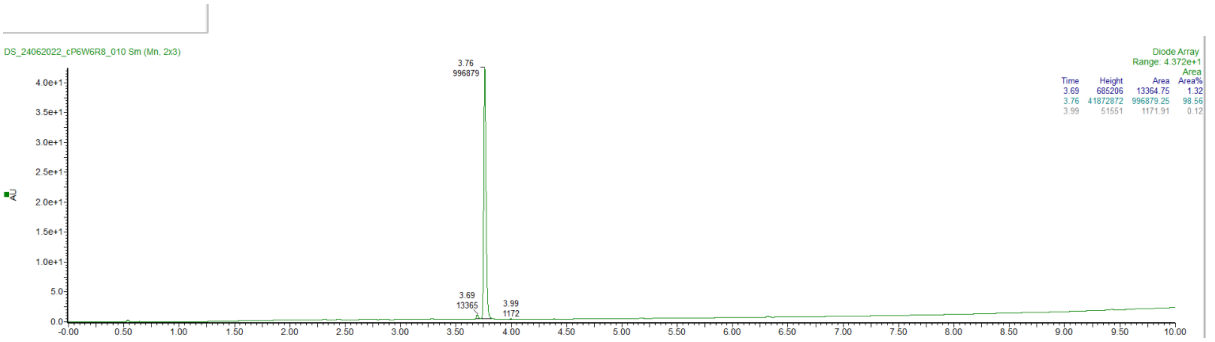

Figure S11. UPLC chromatogram of purified cyclic peptide **cP6-W6R8**. The peptide purity is 98.56 % based on the UPLC calculated area under the curves.

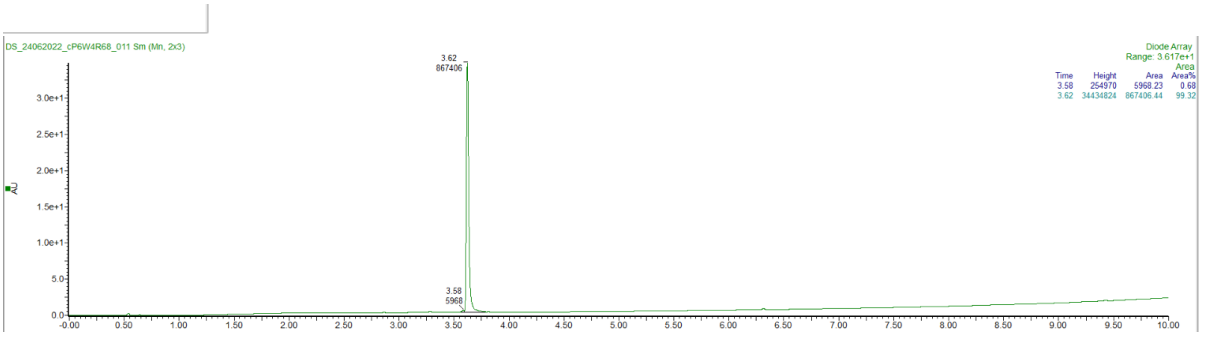

Figure S12. UPLC chromatogram of purified cyclic peptide **cP6-W4R6,8**. The peptide purity is 99.32 % based on the UPLC calculated area under the curves.

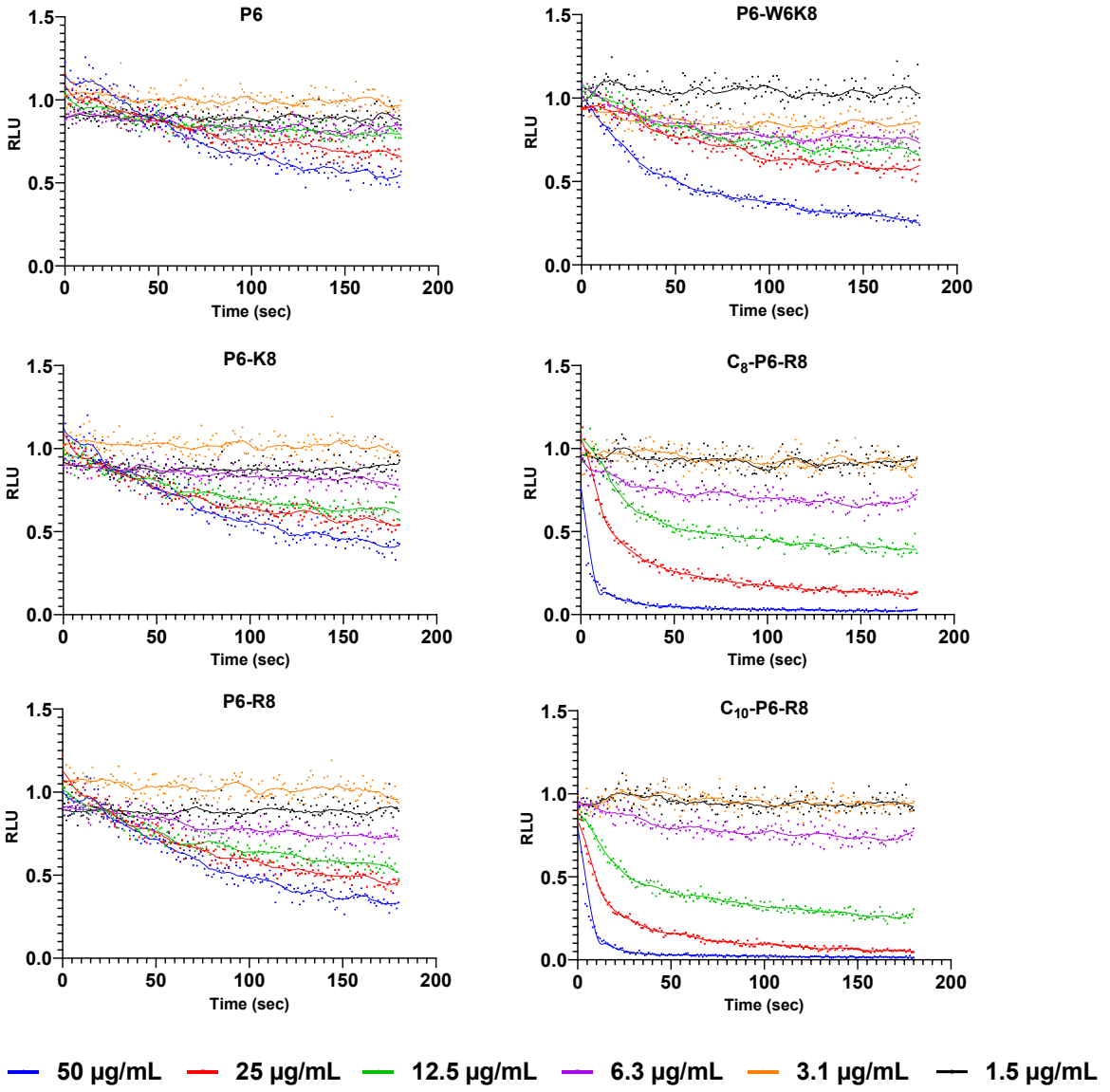

Figure S13. Kinetics of the effect on viability as measured by relative luminescence in *B. subtilis* (pCGLS11) treated with different concentrations of **P6**, **P6-K8**, **P6-R8**, **P6-W6K8**, **C_8-P6-R8** and **C_{10}-P6-R8**.

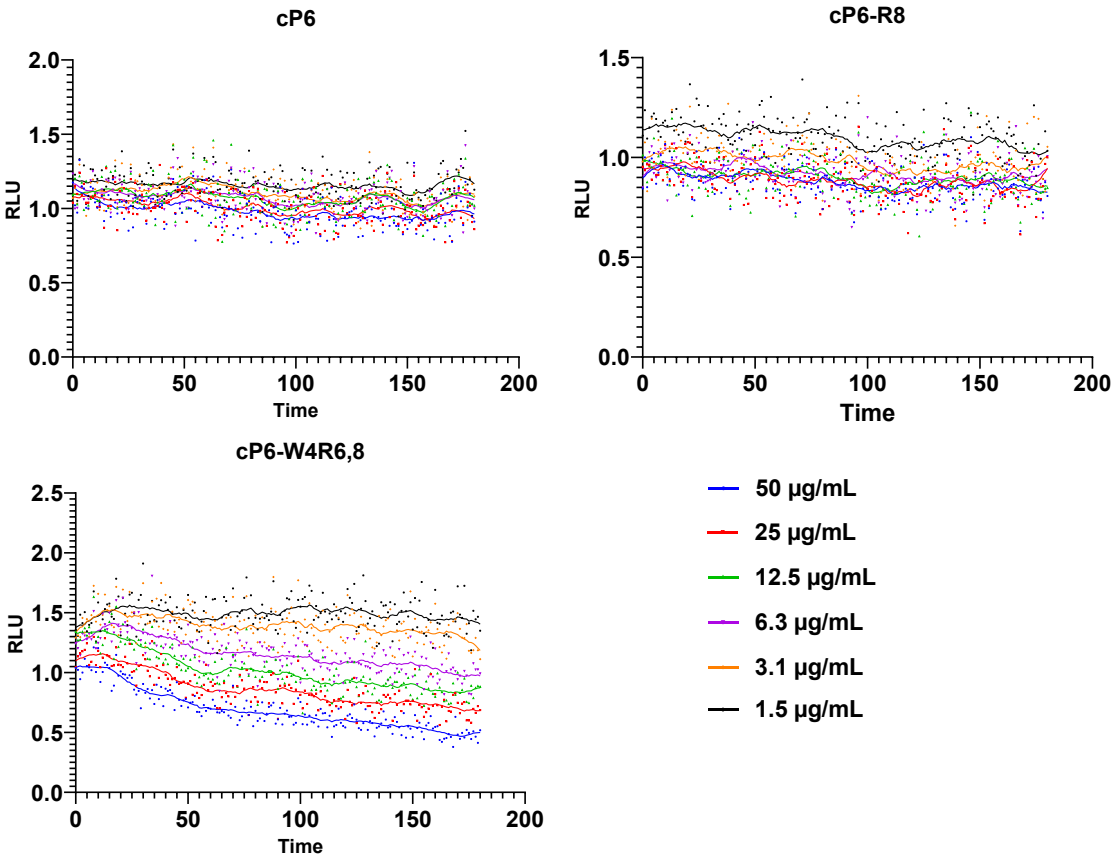

Figure S14. Kinetics of the effect on viability as measured by relative luminescence in *B. subtilis* (pCGLS11) treated with different concentrations of **cP6**, **cP6-R8** and **cP6-W4R6,8**.

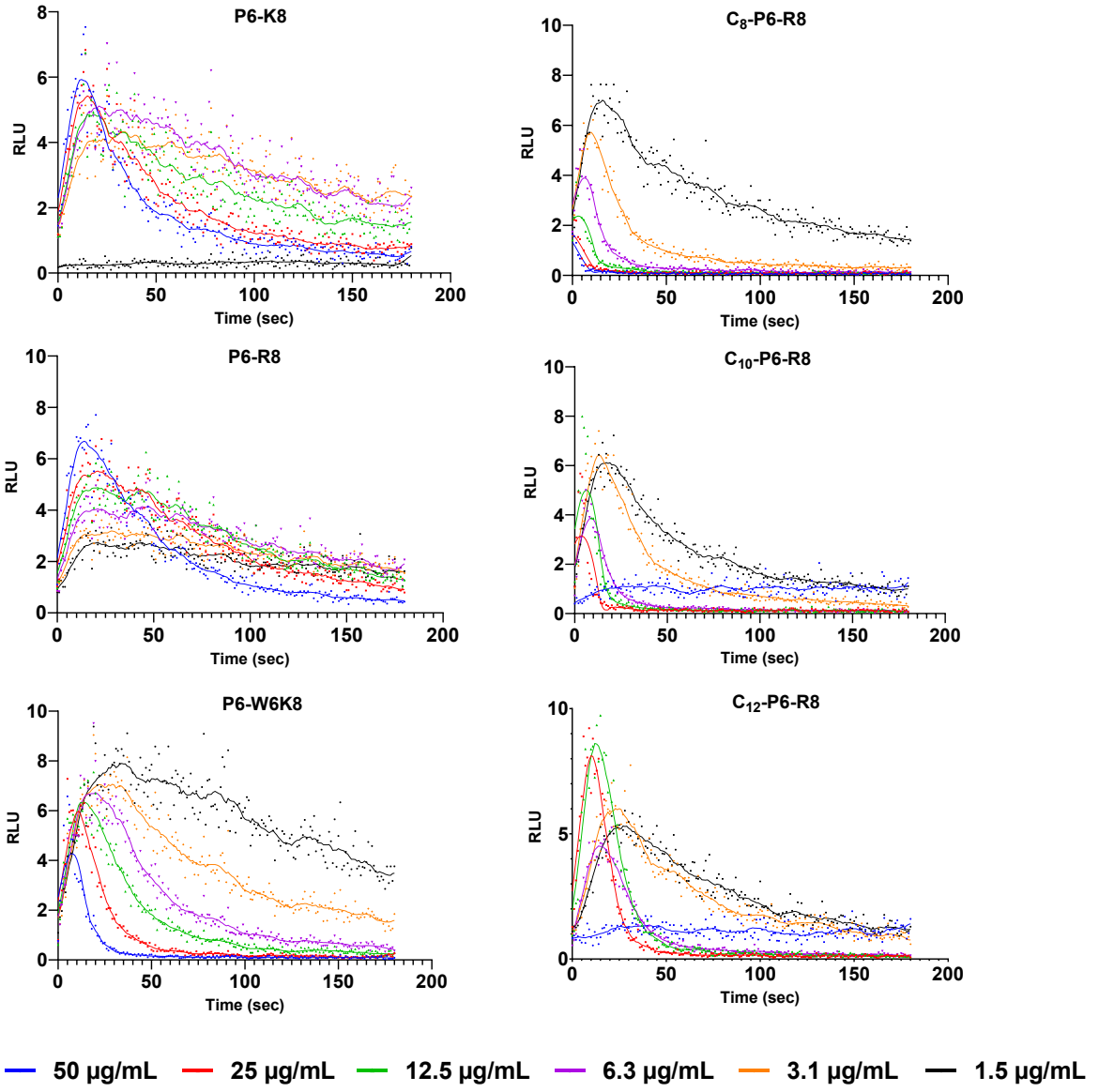

Figure S15. Kinetics of the effect on membrane integrity as measured by relative luminescence in *B. subtilis* (pCSS962) treated with different concentrations of **P6-K8**, **P6-R8**, **P6-W6K6**, **C_8-P6-R8**, **C_{10}-P6-R8** and **C_{12}-P6-R8**.

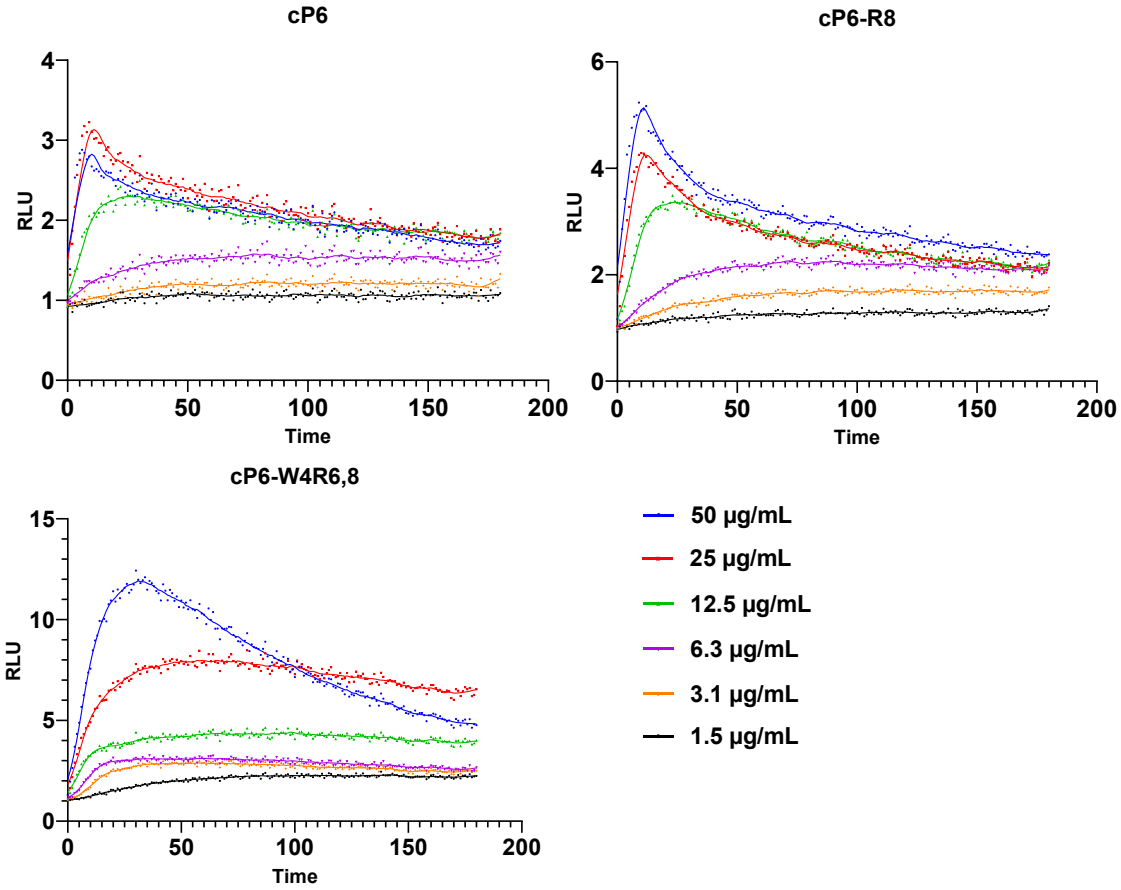

Figure S16. Kinetics of the effect on membrane integrity as measured by relative luminescence in *B. subtilis* (pCSS962) treated with different concentrations of **cP6**, **cP6-R8** and **cP6-W4R6,8**.

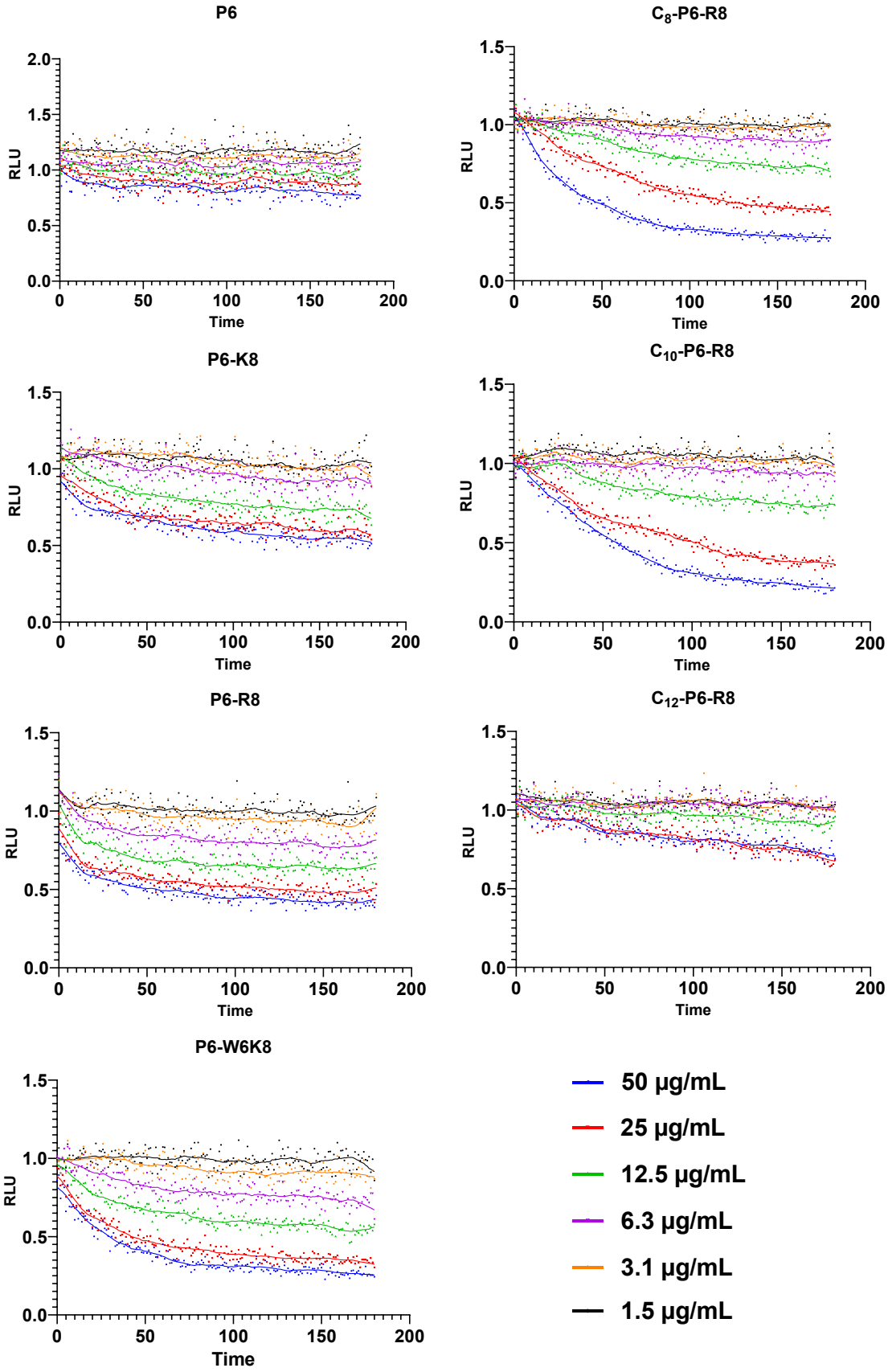

Figure S17. Kinetics of the effect on viability as measured by relative luminescence in *E. coli* (pCGLS-11) treated with different concentrations of **P6**, **P6-K8**, **P6-R8**, **P6-W6K8**, **C_8-P6-R8**, **C_{10}-P6-R8** and **C_{12}-P6-R8**.

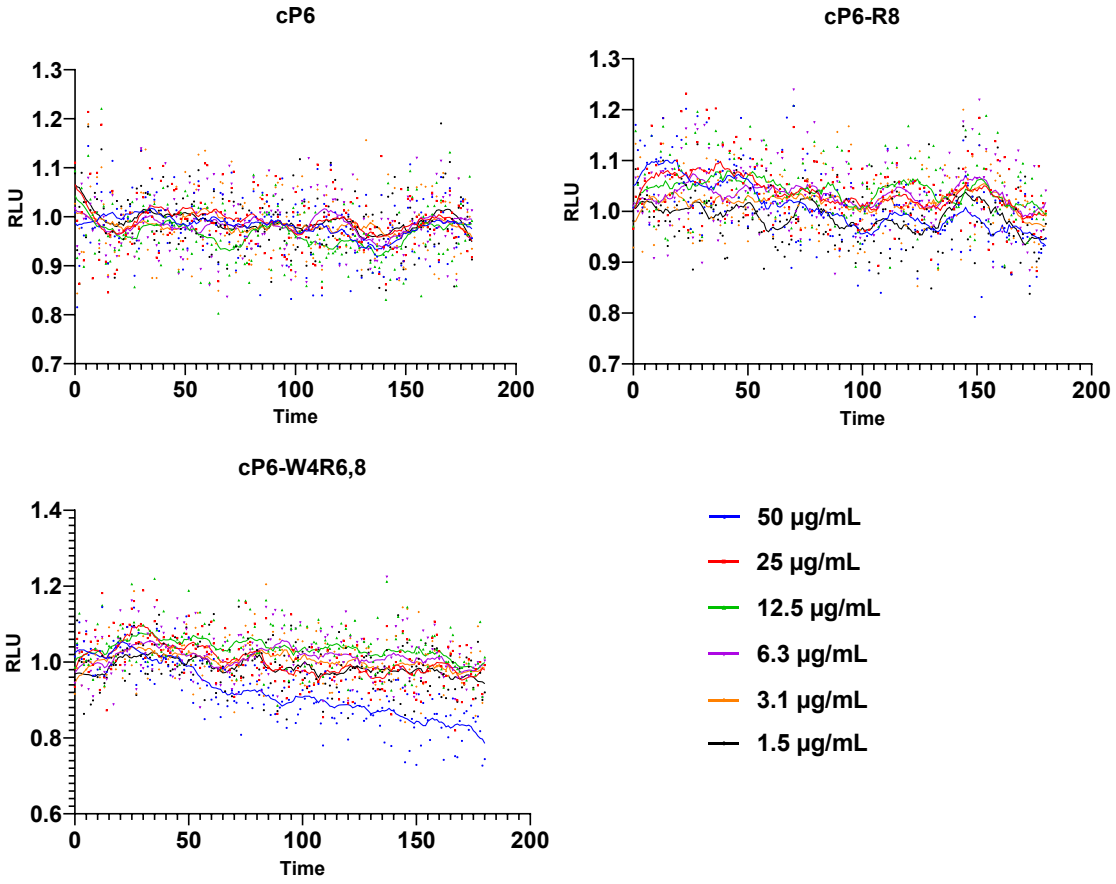

Figure S18. Kinetics of the effect on viability as measured by relative luminescence in *E. coli* (pCGLS-11) treated with different concentrations of **cP6**, **cP6-R8** and **cP6-W4R6,8**.

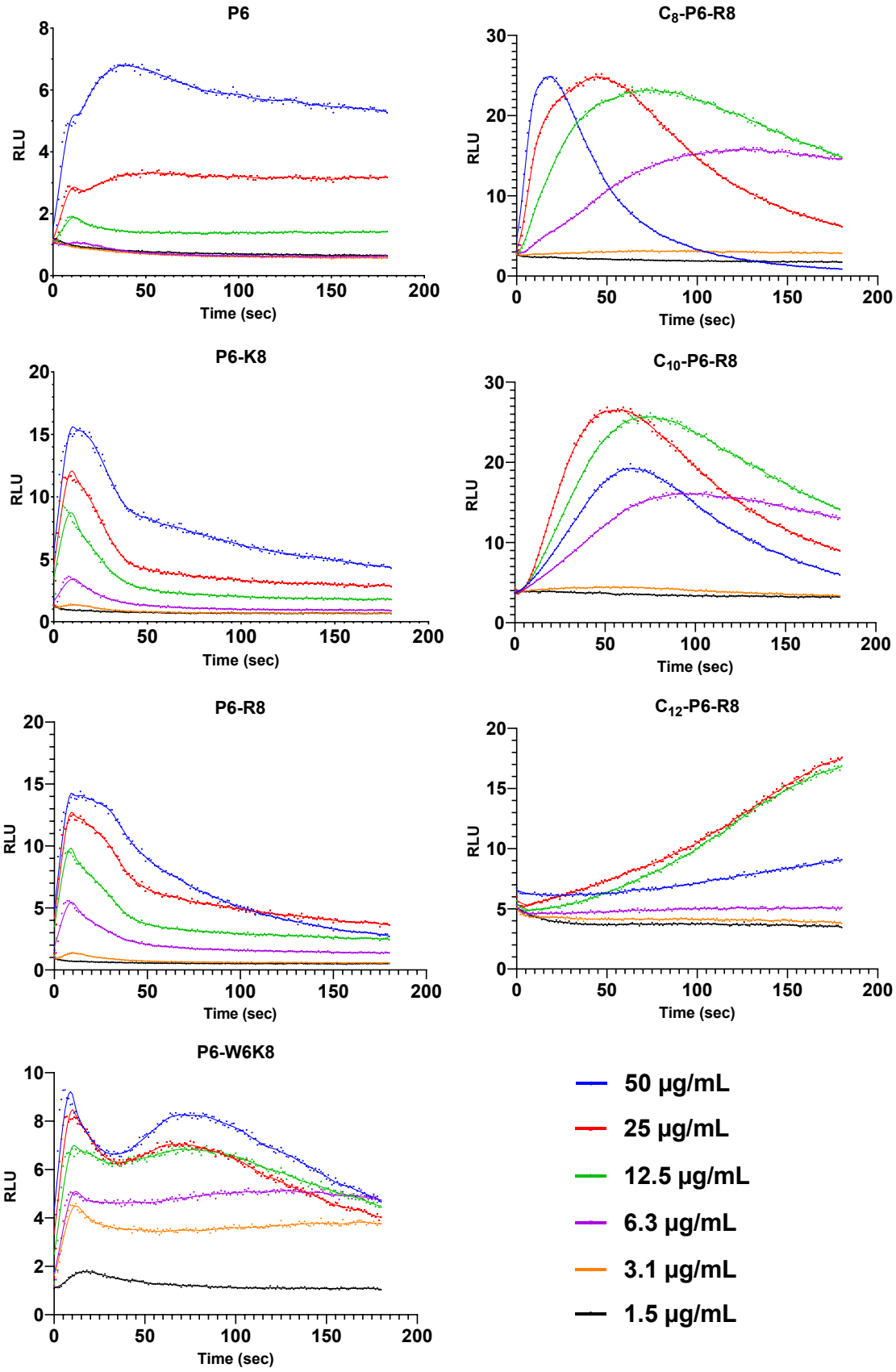

Figure S19. Kinetics of the effect on membrane integrity as measured by relative luminescence in *E. coli* (pCSS962) treated with different concentrations of **P6**, **P6-K8**, **P6-R8**, **P6-W6K8**, **C_8-P6-R8**, **C_{10}-P6-R8** and **C_{12}-P6-R8**.

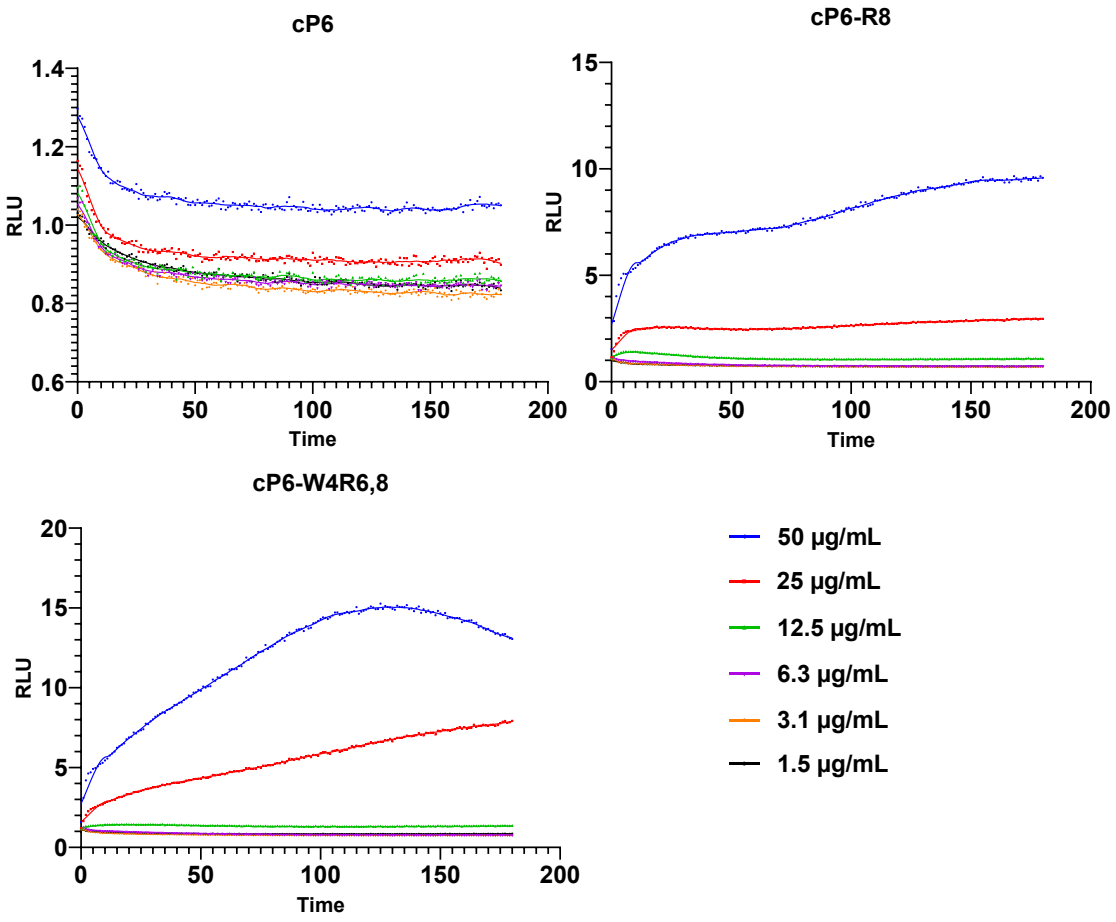

Figure S20. Kinetics of the effect on membrane integrity as measured by relative luminescence in *E. coli* (pCSS962) treated with different concentrations of **cP6**, **cP6-R8** and **cP6-W4R6,8**.

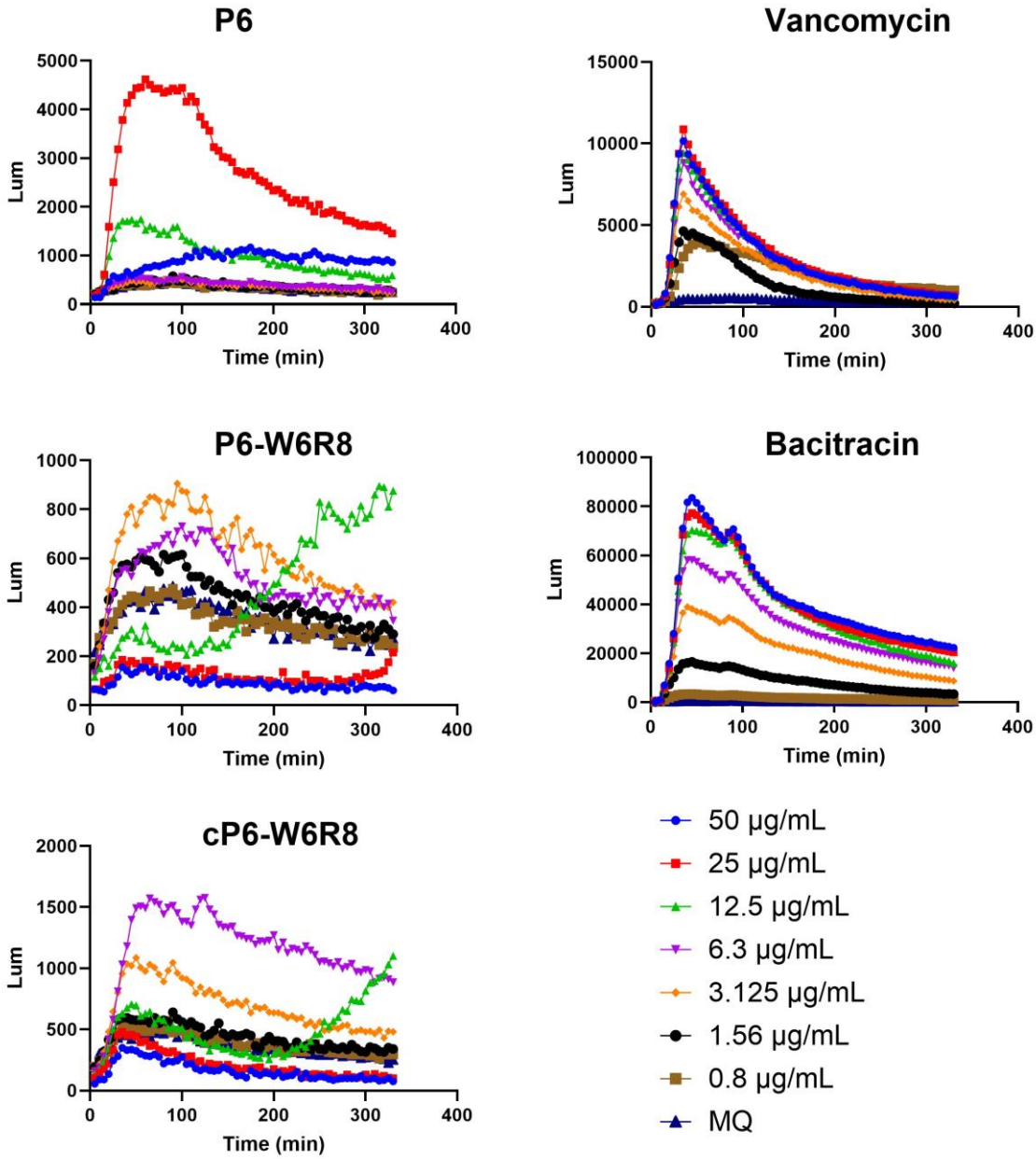

Figure S21. *B. subtilis* biosensor with P*liaI* fusion, specific for cell envelope stress, responded by increased light output compared to the water control, and where the peptides P6, P6-W6R8 and cP6-W6R8 reproducibly induced light output.

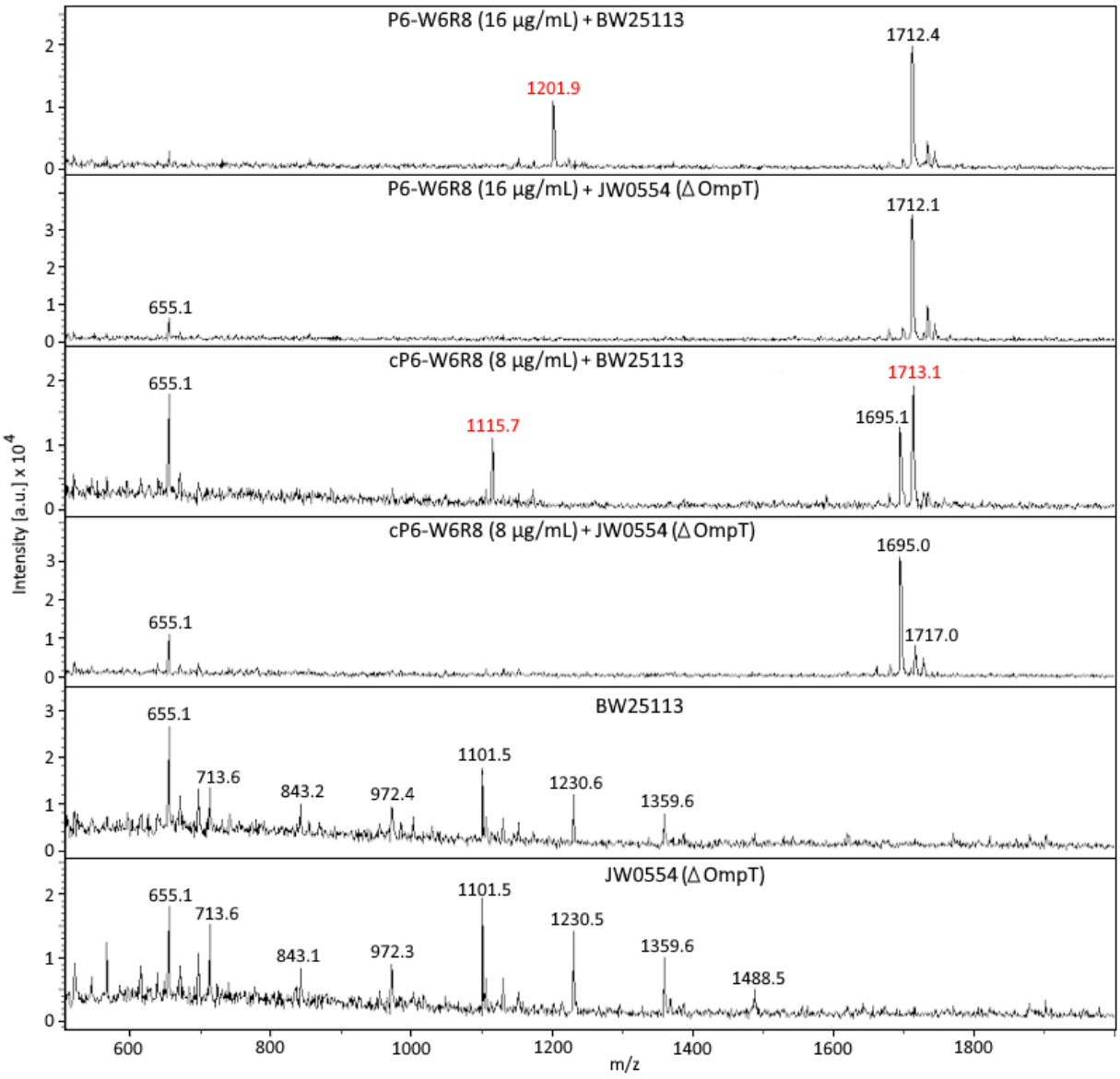

Figure S22. Selected MALDI-TOF MS spectra of *E. coli* BW25113 and JW0554 ΔOmpT exposed to the linear peptide **P6-W6R8** or the cyclic peptide **cP6-W6R8**, or without exposure to peptides. Peptide fragments detected are shown in red. The series of m/z-values with 129 Da apart (observed in the bacterial spectra) are probably degradation products of the peptidoglycan layer (loss of pentose rings and/or glutamic acid)(1, 2).

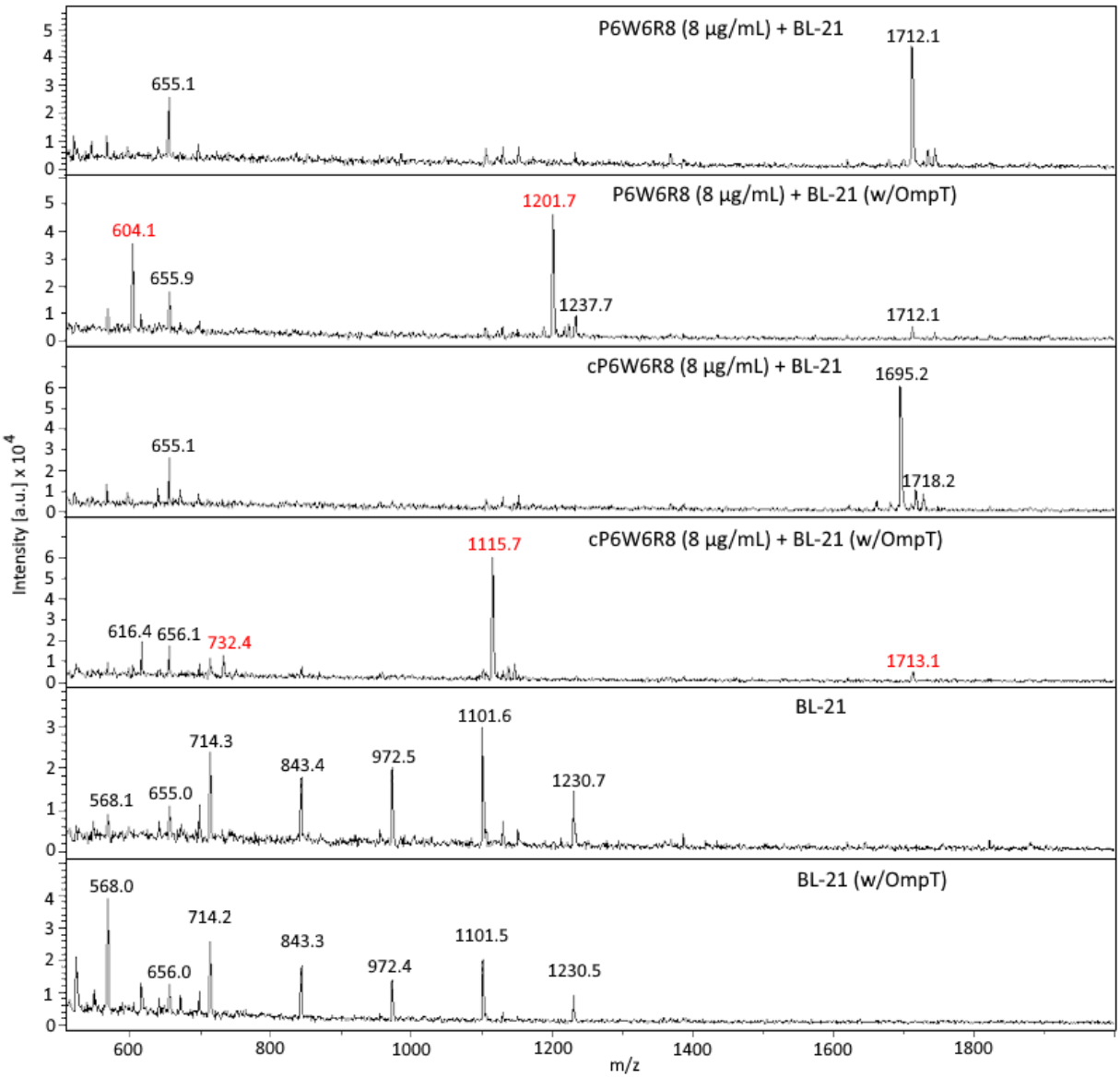

Figure S23. Selected MALDI-TOF MS spectra of *E. coli* BL-21 and BL-21+OmpT exposed to the linear peptide **P6-W6R8** or the cyclic peptide **cP6-W6R8**, or without exposure to peptides. Peptide fragments detected are shown in red. The series of m/z-values with 129 Da apart (observed in the bacterial spectra) are probably degradation products of the peptidoglycan layer (loss of pentose rings and/or glutamic acid)(1, 2).

Table S1. Theoretical and calculated monoisotopic mass (Da), and theoretical and measured m/z ions during HRMS of the synthesised peptides.

	Monoisotopic mass (Da)		$[M+2H]^{2+}$		$[M+3H]^{3+}$		$[M+4H]^{4+}$	
Peptide	Theoretical	Calculated	Theoretical	Measured	Theoretical	Measured	Theoretical	Measured
P6	1540.9215	1540.9226	771.4680	771.4680	514.6478	514.6481	386.2377	386.2383
P6-K8	1597.9794	1597.9802	799.9970	799.9966	533.6671	533.6673	400.5021	400.5028
P6-R8	1625.9855	1626.0196	814.0000	813.9997	543.0024	543.0026	407.5037	407.5043
P6-W6K8	1683.0110	1683.0124	842.5128	842.5123	562.0110	562.0112	421.7600	421.7611
P6-W6R8	1711.0171	1711.0173	856.5158	856.5151	571.3463	571.3465	428.7616	428.7619
C_8-P6-R8	1752.0900	1752.0911	877.0523	877.0516	585.0373	585.0376	439.0298	439.0307
C_{10}-P6-R8	1780.1213	1780.1231	891.0679	891.0677	594.3810	594.3815	446.0376	446.0387
C_{12}-P6-R8	1808.1526	1808.1545	905.0836	905.0831	603.7248	603.7253	453.0454	453.0467
cP6	1523.8950	1523.8955	762.9548	762.9548	508.9723	508.9725	381.9810	381.9813
cP6-R8	1608.9590	1608.9600	805.4868	805.4870	537.3269	537.3273	403.2470	403.2474
cP6-W6R8	1693.9906	1693.9910	848.0026	848.0023	565.6708	565.6709	424.5049	424.5053
cP6-W4R6,8	1693.9906	1693.9912	848.0026	848.0023	565.6708	565.6710	424.5049	424.5054

Table S2. Purity of synthesized peptides (%) and retention time (min) determined by UPLC using a reversed phase column.

Peptide	Purity (%)	Retention time (min)
P6	98.43	3.32
P6-K8	98.41	3.18
P6-R8	98.13	3.20
P6-W6K8	93.67	3.67
P6-W6R8	96.84	3.61
C_8-P6R8	99.41	4.70
C_{10}-P6R8	99.66	5.16
C_{12}-P6R8	100.00	5.67
cP6	100.00	3.36
cP6-R8	97.54	3.20
cP6-W6R8	98.56	3.76
cP6-W4R6,8	99.32	3.62

Table S3. Antimicrobial activity (MIC in μg/mL) of synthesized peptides against the biosensor strain *E. coli* MC1061.

Name	Sequence	*E. coli* MC1061
P6	GWWRRTVAKVRK-NH_2	4
P6-K8	GWWRRTVKKVRK-NH_2	4
P6-R8	GWWRRTVRKVRK-NH_2	8
P6-W6K8	GWWRRWVKKVRK-NH_2	4
P6-W6R8	GWWRRWVRKVRK-NH_2	8
C_8-P6-R8	C_8-GWWRRTVRKVRK-NH_2	8
C_{10}-P6-R8	C_{10}-GWWRRTVRKVRK-NH_2	8
C_{12}-P6-R8	C_{12}-GWWRRTVRKVRK-NH_2	16
cP6	c(GWWRRTVAKVRK)	8
cP6-R8	c(GWWRRTVRKVRK)	8
cP6-W6R8	c(GWWRRWVRKVRK)	4
cP6-W4R6,8	c(GWWWRRVRKVRK)	Nt[1]

[1] Not tested

References

1. Claydon, M.A., Davey, S.N., Edwards-Jones, V. and Gordon, D.B. (1996). The rapid identification of intact
   microorganisms using mass spectrometry. Nature Biotechnology, 14:1584-1586.
2. Liu, H., Du, Z, Wang, J. and Yang, R. (2007). Universal sample preparation method for characterization of bacteria by matrix-assisted laser desorption ionization–time of flight mass spectrometry. Applied and Environmental Microbiology, 73(6):1899-1907.

Paper III

biosensors

MDPI

Article

Outer Membrane Integrity-Dependent Fluorescence of the Japanese Eel UnaG Protein in Live *Escherichia coli* Cells

Céline S. M. Richard, Hymonti Dey, Frode Øyen, Munazza Maqsood and Hans-Matti Blencke *

The Norwegian College of Fishery Science, Faculty of Biosciences, Fisheries and Economics, UiT The Arctic University of Norway, N-9037 Tromsø, Norway
* Correspondence: hans-matti.blencke@uit.no

Abstract: Reporter genes are important tools in many biological disciplines. The discovery of novel reporter genes is relatively rare. However, known reporter genes are constantly applied to novel applications. This study reports the performance of the bilirubin-dependent fluorescent protein UnaG from the Japanese eel *Anguilla japonicas* in live *Escherichia coli* cells in response to the disruption of outer membrane (OM) integrity at low bilirubin (BR) concentrations. Using the *E. coli* wild-type strain MC4100, its isogenic OM-deficient mutant strain NR698, and different OM-active compounds, we show that BR uptake and UnaG fluorescence depend on a leaky OM at concentrations of 10 µM BR and below, while fluorescence is mostly OM integrity-independent at concentrations above 50 µM BR. We suggest that these properties of the UnaG–BR couple might be applied as a biosensor as an alternative to the OM integrity assays currently in use.

Keywords: reporter gene; synthetic biology; UnaG; outer membrane; bilirubin; biosensor

1. Introduction

Reporter genes are important tools and are widely used in synthetic biology and cellular biosensors. Due to the ease of use and signal detection, fluorescent and bioluminescent reporter genes are utilized in different types of applications. They are usually fused to either a promoter–operator regulatory sequence or genes of interest and convert biological events into optically detectable signals, which can easily be read by appropriate instrumentation. The most common reporter genes currently in use are the green fluorescent protein *gfp* from the cnidarian *Aequorea victoria* [1–3] and the red fluorescent protein *rfp* from *Discosoma* coral [4–6], as well as different luciferases [7–9]. During the last decade, several alternatives to the traditional fluorescent proteins have emerged, most notably fluorescent proteins belonging to the fatty-acid-binding protein family, such as UnaG and SmurfP [10], as well as RNA-based light-up aptamers [11–13] such as spinach, broccoli, and pepper. They all have in common that they require a fluorogenic ligand for fluorescence, which often must be provided externally.

In this work, we tried to apply the fluorescent protein from a Japanese eel (*Anguilla japonica*), UnaG, for the ligand-dependent labeling of *Escherichia coli* cells [14]. This protein belongs to the fatty-acid-binding protein (FABP) family and produces fluorescence by binding to its ligand bilirubin (BR) ($C_{33}H_{36}N_4O_6$), a yellow–orange pigment. This molecule is an antioxidant tetrapyrrole, formed by the breakdown of heme—for example, from hemoglobin from dead red blood cells in the mammalian body. UnaG and the unconjugated BR bind noncovalently, but with high specificity and affinity. This protein has been successfully used as an imaging tool for live-cell fluorescence microscopy in mammalian cells [15–17], in yeast [18], as well as in bacteria for anaerobic imaging [19,20], or as a dark-to-green photoswitchable fluorescent protein for super-resolution imaging [17].

The necessity of ligands is not problematic if the host readily provides the molecules in sufficient quantities through its inherent metabolism. Therefore, the use of UnaG does not

check for updates

Citation: Richard, C.S.M.; Dey, H.; Øyen, F.; Maqsood, M.; Blencke, H.-M. Outer Membrane Integrity-Dependent Fluorescence of the Japanese Eel UnaG Protein in Live *Escherichia coli* Cells. *Biosensors* **2023**, *13*, 232. https://doi.org/10.3390/bios13020232

Received: 9 December 2022
Revised: 28 January 2023
Accepted: 3 February 2023
Published: 7 February 2023

require the addition of BR in vertebrate systems. However, when UnaG is used as a reporter in bacteria, BR must be added externally, and, in the case of cytoplasmic expression of the protein, BR must pass the cell envelope and plasma membrane. As BR is a hydrophobic molecule with a size (584.7 Dalton) close to the exclusion threshold of outer membrane (OM) porins (ca. 600 Daltons) [21], sufficient access to BR inside the cell might be a limiting factor when expressed in Gram-negative bacteria. On the other hand, ligands, fluorophores, and enzyme substrate exclusion by cellular barriers such as the OM or plasma membrane can be used in assays or cellular biosensors to evaluate barrier integrity. This principle is used, for instance, in live–dead assays based on the fluorophores [22,23], where plasma membrane disruption is probed by propidium iodide access to the nucleic acids in the cytoplasm. Similarly, the exclusion of D-luciferin of intact plasma membranes is used in assays for plasma membrane integrity [24].

Several methods that are used to study the permeabilization of the OM of Gram-negative bacteria are based on similar principles—for instance, the use of the fluorescent probes 1-*N*-phenylnaphthylamine (NPN) [25–29] or 8-anilino-1-naphthylenesulfonic acid (ANS) [27,30], and ethidium bromide (EtBr) in a different assay [31], and spectrophotometric assays based on periplasmic β-lactamase activity and cytoplasmic β-galactosidase and the activation of respective enzyme-activated dyes [32]. In addition, GFP exported to the periplasm of Gram-negative bacteria has been used to assess damage to the OM in microscopy-based assays [33]. The latter principle has been further applied to multi-color fluorescent flowcytometry assays with GFP localized in the cytoplasm and mCherry in the periplasm [34,35]. The currently most widely applied approach seems to be the use of the fluorescent probe NPN.

The toxicity of ligand, substrate, or probe to the cells of interest might negatively affect experiments or limit the usability for end point measurements rather than real-time assays. For example, a common assay for the evaluation of membrane potential in bacteria is based on the fluorescent dye DiOC2 [36]. The dye itself is cytotoxic and is therefore only used in end point assays. It has been found that also BR affects bacterial viability in the gut. A study by Nobles et al. [37] showed that BR can have a positive effect on the Gram-negative bacteria by protecting them from reactive oxygen species (ROS) but also a negative effect on Gram-positive bacteria by disrupting the plasma membrane at concentrations of at least 100 μM.

In this study, we show that UnaG-dependent fluorescence in living *E. coli* cells depends on OM disruption under the in vitro conditions that we tested when BR is added externally at relatively low concentrations.

2. Materials and Methods

2.1. Media and Growth Conditions

For cloning, *E. coli* strains were routinely grown in Luria–Bertani (LB) broth at 37 °C with aeration. For fluorescence measurements, the bacteria were grown in Mueller–Hinton (MH; Merck, Darmstad, Germany) broth medium at room temperature (RT) over-night, which was then diluted 1:100 in MH broth medium and grown to an OD_{600} of approximately 0.5 at RT. To avoid a fluorescence background, after centrifugation at 3000× *g* for 5 min, the bacteria pellet was washed by careful pipetting in 0.9% NaCl solution, 0.9% NaCl solution with 20 mM Tris HCl pH 7.5, phosphate-buffered saline (PBS), or 5 mM HEPES buffer (Sigma-Aldrich, St Louis, MO, USA), free of bilirubin (BR), before measuring fluorescence. Then, 1 mM BR (Sigma-Aldrich, St Louis, MO, USA) stocks were created in dimethyl sulfoxide (DMSO; Sigma-Aldrich, St Louis, MO, USA). Different concentrations of ampicillin (Merck KGaA, Darmstad, Germany), 100 μg/mL and 5 μg/mL, were used for the plasmid selection in *E. coli* MC4100 and NR698, respectively.

2.2. Bacterial Strains and Plasmids

In this study, we used the isogenic *E. coli* K-12 strains MC4100 and NR698. To express UnaG constitutively in the cytoplasm, the plasmid pMM001 (Figure S11 and Sequence S1)

was designed and then synthetized through Invitrogen GeneArt Gene Synthesis (Thermofisher, Waltham, MA, USA) with codon optimization for *E. coli*. In this plasmid, the synthetic construct UnaG [14] is expressed from the constitutive OBX15 promoter [38]. The strain NR698 was constructed by Ruiz et al. [39], where the permeability of the OM increases by introducing the *imp4213* allele of *E. coli* BE100 [40] into the *E. coli* MC4100. This in-frame deletion of the *imp* gene, which encodes an essential protein of the OM assembly, results in a loss of OM integrity. For the membrane integrity assay, the strains were transformed with plasmid pCSS962 containing a constitutively expressed gene, *LucGR* [24].

2.3. Transformation

Competent *E. coli* MC4100 and NR698 were prepared by the transformation and storage solution (TSS) method [41]. Here, 100 µL of the competent strain was transformed with 100–500 ng plasmid. Cells were incubated at 37 °C, with agitation for 1 h, before being spread on LB agar plates with the appropriate antibiotics and incubated at 37 °C overnight.

2.4. Fluorescence Detection

A Synergy H1 Hybrid Reader (BioTek, Winooski, VT, USA) was used to measure the UnaG fluorescence of bacterial populations. To avoid excessive background fluorescence, the monochromator was set to an excitation wavelength of 508/8 nm and an emission wavelength of 538/8 nm, and fluorescence was measured in 30 s intervals at RT (the temperature inside the device was at 25.5 °C, slightly above ambient, throughout the measurements). The gain was kept at 100 in all experiments. Then, 90 µL of the bacterial suspension was added to a black round-bottom 96-well microtiter plate (Nunc, Roskilde, Denmark). BR and outer- and plasma-membrane-active compounds were added to the indicated concentrations. The following compounds were used: polymyxin B sulfate (PMB; Sigma-Aldrich, St Louis, MO, USA), polymyxin B nonapeptide (PMBN; GLPBIO, Montclair, CA, USA), chlorhexidine acetate (CHX; Fresenius Kabi, Halden, Norway). BR-free bacterial suspension served as the background, with water instead of PMB as a negative control. Data were processed with GraphPad Prism 9 software version 9.5.0 (GraphPad Software; Boston, MA, USA).

2.5. NPN Assays for Outer Membrane Integrity

The increased permeability of the OM was analyzed by measuring increased fluorescence as kinetics of 1-N-phenylnaphthylamine (NPN) uptake following the protocol described by Helander and Mattila-Sandholm [42]. Briefly, *E. coli* MC4100 and NR698 were grown overnight in MH broth medium. The cultures were further diluted and grown to OD_{600} 0.5, rinsed once using centrifugation at 3000× *g* for 5 min, and suspended in 5 mM HEPES buffer supplanted with 5 mM glucose (pH 7.2) and diluted to OD_{600} 0.5. NPN was added to a concentration of 20 µM containing 1 mL of cell suspension in HEPES buffer immediately prior to fluorescence monitoring using 96-well black-bottom microtiter plates. After 10 µL of the permeating agent was added to 90 µL of the cell suspension with NPN, fluorescence was measured using a microplate reader with excitation and emission wavelengths set to 350 and 420 nm, respectively. For the NPN OM assay with BR, *E. coli* cells were grown, harvested, and suspended as described above, before they were preincubated with different concentrations of BR for 10 min. BR-treated cells were washed once and resuspended in HEPES buffer, followed by the addition of NPN to obtain a final concentration of 20 µM for the measurement of fluorescence for 15 min.

2.6. Luminescence Assays for Plasma Membrane Integrity

The *E. coli* strains MC4100 and NR698 constitutively expressing the luciferase LucGR from the pCSS692 plasmid were cultured overnight in MH broth medium supplemented with 5 µg/mL chloramphenicol (Merck KGaA, Darmstad, Germany) for *E. coli* NR698 and 20 µg/mL for MC4100. New day cultures were made by 1% inoculation in MH broth medium and incubated at RT with aeration until the OD_{600} reached 0.5. The final

concentration of D-luciferin potassium salt (Synchem Inc., Elk Grove Village, IL, USA) in the medium was 2 mM.

The real-time membrane integrity assay was modified from a previously described protocol for the membrane integrity assay [24]. This assay was performed on different strains of *E. coli*, including the wild-type (WT) MC4100 and the OM-deficient NR698 strains. The LucGR protein is dependent on its substrate D-luciferin to emit luminescence. PMB at a final concentration of 10 μg/mL was used as a positive control. Milli-H_2O was used as a negative control.

All values were normalized to the water control for the normalization of the luminescence. Data were processed with GraphPad Prism 9 software.

2.7. Microscopy

Suspensions of UnaG-expressing *E. coli* strains MC4100 and NR698 in PBS buffer were prepared as described earlier. Sample preparation was identical as for the assays in the plate reader in PBS. First, 5 μL of bacterial suspension was transferred onto a microscopic slide and covered with a cover slip for immediate microscopic analysis. Fluorescence was analyzed at several time points after the addition of BR to 5 μM and PMB 10 μg/mL with a Leica DM6000B fluorescence microscope and an excitation light source, a Leica CTR6000, with the filter system Cube I3 DM 513828. Fluorescence was documented with a camera, a Leica DFC7000T, attached to the microscope. Identical camera settings were applied for all images taken. The imaging software used for image analysis was the Leica application suite LAS X, where identical settings for contrast enhancement were applied to the original micrographs. In addition, the brightness of the fluorescent images as a whole was increased to 150% in Photoshop CS6 version 13.0 (Adobe; San Jose, CA, USA) for better on-screen visibility. The original figure without enhanced brightness is supplied as Figure S12.

3. Results and Discussion

3.1. UnaG Fluorescence in Complex Growth Media

To evaluate the fluorescence of UnaG expressed from a plasmid-based, constitutive promoter construct (pMM001) in the wild-type (WT) strain *E. coli* MC4100, the bacteria were grown in either MH or LB broth medium, two different complex media typically in use for different purposes and assays in our laboratory. Green fluorescence was analyzed after incubation in the presence of 5 μM BR. However, within the 15 min measurement window, no UnaG/BR-dependent increase in fluorescence was observed (Figure 1a). In addition, the background fluorescence of complex media is very high. It has been speculated that BR is excluded from entering bacterial cells by the wall of Gram-negative bacteria [43]. Therefore, we tried to compromise the OM with PMB, which is known to affect OM integrity [44]. Again, the addition of PMB did not result in an increase in UnaG-dependent fluorescence.

3.2. The Effect of Different Buffers and Solutions on UnaG Fluorescence Signal-to-Noise Ratio after Membrane Disruption

To investigate whether the background fluorescence of complex media might camouflage any UnaG-dependent changes in fluorescence, we measured the fluorescence of the bacteria suspended in different buffers and solutions, which are often used with viable cells. Again, the WT strain *E. coli* MC4100 carrying the plasmid pMM001 was tested for UnaG-specific fluorescence. In addition, the influence of bacterial concentrations on signal-to-noise ratios was evaluated by testing the fluorescence of the bacterial suspension in HEPES buffer and in 0.9% NaCl solution at an OD_{600} of 0.1, 0.3, 0.5, 0.7, and 1.0. The signal-to-noise ratio seemed to increase with increasing cell concentrations until an OD_{600} of 0.5. Above this concentration, the fluorescence ratio of PMB+BR-treated cells to BR-treated cells stabilized (Figure S13). Hence, an OD_{600} of 0.5 was chosen for further experiments.

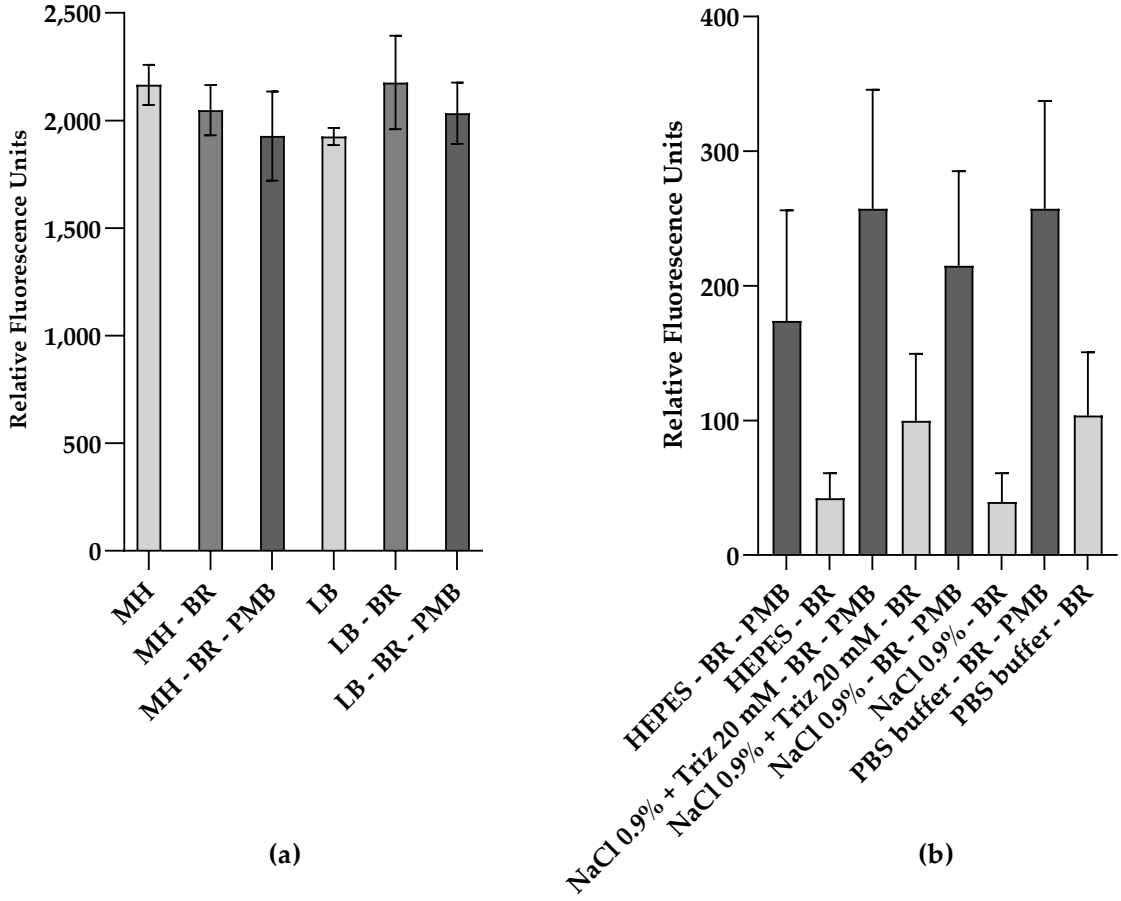

Figure 1. Relative fluorescence of UnaG in live *E. coli* cells is affected by the fluorescent background and the cell envelope active peptide polymyxin B (PMB). Relative fluorescence of *E. coli* MC4100 constitutively expressing UnaG from pMM001 after 15 min exposure to 5 μM bilirubin (BR) and 10 μg/mL of PMB in (**a**) MH medium or LB medium; (**b**) buffers and solutions, at an OD_{600} of 0.5. Relative fluorescence values are blanked to the respective control without BR. Each data point is the mean of three independent measurements.

Figure 1b shows the comparison of the relative fluorescence emission of UnaG in the different buffer conditions at an OD_{600} of 0.5, after 15 min in the presence and absence of PMB at a final concentration of 10 μg/mL. The relative fluorescence was blanked to the background fluorescence in the absence of BR in each buffer/solution. Overall, the relative fluorescence of UnaG is strongest in cells treated with PMB when the cells are resuspended in PBS and HEPES, while the fluorescence increase in response to PMB treatment is most pronounced in 0.9% NaCl solution. In all tested conditions, the fluorescence increased at least two-fold after the addition of PMB, while the increase in 0.9% NaCl solution was approximately five-fold. The individual differences in UnaG fluorescence between the independent replicates resulted in a relatively high standard deviation. At the same time, the fold changes in all individual measurements were always largest when conducted in 0.9% NaCl solution. Comparing the effect of PMB on fluorescence in complex media with corresponding data in buffers and solutions clearly indicated that the complex media affected the PMB-induced UnaG fluorescence (Figure 1a,b). Therefore, 0.9% NaCl solution was chosen for further experiments. This difference in fluorescence in response to PMB might be explained by the OM being impermeable to BR at these low concentrations. However, PMB also affects the membrane permeability of the plasma membrane, and, in our construct, UnaG was expressed and localized in the cytoplasm.

3.3. Outer-Membrane-Dependent Uptake of Bilirubin

To determine whether the fluorescence increase after the addition of PMB was caused by OM damage, the OM-deficient *E. coli* strain NR698 was transformed with pMM001. To study the effect of this OM deficiency on BR uptake, we compared the fluorescence kinetics of this mutant and its isogenic WT strain *E. coli* MC4100, both carrying the pMM001 plasmid. Figure 2a illustrates that the addition of BR alone immediately increases the fluorescence only in NR698, while the fluorescence of MC4100 remains at a constant low level. Within the 15 min measuring window used in this experiment, the fluorescence in the OM-deficient strain increases to four-fold compared to the WT strain. The addition of PMB, on the other hand, increases the relative fluorescence in the WT two-fold. Interestingly, the fluorescence of the OM-deficient strain also increases and stabilizes at approximately five-fold after the addition of PMB. This might be caused by the effect of PMB on the plasma membrane or additional damage to the OM. Moreover, when extending the measurement window to 3 h, the fluorescence of MC4100 stays at a low level, while the fluorescence of NR698 is constantly rising (Figure 2b).

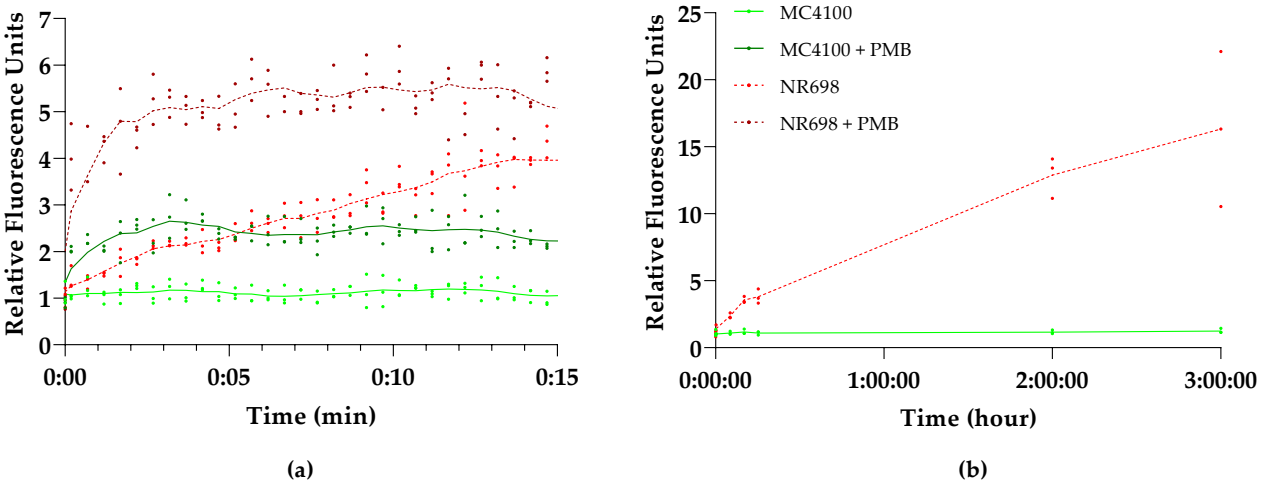

Figure 2. *E. coli* outer membrane (OM) integrity affects UnaG fluorescence. Kinetics of UnaG fluorescence in *E. coli* wild-type (WT) strain MC4100 (solid shades of green) and the isogenic *E. coli* OM-defective mutant NR698 (dashed shades of red) after (**a**) 15 min exposure of 10 µg/mL PMB and subsequent addition of 5 µM BR (dark shades) or 5 µM BR only (light shades); (**b**) 3 h exposure of 5 µM BR only. The data points represent three independent measurements normalized to the negative control of MC4100 in the presence of BR only. The mean is represented by the line of the same color.

The results indicate that the OM indeed excludes BR from entering the cells as only the OM-compromised cells allow for the emission of fluorescence, either by mutation (NR698) or a permeabilizing agent (PMB). This seems to confirm the prediction by Chia et al. that the impermeability of bacterial cell walls to BR limits the use of UnaG to outer cell wall targets [43]. This might be caused by the size of BR as the exclusion threshold of OM porins is around 600 Daltons [21] and the molecular weight of BR is 584.7 Daltons. Possibly, BR is also actively removed from the cells with the help of efflux pumps. However, these experiments were conducted at relatively low concentrations of BR. At higher concentrations of BR, a rapid and concentration-dependent increase of fluorescence could be observed in the absence of compounds affecting OM integrity (see Figure S3 in Supplementary Materials), which coincides with the results from the original study in *E. coli* [14] and studies conducted in anaerobic conditions with different *Bacteroidetes* species [43] at 200 µM and 25 µM, respectively. We were not able to rule out or confirm that BR itself has an OM-permeabilizing effect at higher concentrations, as its absorbance spectrum interferes with the NPN-based fluorescence. To exclude any major damage to the OM by BR, we also conducted synergy studies incubating both strains in

Minimum Inhibitory Concentration (MIC) assays with different combinations of BR and erythromycin or vancomycin. These antibiotics are efficiently excluded by the OM and therefore render Gram-negative bacteria relatively insensitive, compared to Gram-positive bacteria [45–48]. While the NR698 was sensitive to all antibiotic concentrations tested, MC4100 did not become more sensitive in the presence of BR. On the contrary, the highest BR concentrations seemed to reduce sensitivity at the MIC (see Table S1 in Supplementary Materials). This observation seems to be in accordance with BR protecting *E. coli* against oxidative stress, as shown in earlier studies [37].

3.4. Confirming Outer Membrane Integrity by NPN Assays

To confirm the hypothesis that the OM is responsible for BR exclusion at low concentrations, we wanted to test the differences in OM integrity in both strains with the fluorescent probe 1-N-phenylnapthylamine (NPN), which is often used in OM integrity assays [25–29]. In addition, we confirmed the effects of PMB and EDTA on the OM of these *E. coli* strains. As mentioned above, PMB is known to disrupt the LPS layer of Gram-negative bacteria. NPN is a small hydrophobic molecule (219 Da) that cannot effectively cross the OM and fluoresces only weakly in aqueous solution but strongly when it is in close contact with phospholipid (PL) moieties, which become exposed in response to OM damage. When we compared the background fluorescence taking the same number of cells, the WT strain with intact OM (MC4100) produced weaker fluorescence than the strain with deficient OM (NR698). This difference in fluorescence decreases over time, since the fluorescence intensity of the OM-compromised strain decreases over time, as shown in Figure 3. It seems that NPN can easily access the periplasmic space and bind to the PL of the OM and outer leaflet of the inner membrane when the OM is compromised.

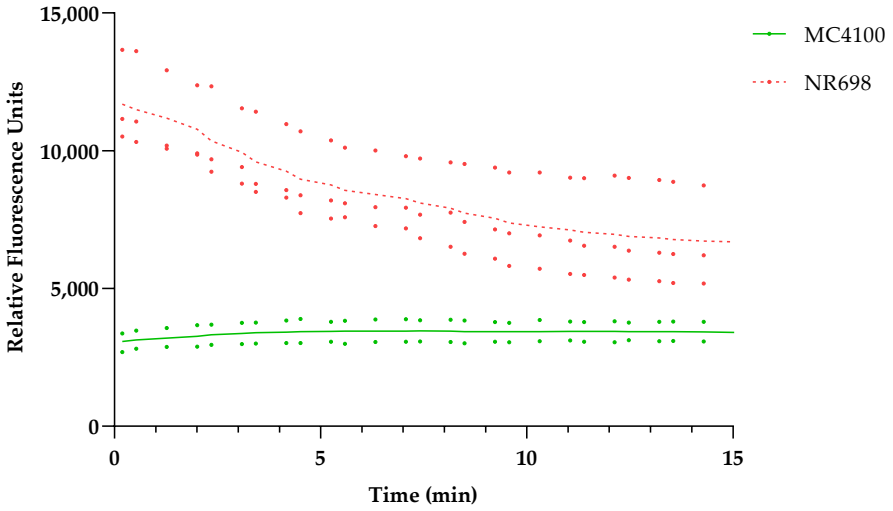

Figure 3. *E. coli* MC4100 and NR698 cells were used to detect fluorescence resulting from OM permeability to the small hydrophobic molecule 1-N-phenylnapthylamine (NPN). The data points represent two (MC4100, solid shade of green) or three (NR698, dashed shade of red) independent measurements normalized to the water-treated control (bacteria in 5 mM HEPES buffer). The mean is represented by the line of the same color.

We then compared the effect of different OM-active compounds on the NPN fluorescence of both strains (Figure 4). MC4100 treated with 10 µg/mL PMB fluoresced almost six-fold more compared to the non-treated control, whereas CHX and EDTA showed a four-fold increase in fluorescence at the 2 min point, which is usually used for OM effects in the NPN assay [25,26]. It is worth noting that MC4100 became slightly more fluorescent in the presence of 10 µg/mL PMB and 5 mM EDTA than NR698 alone, even though a 1.5–2-fold increase in fluorescence was observed when NR698 cells were treated with 10 µg/mL PMB. However, MC4100 cells were less permeable when treated with 100 µg/mL CHX, which

is known to be a strong membranolytic agent with an immediate effect on the viability of bacterial cells, although its OM activity at a sub-MIC level has not been established yet. In our assay, the higher fluorescence values in the NR698 strain with porous OM indicated that NR698 was already more permeable to NPN and reached its higher saturation level in the absence of membrane permeabilizers.

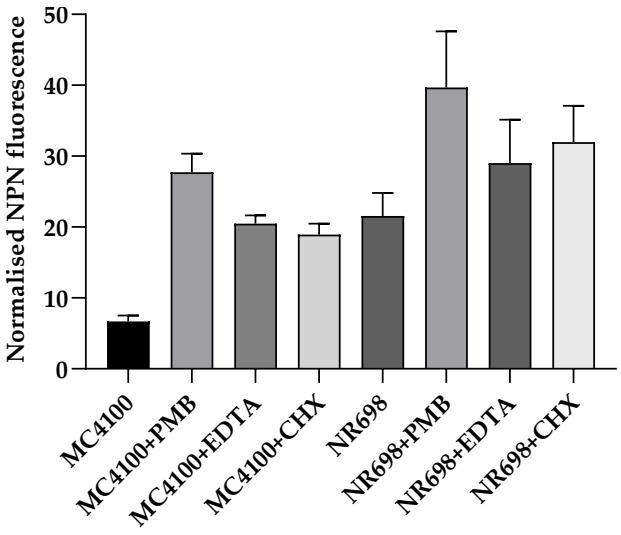

Figure 4. Relative NPN fluorescence in response to different membrane- and OM-active compounds. The permeability of the OM was assessed by measuring the fluorescence of NPN in both *E. coli* strains (MC4100 and NR698) after 2 min in the presence of 10 µg/mL PMB, 5 mM EDTA, or 100 µg/mL chlorhexidine (CHX). The fluorescence emission was plotted after normalizing all the samples to the bacteria in 5 mM HEPES buffer.

3.5. Bilirubin Uptake Is Mostly Independent of Plasma Membrane Integrity

To evaluate the plasma membrane integrity of the mutant strain NR698 and the isogenic WT MC4100, we transformed both strains with plasmid pCSS962 coding for a constitutively expressed eukaryotic luciferase LucGR. This construct was used to evaluate the integrity of the plasma membrane [24]. In addition, we wanted to confirm that a derivative of PMB, the PMB nonapeptide (PMBN), did not affect the plasma membrane of either strain at 10 µg/mL, as we planned to use it as an example for a substance specifically damaging the OM. This peptide is described to be highly specific for the efficient perturbation of the OM and affects the plasma membrane only at high concentrations [49]. The integrity of the plasma membrane of *E. coli* MC4100 and NR698 (Figure 5) was tested in response to PMB and PMBN at a concentration of 12.5 µg/mL, and the kinetics of the bioluminescence of the protein LucGR was measured for 10 min after the addition of each compound. The luminescence increased directly after the addition of PMB in both strains. This indicates that the plasma membrane is compromised, allowing D-luciferin to diffuse into the cells and the enzyme to emit luminescence. PMBN, on the other hand, did affect luminescence to a lower extent in either strain at the tested concentration. Furthermore, the luminescence stabilized to a level similar to the non-treated control, confirming that plasma membrane integrity is not severely perturbed by PMBN in either *E. coli* strain and that the plasma membrane of the mutant NR698 in the absence of antimicrobial compounds is still excluding D-luciferin. As BR itself has earlier been described to affect membrane stability [37,50–52], we also analyzed how different concentrations of BR affect plasma membrane integrity. Although the highest concentration of BR resulted in a two-fold increase in luminescence in MC4100, the luminescence levels did not reflect the same pattern as known for membrane-active compounds (see Figures S4 and S5). We also tested different concentrations of BR against an *E. coli* viability sensor based on the *lux* operon, without observing a concentration-dependent specific effect apart from partial light

absorption by bilirubin (see Figures S7 and S8). This is also in agreement with MIC studies conducted earlier, where BR, even at the highest concentrations tested, did not inhibit growth [53], and which we have confirmed in our lab for both strains used in this study.

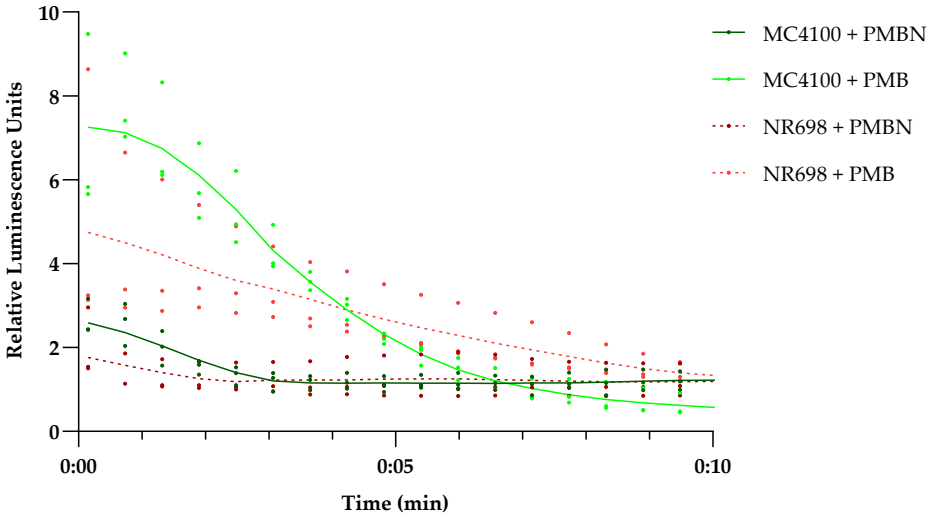

Figure 5. Effect of PMB and PMBN on plasma membrane integrity of *E. coli* MC4100 and NR698. Luminescence kinetics of LucGR in *E. coli* MC4100 (solid shades of green) and *E. coli* NR698 (dashed shades of red) in response to the presence of 12.5 µg/mL PMB (light color) or polymyxin B nonapeptide (PMBN) (dark color) and due to D-luciferin influx caused by plasma membrane permeabilization. The data points represent three independent measurements normalized to the negative control in the presence of D-luciferin only. The mean is represented by the solid line of the same color. An initial luminescence increase represents membrane permeabilization, the subsequent luminescence decrease represents ATP depletion due to bacterial cell death because of lost membrane integrity, while luminescence stabilization on the level of the control indicates survival of the main population with limited or no plasma membrane damage.

3.6. Is UnaG a Suitable Sensor for Outer Membrane Damage?

To evaluate whether UnaG-expressing *E. coli* strains could be used as indicators of OM damage, the effect of PMBN on UnaG fluorescence, and therefore BR diffusion through the OM, was tested. *E. coli* MC4100 was subjected to PMB and PMBN carrying the plasmid pMM001 with the constitutively expressed UnaG gene. Figure 6 shows the kinetics of the fluorescence increase after the addition of 10 µg/mL of either peptide. It is evident that both peptides substantially increase the fluorescence. As we showed earlier that the PMBN does not seem to have a major effect on plasma membrane integrity at the tested concentration, this effect is specific for OM damage. However, as studies with *Bacteroidetes* [19] grown anaerobically have shown that BR is taken up by the cells when provided with the growth medium over time, use of the UnaG–BR combination might require strict control of the assay conditions. Although there are already several different assays to test OM damage, in some cases, there might be advantages of using UnaG in combination with BR. Interestingly, the long-term stability of the system over several hours (Figure 2b) suggests a possible application of the system in assays with living bacterial biosensors for the longer-term monitoring of OM integrity in real time.

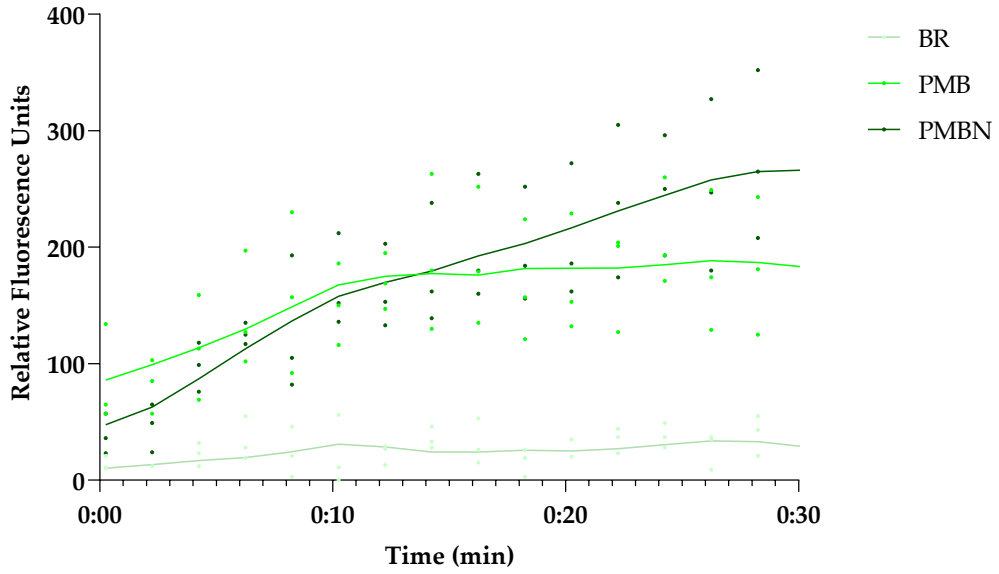

Figure 6. Both the OM-active PMBN and PMB induce UnaG fluorescence in the presence of BR, but show differences in the kinetics over time. The 30 min fluorescence kinetics of UnaG in *E. coli* MC4100 after exposure to 10 µg/mL PMB and 5 µM BR (medium green), 10 µg/mL PMBN and 5 µM BR (dark green), or 5 µM BR only (light green). The data points represent three independent measurements normalized to the negative control in the presence of bacteria only. The mean is represented by the solid line of the same color.

To test this hypothesis, the fluorescence of *E. coli* MC4100 carrying the plasmid pMM001 was measured for 10 h in the presence of different concentrations of compounds that are known or suspected to show OM-disrupting activity, plasma-membrane-disruptive activity, or both. PMB has been described to affect the integrity of Gram-negative membranes [44,54], while its derivative PMBN seems to permeabilize the OM down to concentrations around 1 µg/mL [55] and it does not seem to affect plasma membrane activity at 12.5 µg/mL (compare Figure 5); hence, its permeabilizing activity is likely exclusively affecting the OM at concentrations between 1 and 10 µM. Here, we show that PMB induces UnaG fluorescence only at the lowest concentration tested (2.5 µg/mL), while PMBN-induced fluorescence is up to three-fold higher at all concentrations tested, including 10 µM. The fluorescence intensities of bacteria treated with PMBN resemble the fluorescence intensity of the OM mutant NR698. The concentration-dependent fluorescence of PMB might be explained by its bacteriostatic effect at low concentrations and its bactericidal effect at high concentrations [54]. Chlorhexidine (CHX), on the other hand, only slightly induces fluorescence at the tested concentrations, while both PMB and CHX permeabilize the plasma membrane at the higher concentrations. This possibly indicates that CHX attacks the OM to a lesser extent, with the plasma membrane being the main target. In addition, we tested two recently described cyclic antimicrobial peptide (Turgencins) derivatives, the peptide analogue cTurg-2 as well as the lipopeptide analogue C_{12}-cTurg-1 [56], against the prospective UnaG-based biosensor. Again, the fluorescence levels in response to the analytes varied. C_{12}-cTurg-1, which was previously described to disrupt both the plasma membrane and OM, causes an increase in UnaG fluorescence at both concentrations tested, while the observed fluorescence is more than two-fold stronger at the lower concentration. cTurg-2, on the other hand, was described as mostly OM-active and, in its presence, UnaG fluorescence rose to above the level of the lower concentration of C_{12}-cTurg-1 at both concentrations tested (Figure 7). This might indicate that cTurg-2 is indeed mostly active against the OM. NPN assays conducted for chlorhexidine published previously [56], and related unpublished data on PMB and the Turgencin derivatives summarized in Figure 7b, all show increasing fluorescence with increasing concentrations of active analytes. The NPN assay seems to quantify the combined membrane damage of both the OM and the

plasma membrane. Therefore, the fluorescence intensity tends to increase with increasing analyte concentrations as opposed to the UnaG-based fluorescence, which decreases with increasing analyte concentrations. It is tempting to speculate that plasma-membrane-active compounds kill the bacterial cells due to plasma membrane permeabilization at and above the MIC. Loss of viability shuts down all cellular metabolism, including protein/UnaG synthesis. On the other hand, OM-active compounds such as PMBN will not damage the plasma membrane and cells stay alive, constantly expressing UnaG, with BR diffusing through the compromised OM as it is bound to the protein in the cytoplasm. The steady fluorescence increases over 10 h is represented in the kinetic fluorescence curves shown in Figures S9 and S10 for all the compounds tested. Therefore, we propose that this sensor construct could be used in assays to identify outer membrane active compounds as illustrated in Figure 8.

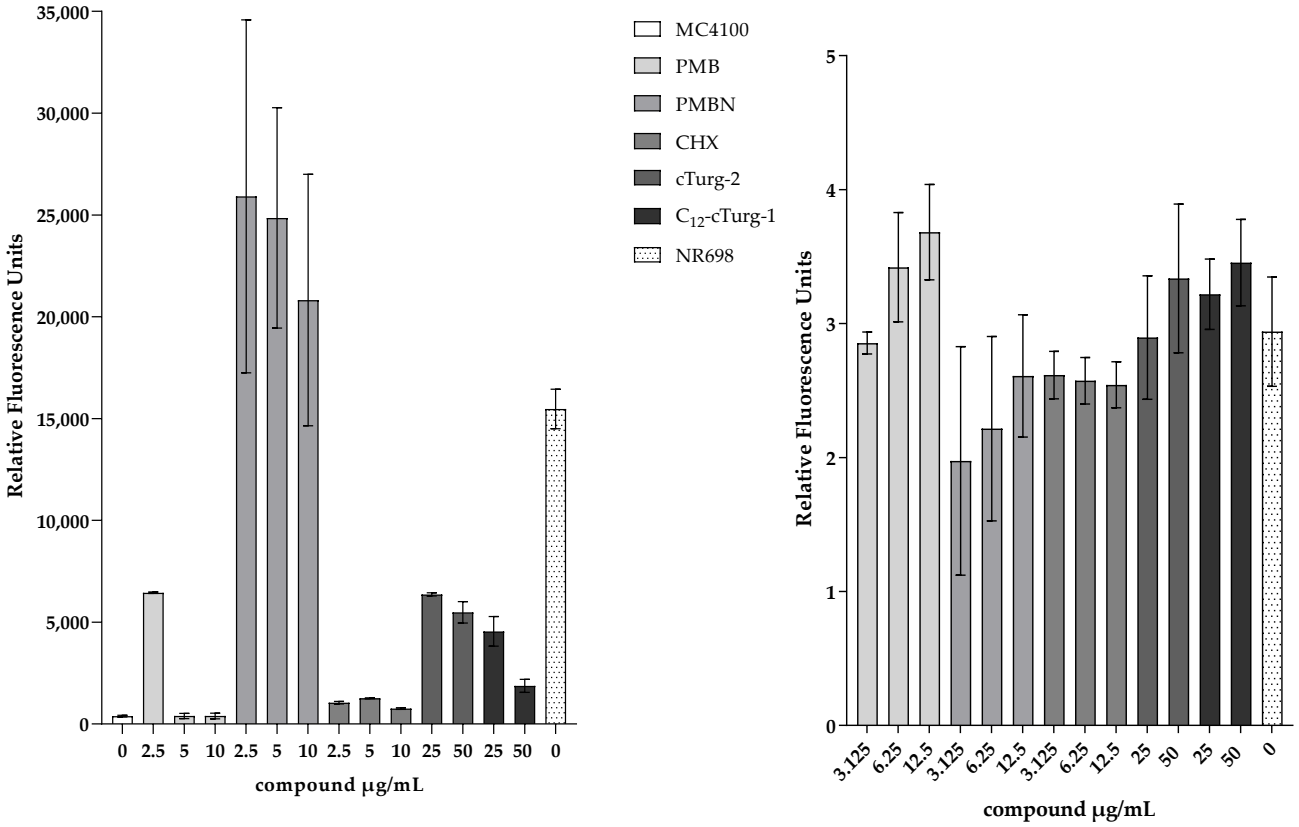

(a) **(b)**

Figure 7. Comparison of relative fluorescence readouts of the proposed UnaG-based OM integrity biosensor and the traditional NPN assay in response to membrane damage. Representative fluorescence values from three independent measurements are shown. (**a**) Fluorescence of MC4100 constitutively expressing UnaG from pMM001 in 0.9% NaCl 10 h after addition of 5 µM BR and indicated concentrations of OM- or plasma-membrane-active compounds. The measurements were blanked to the respective control without BR. (**b**) Normalized fluorescence in presence of NPN and different concentrations of OM- or plasma-membrane-active compounds in 5 mM HEPES after 3 min to the MC4100 control with NPN and only water.

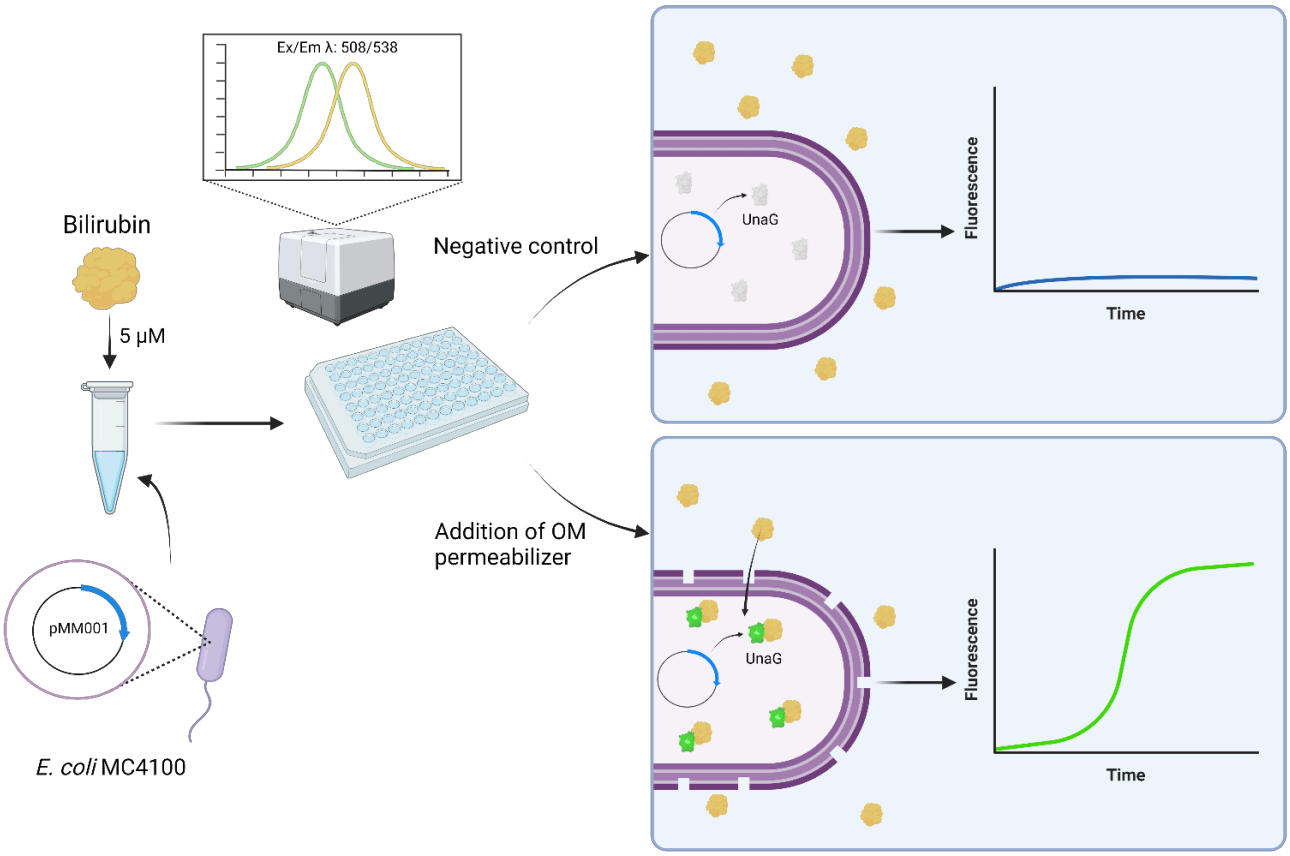

Figure 8. Schematic of the use of the reporter protein UnaG as an OM permeabilization whole-cell biosensor. Created with BioRender.com (accessed on 6 December 2022).

3.7. Is There a Variation in the OM Effect within the Population?

To rule out the possibility that a minor subpopulation is responsible for the increase in fluorescence in response to treatment with OM-disrupting agents observed by the experiments in the plate reader, samples treated in a similar fashion with PMB were analyzed under a fluorescence microscope. Several fluorescent microscope images of the different suspensions of UnaG-expressing *E. coli* strains MC4100 and NR698 in PBS were taken at two different time points after exposure to PMB at 10 µg/mL and BR at 5 µM or BR only (Figure 9). The bacteria were planktonic, viable, and freely moving in the buffer. Therefore, the exposure time could not be increased to achieve brighter images as the moving bacteria resulted in blurry images; this is also visible as a slight positional change between phase contrast and fluorescent images. The fluorescence of the WT MC4100 after exposure to BR was significantly lower compared to the fluorescence after exposure to BR and PMB. Moreover, fluorescence seemed to be mostly constant throughout the population in the focal plane. The effect of PMB was detectable 5 min after its addition. As expected, the fluorescence was significantly lower in the WT compared to the OM-deficient strain when exposed to BR only. This confirms the results observed with PMB performed in the plate reader and indicates that the observed fluorescence is due to the relatively equal fluorescence of the whole population, rather than strongly fluorescent subpopulations. However, an earlier study used the protein UnaG for the imaging of anaerobic bacteria without any OM-disrupting agent [19]. In their study, the concentration of BR in the medium was 25 µM—a concentration only five-times higher than used in this study. Therefore, higher concentrations of BR might increase the diffusion rate to an extent, where sufficient BR molecules accumulate inside the cytoplasm to induce fluorescence also in the absence of OM permeabilizers. It is important to note that this microscopic study was conducted before deciding on the use of 0.9 % NaCl solution as

the medium of choice for conducting experiments, and it was conducted in PBS. More importantly, in the microscopic study, PMB was used as the OM-permeabilizing agent at 10 μg/mL. We later showed, in microtiter plate assays, that the addition of PMBN or PMB at 2.5 μg/mL resulted in substantially higher fluorescence emission than PMB at 10 μg/mL, indicating a more OM-specific effect (Figures 7 and S9). However, in the presence of BR, the untreated OM-compromised NR698 strain emitted strong fluorescence, which was independent of any compromising agents used, and it can therefore serve as a benchmark to compare fluorescence between the assays conducted in the plate reader and the microscopic observations. In conclusion, the microscopic images show that the fluorescence throughout the treated and untreated populations seems to be mostly homogenous and confirms that a breach in OM integrity is necessary for strong fluorescence.

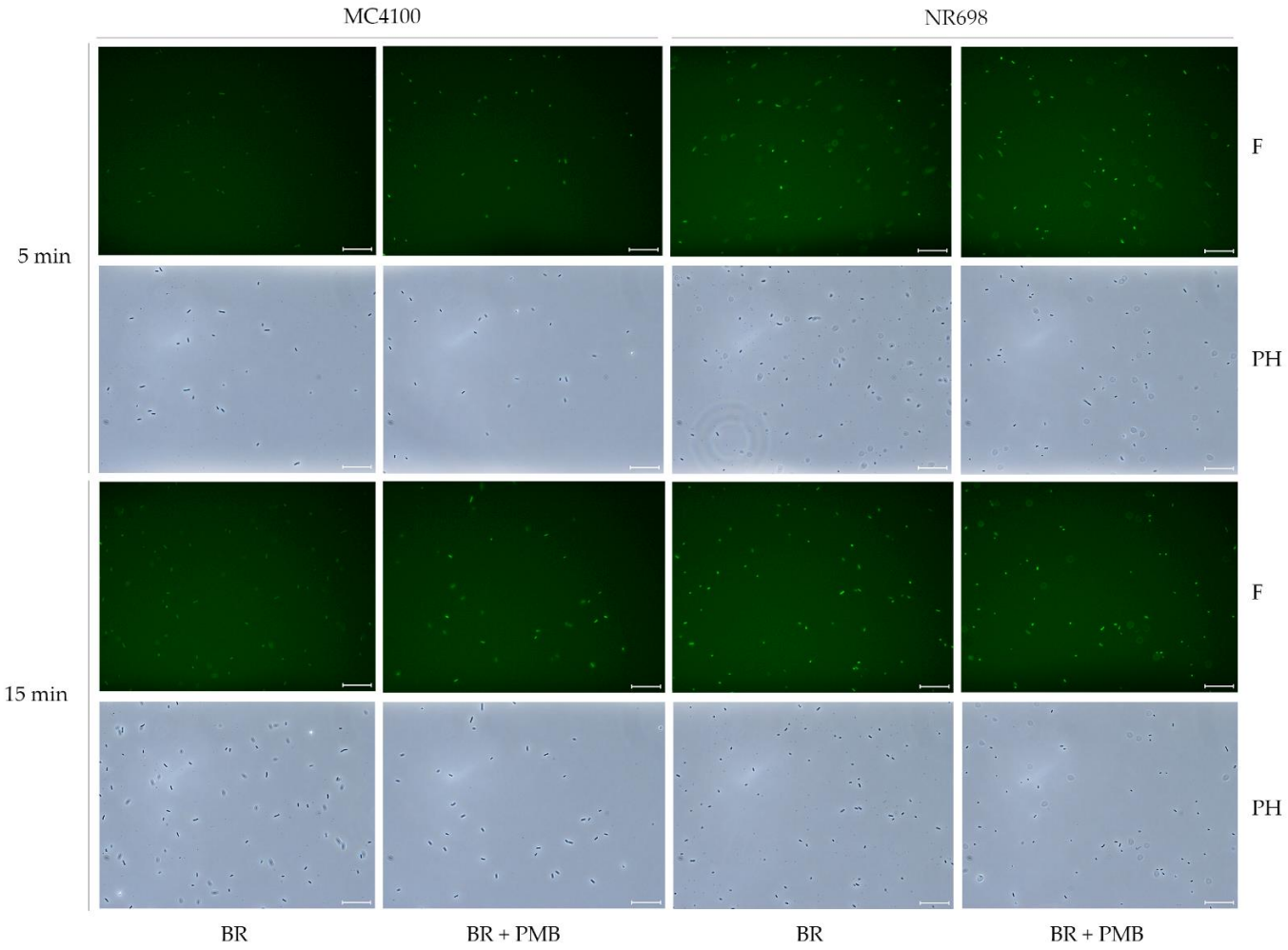

Figure 9. PMB induces population-wide fluorescence of UnaG-expressing *E. coli* cells. Fluorescence images of *E. coli* MC4100 and NR698 at time points of 5 min and 15 min after exposure to BR (5 μM) (BR) or BR and PMB (10 μg/mL) (BR + PMB) at x400 magnification. The images were taken with the phase contrast (PH) and with fluorescence (F) through the software LAS X. The scale bars represent 25 μm. For better visibility on all monitors, the brightness of the fluorescent pictures (F) was equivalently increased to 150 with Adobe Photoshop CS6 version 13.0.

4. Conclusions

UnaG fluorescence in *E. coli* is completely dependent on the external addition of its ligand BR. At concentrations of 50 μg/mL and above, the presence of BR alone ensures the sufficient diffusion of BR through the cell envelope for maximal fluorescence in live cells. At low concentrations of BR (5 μg/mL), diffusion and subsequent fluorescence is

dependent on OM disruption. Furthermore, BR does not seem to affect plasma membrane integrity or the survival of *E. coli* cells negatively. Therefore, the UnaG–BR couple might be used as a real-time reporter system in OM integrity biosensors, especially in cases where non-immediate activity and/or OM-specific activity needs to be detected over an extended period, beyond the 2 min mostly used for NPN-based assays. Due to the relatively simple setup, the system might be used as a biosensor that can distinguish OM from OM- and plasma-membrane-active compounds in high-throughput screening applications.

Supplementary Materials: The following supporting information can be downloaded at: https://www.mdpi.com/article/10.3390/bios13020232/s1, Figure S1: NPN kinetics in response to different permeabilizing analytes; Figure S2: The dose-dependent short-term effect of PMB and PMBN on UnaG fluorescence kinetics; Figure S3: Fluorescence kinetics of UnaG of *E. coli* MC4100 after exposure of different concentrations of BR; Figure S4: Luminescence kinetics of LucGR in *E. coli* NR698 after exposure of different concentrations of BR; Figure S5: Luminescence kinetics of LucGR in *E. coli* MC4100 after exposure of different concentrations of BR; Figure S6: Plasma membrane remains intact after exposure to PMBN; Figure S7: No effect of BR concentrations on short-term viability of *E. coli* MC4100; Figure S8: *E. coli* NR698 stays alive after exposure to different BR concentrations; Figure S9: Long-term fluorescence kinetics of the proposed OM biosensor to well-known model peptides; Figure S10: Long-term fluorescence kinetics of the proposed OM biosensor to novel cyclic peptide derivatives; Figure S11: Map of the plasmid pMM001 (Benchling.com; accessed on 2 December 2022); Figure S12: PMB induces population-wide fluorescence of UnaG-expressing *E. coli* cells; Figure S13: The influence of bacterial density on UnaG fluorescence; Table S1: Antimicrobial activity (MIC in μg/mL); Sequence S1: DNA sequence of the plasmid pMM001.

Author Contributions: Conceptualization, C.S.M.R., M.M. and H.-M.B.; methodology, C.S.M.R., H.D. and H.-M.B.; software and validation, C.S.M.R., H.D. and H.-M.B.; formal analysis, C.S.M.R.; investigation, C.S.M.R., H.D., M.M. and F.Ø.; resources, H.-M.B.; data curation and writing—original draft preparation, C.S.M.R. and H.-M.B.; writing—review and editing, C.S.M.R., H.D., F.Ø., M.M. and H.-M.B.; visualization, C.S.M.R.; supervision, H.-M.B.; project administration, H.-M.B.; funding acquisition, H.-M.B. All authors have read and agreed to the published version of the manuscript.

Funding: This work was supported by a grant (no. 217/6770) from UiT, the Arctic University of Norway, and a PhD fellowship also granted through the UiT. The publication charges for this article have been covered by the publication fund of UiT, the Arctic University of Norway.

Institutional Review Board Statement: Not applicable.

Informed Consent Statement: Not applicable.

Data Availability Statement: Not applicable.

Acknowledgments: We thank Chun Li for the fruitful discussions, valuable advice, and review of the manuscript. We acknowledge Danijela Simonovic and Ingrid Norberg-Schulz Hagen for synthesizing the marine antimicrobial peptide Turgencin A analogues cTurg-2 and C_{12}-cTurg-1 used in this paper.

Conflicts of Interest: The authors declare no conflict of interest.

References

1. Soboleski, M.R.; Oaks, J.; Halford, W.P. Green fluorescent protein is a quantitative reporter of gene expression in individual eukaryotic cells. *FASEB J.* **2004**, *19*, 440–442. [CrossRef]
2. Prasher, D.C. Using GFP to see the light. *Trends Genet.* **1995**, *11*, 320–323. [CrossRef]
3. Martin Chalfie. Green Fluorescent Protein. *Photochem. Photobiol.* **1995**, *62*, 651–656. [CrossRef]
4. Matz, M.; Fradkov, A.F.; Labas, Y.A.; Savitsky, A.; Zaraisky, A.G.; Markelov, M.L.; Lukyanov, S.A. Fluorescent proteins from nonbioluminescent Anthozoa species. *Nat. Biotechnol.* **1999**, *17*, 969–973. [CrossRef]
5. Schalén, M.; Anyaogu, D.C.; Hoof, J.B.; Workman, M. Effect of secretory pathway gene overexpression on secretion of a fluorescent reporter protein in Aspergillus nidulans. *Fungal Biol. Biotechnol.* **2016**, *3*, 3. [CrossRef]
6. Fradkov, A.F.; Chen, Y.; Ding, L.; Barsova, E.V.; Matz, M.V.; Lukyanov, S.A. Novel fluorescent protein from *Discosoma* coral and its mutants possesses a unique far-red fluorescence. *FEBS Lett.* **2000**, *479*, 127–130. [CrossRef]
7. Olsson, O.; Koncz, C.; Szalay, A.A. The use of the luxA gene of the bacterial luciferase operon as a reporter gene. *Mol. Genet. Genom.* **1988**, *215*, 1–9. [CrossRef]

8. Stewart, G.S.A.B.; Williams, P. lux genes and the applications of bacterial bioluminescence. *J. Gen. Microbiol.* **1992**, *138*, 1289–1300. [CrossRef]
9. Williams, T.M.; Burlein, J.E.; Ogden, S.; Kricka, L.J.; Kant, J.A. Advantages of firefly luciferase as a reporter gene: Application to the interleukin-2 gene promoter. *Anal. Biochem.* **1989**, *176*, 28–32. [CrossRef]
10. Rodriguez, E.A.; Tran, G.N.; Gross, L.A.; Crisp, J.L.; Shu, X.; Lin, J.Y.; Tsien, R.Y. A far-red fluorescent protein evolved from a cyanobacterial phycobiliprotein. *Nat. Methods* **2016**, *13*, 763–769. [CrossRef]
11. Paige, J.S.; Nguyen-Duc, T.; Song, W.; Jaffrey, S.R. Fluorescence Imaging of Cellular Metabolites with RNA. *Science* **2012**, *335*, 1194. [CrossRef]
12. Ouellet, J. RNA Fluorescence with Light-Up Aptamers. *Front. Chem.* **2016**, *4*, 29. [CrossRef]
13. Swetha, P.; Fan, Z.; Wang, F.; Jiang, J.-H. Genetically encoded light-up RNA aptamers and their applications for imaging and biosensing. *J. Mater. Chem. B* **2020**, *8*, 3382–3392. [CrossRef]
14. Kumagai, A.; Ando, R.; Miyatake, H.; Greimel, P.; Kobayashi, T.; Hirabayashi, Y.; Shimogori, T.; Miyawaki, A. A Bilirubin-Inducible Fluorescent Protein from Eel Muscle. *Cell* **2013**, *153*, 1602–1611. [CrossRef]
15. Shitashima, Y.; Shimozawa, T.; Asahi, T.; Miyawaki, A. A dual-ligand-modulable fluorescent protein based on UnaG and calmodulin. *Biochem. Biophys. Res. Commun.* **2018**, *496*, 872–879. [CrossRef]
16. To, T.-L.; Zhang, Q.; Shu, X. Structure-guided design of a reversible fluorogenic reporter of protein-protein interactions. *Protein Sci.* **2015**, *25*, 748–753. [CrossRef]
17. Kwon, J.; Park, J.S.; Kang, M.; Choi, S.; Park, J.; Kim, G.T.; Lee, C.; Cha, S.; Rhee, H.W.; Shim, S.H. Bright ligand-activable fluorescent protein for high-quality multicolor live-cell super-resolution microscopy. *Nat. Commun.* **2020**, *11*, 273.
18. Zahradník, J.; Dey, D.; Marciano, S.; Kolářová, L.; Charendoff, C.I.; Subtil, A.; Schreiber, G. A Protein-Engineered, Enhanced Yeast Display Platform for Rapid Evolution of Challenging Targets. *ACS Synth. Biol.* **2021**, *10*, 3445–3460. [CrossRef]
19. Chia, H.E.; Zuo, T.; Koropatkin, N.M.; Marsh, E.N.G.; Biteen, J.S. Imaging living obligate anaerobic bacteria with bilin-binding fluorescent proteins. *Curr. Res. Microb. Sci.* **2020**, *1*, 1–6. [CrossRef]
20. Chia, H.E.; Koebke, K.J.; Rangarajan, A.A.; Koropatkin, N.M.; Marsh, E.N.G.; Biteen, J.S. New Orange Ligand-Dependent Fluorescent Reporter for Anaerobic Imaging. *ACS Chem. Biol.* **2021**, *16*, 2109–2115. [CrossRef]
21. Decad, G.M.; Nikaiko, H. Outer Membrane of Gram-Negative Bacteria XII. Molecular-Sieving Function of Cell Wall. *J. Bacteriol.* **1976**, *128*, 325–336. [CrossRef]
22. Boulos, L.; Prévost, M.; Barbeau, B.; Coallier, J.; Desjardins, R. LIVE/DEAD BacLight: Application of a new rapid staining method for direct enumeration of viable and total bacteria in drinking water. *J. Microbiol. Methods* **1999**, *37*, 77–86. [CrossRef]
23. *LIVE/DEAD BacLight Bacterial Viability Kits Technical Sheet*; Molecular Probes: Eugene, OR, USA, 2004.
24. Virta, M.; Åkerman, K.E.O.; Saviranta, P.; Oker-Blom, C.; Karp, M. Real-time measurement of cell permeabilization with low-molecular-weight membranolytic agents. *J. Antimicrob. Chemother.* **1995**, *36*, 303–315. [CrossRef]
25. Loh, B.; Grant, C.; Hancock, R.E. Use of the fluorescent probe 1-N-phenylnaphthylamine to study the interactions of aminoglycoside antibiotics with the outer membrane of Pseudomonas aeruginosa. *Antimicrob. Agents Chemother.* **1984**, *26*, 546–551. [CrossRef]
26. Hancock, R.E.; Farmer, S.W.; Li, Z.S.; Poole, K. Interaction of aminoglycosides with the outer membranes and purified lipopolysaccharide and OmpF porin of *Escherichia coli*. *Antimicrob. Agents Chemother.* **1991**, *35*, 1309–1314. [CrossRef]
27. Domadia, P.N.; Bhunia, A.; Ramamoorthy, A.; Bhattacharjya, S. Structure, Interactions, and Antibacterial Activities of MSI-594 Derived Mutant Peptide MSI-594F5A in Lipopolysaccharide Micelles: Role of the Helical Hairpin Conformation in Outer-Membrane Permeabilization. *J. Am. Chem. Soc.* **2010**, *132*, 18417–18428. [CrossRef]
28. Briers, Y.; Walmagh, M.; Lavigne, R. Use of bacteriophage endolysin EL188 and outer membrane permeabilizers against Pseudomonas aeruginosa. *J. Appl. Microbiol.* **2011**, *110*, 778–785. [CrossRef]
29. Saravanan, R.; Mohanram, H.; Joshi, M.; Domadia, P.N.; Torres, J.; Ruedl, C.; Bhattacharjya, S. Structure, activity and interactions of the cysteine deleted analog of tachyplesin-1 with lipopolysaccharide micelle: Mechanistic insights into outer-membrane permeabilization and endotoxin neutralization. *Biochim. Biophys. Acta (BBA)-Biomembr.* **2012**, *1818*, 1613–1624. [CrossRef]
30. Lamers, R.P.; Cavallari, J.F.; Burrows, L.L. The Efflux Inhibitor Phenylalanine-Arginine Beta-Naphthylamide (PABN) Permeabilizes the Outer Membrane of Gram-Negative Bacteria. *PLoS ONE* **2013**, *8*, e60666. [CrossRef]
31. Miki, T.; Hardt, W.-D. Outer Membrane Permeabilization Is an Essential Step in the Killing of Gram-Negative Bacteria by the Lectin RegIIIB. *PLoS ONE* **2013**, *8*, e69901. [CrossRef]
32. Lehrer, R.I.; Barton, A.; Ganz, T. Concurrent assessment of inner and outer membrane permeabilization and bacteriolysis in E. coli by multiple-wavelength spectrophotometry. *J. Immunol. Methods* **1988**, *108*, 153–158. [CrossRef] [PubMed]
33. Rangarajan, N.; Bakshi, S.; Weisshaar, J.C. Localized Permeabilization of *E. coli* Membranes by Antimicrobial Peptide Cecropin A. *Biochemistry* **2013**, *52*, 6584–6594. [CrossRef] [PubMed]
34. Heesterbeek, D.A.C.; Martin, N.I.; Velthuizen, A.; Duijst, M.; Ruyken, M.; Wubbolts, R.; Rooijakkers, S.H.M.; Bardoel, B.W. Complement-dependent outer membrane perturbation sensitizes Gram-negative bacteria to Gram-positive specific antibiotics. *Sci. Rep.* **2019**, *9*, 3074. [CrossRef] [PubMed]
35. Heesterbeek, D.A.C.; Muts, R.M.; van Hensbergen, V.P.; Aulaire, P.D.S.; Wennekes, T.; Bardoel, B.W.; van Sorge, N.M.; Rooijakkers, S.H.M. Outer membrane permeabilization by the membrane attack complex sensitizes Gram-negative bacteria to antimicrobial proteins in serum and phagocytes. *PLOS Pathog.* **2021**, *17*, e1009227. [CrossRef]

36. Novo, D.; Perlmutter, N.G.; Hunt, R.H.; Shapiro, H.M. Accurate flow cytometric membrane potential measurement in bacteria using diethyloxacarbocyanine and a ratiometric technique. *Cytometry* **1999**, *35*, 55–63. [CrossRef]
37. Nobles, C.L.; Green, S.I.; Maresso, A.W. A Product of Heme Catabolism Modulates Bacterial Function and Survival. *PLOS Pathog.* **2013**, *9*, e1003507. [CrossRef]
38. Oxford Genetics. pSF-OXB15 (OG558) Strong Promoter *E. coli*. Available online: https://connex.oxgene.com/Products/Details?code=OG558 (accessed on 25 January 2016).
39. Ruiz, N.; Falcone, B.; Kahne, D.; Silhavy, T.J. Chemical Conditionality: A GeneticStrategy to Probe Organelle Assembly. *Cell* **2005**, *121*, 307–317. [CrossRef]
40. Eggert, U.S.; Ruiz, N.; Falcone, B.V.; Branstrom, A.A.; Goldman, R.C.; Silhavy, T.J.; Kahne, D. Genetic Basis for Activity Differences Between Vancomycin and Glycolipid Derivatives of Vancomycin. *Science* **2001**, *294*, 361–364. [CrossRef]
41. Chung, C.T.; Niemela, S.L.; Miller, R.H. One-step preparation of competent *Escherichia coli*: Transformation and storage of bacterial cells in the same solution. *Proc. Natl. Acad. Sci. USA* **1989**, *86*, 2172–2175. [CrossRef]
42. Helander, I.M.; Mattila-Sandholm, T. Fluorometric assessment of Gram-negative bacterial permeabilization. *J. Appl. Microbiol.* **2000**, *88*, 213–219. [CrossRef]
43. Chia, H.E.; Marsh, E.N.G.; Biteen, J.S. Extending fluorescence microscopy into anaerobic environments. *Curr. Opin. Chem. Biol.* **2019**, *51*, 98–104. [CrossRef] [PubMed]
44. Evans, M.E.; Feola, D.J.; Rapp, R.P. Polymyxin B Sulfate and Colistin: Old Antibiotics for Emerging Multiresistant Gram-Negative Bacteria. *Ann. Pharmacother.* **1999**, *33*, 960–967. [CrossRef] [PubMed]
45. Watanakunakorn, C. Mode of action and in-vitro activity of vancomycin. *J. Antimicrob. Chemother.* **1984**, *14*, 7–18. [CrossRef]
46. Dhanda, G.; Sarkar, P.; Samaddar, S.; Haldar, J. Battle against Vancomycin-Resistant Bacteria: Recent Developments in Chemical Strategies. *J. Med. Chem.* **2019**, *62*, 3184–3205. [CrossRef]
47. Delcour, A.H. Outer membrane permeability and antibiotic resistance. *Biochim. Et Biophys. Acta (BBA)-Proteins Proteom.* **2009**, *1794*, 808–816. [CrossRef] [PubMed]
48. Chollet, R.; Chevalier, J.; Bryskier, A.; Pagès, J.-M. The AcrAB-TolC Pump Is Involved in Macrolide Resistance but Not in Telithromycin Efflux in Enterobacter aerogenes and *Escherichia coli*. *Antimicrob. Agents Chemother.* **2004**, *48*, 3621–3624. [CrossRef]
49. Tsubery, H.; Ofek, I.; Cohen, S.; Fridkin, M. Structure−Function Studies of Polymyxin B Nonapeptide: Implications to Sensitization of Gram-Negative Bacteria. *J. Med. Chem.* **2000**, *43*, 3085–3092. [CrossRef] [PubMed]
50. Vázquez, J.; García-Calvo, M.; Valdivieso, F.; Mayor, F. Interaction of bilirubin with the synaptosomal plasma membrane. *J. Biol. Chem.* **1988**, *263*, 1255–1265. [CrossRef]
51. Cowger, M.L.; Mustafa, M.G. Some membrane effects of bilirubin. *Pediatr. Res.* **1971**, *5*, 419–420. [CrossRef]
52. Rodrigues, C.M.; Solá, S.; Brito, M.A.; Brites, D.; Moura, J.J. Bilirubin directly disrupts membrane lipid polarity and fluidity, protein order, and redox status in rat mitochondria. *J. Hepatol.* **2002**, *36*, 335–341. [CrossRef]
53. Terzi, H.A.; Kardes, H.; Atasoy, A.R.; Aykan, S.B.; Karakece, E.; Ustundag, G.H.; Ermis, B.; Ciftci, I.H. The antibacterial effects of bilirubin on gram-negative bacterial agents of sepsis. *Biomed. Res.* **2016**, *27*, 207–209.
54. Storm, D.R.; Rosenthal, K.S.; E Swanson, P. Polymyxin and Related Peptide Antibiotics. *Annu. Rev. Biochem.* **1977**, *46*, 723–763. [CrossRef]
55. Vaara, M. The outer membrane permeability-increasing action of linear analogues of polymyxin B nonapeptide. *Drugs Under Exp. Clin. Res.* **1991**, 17.
56. Dey, H.; Simonovic, D.; Hagen, I.N.-S.; Vasskog, T.; Fredheim, E.G.A.; Blencke, H.-M.; Anderssen, T.; Strøm, M.B.; Haug, T. Synthesis and Antimicrobial Activity of Short Analogues of the Marine Antimicrobial Peptide Turgencin A: Effects of SAR Optimizations, Cys-Cys Cyclization and Lipopeptide Modifications. *Int. J. Mol. Sci.* **2022**, *23*, 13844. [CrossRef] [PubMed]

biosensors

MDPI

Supporting Information

Outer Membrane Integrity-Dependent Fluorescence of the Japanese Eel UnaG Protein in Live *Escherichia coli* Cells

Céline S. M. Richard, Hymonti Dey, Frode Øyen, Munazza Maqsood and Hans-Matti Blencke

Methods

Minimum inhibitory concentration (MIC) assay

Stock solutions of Bilirubin and further dilutions were prepared by dissolving them in 100% DMSO. The final DMSO concentration remained 2% in all the concentration of each antibiotic, Bilirubin or DMSO alone. A modified broth microdilution susceptibility assay, based on the CLSI M07-A9 protocol, was used to determine minimal inhibitory concentrations (MIC) [1]. Briefly, overnight bacterial cultures were grown in Mueller-Hinton (MH) medium (Difco Laboratories, USA) for 2 hours at room temperature. The bacterial inoculum was diluted to 5 x 10^5 cells/mL in MH medium and added in 96-well plates (Nunc, Roskilde, Denmark) preloaded with two-fold dilution series of Bilirubin (200 to 1.6 μM) and antibiotic solutions (64 to 0.5 μg/mL) in a ratio of 1:10 giving a final well volume of 100 μL with bacterial inoculum. The microplates were incubated in an EnVision 2103 microplate reader (PerkinElmer, Llantrisant, UK) at 35 ˚C, with OD_{595} recorded every hour for 24 h. The minimal inhibitory concentration (MIC) value was defined the lowest concentration of antibiotics either in presence or absence of Bilirubin showing an optical density less than 10% of the negative (growth) control, consisting of bacteria and MQ- water.

Bacterial viability assay (luminescence based)

The *E. coli* strains MC4100 and NR698 were transformed with plasmid pCGLS-11 [2] expressing a *luxCDABE* operon from a constitutive promoter. Both strains were cultured overnight in MH broth medium supplemented with 100 and 5 μg/mL Ampicillin (Merck KGaA, Darmstad, Germany), respectively. New day cultures were made by 1% inoculation in MH broth medium and incubated at RT with aeration until the OD600 reached 0.5. This was changed from earlier use of the viability assay to adjust the cell density to the UnaG assays. To evaluate the effect of Bilirubin on bacterial viability the luminescence values were normalized to the DMSO control to account for DMSO related increase of luminescence. Data were processed with GraphPad Prism 9 software.

Figures and tables

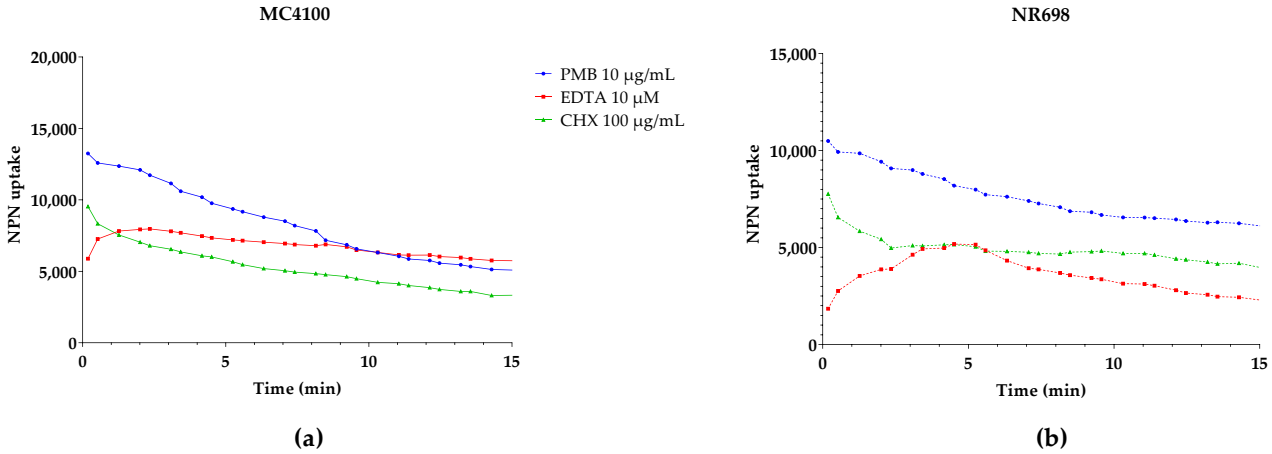

(a) (b)

Figure S1. NPN kinetics in response to different permeabilizing analytes. *E. coli* MC4100 (**a**) and NR698 (**b**) cells were used to detect fluorescence as a result of outer membrane (OM) permeabilization to the small hydrophobic molecule 1-N-phenylnapthylamine (NPN). Fluorescence emission normalized to the water treated control (bacteria in HEPES buffer) is plotted as NPN uptake over time (min).

Table S1. Antimicrobial activity (MIC in µg/mL)

	MIC (µg/mL)	
Antibiotic	**MC4100**	**NR698**
Vancomycin in 2% DMSO	64	0.25 – 0.4
Vancomycin + BR (2% DMSO)	>64	>0.4
Erythromycin 2% DMSO	16	0.25 – 0.4
Erythromycin + BR (2% DMSO)	32	>0.8

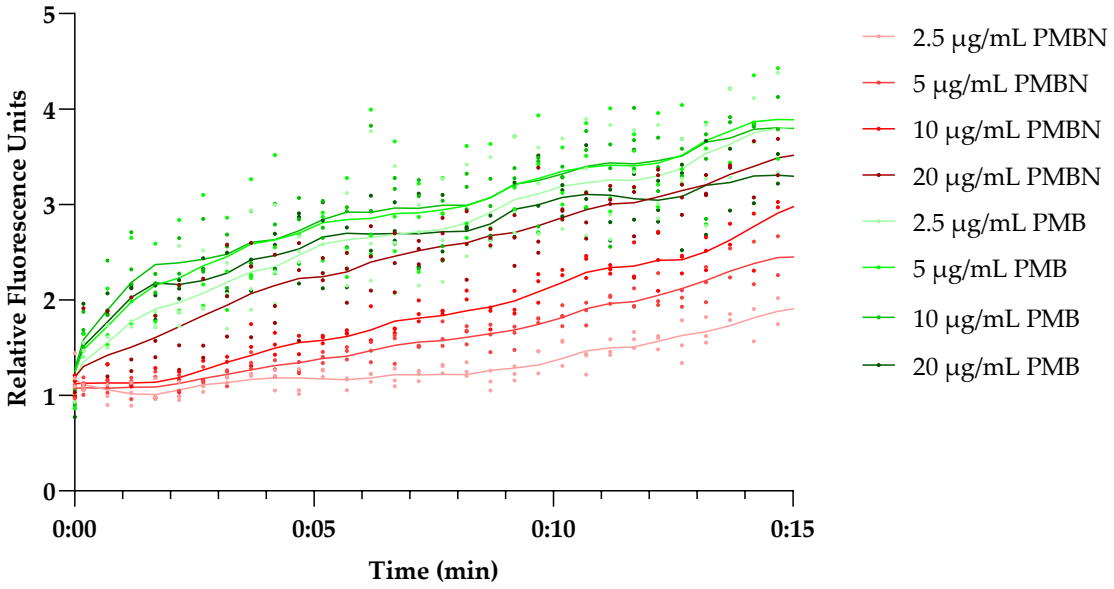

Figure S2. The dose dependent short-term effect of PMB and PMBN on UnaG fluorescence kinetics. Fluorescence kinetic of UnaG of *E. coli* MC4100 after exposure of different concentrations of polymyxin B (PMB; solid shades of green) or polymyxin B nonapeptide (PMBN; solid shades of red).

The data points represent three independent measurements normalized to the negative control in presence of BR only. The mean is represented by the solid line of the same color.

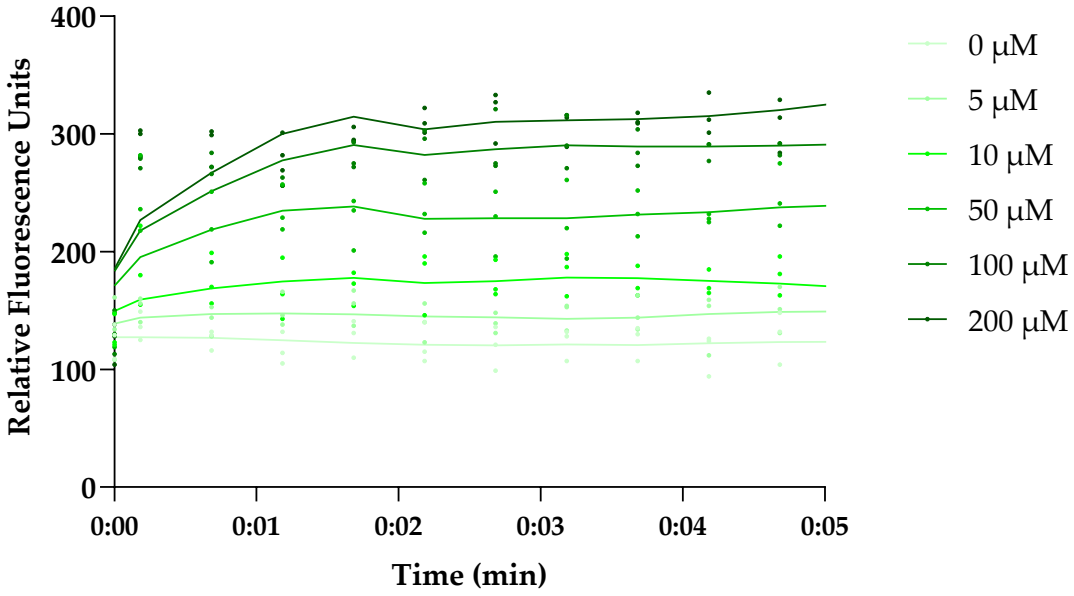

Figure S3. Fluorescence kinetic of UnaG of *E. coli* MC4100 after exposure of different concentration of BR. The data points represent three independent measurements normalized to the negative control in presence of bacteria only. The mean is represented by the solid line of the same color.

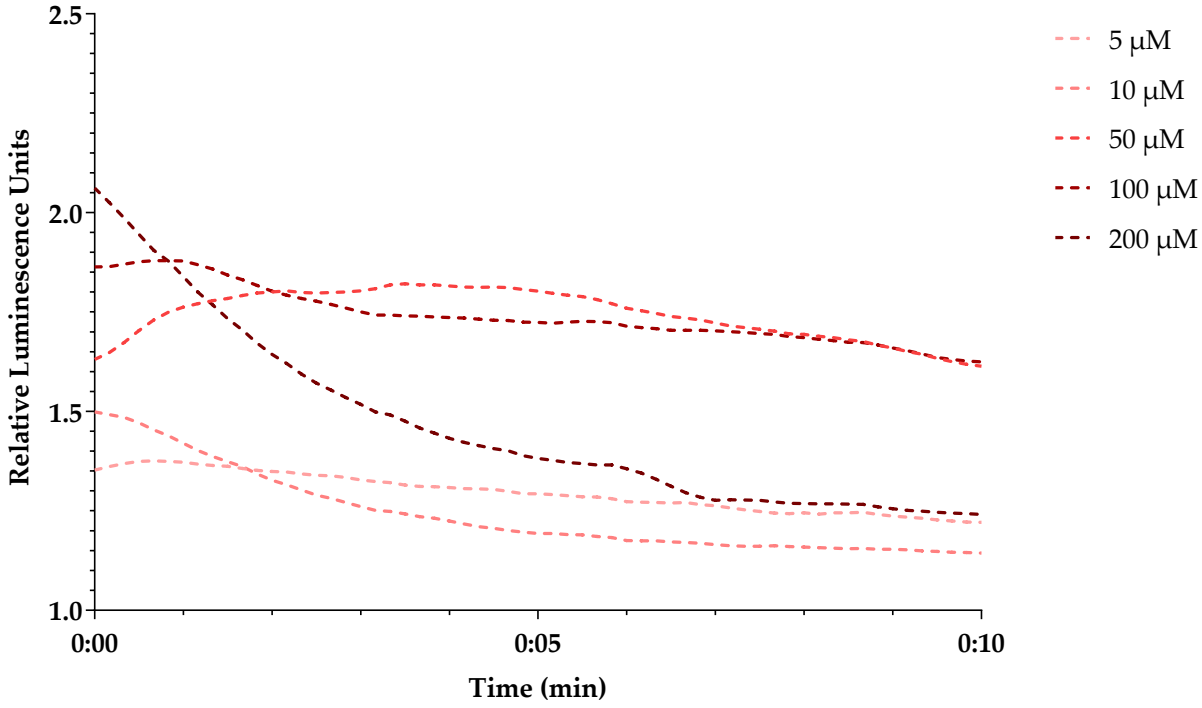

Figure S4. Luminescence kinetic of LucGR in *E. coli* NR698 after exposure of different concentration of BR. The mean of three independent measurements normalized to the negative control in presence of D-luciferin only is represented by the dashed line of the same color.

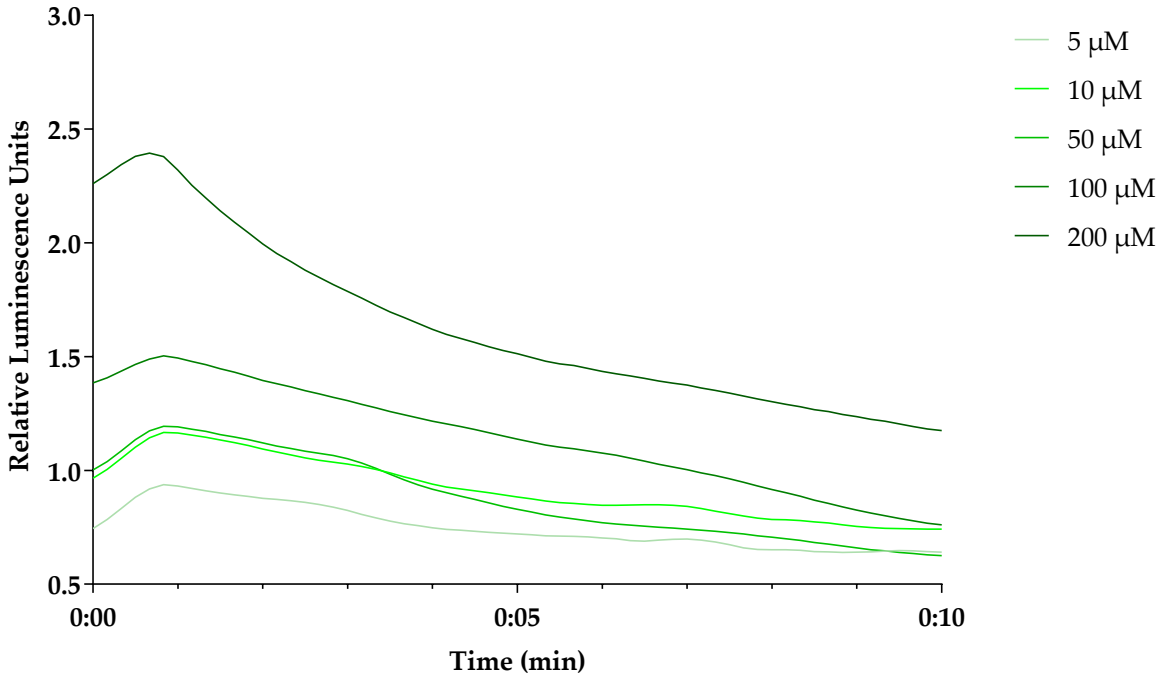

Figure S5. Luminescence kinetic of LucGR in *E. coli* MC4100 after exposure of different concentration of BR. The mean of three independent measurements normalized to the negative control in presence of D-luciferin only is represented by the solid line of the same color.

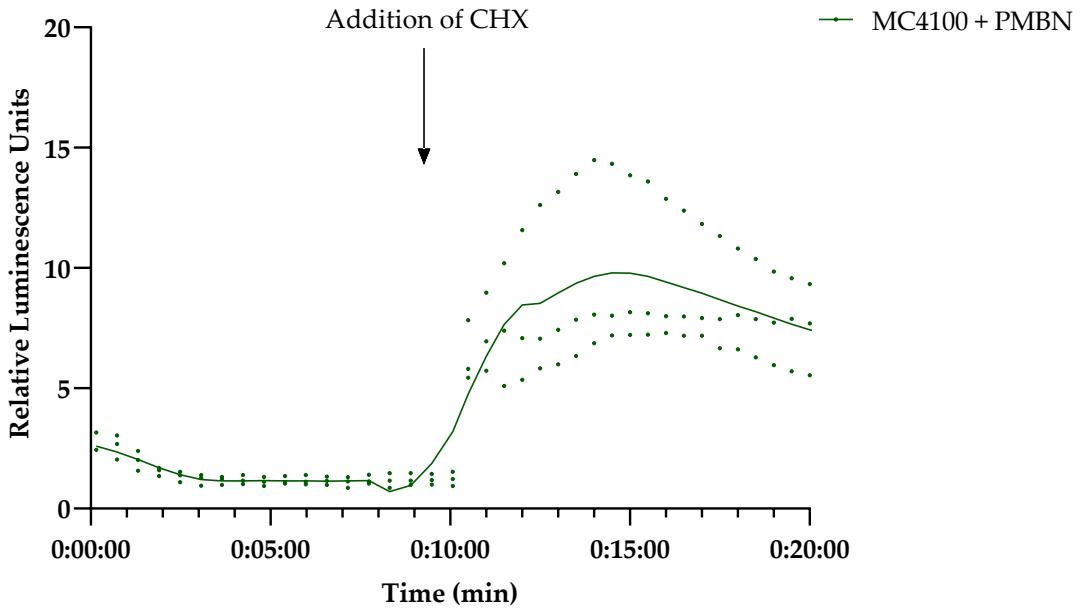

Figure S6. Plasma membrane remains intact after exposure to PMBN. Luminescence kinetic of LucGR in *E. coli* MC4100 after initial exposure to 12,5 μg/mL PMBN and 5 μM of BR and subsequent addition of 5 μg/mL chlorhexidine (CHX) at the 10 minutes mark. The data points represent three independent measurements normalized to the negative control in presence of D-luciferin only. The mean is represented by the solid line of the same color.

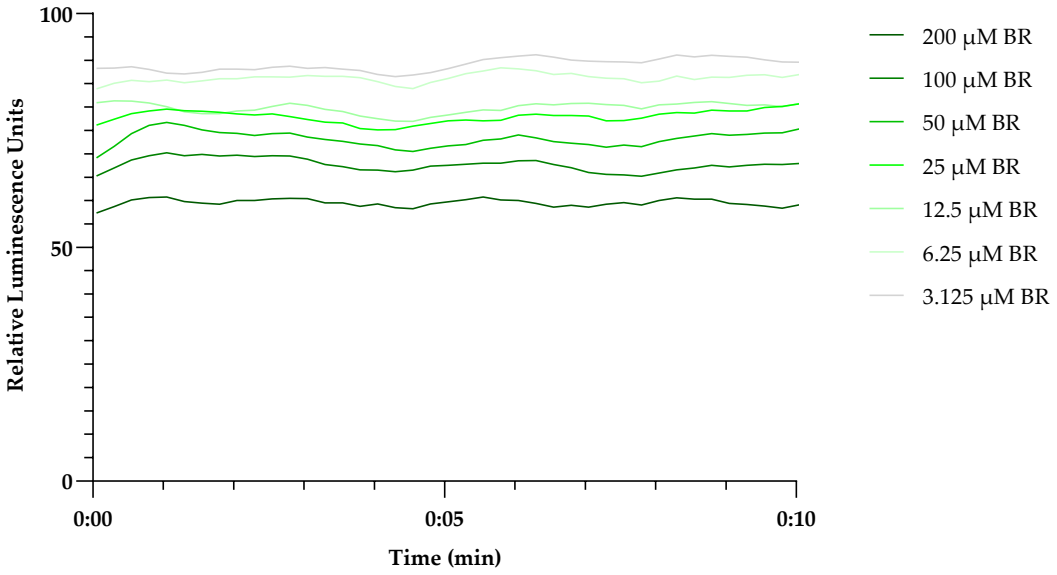

Figure S7. No effect of BR concentrations on short-term viability of *E. coli* MC4100. Luminescence kinetic of lux operon in *E. coli* MC4100 after exposure to different concentrations of BR. The mean of three independent measurements normalized to the negative control in presence of DMSO only is represented by the solid lines. Concentration dependent reduction of luminescence is likely caused by the absorbance spectrum of BR overlapping with the emission spectrum of the luciferase. A decrease in luminescence over time would indicate reduced viability.

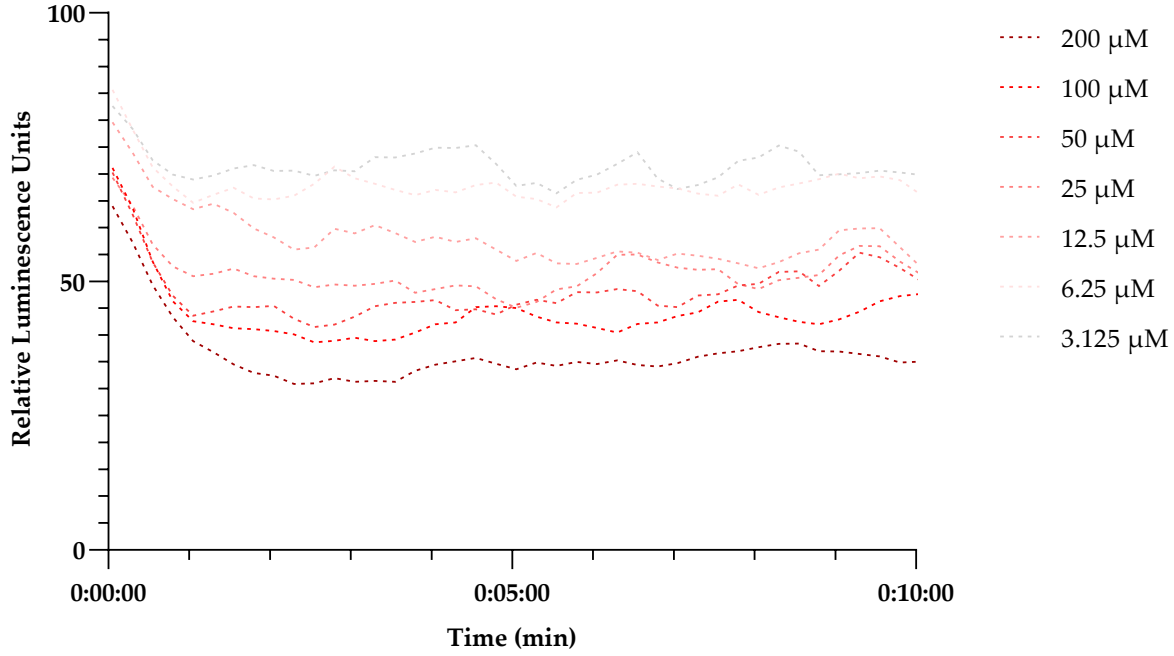

Figure S8. *E. coli* NR698 stays alive after exposure to different BR concentrations. Luminescence kinetic of the lux operon in *E. coli* NR698 after exposure of different concentration of BR. The mean of three independent measurements normalized to the negative control in presence of DMSO only is represented by the dashed line of the same color. Concentration dependent reduction of luminescence is likely caused by the absorbance spectrum of BR overlapping with the emission spectrum of the luciferase.

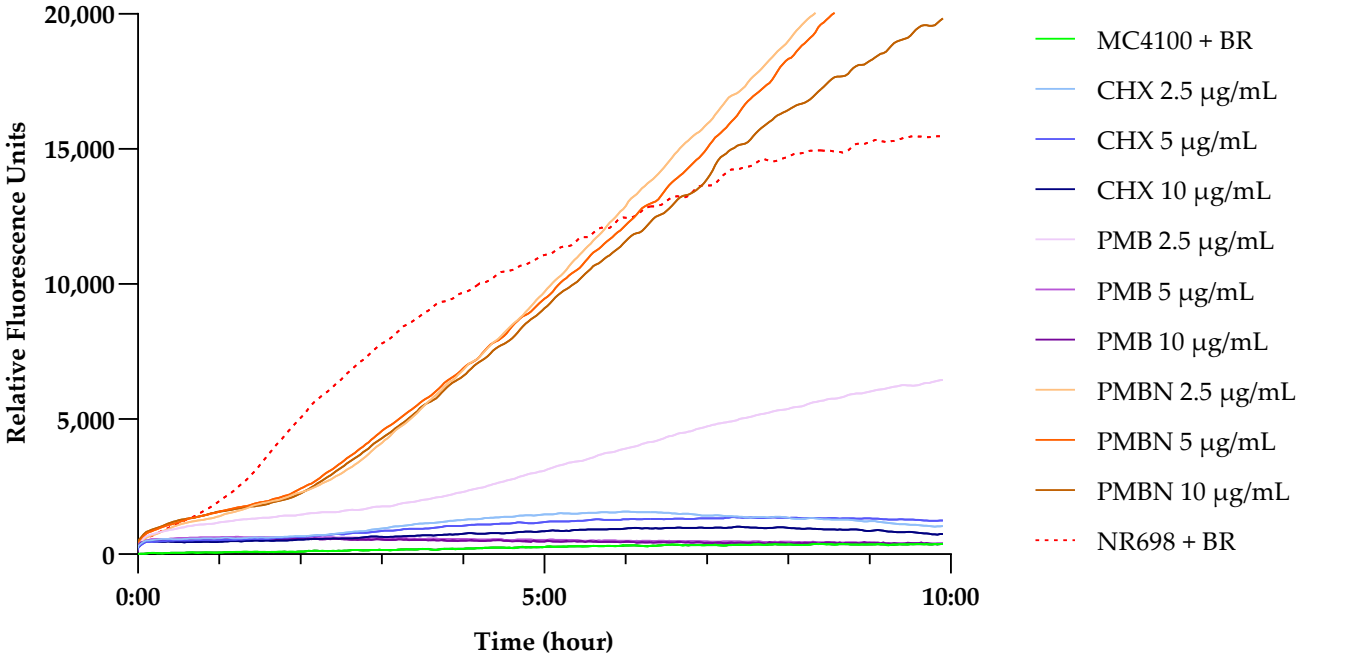

Figure S9. Long-term fluorescence kinetic of the proposed OM biosensor to well-known model peptides. Fluorescence kinetic of UnaG of *E. coli* MC4100 after exposure to different concentrations of PMB (solid shades of purple), PMBN (solid shades of orange), and CHX (solid shades of blue) for 10 hours. The *E. coli* MC4100 negative control with bilirubin only is represented by a solid green line and *E. coli* NR698 with bilirubin only by a dashed red line. All the data are normalized to bacteria with no addition of bilirubin. The mean of three independent measurements is represented by the solid line of the same color.

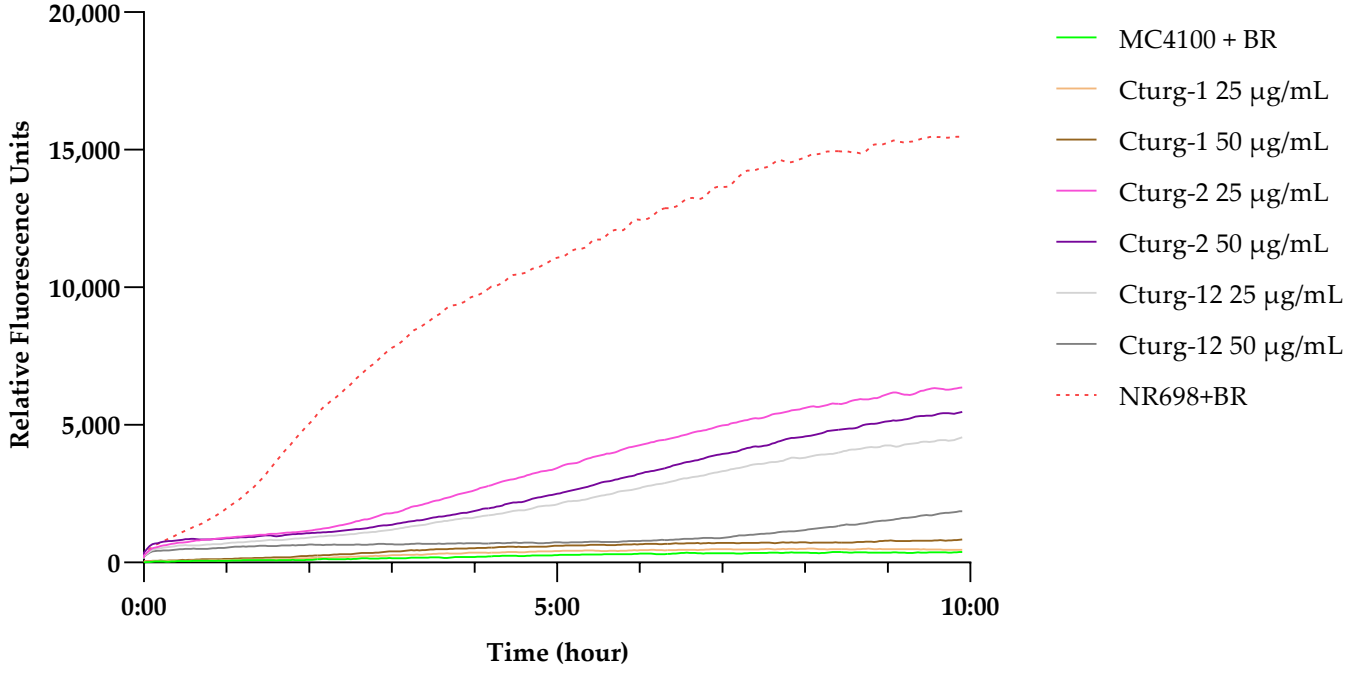

Figure S10. Long term fluorescence kinetic of the proposed OM biosensor to novel cyclic peptide derivatives. Fluorescence kinetic of UnaG in *E. coli* MC4100 after exposure to different concentrations of cyclic marine antimicrobial peptide derivatives cTurg-1 (solid shades of brown), cTurg-2

(solid shades of pink), and derivate C_{12}-Turg-1 (solid shades of blue) for 10 hours. The control of *E. coli* MC4100 with bilirubin only is represented by a solid green line and *E. coli* NR698 with bilirubin only by a dashed red line. All the data are normalized to bacteria with no addition of bilirubin. The mean of three independent measurements is represented by the solid line of the same color.

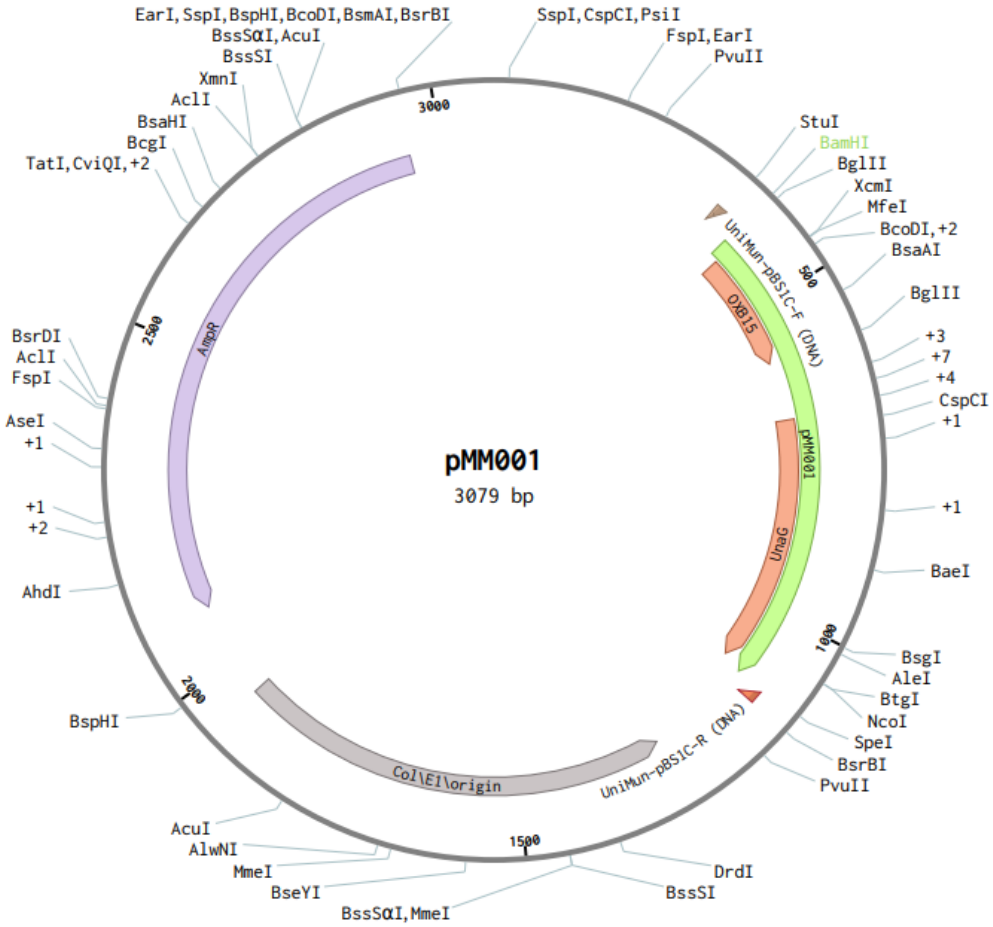

Figure S11. Map of the plasmid pMM001 (Benchling.com; accessed on 2 December 2022).

Sequence S1. DNA sequence of the plasmid pMM001.

CTAAATTGTAAGCGTTAATATTTTGTTAAAATTCGCGTTAAATTTTTGTTAAATCA
GCTCATTTTTTAACCAATAGGCCGAAATCGGCAAAATCCCTTATAAATCAAAAG
AATAGACCGAGATAGGGTTGAGTGGCCGCTACAGGGCGCTCCCATTCGCCATTC
AGGCTGCGCAACTGTTGGGAAGGGCGTTTCGGTGCGGGCCTCTTCGCTATTACGC
CAGCTGGCGAAAGGGGGATGTGCTGCAAGGCGATTAAGTTGGGTAACGCCAGG
GTTTTCCCAGTCACGACGTTGTAAAACGACGGCCAGTGAGCGCGACGTAATACG
ACTCACTATAGGGCGAAGGAAGGCCGTCAAGGCCTTGGCGGAAGGCCGTCAAG
GCCGCATGGATCCCCAGATCTAAGCTGTTGTGACCGCTTGCTCTAGCCAGCTATC
GAGTTGTGAACCGATCCATCTAGCAATTGGTCTCGATCTAGCGATAGGCTTCGAT
CTAGCTATGTAGAAACGCCGTGTGCTCGATCGCTTGATAAGGTCCACGTAGCTGC
TATAGTTGCTTCAACAGAACATATTGACTATCCGGTATTACCCGGCAGATCTTTG
TCGATCCTACCATCCACTCGACACACCCGCCAGCGGCCGCTGCCAAGCTTCCGA
GCTCTCGAATTCAAAGGAGGTACCCACCATGGTTGAAAAATTTGTTGGCACCTG
GAAAATTGCCGATAGCCATAATTTTGGCGAATACCTGAAAGCCATTGGTGCACC
GAAAGAACTGAGTGATGGTGGTGATGCAACCACACCGACACTGTATATTAGCCA
GAAAGATGGTGATAAGATGACCGTGAAAATTGAAAATGGTCCGCCTACCTTTCT
GGATACCCAGGTTAAATTCAAACTGGGCGAAGAATTTGATGAATTTCCGAGCGA
TCGTCGTAAAGGTGTTAAAAGCGTTGTTAATCTGGTGGGTGAAAAACTGGTTTAT
GTGCAGAAATGGGATGGTAAAGAAACCACCTATGTGCGCGAAATCAAAGATGG
TAAACTGGTTGTTACCCTGACCATGGGTGATGTTGTTGCAGTTCGTAGCTATCGTC
GTGCAACCGAATAAACTAGTCTGGGCCTCATGGGCCTTCCGCTCACTGCCCGCTT
TCCAGTCGGGAAACCTGTCGTGCCAGCTGCATTAACATGGTCATAGCTGTTTCCT

TGCGTATTGGGCGCTCTCCGCTTCCTCGCTCACTGACTCGCTGCGCTCGGTCGTTC
GGGTAAAGCCTGGGGTGCCTAATGAGCAAAAGGCCAGCAAAAGGCCAGGAAC
CGTAAAAAGGCCGCGTTGCTGGCGTTTTTCCATAGGCTCCGCCCCCCTGACGAGC
ATCACAAAAATCGACGCTCAAGTCAGAGGTGGCGAAACCCGACAGGACTATAA
AGATACCAGGCGTTTCCCCCTGGAAGCTCCCTCGTGCGCTCTCCTGTTCCGACCC
TGCCGCTTACCGGATACCTGTCCGCCTTTCTCCCTTCGGGAAGCGTGGCGCTTTCT
CATAGCTCACGCTGTAGGTATCTCAGTTCGGTGTAGGTCGTTCGCTCCAAGCTGG
GCTGTGTGCACGAACCCCCCGTTCAGCCCGACCGCTGCGCCTTATCCGGTAACTA
TCGTCTTGAGTCCAACCCGGTAAGACACGACTTATCGCCACTGGCAGCAGCCAC
TGGTAACAGGATTAGCAGAGCGAGGTATGTAGGCGGTGCTACAGAGTTCTTGAA
GTGGTGGCCTAACTACGGCTACACTAGAAGAACAGTATTTGGTATCTGCGCTCTG
CTGAAGCCAGTTACCTTCGGAAAAAGAGTTGGTAGCTCTTGATCCGGCAAACAA
ACCACCGCTGGTAGCGGTGGTTTTTTTGTTTGCAAGCAGCAGATTACGCGCAGAA
AAAAAGGATCTCAAGAAGATCCTTTGATCTTTTCTACGGGGTCTGACGCTCAGTG
GAACGAAAACTCACGTTAAGGGATTTTGGTCATGAGATTATCAAAAAGGATCTT
CACCTAGATCCTTTTAAATTAAAAATGAAGTTTTAAATCAATCTAAAGTATATAT
GAGTAAACTTGGTCTGACAGTTACCAATGCTTAATCAGTGAGGCACCTATCTCA
GCGATCTGTCTATTTCGTTCATCCATAGTTGCCTGACTCCCCGTCGTGTAGATAAC
TACGATACGGGAGGGCTTACCATCTGGCCCCAGTGCTGCAATGATACCGCGAGA
ACCACGCTCACCGGCTCCAGATTTATCAGCAATAAACCAGCCAGCCGGAAGGG
CCGAGCGCAGAAGTGGTCCTGCAACTTTATCCGCCTCCATCCAGTCTATTAATTG
TTGCCGGGAAGCTAGAGTAAGTAGTTCGCCAGTTAATAGTTTGCGCAACGTTGTT
GCCATTGCTACAGGCATCGTGGTGTCACGCTCGTCGTTTGGTATGGCTTCATTCA
GCTCCGGTTCCCAACGATCAAGGCGAGTTACATGATCCCCCATGTTGTGCAAAA
AAGCGGTTAGCTCCTTCGGTCCTCCGATCGTTGTCAGAAGTAAGTTGGCCGCAGT
GTTATCACTCATGGTTATGGCAGCACTGCATAATTCTCTTACTGTCATGCCATCCG
TAAGATGCTTTTCTGTGACTGGTGAGTACTCAACCAAGTCATTCTGAGAATAGTG
TATGCGGCGACCGAGTTGCTCTTGCCCGGCGTCAATACGGGATAATACCGCGCC
ACATAGCAGAACTTTAAAAGTGCTCATCATTGGAAAACGTTCTTCGGGGCGAAA
ACTCTCAAGGATCTTACCGCTGTTGAGATCCAGTTCGATGTAACCCACTCGTGCA
CCCAACTGATCTTCAGCATCTTTTACTTTCACCAGCGTTTCTGGGTGAGCAAAAA
CAGGAAGGCAAAATGCCGCAAAAAAGGGAATAAGGGCGACACGGAAATGTTG
AATACTCATACTCTTCCTTTTTCAATATTATTGAAGCATTTATCAGGGTTATTGTCT
CATGAGCGGATACATATTTGAATGTATTTAGAAAAATAAACAAATAGGGGTTCC
GCGCACATTTCCCCGAAAAGTGCCAC

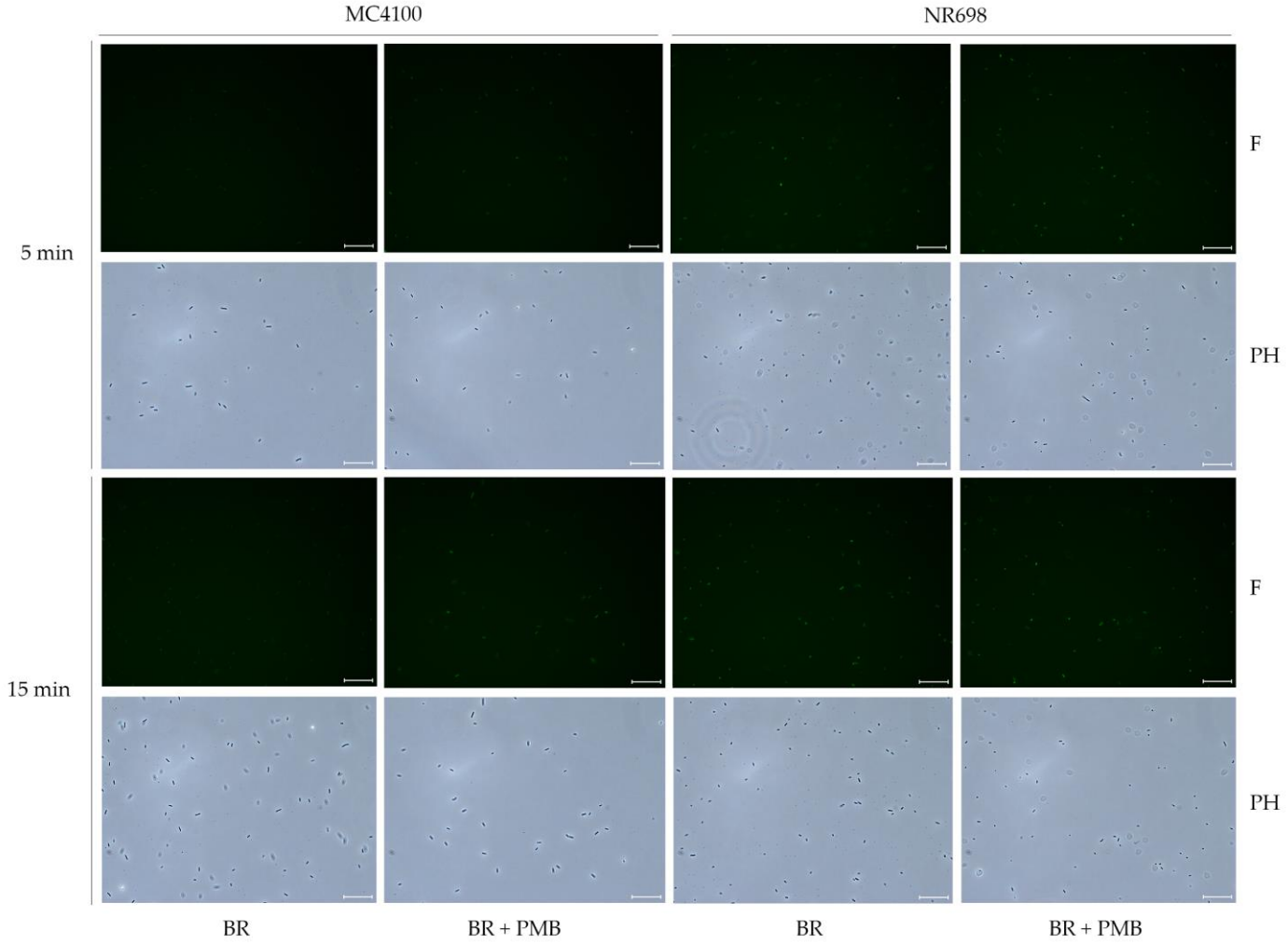

Figure S12. PMB induces population wide fluorescence of UnaG expressing *E. coli* cells. Fluorescence images of *E. coli* MC4100 and NR698 at time points of 5 minutes and 15 minutes after exposure to BR (5 μM) (BR) or BR and PMB (10 μg/mL) (BR + PMB) at x400 magnification. The images were taken with the phase contrast (PH) and with fluorescence (F) through the software LAS X. The scale bars represent 25 μm. Version without the increase of the brightness through Adobe Photoshop CS6 version 13.0.

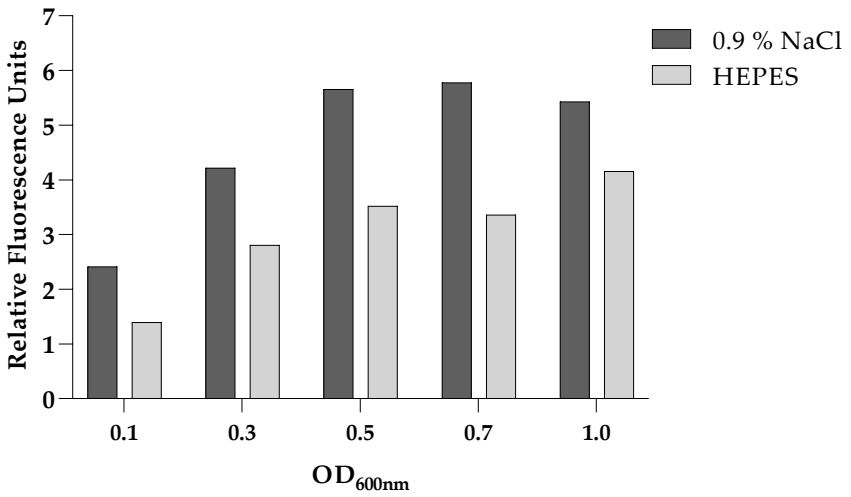

Figure S13. The influence of bacterial density on UnaG fluorescence. Relative fluorescence of UnaG in E. coli MC4100 after 15 min exposure to 10 μg/mL PMB normalised to the control in absence of PMB at different ODs in 0.9% NaCl and HEPES buffer

Paper IV

Combining outer membrane active synthetic antimicrobial peptides with vancomycin or erythromycin increases antibacterial and antibiofilm activities

Hymonti Dey[1], Danijela Simonovic[2], Céline S. M. Richard[1], Ingrid Norberg-Schulz Hagen[2], Natascha Johansen[2], Frode J. Øyen[1], Elizabeth G. Aarag Fredheim[2], Morten B. Strøm[2], Roger Simm[3], Tor Haug[1*], Hans-Matti Blencke[1*]

[1] The Norwegian College of Fishery Science, Faculty of Biosciences, Fisheries and Economics, UiT the Arctic University of Norway, NO-9037 Tromsø, NORWAY.

[2] Department of Pharmacy, Faculty of Health Sciences, UiT the Arctic University of Norway, NO-9037 Tromsø, NORWAY.

[3] Department of Biosciences, University of Oslo, NO-0371 Oslo, NORWAY

* Corresponding authors. Correspondence: tor.haug@uit.no and hans-matti.blencke@uit.no

Keywords:
Antimicrobial peptides
Turgencin
EeCentrocin
Lipopeptides
Cyclic peptides
Biofilm
Biosensor
Synergy

ABSTRACT

With the surge of antibiotic resistance and its adverse consequences, the development of new antimicrobials with new therapeutic strategies is urgently needed. Antimicrobial peptides (AMPs) have emerged as promising alternatives to conventional antibiotics due to their rapid membranolytic mode of action against microorganisms in both planktonic and biofilm lifestyles. In this study, we investigated the antimicrobial and antibiofilm activity of synthetic peptide derivatives against *Pseudomonas aeruginosa*, *Salmonella enterica serovar* Typhimurium, and *Staphylococcus epidermidis*. The peptides were also screened for synergistic activities in combination with erythromycin and vancomycin. We found that peptides with moderate-to-weak antimicrobial activity were able to inhibit biofilm formation at sub-inhibitory levels. Using an *Escherichia coli* dual biosensor strain, both plasma membrane and outer membrane disruptive effects were confirmed for selected peptides. In addition to inhibiting planktonic growth in a synergistic manner, the synthetic peptides showed more pronounced effects in inhibiting static biofilm growth when used in combination with erythromycin or vancomycin. Overall, these results suggest that the structural disruption of the outer and plasma membrane by synthetic peptide derivatives provides a basis for the development of AMPs as adjuvants to erythromycin and vancomycin to treat both planktonic and biofilm infections.

1. Introduction

Emerging microbial resistance to conventional antibiotics is a public threat (1). Bacterial infections are to an increasing extent associated with treatment failures. Particularly, biofilm related infections are difficult to treat due to the inherent increased tolerance and resistance to antimicrobials (2). The biofilm lifestyle of microbes is common in nature and frequently occurs in infections (3). Current treatment strategies for the eradication of biofilm infections commonly include high doses of antibiotics. However, antibiotic treatment has high risks of long-term damage to host microbiota and the emergence of multidrug-resistant bacteria (4). To combat the problems related to antimicrobial resistance and biofilms, alternative strategies hold a huge potential (5).

Antimicrobial peptides (AMPs) are important components of the innate immunity and host defence (6). AMPs can target a broad range of Gram-positive and Gram-negative pathogens (7, 8). In addition to their diverse functionality, effectiveness of AMPs on biofilms and non-growing microbes suggests a great advantage for developing AMPs as antibiofilm agents (9, 10). Several studies have previously demonstrated that AMPs can be modified to obtain new analogues with increased activity and proteolytic stability (5). In order to design new derivatives with stronger antibiofilm activity against *Staphylococcus aureus* and *Pseudomonas aeruginosa*, LL-37 was one of the AMPs that has been extensively studied (11). In addition to the inhibition of biofilm formation and eradication of preformed biofilm, small synthetic derivatives reduced the expression of various genes involved in the formation of *P. aeruginosa* biofilms at sub-growth inhibitory concentrations (5, 11). Combination therapies between antibiotics and AMPs are also effective against biofilms (12). The synthetic biofilm active

peptide 1018 was reported to display synergy with different classes of conventional antibiotics to inhibit and eradicate biofilms (13). Most AMPs can disrupt cell membranes, facilitating the entry of larger antibiotics as well as other AMPs with intracellular targets, which generally exceed the exclusion limit of outer membrane (OM) porins (>600 da) (9, 10). Therefore, employment of effective combinations of peptides and antibiotics is an important strategy to rescue the efficiency of preexisting drugs as well as increase their antibiofilm efficacy (13).

In this study, we investigated the activity of short synthetic analogues of two marine AMPs; Turgencin A and EeCentrocin 1, originally isolated from the colonial ascidian *Synoicum turgens* (14) and the sea urchin *Echinus esculentus* (15), respectively. The peptide analogues were screened for activity against the Gram-positive anaerobic *Clostridium difficile*, and three biofilm forming strains: *Staphylococcus epidermidis*, *P. aeruginosa* and *Salmonella enterica* serovar Typhimurium (*S.* Typhimurium). *P. aeruginosa* is frequently found in infections in patients with cystic fibrosis, while *Salmonella*, a foodborne pathogen known to cause diarrhoea, has been reported to be responsible for approximately 2.8 billion cases of infection globally every year (12, 16). The alarming aspect of these pathogens is their ability to produce biofilms on foreign body implants, medical devices, and plastic materials. The bacteria in biofilms are protected against antimicrobial attack because of their altered metabolic activity and the presence of extracellular polymeric substances (EPS). *C. difficile* on the other hand is one of the most challenging opportunistic pathogens, causing antibiotic associated diarrhea and colitis (17). *C. difficile* possesses a unique cell wall structure that distinguishes them from several other Gram-positive bacteria, possibly affecting the activity spectrum of AMPs. Additionally, their ability to form endospores allows them to survive adverse conditions.

We also investigated whether the peptide´s OM permeabilization allows larger antibiotics, such as vancomycin and erythromycin, to gain access to their target site in the periplasm and cytoplasm, respectively. Although both OM and plasma membrane (PM) integrity were evaluated in the presence of synthetic Turgencin-analogues in a previous study (18), we further investigated their membrane activity using a novel *Escherichia coli* biosensor expressing UnaG and LucGR that allow us to monitor both the OM and the PM function in single experimental settings (19). Finally, the antibiofilm activity of the peptides was analyzed alone and in synergistic manner using the crystal violet (CV) staining assay. Overall, this study provides promising results on synergy and biofilm properties by synthetic AMPs that may help develop potent antibiotic adjuvants for biofilm inhibition and mitigation of problems with antimicrobial resistance.

2. Results and Discussion

2.1 Minimum inhibitory concentrations (MICs) of cyclic and linear peptides

In this study we wanted to investigate how pathogens associated with different inherent antibiotic evasion strategies are affected by a set of novel AMP derivatives. *S. epidermidis, P. aeruginosa* and *S.* Typhimurium are common human pathogens that can cause hospital acquired infections in immunocompromised patients (20). Despite the clinical success of metronidazole and vancomycin against this pathogen, virulent *C. difficile* strains are often found to be intrinsically resistant to several antibiotics, causing recurrent infections (21). Therefore, we wanted to investigate the antimicrobial activity of some novel AMPs against *C. difficile*.

In our previous studies, a total of 38 12-amino acid synthetic peptide derivatives derived from the marine AMPs Turgencin A and EeCentrocin 1 were investigated for their antimicrobial activity and structure-activity relationship (SAR) against a panel of Gram-positive and Gram-negative bacterial reference strains (18, 22, 23). In the present study we screened a selection of these peptides against the Gram-positive obligate anaerobe *C. difficile*, and the three-biofilm forming *S. epidermidis* RP62A, *P. aeruginosa* PA01 and *S.* Typhimurium UMR1. A total of nine analogues of Turgencin A (1 linear and 8 cyclic) and seven analogues of EeCentrocin 1 (6 linear and 1 cyclic) were tested against the isolates. A broth microdilution method was used for antimicrobial activity testing, following the Clinical and Laboratory Standards Institute (CLSI) guidelines (24). The antibacterial activities determined are shown in **Table 1**.

Under standard aerobic assay conditions all tested analogues but cTurg-1 inhibited growth of at least one of the Gram-negative strains *S. epidermidis*, *P. aeruginosa or S.* Typhimurium at 16 µg/mL or below. No MIC could be determined for cTurg-1 as it remained completely inactive at all tested concentrations. The situation was different when MIC assays were performed in anaerobic condition against Gram-positive *C. difficile* and a selection of facultative and obligate anaerobic strains commonly found in the human oral cavity. Only four of the peptides (all lipopeptides), including the eight-residues peptide C_{12}-Turg-1(18-25), had MIC values ranging between 8-32 µg/mL against *C. difficile*. The two most potent Turgencin A-derived peptides, C_{12}-cTurg-1 and C_8-cTurg-2 were also the most active peptides among 25 Turgencin A analogues screened against a panel of standard Gram-positive and Gram-negative bacterial strains in aerobic conditions (18). As most of the analogues tested in the present study showed either modest or no activity against *C. difficile* and the panel of bacteria associated with the human oral cavity (**Table S4**) we did not continue with further studies using these strains.

Table 1. Antimicrobial activity of synthetic Turgencin A and EeCentrocin 1 derivatives. Peptide sequences in parentheses denote cyclic peptides. Amino acid modifications in the peptides, compared to the original AMP sequences, are shown in bold.

Peptides	Sequence	Antimicrobial activity[1] (MIC in µg/mL)			
		Gram-positive		Gram-negative	
		C. diff	*S. epi*	*P. aer*	*S.* Typh
Turgencin A derivatives					
cTurg-1	(CGKKPGGWKC)KL-NH_2	>128	>256	>256	>128
cTurg-2	(CGKK**WW**GWKC)KL-NH_2	>64	16	64	32
cTurg-3	(CGKK**W**G**W**WKC)KL-NH_2	>64	16	64	16
cTurg-4	(CGKKP**WW**WKC)KL-NH_2	>64	32	32	16
cTurg-5	(CG**RRWW**GWRC)RL-NH_2	>64	8	8	8
cTurg-6	(CG**RRW**G**W**WRC)RL-NH_2	>64	8	32	8
C_{12}-Turg-1(18-25)	**C_{12}**-GKKPGGWK-NH_2	32	16	128	64
C_{12}-cTurg-1	**C_{12}**-(CGKKPGGWKC)KL-NH_2	8	4	16	8
C_8-cTurg-2	**C_8**-(CGKK**WW**GWKC)KL-NH_2	16	4	16	8
EeCentrocin 1 derivatives					
P6	GWWRRTVAKVRK-NH_2	>128	64	32	16
P6-K8	GWWRRTV**K**KVRK-NH_2	>128	64	32	16
P6-W6K8	GWWRR**W**V**K**KVRK-NH_2	64	8	8	4
P6-W6R8	GWWRR**W**V**R**KVRK-NH_2	64	4	8	4
C_8-P6R8	**C_8**-GWWRRTV**R**KVRK-NH_2	64	4	8	8
C_{10}-P6R8	**C_{10}**-GWWRRTV**R**KVRK-NH_2	32	4	8	8
cP6-W6R8	(GWWRR**W**V**R**KVRK)	>128	64	16	8

[1] Bacterial strains; *Clostridium difficile*, *Staphylococcus epidermidis* RP62A, *Pseudomonas aeruginosa* PA01, and *Salmonella.* Typhimurium UMR1.

2.2 Synergistic activity in combination with erythromycin or vancomycin against E. coli

We have previously shown that the amphipathic (both cationic and hydrophobic) properties of the short synthetic analogues of the marine AMPs Turgencin A and EeCentrocin 1 were responsible for antimicrobial and membrane-disrupting activity (18, 23). We also established that some of these derivatives interfere with PM integrity at higher concentrations, while they retained the ability to compromise the OM at several dilution steps below the PM activity (NPN uptake data) (18, 23). We hypothesize that this activity can give synergistic effects when combined with relatively high molecular weight antibiotics such as erythromycin and vancomycin, which are mostly excluded by the OM of Gram-negative bacteria. Therefore, we used a checkerboard assay and calculated the fractional inhibitory concentration index (FICI) to investigate any synergistic effects against *Escherichia coli* for the nine Turgencin A analogues and two of the EeCentrocin 1 analogues in combination with erythromycin or vancomycin.

In our study, all peptide analogues, except for cTurg-5 and cTurg-6, demonstrated synergy (FICI ≤ 0.5) when combined with erythromycin (**Table 2**). Notably, cTurg-5 and cTurg-6 are the only arginine-modified analogues from the synthetic Turgencin A series that were tested. The absence of synergy

observed with these analogues might be attributed to their increased penetration into the membrane resulting in irreversible membrane damage and rapid cell death. Interestingly, the 8-residues linear peptide, C_{12}-Turg-1-(18-25), composed of the original Turgencin A core sequence, exhibited the strongest synergy with erythromycin. Additionally, analogues such as cTurg-1, cTurg-2, cTurg-3 and C_8-cTurg-2 showed a synergistic effect when combined with vancomycin. For the remaining analogues, additive effects ($0.5 \leq FICI \leq 1$) were observed when combined with either erythromycin or vancomycin. Moreover, several analogues, including the active lipopeptides C_{12}-cTurg-1 and C_8-cTurg-2 (at concentrations between 4-8 µg/mL), were found to reduce the MIC of the antibiotics when combined. The effective growth inhibition was achieved at 0.03x-0.008x MIC of both erythromycin and vancomycin (**Table 2**), suggesting a pronounced effect in sensitizing the bacteria to allow entry of both antibiotics.

Table 2. Antibacterial activities (MIC in µg/mL) and synergy calculations (FICI) of selected Turgencin A and EeCentrocin analogues against *E. coli* (ATCC 25922) in combination with either erythromycin or vancomycin. $FICI \leq 0.5$ is interpreted as synergy, whereas $0.5 < FICI \leq 1.0$ is interpreted as additive effects.

Peptides/antibiotics	MIC (µg/mL) alone	MIC (µg/mL) in combination		FICI	MIC (µg/mL) in combination		FICI
		Peptide	Erythromycin		Peptide	Vancomycin	
Turgencin A derivatives							
cTurg-1	>256	32	8	0.25	8	64	0.50
cTurg-2	64	4	1	0.09	16	16	0.38
cTurg-3	32	4	1	0.16	8	16	0.38
cTurg-4	64	8	1	0.16	32	32	0.75
cTurg-5	8	4	0.5	0.52	4	32	0.75
cTurg-6	8	4	2	0.56	4	8	0.56
C_{12}-Turg-1-(18-25)	128	4	1	0.06	8	64	0.56
C_{12}-cTurg-1	8	2	8	0.50	4	4	0.53
C_8-cTurg-2	8	4	0.25	0.50	4	1	0.50
EeCentrocin 1 derivatives							
P6-W6R8	8	2	4	0.37	4	8	0.56
cP6-W6R8	8	2	8	0.50	4	64	1.00
Antibiotics							
Erythromycin	32						
Vancomycin	128						

2.3 Do different membrane compositions influence the synergistic action?

Clinically relevant Gram-negative bacteria represent a plethora of different membrane structures as well as LPS compositions. To investigate whether the synergistic potential of cTurg-2 found in *E. coli* is influenced by different properties of the OM in Gram-negative species, we determined the MIC of cTurg-2 alone and in combination with erythromycin and/or vancomycin against *E. coli* BL-21, *S.* Typhimurium UMR1, *P. aeruginosa* (ATCC 27853), *Klebsiella aerogenes* (ATCC 51697) and *Acinetobacter baylyi* (DSM 24193). Based on the MIC-values obtained, the FICI was calculated.

The results show that in all the Gram-negative bacterial strains tested, the MIC of cTurg-2, erythromycin and vancomycin alone was in the range of 16 to >64 µg/mL, except for erythromycin which showed a MIC of 2 µg/mL against *A. baylyi* (**Table 3**). The combination of cTurg-2 with erythromycin showed synergy against all strains tested. The strongest synergy was observed against *E. coli* BL21, *K. aerogenes*, and *A. baylyi* ($FICI < 0.2$). However, in combination with vancomycin, higher concentrations of both compounds were needed to observe growth inhibitory and synergistic effects. Although the interaction was mostly additive, cTurg-2 was able to display synergy with vancomycin against *S.* Typhimurium UMR1 and A. *baylyi* (**Table 3**). Additionally, the linear P6-W6R8 and cyclic cP6W6R8 were tested for synergy in combination with vancomycin and erythromycin against several

different *E. coli* strains (**Table S1-S3)**. We also evaluated the OM deficient *E. coli* NR698 which is hypersensitive to vancomycin and erythromycin. No synergy was observed against *E. coli* NR698, indicating that OM active analogues cannot further sensitize the strain to improve the effectiveness of vancomycin and erythromycin when the OM is already disrupted or hyper porous. In addition, several peptide and antibiotic combinations were analysed for synergy against *E. coli* BL-21. In accordance with our previous studies, polymyxin B (PMB) and erythromycin combination showed strong synergy (**Table S1**), however, PMB it did not show synergy in combination with vancomycin (**Table S1**).

To evaluate the hypothesis that OM permeabilization was responsible for the synergistic function, we tested the antimicrobial activity of cTurg-2 in combination with erythromycin or vancomycin against the Gram-positive bacteria *Staphylococcus aureus* (ATCC 9144) and *S. epidermidis* RP62A, which do not contain an OM. Consistent with the OM activities previously shown for of cTurg-2 (19), neither erythromycin nor vancomycin (in combination with cTurg-2) showed synergy against the Gram-positive strains (**Table 3**).

Table 3. Antibacterial (MIC in μg/mL) and synergistic activities of cTurg-2 in combination with erythromycin or vancomycin against different Gram-negative and Gram-positive bacteria.

Bacterial strains	MIC (μg/mL) of peptides/antibiotics alone or in combination				FICI
	Alone		In combination		
	cTurg-2	Erythromycin	cTurg-2	Erythromycin	
E. coli BL-21	64	64	8	2	0.16
S. Typhimurium UMR1	32	32	8	8	0.5
P. aeruginosa (ATCC 27853)	32	64	8	16	0.5
K. aerogenes (ATCC 51697)	>64	128	4	4	<0.09
A. baylyi (DSM 24193)	16	2	1	0.25	0.19
S. aureus (ATCC 9144)	32	0.5	>32	0.5	>2
S. epidermidis RP62A (ATCC 35984)	16	>64	16	64	>1
	cTurg-2	**Vancomycin**	**cTurg-2**	**Vancomycin**	**FICI**
E. coli BL-21	64	32	32	4	0.63
S. Typhimurium UMR1	32	64	8	16	0.5
P. aeruginosa (ATCC 27853)	64	>64	>32	>64	-
K. aerogenes (ATCC 51697)	>64	256	32	128	>0.75
A. baylyi (DSM 24193)	16	64	4	16	0.5
S. aureus (ATCC 9144)	32	1	32	1	2
S. epidermidis RP62A (ATCC 35984)	16	1	16	1	2

2.4. Outer and plasma membrane activity in a dual biosensor E. coli strain

Nine derivatives of Turgencin A and six derivatives of EeCentrocin 1 were tested for both OM and PM activity using a dual function *E. coli* biosensor. The Turgencin A analogues, cTurg-2, C_{12}-Turg-1-(18-25), C_{12}-cTurg-1 and C_8-cTurg-2 showed the strongest UnaG dependent fluorescence response, indicating OM activity (**Figure 1A**). In addition, C_{12}-Turg-1-(18-25) and C_{12}-cTurg-1 showed relatively strong peaks of light emission indicating membrane activity at both 12.5 μg/mL and 6.3 μg/mL, while cTurg-2 and C_8-cTurg-2 with modest antimicrobial activity did not seem to affect the PM at the tested concentrations. However, in the presence of cTurg-2, only a two-fold fluorescence increase was detected at 6.3 μg/mL. For cTurg-2 and C8-Turg-2 OM disruption seems to happen at concentrations with little or no effect on PM integrity, possibly indicating more specific binding to the OM. Interestingly, C_{12}-cTurg-1 and C_{12}-cTurg-1(18-25) affect both membranes, although the effect on the PM does not seem

to kill the whole population as indicated by the relatively strong fluorescence increase up to 12.5 µg/mL and remaining light emission throughout the measurement at concentrations at 6.3 µg/mL.

On the other hand, the EeCentrocin 1 analogues, the linear P6-W6R8 and the cyclic cP6-W6R8 were found to affect the integrity of both the OM and PM. Due to the rapid effect on cell viability at concentrations above 6.3 µg/mL, light emission dropped before we could detect luminescence peaks. As UnaG stability in its apo-protein form is limited, no fluorescence was detected at these bactericidal concentrations (**Figure 1B**). At lower concentrations, however, addition of the sensor bacteria to P6-W6R8 and cP6-W6R8 consistently increased fluorescence, indicating interference with OM integrity. For both these peptides OM and PM integrity interference seems to coincide (**Figure 1B**). These results suggest that not all peptides with OM permeabilizing ability at sub-MIC concentrations will interfere with PM integrity, some peptides seem to be more specific for the OM while other peptides will disrupt both membranes simultaneously. When the dual biosensor is used with AMPs affecting both PM and OM the response pattern is likely to reflect seemingly OM specific activity at lower concentrations as loss of PM integrity is lethal and thus inhibiting expression of UnaG and the much slower response of the OM sensing construct. The data showing the OM and PM activity for the rest of the analogues can be found in the supporting information, **Figure S1**.

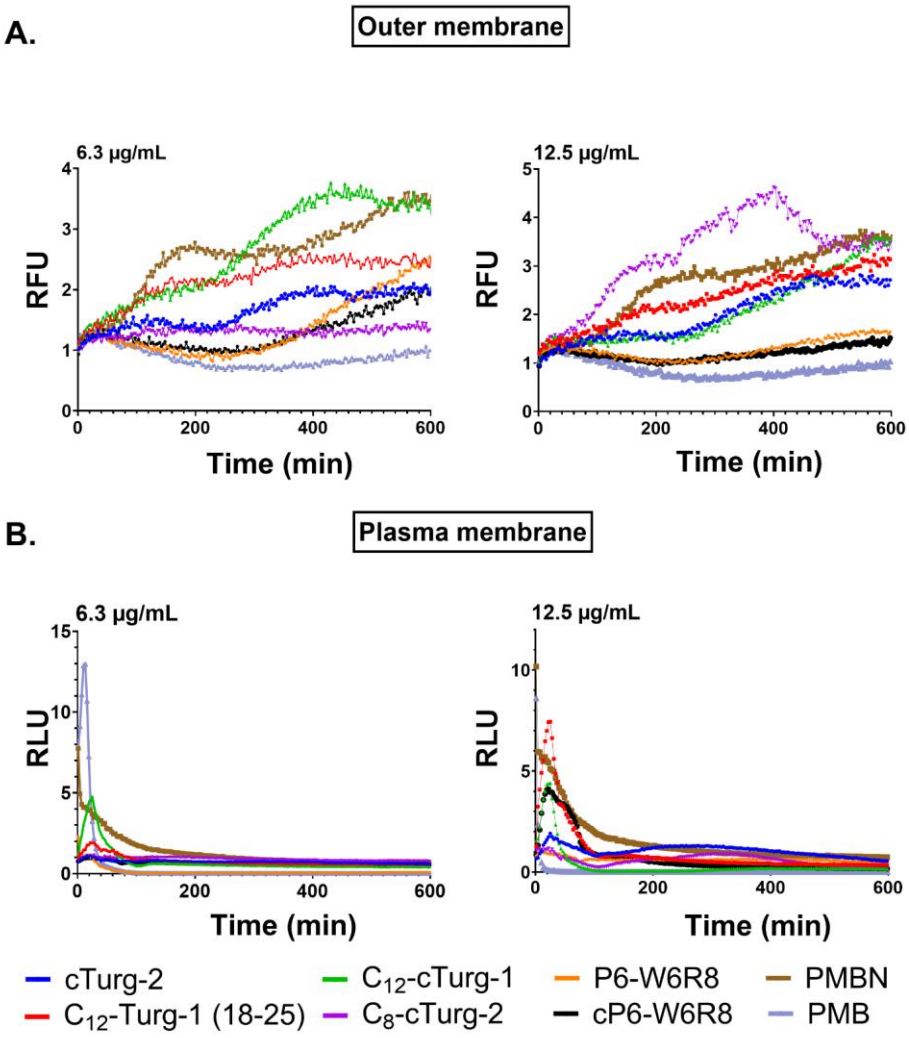

Figure 1. A. Outer membrane and B. plasma membrane activity at concentrations of 6.3 and 12.5 µg/mL of selected Turgencin A analogues and EeCentrocin 1 analogues, determined using an *E. coli* dual biosensor strain. The figure depicts fluorescence and luminescence normalized to the untreated control. PMB and PMBN were used as controls.

2.5. Antibiofilm effects of synthetic cyclic and linear analogues of Turgencin A and EeCentrocin 1

The OM in Gram-negative bacteria functions as a protective barrier. The biofilm matrix is known to comprise various components, including proteins adhered to the bacterial membrane. Since the OM forms the direct interface to the bacterial environment and as such is the structure directly in contact with biofilm matrix, we hypothesized that interfering with OM integrity might also affect the bacteria's ability to form biofilms. Hence, we investigated if these peptide derivatives inhibited biofilm formation and removed preformed biofilms.

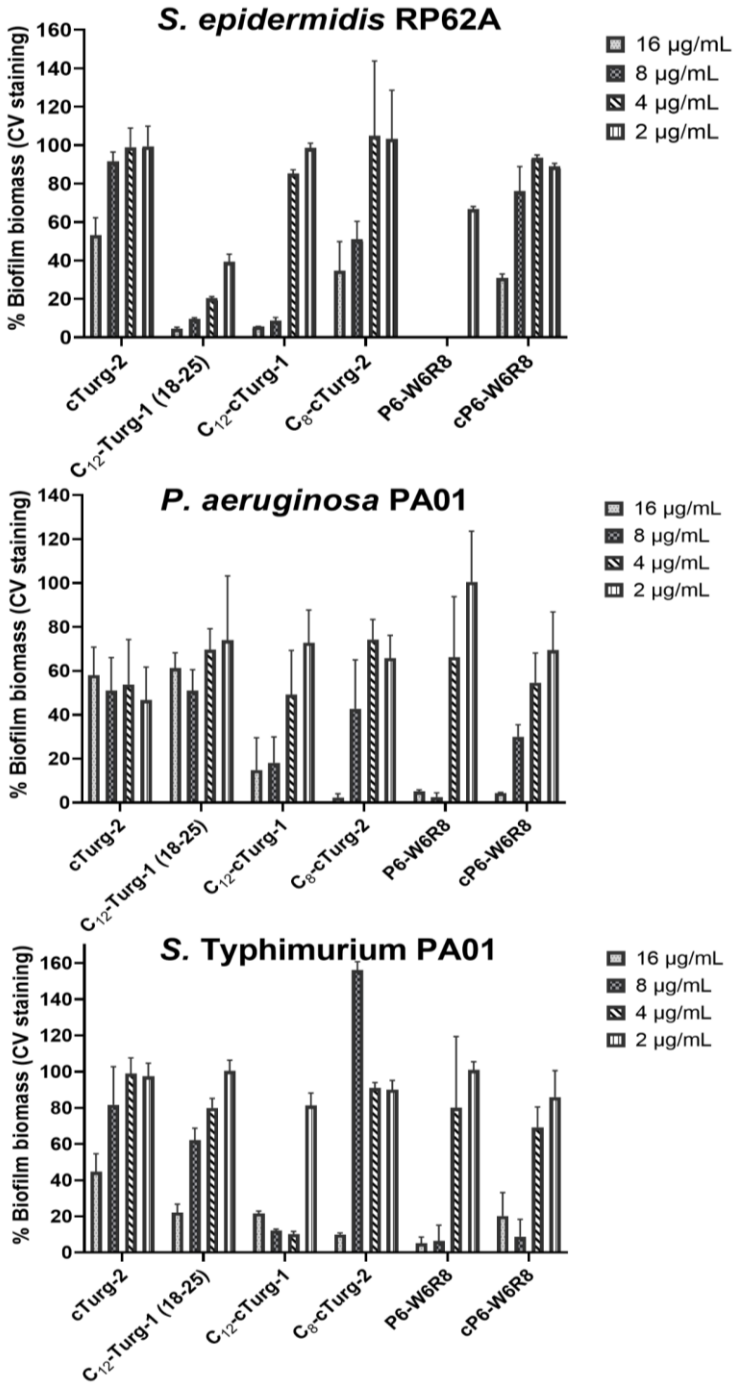

Figure 2. The effects of selected Turgencin A and EeCentrocin analogues at different concentration on biofilm formation by *S. epidermidis* RP62A, *P. aeruginosa* PA01 and *S.* Typhimurium UMR1. The data represent relative remaining biomass compared to the untreated control (100% biofilms).

Hence, we investigated if these peptide derivatives inhibited biofilm formation and removed preformed biofilms. We also compared the antibiofilm effect of the OM active peptides to the antibiofilm effect of the PM active counterparts and compared their minimal biofilm inhibitory concentrations (MBIC) to the MIC observed in liquid planktonic cultures. Biofilms of *S. epidermidis*, *P. aeruginosa*, and *S.* Typhimurium are known to form a very sticky EPS matrix on plastic surfaces consisting of polysaccharide, lipid, DNA, and various ions (25-27). It was previously reported that the EPS of *S.* Typhimurium contains cellulose and thin aggregative fimbriae (28).

To analyse the effects of the synthetic analogues of Turgencin A and EeCentrocin 1 on biofilm formation, a crystal violet (CV) biomass staining assay was used to screen a total of 18 synthetic analogues. As shown in the **Figure 2**, all the Turgencin A and the EeCentrocin 1 analogues effectively inhibited biofilm formation in all three strains with a 40-100% inhibition at 16 µg/mL. The linear analogues C_{12}-Turg-1 (18-25) exhibited a concentration-dependent inhibition of biofilm formation against *S. epidermidis* RP62A, with a strong inhibition observed at concentrations ranging from 16-4 µg/mL. Interestingly, both cTurg-2 and C_{12}-Turg-1 (18-25) demonstrated a reduced biomass formation in *S.* Typhimurium UMR1 and *P. aeruginosa* PA01 without a substantial effect on the viability or turbidity of the planktonic growth. In contrast, Turgencin A analogues C_{12}-cTurg-1 and C_8-cTurg-2 as well as EeCentrocin 1 analogues P6-W6R8 and cP6-W6R8 with high antimicrobial activity (i.e. low MIC) in Gram-negative strains (**Table 1**), did not show significant antibiofilm effects below 0.5x-MIC (conc 2-4 µg/mL). However, the biofilm reproducibility in *P. aeruginosa* turned out to be rather difficult. This suggests a membranolytic function that inhibits growth, resulting in reduced overall biomass formation in the presence of high concentration of these analogues. The EeCentrocin cyclic analogue cP6-W6R8 showed less biofilm inhibitory activity against *S. epidermidis* RP62A.

Some active analogues showed a tendency for higher CV-staining or induced biomass formation, indicating a potential stress response or the release of cellular components or charged molecules from dead bacteria. While most analogues may prevent or interrupt the initial attachment of biofilm forming cells, moderately active analogues cTurg-2 and C_{12}-Turg-1 (18-25) likely employ targeted action against biofilm formation. The tendency of biofilm inhibition on Congo red agar has also been observed (**Figure S3** and **Assay S1**). Additional biofilm inhibitory data for the remaining analogues against all three biofilm forming strains are available in the supplementary material (**Table S5-S7**).

2.6. Effects of synthetic analogues against preformed biofilms

A selection of the synthetic peptide analogues was tested for their ability to eradicate 22 h preformed biofilms of the three biofilm-producing strains: *S. epidermidis* RP62A, *P. aeruginosa* PA01 and *S.* Typhimurium UMR1. The biofilm eradicating capability of four Turgencin A analogues were tested only against the *S.* Typhimurium UMR1 strain. After washing the unattached cells, peptide concentrations of 8-128 µg/mL were added, which was followed by an additional 22 h incubation in the presence of AMPs. It is possible that during this 22 h incubation period, viable bacteria in the biofilm might grow and produce thicker biofilm. Since we have used 2- to 16-fold higher concentrations than MIC for some peptides, we expected that the peptides may have to kill the bacteria within the biofilms as well as disrupt the matrix to show eradicating effects. However, the effect may also be prevention of further biofilm formation if fast membrane permeabilization can affect the viability of the biofilm-embedded cells. Several synthetic analogues were able to remove 60-99% of the preformed biofilms of *S.* Typhimurium UMR1 (**Figure 3**) and the EeCentrocin analogues were also able to remove >90% biofilms formed by *P. aeruginosa* PA01 (**Table 4**). No significant reduction in biomass was observed for *S. epidermidis* RP62A at the highest peptide concentrations tested (**Table 4**). Eradication data for the rest of the EeCentrocin analogues can be found in supporting info (**Table S8**). In addition, the effective concentration needed to eradicate *S.* Typhimurium pre-formed biofilm was surprisingly lower (0.5-2 xMIC) than what was needed to eradicate *P. aeruginosa* and *S. epidermidis* biofilms. However, it is quite common that the concentration needed to eradicate biofilms is several times higher than the concentration needed for bactericidal or bacteriostatic effects, observed for planktonic growth.

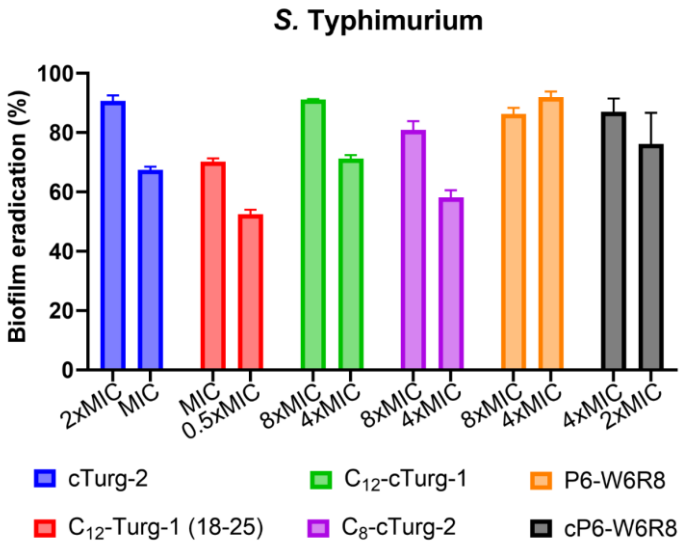

Figure 3: Removal of 22h preformed biofilms in the presence of Turgencin A and EeCentrocin 1 analogues. The data are represented as % of eradication/removal at the concentration of 64 and 32 µg/mL after 22h treatments compared to the untreated control.

Table 4. Antimicrobial activity (MIC, µg/ml) and antibiofilm eradication activity of C_{12}-cTurg-1, C_8-cTurg-2, P6-W6R8 and cP6-W6R8 after 24h treatment at 64 µg/mL against 22h preformed biofilms of *P. aeruginosa* PA01 and *S. epidermidis* RP62A.

Peptide	*P. aeruginosa* PA01			*S. epidermidis* RP62A		
	MIC (µg/mL)	Eradication		MIC (µg/mL)	Eradication	
		%	x MIC		%	x MIC
C_{12}-cTurg-1	16	50	4	4	50	16
C_8-cTurg-2	16	50	4	4	50	16
P6-W6R8	8	90	8	4	60	16
cP6-W6R8	16	90	4	64	50	2

2.7. Is the peptide effect limited to initial adherence?

The previous experiments showed that all peptides tested were able to inhibit biofilm formation at 0.5xMIC, while most peptides were not able to completely remove mature biofilms at MIC. We wanted to know whether the activity of the peptides was limited to the initial adherence of the bacteria or if the activity extended to biofilm proliferation and maturation. To resolve a possible limitation to adhesion, requiring presence of the peptide from the start, the experiment was conducted by adding 25 µg/mL of the peptides at either 0h, 2h, 4h or 6h after the assay start for both *S.* Typhimurium UMR1 and *P. aeruginosa* PA01, followed by 22h of incubation. In *P. aeruginosa*, C_{12}-cTurg-1 and P6-W6R8 displayed significant inhibition of biofilm formation, with a stronger inhibition observed at the earlier timepoints that also affected planktonic growth. While C_8-cTurg-2, cTurg-2 and C_{12}-Turg-1 (18-25) did not show any growth inhibition at all tested timepoints, however, 30-50% biofilm inhibitory effects were still observed. cP6-W6R8 exhibited a strong growth inhibition at 0-2h exposure, correlating with the biofilm inhibition, while both the planktonic biomass and biofilm formation remained unaffected at later timepoints (**Figure 4** and **Figure S2**). In *S.* Typhimurium, both cTurg-2 and C_{12}-Turg-1 (18-25) inhibited biofilm formation, with maximal inhibition of approximately 55% observed at 0-2h timepoints. Similarly, C_{12}-cTurg-1 and C_8-cTurg-2 affected the planktonic growth of *S.* Typhimurium at the initial timepoints after addition of each peptide, whereas the viability of the cells was not affected at the later stages of exposure (**Figure S2**). Both peptides exhibited stronger inhibition at timepoints 0-4h, with around 75% inhibition, and at 6h, with 40% in *S.* Typhimurium (**Figure 4**). Although the linear EeCentrocin 1 analogue P6-W6R8 affected the growth of *S.* Typhimurium by 75-90% at 0-2h exposure, it showed stronger effects on biofilm inhibition at 4-6h with an average inhibition of 80% (**Figure 4**).

Overall, our results suggest that if biofilms are allowed to grow for a longer time before adding peptide samples, the growth and biofilm inhibition are significantly reduced for the active analogues at 25 µg/mL while moderately active peptides are still able to show a consistent effect on 22-28h biofilm formation and 2-6 h preformed biofilms. Since both cTurg-2 and C_{12}-Turg-1 (18-25) showed >50% biofilm inhibition at sub-inhibitory concentrations against S. Typhimurium UMR1 strain, we wanted to investigate the effects of these analogues on red, dry and rough (*rdar*) morphotype typically formed by S. Typhimurium. Interestingly, in the presence of cTurg-2 or C_{12}-Turg-1 (18-25), *S.* Typhimurium UMR1 loss *rdar* morphotype as the macrocolony on the Congo-red agar appears to be whitish for cTurg-2, while for C_{12}-Turg-1 (18-25), the colonies looked smooth and less wrinkly (**Assay S1, Figure S3**).

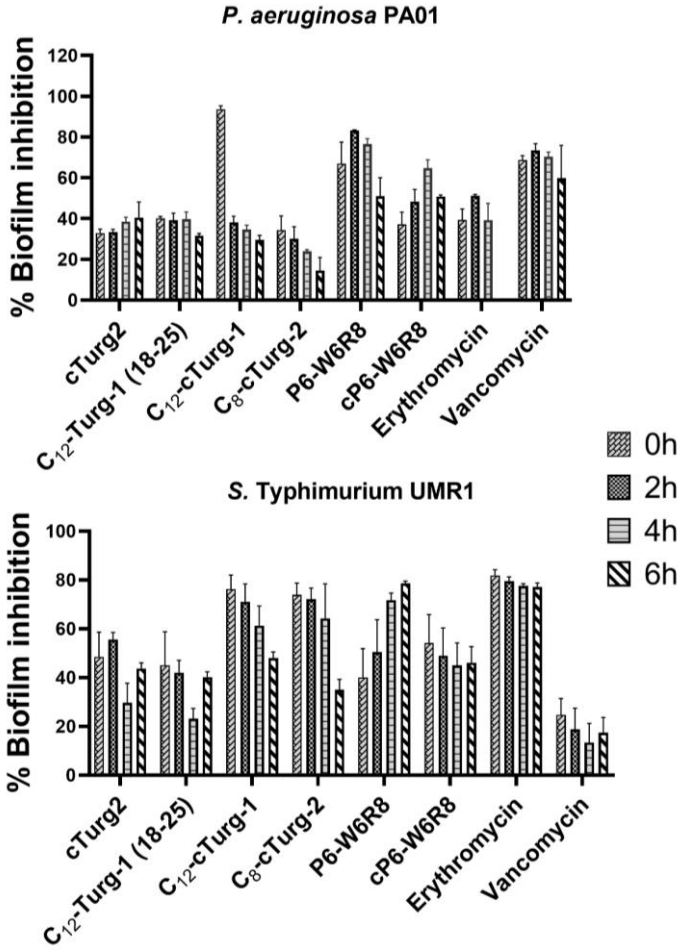

Figure 4. Effects of linear and cyclic peptides on inhibition of *P. aeruginosa* PA01 and *S.* Typhimurium UMR1 biofilm formation at varying timepoints at the concentration 25 µg/mL.

2.8. Synergistic effect on biofilm inhibition in P. aeruginosa PAO1 and S. Typhimurium UMR1

The two-way interaction of the linear Turgencin A core peptide C_{12}-Turg-1 (18-25) combined with both erythromycin and vancomycin was assessed for their effect on inhibition of S. Typhimurium UMR1 biofilm formation. It is worth noting that among several inhibitory concentrations assessed for C_{12}-Turg-1 (18-25) to prevent biofilm formation, 8-32 µg/mL showed around 50% inhibition of biofilm formation despite limited effects on growth inhibition (Figure 2 and Figure 4). In combination with erythromycin, the effective inhibitory concentration decreased to 2 µg/mL for both the peptide and for erythromycin. Although C_{12}-Turg-1 (18-25) did not show synergy with vancomycin in E. coli as previously shown in Table 2, synergistic interaction with vancomycin was correlated with stronger biofilm inhibitory effects against S. Typhimurium biofilms, with a slight decrease in the FICI value from 0.25 to 0.19 (**Figure 5A**). Although the amino acid sequences of cTurg-2 and the core peptide C_{12}-Turg-1 (18-25) are somewhat similar, their antibiofilm mechanism seems to be different. This might be due to their structural differences as cyclic and linear peptides.

A.

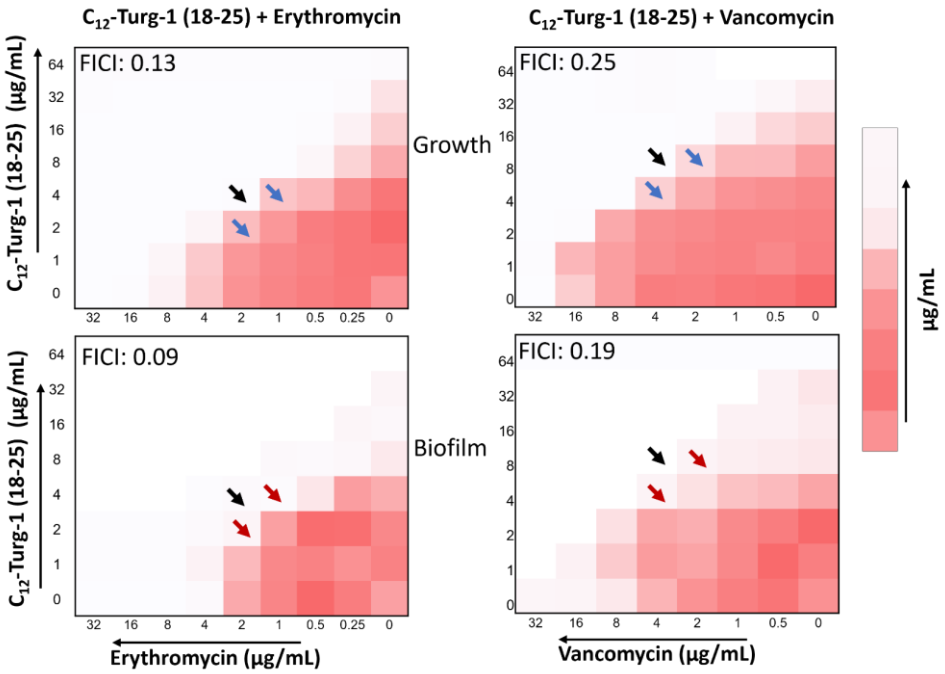

B.

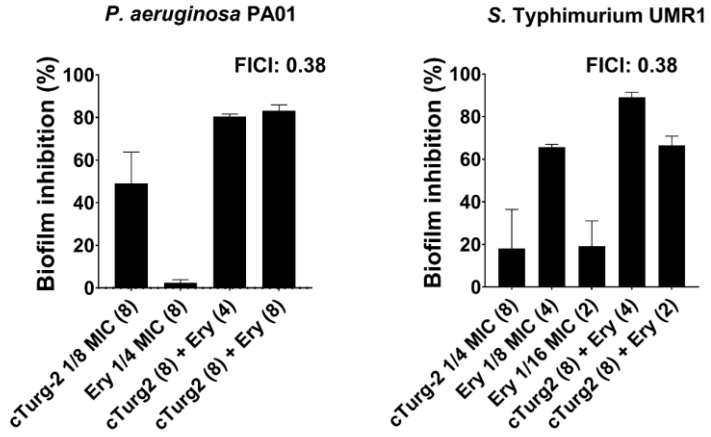

Figure 5. Checkerboard synergy assay to determine A) *S.* Typhimurium UMR1 biofilm inhibitory effects (formation of static biofilm) of C12-Turg-1 (18-25) alone or in combination with either erythromycin or vancomycin, and B) *S.* Typhimurium UMR1 and *P. aeruginosa* PA01 biofilm inhibitory effects of cTurg-2 alone or in combination with erythromycin. Blue and red arrows indicate growth and biofilm biomass, respectively. The black arrows indicate inhibition of growth and biofilms.

Given that the combination of cTurg-2 and erythromycin showed a synergistic effect (FICI of 0.5) on the growth of planktonic *P. aeruginosa* PAO1 and *S.* Typhimurium UMR1 cells (**Table 3**), we wanted to assess whether this two-compound combination could prevent biofilm formation in these strains. In *P. aeruginosa* PAO1, cTurg-2 alone inhibited approximately 50% biofilm formation at concentrations of 8-16 µg/mL (**Figure2**), while erythromycin was less effective. However, combining both compounds resulted in increased biofilm inhibition at concentrations less than one-fourth of their MIC-values. The synergistic combination decreased the effective concentrations required from 64 µg/mL for cTurg-2 alone to 8 µg/mL in combination and from 32 µg/mL for erythromycin alone to 4-8 µg/mL in combination (**Figure 5B**). The FICI calculated from this compound combination is 0.38, indicating a synergistic effect of this treatment on biofilms. Similarly, in *S.* Typhimurium UMR1, at 0.5x-MIC, cTurg-2 was able to inhibit more than 50% biofilm formation. Treatment with a combination of 0.25x-MIC (8 µg/mL) of cTurg-2 and 0.125x-MIC (4 µg/mL) of erythromycin showed >90% inhibition of biofilm formation (**Figure 5B**).

3. Conclusion

Of the16 synthetic analogues of marine AMPs Turgencin A and EeCentrocin 1, only the lipopeptide analogues showed activity (MIC ≤ 32 µg/mL) against *C. difficile*. The dual *E. coli* biosensor assay, and the synergistic combination studies indicate that most of the OM active derivatives were able to sensitize the Gram-negative bacteria for the entry of erythromycin. However, none of the lipopeptides or the arginine-enriched analogues displayed a synergistic effect in combination with vancomycin, although the interaction was still additive. The shortest lipopeptide C_{12}-Turg-1 (18-25) and the moderately active cyclic peptide cTurg-2 displayed a pronounced synergistic effect with erythromycin. This observation may suggest that the active analogues having both OM and PM activity anchor more into the membrane leading to membrane disintegration instead of pore formation. Most of the peptide analogues were able to inhibit (>50% biofilm formation) at the half-MIC (compared to their corresponding MIC in MH media). The mechanism of action for biofilm inhibition and eradication of the active analogues might be their membranolytic and killing effect, whereas the antibiofilm effects of weakly active analogues suggest inhibition of biofilm development either alone or synergistically at concentrations independent of the effects on growth inhibition. In summary, this study showed that the modified analogues with pronounced OM activity have an inhibiting effect on biofilm development and an eradication effect on preformed biofilms in Gram-negative bacteria, and they can show increased biofilm inhibitory activity in combination with conventional antibiotics.

4. Materials and Methods

4.1. Peptides and antibiotics

All peptides used in this study were synthesized using Fmoc peptide synthesis process as described previously (18, 23). The shortest lipopeptide (8 amino acids) of the Turgencin A series named C_{12}-Turg-1-(18-25) (C_{12}-GKKPGGWK-NH_2) was synthesized by Hagen (22).

Several different antibiotics including vancomycin, erythromycin, polymyxin B (PMB), and polymyxin B Nonapeptide (PMBN), all obtained from commercial sources, were used. Stock solutions of antibiotics were prepared in sterile water except for erythromycin which was dissolved in 96% EtOH.

4.2. Bacterial strains

S. T*yphimurium* UMR1was used with permission from Prof. Ute Römling (Karolinska Institutet). The laboratory strains *E. coli* (ATCC 25922), *E. coli* BL-21 (DE3), *E. coli* MC4100, *E. coli* NR698, *E. coli* BW2511, *E. coli* JW450, *P. aeruginosa* (ATCC 27853), *K. aerogenes* (ATCC 51697), *A. baylyi* (DSM 24193), *S. aureus* (ATCC 9144), *S. epidermidis* RP62A (ATCC 35984) and the non-toxicogenic laboratory strain *C. difficile* (ATCC 700057) were from bacterial culture collections. The bacteria were cultured from frozen glycerol stocks on Mueller-Hinton (MH, Difco Laboratories, USA) agar plates at 37 °C.

4.3 Antibacterial MIC Assay

Standard broth microdilution assay was used to measure the MIC values of the selected antimicrobial peptides (29). Briefly, *S. epidermidis* RP62A, *P. aeruginosa* PA01 and *S.* Typhimurium UMR1 colonies were picked from Mueller Hinton (MH) agar plates and grown overnight at room temperature (RT) in tryptic soy broth (TSB) without glucose, MH broth (MHB) and Lysogeny broth (LB), respectively. All the other bacterial strains used in this study including *E. coli* (ATCC 25922), *E. coli* BL-21 (DE3), *E. coli* MC4100, *E. coli* NR698, *E. coli* BW2511, *E. coli* JW450, *K. aerogenes*, *A. baylyi*, and *S. aureus* were grown in MHB. The next morning bacterial cultures were diluted and grown for 2-3 hours at RT and adjusted to 5 x 10^5 CFU/mL to be used as inoculum. A volume of 50 µL bacterial inoculum was treated with 2-fold serially diluted peptides preloaded in 96-well plates and incubated for 24 h at 35 ˚C.

C. difficile colonies were picked from 1-2 weeks anaerobic culture on Brucella agar supplemented with 5% lysed horse blood, Vitamin K (Sigma-Aldrich, V3501) and hemin (Sigma-Aldrich, 51280). Two-fold serial dilutions of peptide analogues and the bacterial suspensions (OD600 0.01-0.02) were

prepared in Brucella broth base (Sigma-Aldrich, B3051) supplemented with Vitamin-K and hemin. The preparation of bacterial suspensions and inoculation into 96-well plates were carried out in an aerobic atmosphere. Plates were incubated at 35 °C using anaerobic gas generating pouch system with indicator (BD GasPak ™ EZ, 260001) for 48 h.

4.4. Checkerboard synergy assay

The synergistic interaction of the synthetic peptides in combination with either erythromycin or vancomycin were investigated following the stablished checkerboard method (30). Briefly, bacterial strains were grown overnight in MH broth at RT. The bacterial cultures were diluted and grown for 2-3 hours and adjusted to 5 x 10^5 CFU/mL to be used as inoculum. Working concentration of both peptides and antibiotics were prepared by two-fold serial dilutions starting at the four-fold of desired concentrations. Next, 25 µL of peptide and antibiotic dilutions with different concentrations were added to the 96-well plates. Then, 50 µL of diluted bacterial suspension was added to each well containing dilution of peptide and antibiotic combinations to give the final desired concentrations. The plates were subsequently incubated for 24 h at 35 °C. The fractional inhibitory concentration index (FICI) values were calculated using the FICI formula with the highest combination effects: FICI = MIC of drug A in combination/MIC of drug A alone + MIC of drug B in combination/MIC of drug B alone. The antimicrobial combination was defined as synergy when the FICI ≤ 0.5, additive when 0.5 < FICI ≤ 1, no interaction when 1 < FICI ≤ 4, and antagonism when the FICI was >4.

4.5. Long term dual outer membrane and plasma membrane integrity assay

To study the impact of bioactive molecules on the OM and the PM over time in a single assay, we used the *E. coli* K-12 strain MC4100 carrying the plasmid pCSMR01 with *unaG* and *lucGR* expressed from the strong constitutive promoter OBX15. This sensor strain was cultured overnight in MH broth medium supplemented with 100 µg/mL ampicillin to maintain the plasmid. Day cultures were then prepared by diluting the overnight culture to 1% in new MH broth medium followed by incubation at RT until the OD_{600} reached 0.3-0.5. Cells were centrifuged at 3000g for 5 min. The cells were then dissolved in 0.9 % NaCl 20 mM TrisHCl at pH 7.5 and the bacterial density was adjusted to OD_{600}=0.3. A Plate Reader (BioTek, Winooski, VT, USA) was used for luminescence and fluorescence detection. Fluorescence and luminescence were measured in 3 min intervals for 10 hours at 25.5 °C with shaking in advance of each measurement. The excitation wavelength for UnaG detection was set to 508 / 8 nm and emission to 538 / 8 nm. The gain was kept at 100 for both luminescence and fluorescence in all experiments. The experiments were conducted in black round-bottom 96-well microtiter plates (Nunc, Roskilde, Denmark) at a final volume of 100 µL, Bilirubin (BR) was added to a final concentration of 5 µM, D-luciferin to a final concentration of 1 mM and peptide compounds to the specified concentrations. Addition of water instead of peptide was used as negative control and PMBN (GLPBIO, Montclair, CA, USA) was used as a positive control. BR-free bacteria were included to determine background fluorescence. All the data were processed with GraphPad Prism 9 software version 9.5.0 (GraphPad Software; Boston, USA).

4.6. Antibiofilm assays for S. epidermidis RP62A

Three biological replicates were prepared by selecting different colonies of the test strain. The colonies were inoculated in 5 mL of TSB overnight in a shaker (225 rpm) at 37 °C. Preparation of the inoculum was done by centrifuging the overnight cultures. The pellet of each biological replicate was then dissolved in approx. 1 mL of phosphate-buffered saline (PBS) and filtered through a syringe filter with a pore size of 5 µm. Following this step, the filtered bacterial cultures were diluted in 0.9% NaCl to a 2 McFarland solution before being further diluted to 6×10^6 CFU/mL in TSB containing 1% glucose. Working solutions of each synthetic peptide to be assayed were prepared by first making the dilution series of the peptide samples in MQ-H_2O. Following preparation of the test peptides, 50 µL of the bacterial suspension was added into each well of a 96-well microtiter plate preloaded with 50 µL of the diluted peptide solutions. After incubation for 24 h at 37 °C without shaking, the cultures were poured out and the plates were washed with tap water three times to remove planktonic bacterial cells. The plates were incubated at 55 °C for 1 h to fixate the biofilm. Following this, 150 µL of crystal violet (0.1%) was added in each well to stain the biofilm. The plates were further incubated for 20 min in RT,

washed with tap water three times and then 200 µL of ethanol (96%) was added in each well. Assessment of biofilm inhibition was done by measuring the absorbance of the CV that bound to the adherent biofilm using an ELISA reader at 595 nm. Peptides resulting in more than 50% reduction in the amount of biofilm mass at sub-MIC levels were considered antibiofilm active.

4.7. Antibiofilm assay for P. aeruginosa PA01 and Salmonella Typhimurium *UMR1*

Peptides were subjected to investigating MBIC representing the minimum concentration that prevent biofilm formation. Both inhibitory and dispersal activity were investigated at concentration ranging from 64-2 µg/mL. Briefly, bacterial strains were incubated at RT overnight in LB or MH media under shaking. The next day overnight cultures were diluted and grown for two hours in biofilm inducing media for each strain. For *P. aeruginosa* PA01, MH broth was used and for *S.* Typhimurium UMR1, LB broth without NaCl was selected. 50 µL dilution series of each peptide was prepared in 96-well plates in triplicates. A 50 µl aliquote from 2 hr culture (a final bacterial concentration of $5x10^5$ CFU/mL) was added to each well and incubated for 24 h. For optimum biofilm growth of *P. aeruginosa* and *S.* Typhimurium, the preferred incubation temperature was 35 °C and 28 °C, respectively. After overnight incubation, the method described above for *S. epidermidis* RP62A was followed.

4.8. Eradication of preformed biofilm

Bacteria were grown as described above. The amount of bacterial suspension was increased by 2-fold compared to the inhibition assay to allow proper cell attachment and biofilm formation. Briefly, the assay was done by transferring 100 µL cell suspension into wells of the 96-well plate containing approx. $10x10^5$ CFU/mL. Following 22 h incubation, the plates were washed with sterile MQ-H_2O and 50 µL peptide solutions were added to the preformed biofilms and the volume was adjusted by adding 50 µL fresh media. The wells filled with 50 µL MQ-H_2O and 50 µL fresh media were used as controls. The plates were incubated for another 22 h and the treated and untreated biofilm biomass were assessed using the CV assay as described above.

4.9. Time dependent biofilm adhesion

P. aeruginosa PA01 and *S.* Typhimurium UMR1 cultures were prepared the same way as previously described. Briefly, a 100 µL of diluted and freshly grown bacterial suspension (final conc. $5x10^5$ CFU/mL) prepared from overnight cultures, were added to the 96-well microtiter plate. Subsequently, 25 µg/mL of synthetic analogues and antibiotic controls were added to their respective wells at different timepoints (0h, 2h, 4h or 6h) and incubated for an additional 22h. The incubation period varied according to the conditions where different analogues and antibiotics were added at different timepoints. For example, analogues added at the start of the assay (0h) was incubated for a total of 28h followed by the incubation period of 26h, 24h, and 22h for the conditions where the peptides and antibiotics were added at 2h, 4h or 6h, respectively after the assay started. The inhibition of bacterial adhesion/biofilm inhibition was assessed by comparing with untreated control (28h). All experiments were done in triplicate wells and repeated at least twice.

5. References

1. Global burden of bacterial antimicrobial resistance in 2019: a systematic analysis. The Lancet. 2022;399(10325):629-55.
2. Sharma D, Misba L, Khan AU. Antibiotics versus biofilm: an emerging battleground in microbial communities. Antimicrobial resistance and infection control. 2019;8(1):76.
3. Martínez Díaz Y, Vanegas Laverde G, Reina Gamba L, Mayorga Wandurraga H, Arévalo-Ferro C, Ramos Rodríguez F, et al. Biofilm inhibition activity of compounds isolated from two Eunicea species collected at the Caribbean Sea. Revista Brasileira de Farmacognosia. 2015;25(6):605-11.
4. Hooton TM, Bradley SF, Cardenas DD, Colgan R, Geerlings SE, Rice JC, et al. Diagnosis, prevention, and treatment of catheter-associated urinary tract infection in adults: 2009 International

Clinical Practice Guidelines from the Infectious Diseases Society of America. Clinical infectious diseases. 2010;50(5):625-63.
5. Galdiero E, Lombardi L, Falanga A, Libralato G, Guida M, Carotenuto R. Biofilms: Novel Strategies Based on Antimicrobial Peptides. Pharmaceutics. 2019;11(7).
6. Fjell CD, Hiss JA, Hancock REW, Schneider G. Designing antimicrobial peptides: form follows function. Nature Reviews Drug Discovery. 2012;11(1):37-51.
7. Patel H, Huynh Q, Bärlehner D, Heerklotz H. Additive and Synergistic Membrane Permeabilization by Antimicrobial (Lipo)Peptides and Detergents. Biophysical journal. 2014;106(10):2115-25.
8. Lazzaro BP, Zasloff M, Rolff J. Antimicrobial peptides: Application informed by evolution. Science. 2020;368(6490).
9. Ghai I, Ghai S. Understanding antibiotic resistance via outer membrane permeability. Infection and drug resistance. 2018;11:523-30.
10. Gong H, Hu, X., Liao, M., Fa, K., Ciumac, D., Clifton, L. A., Sani, M. A., King, S. M., Maestro, A., Separovic, F., Waigh, T. A., Xu, H., McBain, A. J., & Lu, J. R. Structural Disruptions of the Outer Membranes of Gram-Negative Bacteria by Rationally Designed Amphiphilic Antimicrobial Peptides. ACS Applied Materials & Interfaces. 2021;13(14):16062-74.
11. Fuente-Núñez Cdl, Korolik V, Bains M, Nguyen U, Breidenstein EBM, Horsman S, et al. Inhibition of Bacterial Biofilm Formation and Swarming Motility by a Small Synthetic Cationic Peptide. Antimicrobial Agents and Chemotherapy. 2012;56(5):2696-704.
12. Lu Y, Tian H, Chen R, Liu Q, Jia K, Hu D-L, et al. Synergistic Antimicrobial Effect of Antimicrobial Peptides CATH-1, CATH-3, and PMAP-36 With Erythromycin Against Bacterial Pathogens. Frontiers in Microbiology. 2022;13.
13. Reffuveille F, Fuente-Núñez Cdl, Mansour S, Hancock REW. A Broad-Spectrum Antibiofilm Peptide Enhances Antibiotic Action against Bacterial Biofilms. Antimicrobial Agents and Chemotherapy. 2014;58(9):5363-71.
14. Hansen I, Isaksson J, Poth AG, Hansen K, Andersen AJC, Richard CSM, et al. Isolation and Characterization of Antimicrobial Peptides with Unusual Disulfide Connectivity from the Colonial Ascidian Synoicum turgens. Marine drugs. 2020;18(1).
15. Solstad RG, Li C, Isaksson J, Johansen J, Svenson J, Stensvåg K, et al. Novel Antimicrobial Peptides EeCentrocins 1, 2 and EeStrongylocin 2 from the Edible Sea Urchin Echinus esculentus Have 6-Br-Trp Post-Translational Modifications. PLOS ONE. 2016;11(3):e0151820.
16. Gut AM, Vasiljevic T, Yeager T, Donkor ON. Salmonella infection - prevention and treatment by antibiotics and probiotic yeasts: a review. Microbiology (Reading). 2018;164(11):1327-44.
17. Mylonakis E, Ryan ET, Calderwood SB. Clostridium difficile--Associated diarrhea: A review. Archives of internal medicine. 2001;161(4):525-33.
18. Dey H, Simonovic D, Norberg-Schulz Hagen I, Vasskog T, Fredheim EGA, Blencke H-M, et al. Synthesis and Antimicrobial Activity of Short Analogues of the Marine Antimicrobial Peptide Turgencin A: Effects of SAR Optimizations, Cys-Cys Cyclization and Lipopeptide Modifications. International Journal of Molecular Sciences. 2022;23(22):13844.
19. Richard CSM, Dey H, Øyen F, Maqsood M, Blencke H-M. Outer Membrane Integrity-Dependent Fluorescence of the Japanese Eel UnaG Protein in Live Escherichia coli Cells. Biosensors. 2023;13(2):232.
20. Otto M. Staphylococcus epidermidis pathogenesis. Methods in molecular biology. 2014;1106:17-31.
21. Freeman J, Baines SD, Jabes D, Wilcox MH. Comparison of the efficacy of ramoplanin and vancomycin in both in vitro and in vivo models of clindamycin-induced Clostridium difficile infection. Journal of Antimicrobial Chemotherapy. 2005;56(4):717-25.
22. Hagen IN-S. Synthesis of short lipopeptide analogues of the marine, antimicrobial peptide Turgencin A. Master thesis, 137 pages, UiT - the Arctic University of Norway, Tromsø, Norway. 2021.
23. Simonovic D, Dey H, Johansen N, Anderssen T, Hansen IKØ, Devold H, et al. Antimicrobial activity of short analogues of the marine peptide EeCentrocin 1: Synthesis of lipopeptides and head-to-tail cyclic peptides and mechanism of action studies. In: Norway UTAuo, editor. Manuscript2024.
24. Igumnova EM, Mishchenko E, Haug T, Blencke H-M, Sollid JUE, Fredheim EGA, et al. Synthesis and antimicrobial activity of small cationic amphipathic aminobenzamide marine natural

product mimics and evaluation of relevance against clinical isolates including ESBL–CARBA producing multi-resistant bacteria. Bioorganic & Medicinal Chemistry. 2016;24(22):5884-94.
25. Heilmann C, Schweitzer, O., Gerke, C., Vanittanakom, N., Mack, D., & Götz, F. Molecular basis of intercellular adhesion in the biofilm-forming Staphylococcus epidermidis. Molecular Microbiology. 1996;20(5):1083-91.
26. Gill SR, Fouts DE, Archer GL, Mongodin EF, Deboy RT, Ravel J, et al. Insights on evolution of virulence and resistance from the complete genome analysis of an early methicillin-resistant Staphylococcus aureus strain and a biofilm-producing methicillin-resistant Staphylococcus epidermidis strain. Journal of bacteriology. 2005;187(7):2426-38.
27. Xue T, Ni J, Shang F, Chen X, Zhang M. Autoinducer-2 increases biofilm formation via an ica- and bhp-dependent manner in Staphylococcus epidermidis RP62A. Microbes and infection. 2015;17(5):345-52.
28. Zogaj X, Nimtz M, Rohde M, Bokranz W, Römling U. The multicellular morphotypes of Salmonella typhimurium and Escherichia coli produce cellulose as the second component of the extracellular matrix. Molecular microbiology. 2001;39(6):1452-63.
29. Igumnova EM, Mishchenko E, Haug T, Blencke H-M, Sollid JUE, Fredheim EGA, et al. Synthesis and antimicrobial activity of small cationic amphipathic aminobenzamide marine natural product mimics and evaluation of relevance against clinical isolates including ESBL–CARBA producing multi-resistant bacteria. Bioorg Med Chem. 2016;24(22):5884-94.
30. Zhang Y, Wang X, Li X, Dong L, Hu X, Nie T, et al. Synergistic Effect of Colistin Combined with PFK-158 against Colistin-Resistant Enterobacteriaceae. Antimicrobial Agents and Chemotherapy. 2019;63(7).

Supporting information

Combining outer membrane active synthetic antimicrobial peptides with vancomycin or erythromycin increases antibacterial and antibiofilm activities

Hymonti Dey[1], Danijela Simonovic[2], Céline S. M. Richard[1], Ingrid Norberg-Schulz Hagen[2], Natascha Johansen[2], Frode J. Øyen[1], Elizabeth G. Aarag Fredheim[2], Morten B. Strøm[2], Roger Simm[3], Tor Haug[1*], Hans-Matti Blencke[1*]

[1] The Norwegian College of Fishery Science, Faculty of Biosciences, Fisheries and Economics, UiT the Arctic University of Norway, NO-9037 Tromsø, NORWAY.
[2] Department of Pharmacy, Faculty of Health Sciences, UiT the Arctic University of Norway, NO-9037 Tromsø, NORWAY.
[3] Department of Biosciences, University of Oslo, NO-0371 Oslo, NORWAY
* Corresponding authors. Correspondence: tor.haug@uit.no and hans-matti.blencke@uit.no

Contents:

Table S1. Antimicrobial (MIC in μg/mL) and synergistic activities of AMPs and commercial antibiotic combinations against *E. coli* BL-21.

Compound A + Compound B	MIC (μg/mL) of Compound A and Compound B				FICI
	Alone		In combination		
	A	B	A	B	
P6-W6R8 + Polymyxin B	8	2	4	0.06	0.53
P6-W6R8 + PMBN	8	>256	4	1	0.50
P6-W6R8 + Erythromycin	8	32	1	4	0.25
P6-W6R8 + Vancomycin	8	64	2	4	0.31
P6-W6R8 + cTurg-2	8	64	4	1	0.52
Chlorhexidine + cTurg-1	2	>256	2	25	>1.0
Oxyteracycline + cTurg-1	2	>256	2	25	>1.0
Polymyxin B + cTurg-1	2	>256	1	25	>0.6
Polymyxin B + cTurg-2	2	64	1	1	0.52
Polymyxin B + cTurg-5	2	8	1	4	1.0
Polymyxin B + cTurg-6	2	8	1	8	1.5
Polymyxin B + C_8-cTurg-2	2	8	1	2	0.75
Polymyxin B + Erythromycin	2	32	0.25	2	0.19
Polymyxin B + Vancomycin	2	32	0.25	16	0.75
PMBN + Erythromycin	>256	32	0.5	16	>0.5

Table S2. Antimicrobial (MIC in μg/mL) and synergistic activities of the linear P6-W6R8 in combination with erythromycin or vancomycin against different *E. coli* strains.

Bacterial strains	MIC (μg/mL) of peptides/antibiotics alone or in combination				FICI
	Alone		In combination		
	P6-W6R8	Erythromycin	P6-W6R8	Erythromycin	
E. coli MC4100	8	16	2	2	0.37
E. coli NR698	8	0.5	8	0.25	1.5
E. coli BW2511	16	64	2	8	0.25
E. coli JW450	4	64	2	1	0.37
	P6-W6R8	Vancomycin	P6-W6R8	Vancomycin	
E. coli MC4100	8	64	2	4	0.31
E. coli NR698	8	0.5	4	0.25	1.0
E. coli BW2511	16	64	4	8	0.37
E. coli JW450	4	64	2	8	0.63

Table S3. Antimicrobial (MIC in μg/mL) and synergistic activities of the cyclic cP6-W6R8 in combination with erythromycin or vancomycin against different *E. coli* strains.

Bacterial strains	MIC (μg/mL) of peptides/antibiotics alone or in combination				FICI
	Alone		In combination		
	cP6-W6R8	Erythromycin	cP6-W6R8	Erythromycin	
E. coli MC4100	8	16	2	2	0.37
E. coli NR698	4	0.5	2	0.25	1.0
E. coli BW2511	16	64	4	2	0.28
E. coli JW450	8	32	2	2	0.31
	cP6-W6R8	Vancomycin	cP6-W6R8	Vancomycin	
E. coli MC4100	8	64	2	8	0.38
E. coli NR698	4	0.5	4	0.5	2.0
E. coli BW2511	16	64	4	4	0.31
E. coli JW450	8	64	4	8	0.62

Table S4. Antimicrobial activities (MIC in μg/mL) of synthetic peptides and selected antibiotics against facultative and/or obligate anaerobic bacterial strains commonly found in the human oral cavity.

Peptide/antibiotic	***Streptococcus mitis*** **CCUG 31611** **(Gram-positive)**	***Streptococcus oralis*** **NCTC 11427** **(Gram-positive)**	***Actinomyces naeslundii*** **ATCC 19039** **(Gram-positive)**	***Fusobacterium nucleatum*** **ATCC 10953** **(Gram-negative)**
C_{12}-cTurg-1	16	>64	32	64
C_8-cTurg-2	64	>64	64	>64
cTurg-2	>64	>64	>64	>64
cTurg-3	>64	>64	>64	>64
cTurg-6	>64	>64	>64	>64
P6-W6R8	>64	>64	64	32
Vancomycin	1	<1	<1	>128
Ciprofloxacin	2	4	2	4
Polymyxin B	64	>128	64	0.5
Erythromycin	0.5	1	<0.125	32

Table S5. Effects of selected Turgencin A and EeCentrocin 1 analogues on biofilm formation by *S. epidermidis* RP62A. MIC values were determined during MBIC assay conditions (TSB+glu media) and are based on the relative absorbance/turbidity in the biofilm assay plates before washing away the planktonic cells.

Peptide	MIC (µg/mL)	Percentage biofilm inhibition		
		2xMIC	MIC	0.5xMIC
cTurg-1	>256	-[1]	47	46
cTurg-3	16	81	78	50
cTurg-4	32	92	80	57
cTurg-5	8	95	77	17
cTurg-6	8	95	80	33
P6	64	99	99	70
P6-K8	64	99	71	44
P6-W6K8	8	99	99	76
C_8-P6-R8	4	100	100	35
C_{10}-P6-R8	4	100	100	35
Polymyxin B	1.5	100	100	80
Daptomycin	6.25	97	94	30
Vancomycin	2	100	99	9

[1] Not tested

Table S6. Effects of selected Turgencin A and EeCentrocin 1 analogues on biofilm formation by *P. aeruginosa* PA01 biofilm. MIC values were determined during MBIC assay conditions (MH media) and are based on the relative absorbance/turbidity in the biofilm assay plates before washing away the planktonic cells.

Peptide	MIC (µg/mL)	Percentage biofilm inhibition		
		2xMIC	MIC	0.5xMIC
cTurg-1	>64	-[1]	70	73
cTurg-3	64	-	95	78
cTurg-4	32	95	96	61
cTurg-5	8	95	90	59
cTurg-6	16	96	96	86
P6	16	100	96	84
P6-K8	16	100	100	75
P6-W6K8	8	98	63	63
C_8-P6-R8	16	86	100	47
C_{10}-P6-R8	16	86	88	64
Polymyxin B	1.5	100	86	41

[1] Not tested

Table S7. Effects of selected Turgencin A and EeCentrocin 1 analogues on biofilm formation by *S.* Typhimurium UMR1. MIC values were determined during MBIC assay conditions (LB-salt media) and are based on the relative absorbance/turbidity in the biofilm assay plates before washing away the planktonic cells.

Peptide	MIC (µg/mL)	Percentage biofilm inhibition		
		2xMIC	MIC	0.5xMIC
cTurg-1	>256	-[1]	-	71
cTurg-3	16	83	78	88
cTurg-4	32	79	84	81
cTurg-5	16	76	73	86
cTurg-6	16	67	67	81
P6	16	86	98	90
P6-K8	16	89	95	81
P6-W6K8	16	74	90	91
C_8-P6-R8	8	82	93	92
C_{10}-P6-R8	32	49	77	86
Polymyxin B	1.5	100	99	82
Vancomycin	64	100	100	100

[1] Not tested

Table S8. Effects of selected EeCentrocin analogues on preformed biofilms produced by *S.* Typhimurium UMR1, *P. aeruginosa* PA01 and *S. epidermidis* RP62A. MBIC of the peptides were tested based on the relative absorbance/turbidity in the biofilm assay plates before washing away the planktonic cells.

	***S.* Typhimurium UMR1**		***P. aeruginosa* PA01**		***S. epidermidis* RP62A**	
Peptide	**% removal**	**xMIC**	**% removal**	**xMIC**	**% removal**	**xMIC**
P6	74	1	99	8	24	1
P6-K8	83	1	99	8	28	1
P6-W6K8	83	1	90	8	61	8
C_8-P6-R8	44	1	[1]-	-	21	16
C_{10}-P6-R8	71	1	90	4	41	16
PMB	0	1	100	1	0	1

[1] Not tested

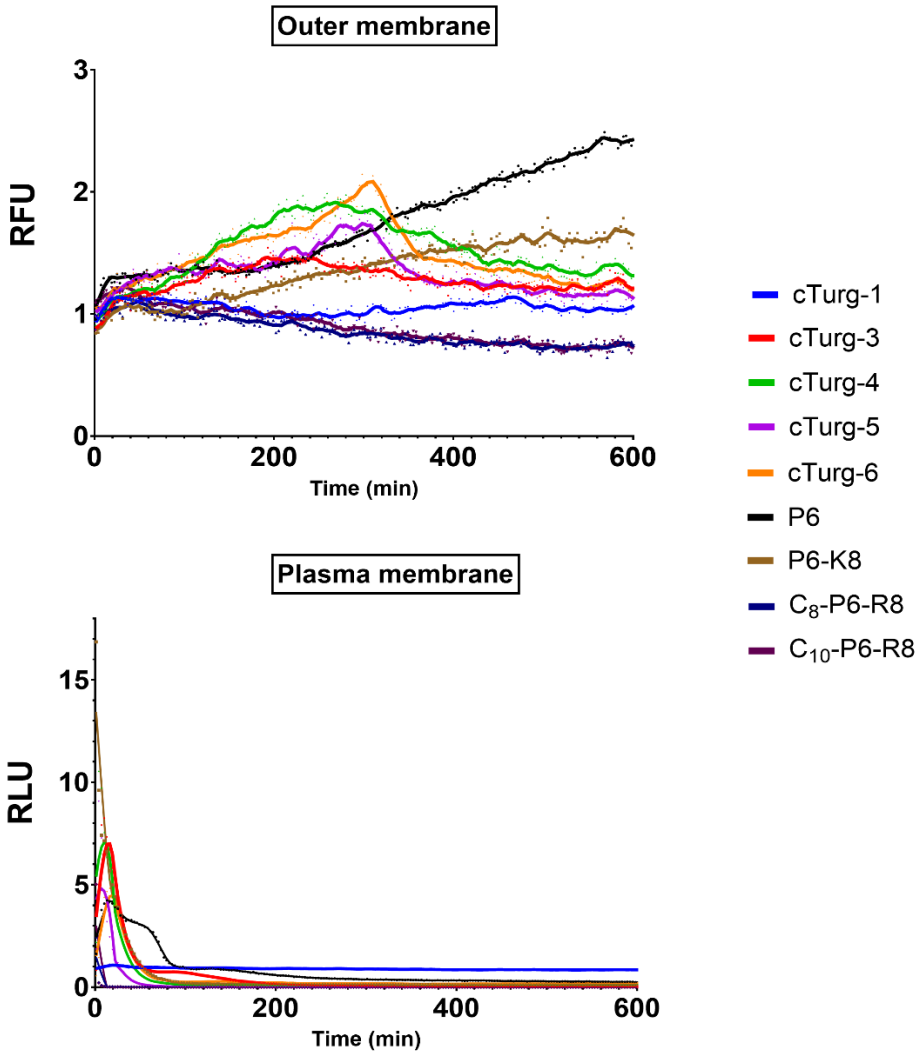

Figure S1. Outer membrane and plasma membrane activity of selected Turgencin A analogues and EeCentrocin 1 analogues, determined at concentration 12.5 µg/mL using an *E. coli* dual biosensor strain. The figure depicts fluorescence and luminescence normalized to the untreated control.

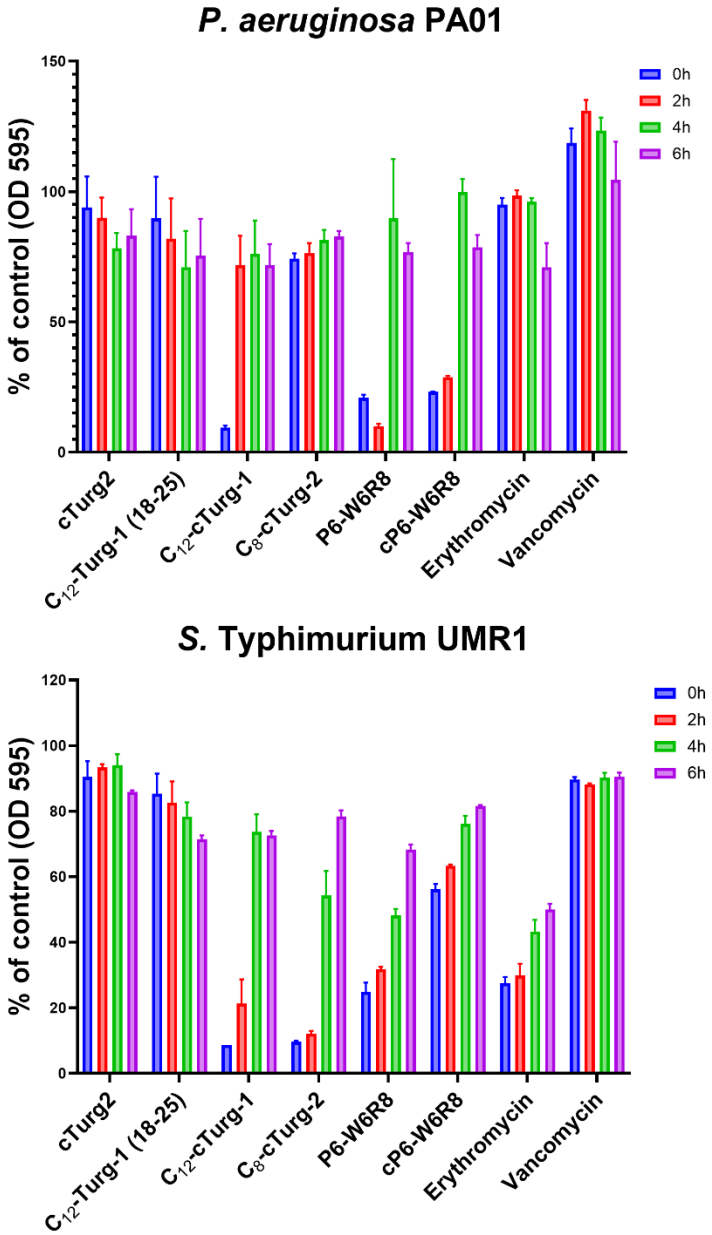

Figure S2. Effects of linear and cyclic peptides on growth of *P. aeruginosa* PA01 and *S.* Typhimurium UMR1 biofilm formation at varying timepoints after adding a concentration of 25 µg/mL of the different peptides.

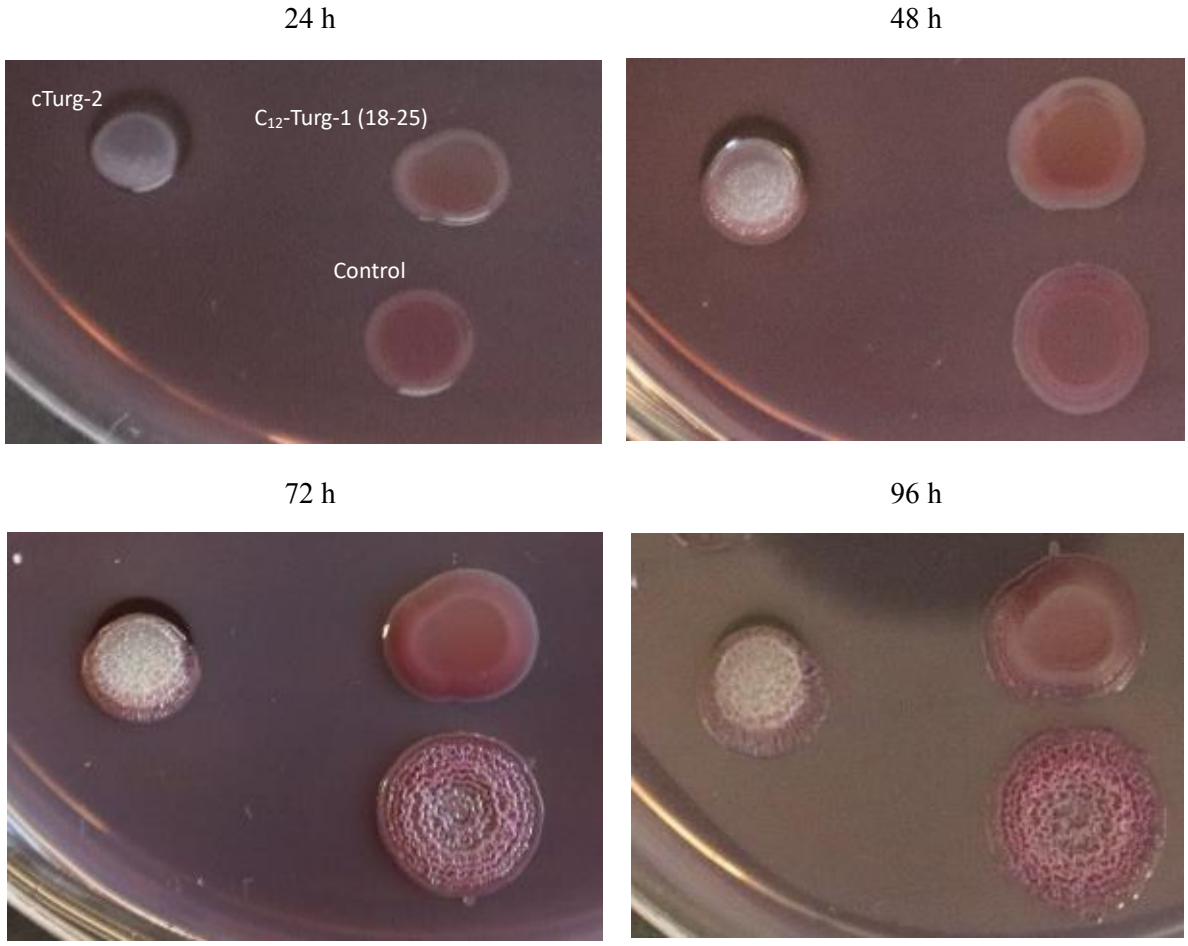

Figure S3. Effects of cTurg-2 and C_{12}-Turg-1 (18-25) on rdar morphotype of *S.* Typhimurium UMR1 biofilm formation Congo red agar plate (LB agar without NaCl, supplemented with the amyloid dye Congo red.

Assay S1. Effects of Turgencin analogues on *S.* Typhimurium morphotype in Congo red agar

Materials and methods:

The biofilm inhibitory effect of cTurg-2 and C_{12}-Turg-1 (18-25) was investigated using the CR-agar method. Agar plates were prepared with 10 g/L Tryptone, 5 g/L yeast extract, 16 g/L agar, 40 µg/mL Congo red (CR) and 20 µg/mL Coomassie Brilliant Blue G-250. Fresh colonies of *S.* Typhimurium colonies were picked from LB agar and grown overnight in LB broth with NaCl. The overnight culture was centrifuged at 3000x*g* for 5 min and dissolved in PBS and adjusted to an OD_{600} of 2.0. Next, 5 µL of peptide analogues (1 µg/mL) were spotted on the CR agar and left to dry for 30 min. An aliquot of 10 µL bacterial suspension were added on top of the peptide containing spots and allowed to dry. The plates were incubated at 28^{o} C for 4 days in a humid atmosphere.

Results and discussion:

The biofilm forming *Salmonella enterica* serovar Typhimurium UMR1 produces a distinct *rdar* (red, dry, and rough) morphotype on CR- agar plates (Monteiro et al., 2011). The rdar morphotype indicates the production of cellulose and curli as biofilm extracellular matrix components. In our studies, the cyclic peptide cTurg-2 showed a distinct saw (white and smooth) morphology after 24 h incubation (Figure S3), indicating a lack of cellulose and/or curli expression. On the other hand, in the presence of the linear lipopeptide C_{12}-Turg-1 (18-25), the bacteria were unable to form the *rdar* (red, dry and rough) morphotype even after 96 hours of incubation.

The CR-agar method is known for the qualitative assessment of biofilm production and the phenotypic characterization of biofilm forming bacteria. Most studies use deletion mutants which show differential expression of curli and cellulose (both or neither) to differentiate between different morphotypes on CR agar. The production of *pdar* (pink, dry and rough) morphotype refers to the expression cellulose but not curli, whereas the *bdar* (brown, dry and rough) morphotype indicates the expression of curli but not cellulose, and smooth and white colonies indicate no production of biofilm (Kim et al., 2022). Accordingly, a pink colored colony morphology represents only cellulose expression and thus disturbance of the curli csgBAC, csgDEFG operon expression, and/or curli assembly (Evans and Chapman, 2013).

Conclusion:

Although staining the biofilm components with CR is a fast and easy method, without complementary genetic analyses and the use of proper controls, there would be a risk of misinterpretation of the results. Further experiments are needed to confirm these results.

References:

Evans ML and Chapman, MR. Curli Biogenesis: Order out of disorder. Biochimica et Biophysica Acta – Molecular Cell Research. 2014;1843(8):1551-1558.

Kim S-H, Jyung S and Kang D-H. Comparative study of *Salmonella* Typhimurium biofilms and their resistance depending on cellulose secretion and maturation temperatures. LWT. 2022;154:112700.

Monteiro C, Fang X, Ahmad I, Gomelsky M and Römling U. Regulation of biofilm components in *Salmonella enterica* serovar Typhimurium by lytic transglycosylases involved in cell wall turnover. Journal of Bacteriology. 2011;193(23):6443-6451.